OXIDATION OF BUTENE OVER PLATINUM CATALYSTS

IN A

ZIRCONIA-YTTRIA ELECTROCHEMICAL REACTOR

by

Mark Richard Stening Manton

B.Sc.(Ind. Chem.), University of the Witwatersrand (1976)

M.Sc., University of South Africa (1978)

SUBMITTED IN PARTIAL FULFILLMENT
OF THE REQUIREMENTS FOR THE
DEGREE OF

DOCTOR OF PHILOSOPHY

at the

MASSACHUSETTS INSTITUTE OF TECHNOLOGY

May 1986

Signature of Author _____
Department of Chemical Engineering
May 16, 1986

Certified By _____
James Wei
Thesis Supervisor

Certified By _____
Herbert H. Sawin
Thesis Supervisor

Accepted By _____
William M. Deen
Chairman, Department Graduate Committee

OXIDATION OF BUTENE OVER PLATINUM CATALYSTS

IN A ZIRCONIA-YTTRIA ELECTROCHEMICAL REACTOR

by

Mark Richard Stening Manton

Submitted to the Department of Chemical Engineering on May 19, 1986
in partial fulfillment of the requiremtents for the degree of
Doctor of Philosophy in Chemical Engineering

Oxidation of Butene: Under butene rich/oxygen lean conditions, and at temperatures between 477°C and 544°C, the platinum catalyst oxidized butene to butadiene with a selectivity of about 80%. At higher P_{O2}/P_{butene} ratios, platinum oxide formed at the expense of the un-oxidized platinum. Butene is oxidized only to deep oxidation products, CO, CO_2 and H_2O, over the oxide surface, resulting in a decrease in the selectivity at high P_{O2}/P_{butene} ratios. The activation energy for deep oxidation (to CO and CO_2) and butadiene formation over the clean Pt surface were 27.1 and 30.2 kcal/mole, respectively.

Butene Fuel Cell: The platinum sponge catalyst used in this study was deposited on the walls of a O^{2-} ion conducting solid electrolyte (yttria doped zirconia) and therefore could act as an electrode of a high temperature fuel cell. The only products obtained when the circuit was closed, however, were CO and CO_2, no butadiene was formed. This was rationalized in terms of an oxide layer forming in the localized area of the electrode/electrolyte interface, which would act as a deep oxidation catalyst only.

Oxide decomposition: When exposed to air, in the absence of butene, platinum oxide forms on the platinum electrode/catalyst. When the ambient gas was changed to helium, the oxide decomposed by reaction between the oxide and a vacant site on the platinum surface with a rate constant of about 0.75 min^{-1} at 477°C. The apparent activation energy for decomposition of the oxide between 423 and 577°C was only about 1.6 kcal/mole.

Adsorption/desorption of oxygen: The enthalpy of adsorption of oxygen on clean platinum was estimated by measuring the "exchange current density" of the electrode/electrolyte interface at various oxygen partial pressures and temperatures, and modelling it in terms of Langmuir-Hinshelwood adsorption of oxygen on platinum. Above 577°C, the model fits well and ΔH_{O2}=53 kcal/mole. Below 523°C, the data deviate significantly from the model probably because of oxide formation.

Electrode/Electrolyte interface: The change in the overpotential, the difference between the potential when current flows and at equilibrium, was recorded as a function of applied current. The slopes of the forward and backward Tafel plots indicate that the transfer coefficients are 1.0. This suggests that the rate controlling step for the electrochemical reaction is the transfer of O^- anions across the interface into the electrolyte, with the anions being subsequently further reduced to O^{2-} ions in the electrolyte.

Thesis Supervisors: Professors James Wei and Herbert Sawin

ACKNOWLEDGEMENTS

My thesis only reached this stage of development in part because of the following people:

* My thesis supervisor Professor James Wei, [illegible]visor Professor Herb Sawin, "previous" advisor (since gone to g[illegible] pastures, and telephone conversations) Professor Costas Vayenas, and my thesis committee Professors Charles Satterfield, Michael Manning and Harry Tuller.

* The Department of Chemical Engineering at M.I.T. and the U.S. Department of Energy for financial support, the latter under contract number DE-AC02-80ER10694.

* For instruction in the art of surface analysis: John R. Martin and Libby Shaw, and assistance with the scanning electron micrographs: Leonard I. Sudenfield. For getting RS/1 to write the y-axis labels sideways and other computational help: Dr William Gilbert, and Professor (nee student) George Truskey for a copy of the non-linear least squares fitting program.

* To my Father for originally encouraging me to come to the States.

* To my Mother for all her support along the way and my step-father for goading me into engineering.

* And last, but by no means least, to all those who tried valiantly to keep me sane throughout the long haul: Kate Sawallisch, Kent Gu[illegible]klen, Mike Gallager, Kris Antonsen, John Tsikoyannis, Phil Westmoreland, Kathleen Beach, Dune, Tom McKinnon, Alan and Marianne Hatton, Gail Gamboa, Lynne Sheinfeld, Barbara Smith, Dave Matsumato, and if I missed you, it's late and I'm tired. Finally, those who beat me to the door, but helped while here: Micky Dalal, John Nenniger, Ian Webster, Chris Schwier and James Nathaniel Michaels.

* Finally, thanks for putting up with me and this, Kate.

K.S.

Thank you

LIST OF FIGURES

LIST OF TABLES

1.INTRODUCTION AND BACKGROUND

1.1 OVERVIEW AND PURPOSE

Butadiene is the 28th largest tonnage chemical in the US and is used primarily as a polymeric precursor for synthetic rubber (styrene-butadiene-rubber) for the polymer ABS (acrylonitrile-butadiene-styrene). It is produced as a by-product of the steam cracking of naptha or by the dehydrogenation or oxidative dehydrogenation of butane and butene.

The dehydrogenation of butane to butene is carried out over a Cr_2O_3/Al_2O_3 catalyst at about 650°C at a high space velocity, diluted in steam (Carra and Forni, 1971). The further dehydrogenation of butene to butadiene is equilibrium limited and requires high temperatures and large steam dilutions to obtain reasonable conversions. As a consequence, dehydrogenation has been largely superseeded by oxidative dehydrogenation, which is an exothermic reaction and is not equilibrium limited. Catalysts for this reaction are typically ferrites (Sterrett and Mc Ilvried, 1974), but bismuth-molybdates and antimony-tin oxides (Sharchenko, 1969) have also been used. Yields, which are typically about 60% (Thomas, 1970), are greatest at temperatures less than 400°C, whereas at higher temperatures, secondary products, mainly CO_2, predominate. Large steam/butene ratios are required to obtain these yields.

The purpose of this thesis was to examine the possibility of producing butadiene from butene by another alternative, viz. the electrochemical oxidation of butene. In this process, butene would be fed as the "fuel" to a solid-electrolyte electrochemical reactor. It was hoped that oxygen from the electrolyte would oxidize butene to butadiene. The advantage of this method would be two-fold. Firstly, the oxidative dehydrogenation of butene

is exothermic and if performed in a fuel cell would release the energy of the reaction as electrical power, which would be more useful than heat (and would also not be subject to Carnot cycle limitations). Secondly, this reactor has the "fuel" and oxidant (air) on separate side of the solid-electrolyte, and therefore explosive limits are by-passed. This would mean that a more compact reactor design could be used.

Processes designed for the synthesis of useful chemicals so that electric power becomes a co-product have been termed "electrogenerative" processes by Langer (1979,1985). He used this technique for the selective reduction of NO to hydroxylamine (Langer and Pate, 1983) and for the oxidation of SO_2 to SO_3 (Spotnitz, Loeffler and Langer, 1981) both with the cogeneration of electricity. This approach has also been investigated for the oxidation of ethylbenzene to styrene (Michaels, 1983) and of ammonia to nitric oxide (Vayenas and Farr, 1979), with reasonable sucess. In the latter study, nitric oxide and electricity were simultaneously produced (Sigal and Vayenas, 1982), whereas in the former, it was found that the thermodynamic limitation of the dehydrogenation could by side-stepped by operating electrochemically.

A limitation of all electrochemical reactors is that are considerably more complex than a comparable catalytic system. To a first approximation, a catalytic reactor is a large drum with pellets in it. An electrochemical reactor, however, requires a catalyst/electrode, supported on an electrolyte, separate gas streams for each side of the electrolyte, and electrical connections between the eletrodes and the outside world. Nevertheless, these types of reactors would serve a useful purpose, if they were able to generate, otherwise discarded, power or to favorably affect the selectivity of a desired reaction.

Unfortunately, as discussed in this thesis, the initial result of the

investigation of this concept, for the partial oxidation of butene to butadiene, was negative. When butene was fed to a zirconia-yttria (solid electrolyte electrochemical) reactor operating as a fuel cell, the only products were CO and CO_2, no butadiene was produced. Furthermore, when oxygen was fed with the butene in the gas phase, instead of through the electrolyte, butene was selectively oxidized to butadiene. This result was not expected, and a substantial fraction of this thesis is directed to the question of why this difference exists between gas phase and "electrochemical" oxygen.

The conclusion is that in excess oxygen, platinum oxide forms over the catalyst surface and butene is oxidized only to CO_2 over this surface. When current, in the form of oxygen anions, flows through the zirconia-yttria solid electrolyte, a region of excess oxygen forms at the electrode/electrolyte interface. This would create platinum oxide and therefore lead exclusively to deep oxidation (to CO and CO_2) of butene, rather than partial oxidation to butadiene as was desired and observed by the use of gas phase oxygen.

The evaluation of this hypothesis involved initially investigating the kinetics for the formation and decomposition of platinum oxide on the catalyst surface in the absence of butene. This constitutes the bulk of chapter three. Chapter four deals with the kinetics of butene oxidation both by gas phase oxygen and by "electrochemical" oxygen (that came through the electrolyte), and also surface spectroscopic analysis of the surface, after different pretreatments, in an attempt to independently reinforce the arguements of the kinetic model.

1.2 LITERATURE REVIEW

The methods employed in this thesis draw extensively on electrochemical techniques, standard kinetic analyses and also on surface analytical techniques. This is a somewhat disparate combination and it is unlikely that the reader is familiar with all these areas. This literature review section attempts to both cover the relevant literature and to provide background to those techniques not known to the reader. Texts for further reference, if required, are Bockris and Reddy (1971) and Newman (1973) on electrochemistry; Froment and Bischoff (1979) and Carberry (1976) on reactor and catalytic kinetics; Briggs and Sheah (1983) on surface analysis by XPS and Auger spectroscopy; Subbarao (1980) and Kleitz and Dupuy (1976) on solid electrolytes and Hegedus and McCabe (1984) on catalyst poisoning.

1.2.1 Butene Dehydrogenation and Oxidative Dehydrogenation

As mentioned briefly in the introduction, butene is converted to butadiene by either dehydrogenation (equation 1) or oxidative dehydrogenation (equation 2):

$$C_4H_8 \longrightarrow C_4H_6 + H_2 \qquad (1)$$

$$C_4H_8 + 1/2\ O_2 \longrightarrow C_4H_6 + H_2O \qquad (2)$$

Dehydrogenation of butene is carried out over chromia-alumina catalysts at high temperature and short contact times in the presence of excess steam (Carra and Forni, 1971). The reaction is equilibrium limited, which is why the large dilution in steam is required. This method has been largely superseeded by the oxidative dehydrogenation route which uses bismuth-molybdate or antimony-tin oxide catalysts.

Antimony-tin oxide catalysts are also used commercially for the

oxidative dehydrogenation of butene and have received extensive academic and industrial investigation both of their catalytic activity (Irvine and Taylor, 1978a and 1978b; McAteer, 1979; and Christie and Taylor, 1976) and of the surface structure and effect of pretreatment (Cross and Pyke, 1979; Herniman, Pyke and Reid (1979); Pyke,Reid and Tilley, 1982). This work was also thoroughly reviewed recently by Perry (1981). Antimony-tin oxide is also a semi-conductor, and oxides of 5% Sb in SnO_2 have conductivities of about 5.7×10^{-2} Ω/cm^2 in air (Herrman and Portefaix, 1979). It therfore appeared that it would be an ideal candidate for the electrode/catalyst in a high temperature electrochemical reactor. Preliminary experiments produced electrodes that were either porous but not conductive (prepared from organometallic resins, or by low temperature deposition of chlorides), or conductive but not porous (prepared by high temperature chemical vapor deposition, CVD, of chlorides). All attempts to synthesise a conductive and porous electrode failed. For this reason, the direction of the thesis changed to at least investigate the feasibility of the concept by using platinum electrodes, which can be readily made into conductive and porous electrodes.

1.2.2 Oxidation over Platinum

The largest use of platinum is in automobile emission control, and although much work has been done, no substitutes for platinum catalysts have been found (Taylor, 1984). They are typically used for the complete oxidation of the hydrocarbons and CO.

1.2.2.1 Oxidation of Butene

There is only a limited amount of data on the oxidation of butene over platinum catalysts. Schwartz, Holbrook and Wise (1971) studied the

oxidation of a number of paraffins and olefins over platinum wires in excess oxygen. They reported an activation energy for the complete oxidation of butene of 17.4±2.4 kcal/mole and observed a negative order dependence of the rate on the oxidation of butene, with a reaction order of about -0.2. In addition, the reaction required oxygen to be adsorbed on the catalyst, causing them to speculate that the O/Pt ratio on the surface could be approaching 2.0.

In a similar study, Cant and Hall (1970) only observed first order dependence on oxygen partial pressure when oxidizing ethylene and propylene over platinum supported on SiO_2, although the rate was also "strongly repressed" by olefin. The activation energies, for the oxidation of ethylene and propylene to CO_2, for $80^oC<T<120^oC$, were similar to those of Schwartz et al.: 18.5±0.5 kcal/mole ($\log_{10}A=23.1\pm0.5$ molecules sec^{-1} cm^{-2}) and 19.8±0.4 kcal/mole ($\log_{10}A=23.6\pm0.4$ molecules $sec^{-1}cm^{-2}$). Only very low selectivities to partial oxidation products were observed over platinum (less than 1% selectivity to acetic acid, the largest partial oxidation product).

In 1984, Yao published data on the oxidation of CO and propylene, 1-hexene and toluene over platinum wires and platinum supported on AL_2O_3. He pretreated his catalysts in air at temperatures above 600^oC, measured the kinetics for CO_2 production, and fitted the results according to a power law fit:

$$\text{rate} = k\ (p_{O2})^m\ (p_{\text{hydrocarbon}})^n \qquad (3)$$

For CO oxidation, the reaction was first order in oxygen pressure (m=1) and minus one order in CO (n=-1), with an activation energies of 30 and 22 - 30 kcal/mole for Pt wire and Pt-Al_2O_3 respectively. When oxidizing propylene, toluene or hexene, however, the reaction orders varied with the oxygen/hydrocarbon ratio in each particular reaction, the temperature and

even the order of adding the reactants. Under strongly oxidizing conditions (O_2/HC > 0.8 of the stoichiometric ratio for oxidation to CO_2) the reaction orders and activation energies for the oxidation of propylene and hexene were similar (Table 1.1).

Table 1.1 Orders of reaction and activation energies for the oxidation of propylene, hexene and toluene over Pt (Yao, 1984).

compound	catalyst	m	n	ΔE(kcal/mole)
propylene	Pt wire	1.8	-0.8	22
	$Pt-Al_2O_3$	2.0-2.2	-0.9 to -1.2	16-20
hexene	Pt wire	1.7	-1.2	16
	$Pt-Al_2O_3$	0.7-1.5	-0.3	12-17
toluene	Pt wire	2.1	-2.0	28
	$Pt-Al_2O_3$	2.2-2.5	-1.2 to -1.9	21-29

The mechanism proposed by Yao for these reactions was between adsorbed oxygen and hydrocarbon (Langmuir-Hinshelwood mechanism) with the latter strongly inhibiting the reaction. He concluded that the similarity between propylene, hexene and toluene indicated that the double bond was more significant than the chain length, with the rate controlling step being adsorption and cleavage of the double bond. If this is the case, then similar behavior would be expected for butene oxidation over Pt in excess oxygen. Yao attributed the apparent non-integral reaction orders to the adsorption and removal of partially oxidized products. When the catalyst was reduced, the reaction orders changed and the reaction was less inhibited by the hydrocarbon, showed smaller partial reaction orders and higher reactivities.

Although not concerned with the oxidation of butene, Ostermaier,

Katzer and Manogue (1976) reported that when studying the oxidation of ammonia over Pt-Al_2O_3 and platinum black at temperatures less than 450°C, the reaction was inhibited by oxygen. The concentration of oxygen on the surface corresponded to PtO_2. Smaller crystallites were almost completely deactivated while larger ones were more resistant. From this they hypothesised that the platinum was probably oxidized to 3-4 monolayers. Furthermore, they concluded that "oxidation reactions over noble metals may involve more a noble metal oxide than a noble metal surface; i.e., in oxidation reactions noble metals may not be as noble as normally assumed".

Over Rh, Ru and Pd catlaysts, Kiss and Gonzalez (1985) found this to be the case because the oxidation of CO was strongly inhibited by the formation of an oxide film.

The formation and decomposition of an oxide film has been independently proposed by both Vayenas, Lee and Michaels (1981) and by Sales, Turner and Maple (1982) to explain the observation of oscillations in the oxidation of ethylene and CO respectively.

There have, however, been an extremely large number of different models proposed to explain the oscillations observed in the oxidation of CO over platinum, besides oxide formation/decomposition. The scource of the oscillations is still a subject of debate (see next section).

1.2.2.2 Oscillations during CO oxidation over Pt

The ultra high vacuum studies relating to the mechanism for the oxidation of CO over platinum metals were reviewed by Engel and Ertl in 1979. Carbon monoxide adsorbs molecularily with electron tansfer to the metal and back-bonding to the π^* antibonding orbital of the CO with bonding to the surface occuring through the carbon atom. The adsorption energy for CO on clean surfaces is about 32 kcal/mole and decreases as the surface

coverage increases, until a maximum coverage of about $1x10^{15}$ cm^{-2}. The descrption energy for CO on Pd(111) is 32±2 kcal/mole with a pre-exponential factor of $10^{14.4}s^{-1}$, and is probably similar for platinum.

Oxygen adsorbs dissociatively on platinum surfaces with a heat of adsorption of between 70 and 45 kcal/mole depending on the coverage (see section 1.2.2.3 below). The oxidation reaction occurs between adsorbed oxygen and butene by a Langmuir-Hinshelwood mechanism at temperatures above 100°C (Bonzel and Ku, 1972). As the temperature is raised oscillations of the CO_2 ouput from the reactor have been observed. Oscillations typically exist above temperatures between about 150°C and have been seen as high as 500°C (figure 1.1), depending on the CO and O_2 pressures (Yeates, Turner, Maple and Somorjai, 1985, figure 1.1).

The current literature for the observation and modelling of oscillation reactions has been reviewed by Razon and Schmitz (1986). A simple Langmuir-Hinshelwood mechanism for the oxidation reaction is capable of explaining reactor multiplicity, but is not of sufficient complexity to explain isothermal oscillations. If complexity is added to the simple model then oscillations may result (Sheintuck 1985). Amongst the "complexities" that have been proposed, besides the formation of a platinum oxide, include making the adsorption of the reactants coverage dependent, non-isothermality of the catalytic surface (Razon and Schmidz, 1986), the formation of islands of non-reactive CO on the Pt surface (Cant and Angove, 1986; Haarland and Williams, 1982), adsorption of inerts or co-reacting species such as 1-butene (Mukesh, et al., 1982), adsorption of CO causing reversible changes in the surface structure of the Pt (Lynch, Emig and Wanke, 1986) and Kaul and Wolf (1984) proposed that the hot CO_2 product acts as a sink to remove excess heat from the platinum surface to the

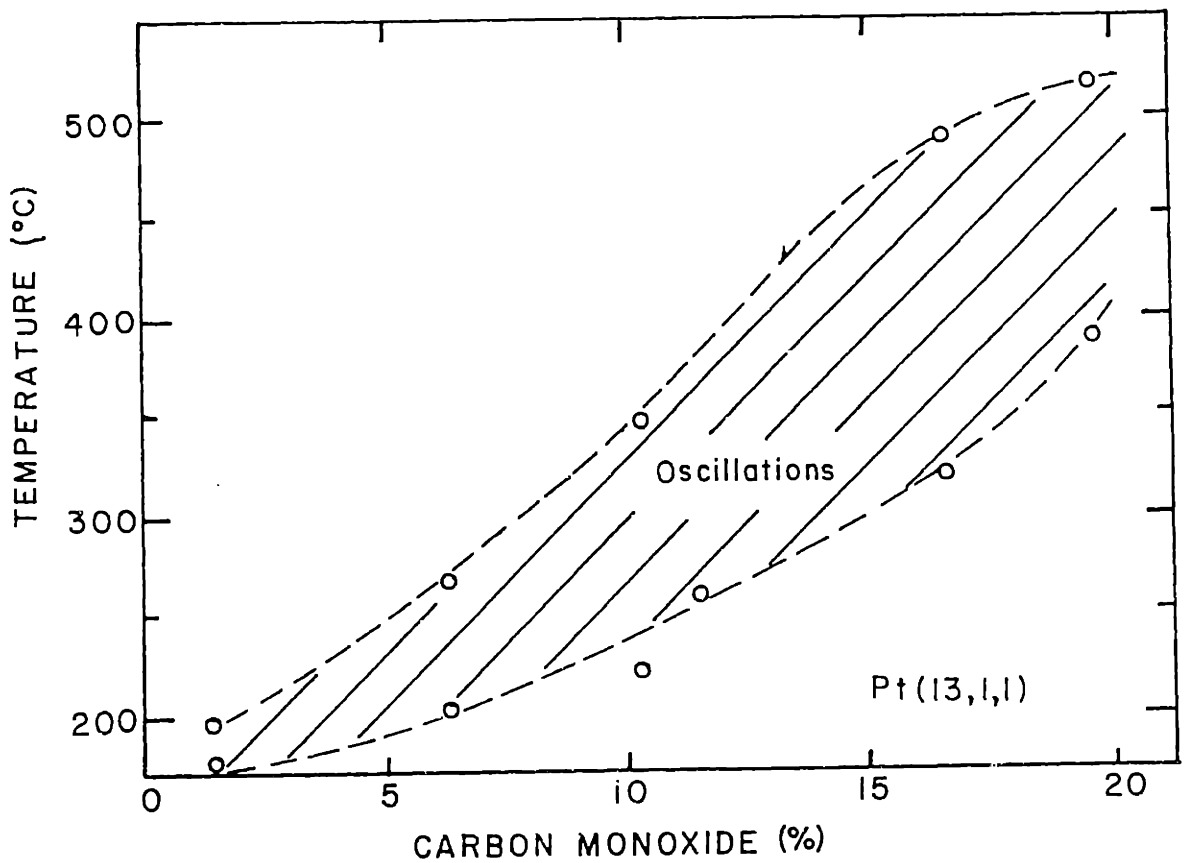

Figure 1.1: Temperature versus CO concentration showing where oscillations are obtained on Pt(13,1,1) contaminated with Si (from Yeates et al., 1985)

diluent gas. When any of the above added complexities is added to the model, oscillations may be predicted.

To date there is little to judge between the different proposals, although they may not be exclusive of each other and some may apply under specific conditions, but not others. In particular, it seems that a slow decrease in the rate of oxidation that is observed under reducing conditions at temperatures < 540 K, may be due to the formation of CO islands which are unreactive and therefore decrease the surface area available for reaction and the overall reaction rate (White and Golchet, 1979). Large concentrations of adsorbed CO were observed by IR which coincided with low catalytic activities (Cant and Angove, 1986 and Behm, Thiel, Norton and Binder, 1984). Surface reconstructions probably do also occur, but may not be sufficiently significant to acconut for all the oscillations observed. The possiblity of a surface platinum oxide existing on the surface has, itself, been a topic of debate in the surface science literature.

1.2.2.3 Adsorption of Oxygen on Platinum

There are four forms of oxygen adsobed on platinum that have been reported in the literature: molecular O_2, dissociatively adsorbed chemisorbed O, platinum oxide, PtO_2, and "ultrastable" platinum oxide.

At temperatures < 100 K oxygen adsorbs molecularily in islands (Steininger, Lehwald and Ibach, 1982) with an activation energy for adsorption of about 3.8 kcal/mole (Gland, 1980). Molecular oxygen desorbs by a first order process with an activation energy of 8 kcal/mole, from a clean Pt surface, and about 3.8 kcal/mole from a surface pre-saturated with O atoms (Gland, 1980). At temperatures above about 160 K, adsorbed molecular oxygen dissociates, or if adsorbed above this temperature, it adsorbes

dissociatively.

The heat of adsorption of oxygen on platinum has been determined by several authors: on Pt foils, Brennan, Hayward and Trapnell (1960) measured it calorimetrically as 62-65 kcal/mole, and decreased with increasing coverage. More recent measurements using temperature programed desorption combined with Auger spectroscopy report an enthalpy of adsorption of oxygen on Pt(321) to be 70 to 47 kcal/mole also decreasing with increasing coverage (McClellan, McFeely and Gland, 1983). They observed two desorption peaks, a low temperature 2nd order peak and a 1st order peak at higher temperatures. The 1st order peak occurs only at higher coverages and is not observed on Pt(111) which is able to adsorb only 1/3rd as much oxygen. A similar 1st order desorption peak, at high coverages, was observed on Pt(110) by Wilf and Dawson (1977), but in their case, the activation energy for desorption was only 32 kcal/mole.

Over the Pt(s)-[12(111)x(111)] surface, Gland and Korchak (1978) measured ΔH_{des}=39±3 kcal/mole over terrace sites and 45±3 kcal/mole for desorption from the stepped sites. And finally, over polycrystalline Pt foils, Kislyuk and Bakuleva (1982) observed two 2nd order peaks which they assumed came from desorption from islets of O, or from individual atoms, with ΔH=49±4 kcal/mole.

Weinberg and Merrill (1973) calculated the dissociative heats of chemisorption of 58-68 kcal/mole using "crystal field surface orbital-bon energy bond order" calculations, which agree reasonably well with experimental results.

1.2.2.4 Oxide Formation on Pt

When adsorbed at temperatures above about 700 K, platinum oxide may form (Lewis and Gomer, 1968), and when adsorbed above about 1000 K,

extremely stable forms of platinum oxide have been reported that were stable to 1000 K under ultra high vacuum conditions (Gland, Sexton and Fischer, 1980; Matsushima, Almy and White, 1977). Bonzel, Franken and Pirug (1981), however, have challenged much of the published data, claiming that the oxide was probably due to impurities such as Si and Ca that could segregrate to the surface and oxidize. They measured the concentration of Si on the surface prior to oxidation, and found that it correlated well with the concentration of oxygen on the surface after oxidation.

Legare, Hilaire and Maire (1984) studied oxygen interactions with polycrystalline Pt and a Pt-Si (3 atm % Si) alloy, by XPS, and could find no platinum oxide in the pure platinum sample. In the Pt-Si alloy, Si surface segregated when the sample was pretreated in air at 1000 K, leading to SiO_2 islands on the surface, with an oxygen binding energy above about 532 eV. The presence of SiO_2 may also cause the Pt to adsorb oxygen in a "sub-surface" manner similar to that reported by Niehaus and Comsa (1980). After oxidation, they were able to observe the presence of oxygen by Auger electron spectroscopy, but not by low energy ion scattering, which is sensitive to only the topmost surface layer.

In a later by study by Hilaire et al. (1984), which contrasts somewhat to their results mentioned above, they found that while pure Pt could not be oxidized, in alloys of platinum and palladium, the platinum could be oxidized, provided the bulk concentration of palladium was greater than a threshold value of more than 3%. They estimated that the surface concentration of palladium, or any impurity, had to be greater than 13 to 20% for oxidation of the platinum to occur.

Yeates, Turner, Gellman and Somorjai (1985) examined platinum catalysts that had exhibited oscillations when oxidizing CO and also observed the presence of silicon on the platinum surface. In this case,

however, they claimed that the Si was not the cause of the surface oxygen, but acted as a catalyst for the conversion of platinum to platinum oxide.

The question of platinum oxide is therefore somewhat muddled by the presence or absence of impurities on the surface and their effects. Platinum oxide is thermodynamically stable at atmospheric pressure up to about 600°C (Berry, 1978). Berry studied the resistance of Pt wires on exposure to oxygen in sealed enclosures, modelling the resistance in terms of a parallel conductors. He determined the heat of formation of platinum oxide to be about -42±3 kcal/mole O_2 with an entropy of formation of -49±2 cal/mole O_2 K (figure 1.2). His value agreed reasonably well with the value reported in Kubaschewski and Alcock, 1979 of ΔH^o_{298}=-40.3±2.5kcal/mole and ΔS=-61.15±cal/deg mole. These values also agree with those reported by Vayenas et al.(1981) of ΔH=-46 kcal/mole and ΔS=-45cal/mol 02 K. Vayenas deduced these values from the limit cycles of oscliiations observed during the oxidation of ethylene on platinum. This agreement with the thermodynamic measurements would appear to provide some independent proof for the oxide formation/decomposition route for oscillations.

In contrast to his earlier work, Bonzel (Peukert and Bonzel, 1984) was in fact able to prepare platinum oxide on clean platinum by thermal oxidation of Pt(111) at 900 K (627°C) and 0.1 MPa O_2. When cooled, and exposed to the UHV, this compound gave an XPS signal at 530.2 eV, which is identical to the values he reports for oxygen chemisorbed on platinum (530.2 eV) and bulk platinum oxide (530.3 eV). When they heated bulk PtO_2 in the UHV, this form of platinum oxide underwent a sharp transition from an O/Pt ratio of 2.0 to about 0.5 at 380±20 K. Decomposition at this temperature and pressure agrees with the thermodynamic data of Berry and Vayenas. The O/Pt ratio did not decrease to zero immediately above this

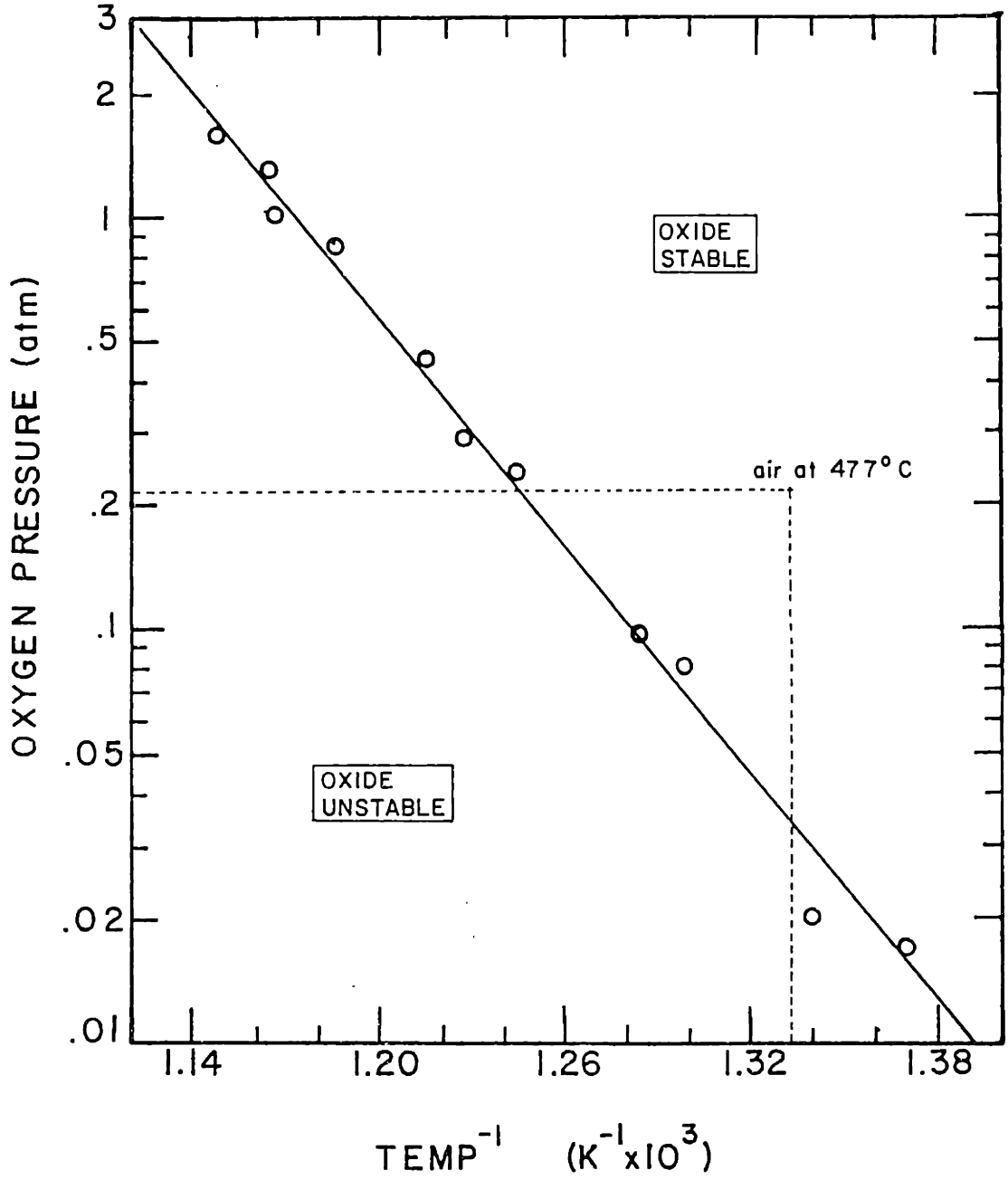

Figure 1.2: Van't Hoff plot of the dissociation pressure for surface platinum oxide versus 1/temperature (from Berry, 1978)

temperature (figure 1.3). The decomposition of bulk PtO_2 above this temperature followed very closely the O/Pt ratio of the oxide layer formed in the Pt surface, indicating that the oxide layer was, in fact, present and decomposing up to about 900 K in the UHV.

The picture is further complicated by consideration of the literature of platinum catalysts used for ammonia oxidation, because under the far higher temperature conditions, where the platinum oxide is unstable, it is invoked as the cause of etching and degradation of platinum-rhodium gauzes (Satterfield, 1982). However, under these conditions, although platinum oxide is not the major stable species on the surface, it does exist in thermodynamic equilibrium with platinum (at 850° C, the equilibrium constant is about 0.003). However, under these conditions, platinum oxide is volatile and this has the effect of enhancing the rate of sintering in the presence of oxygen versus inert or vacuum (Chen and Schmidt, 1978, McCabe, Pignet and Schmidt, 1974).

The oxidation of platinum to gaseous oxide:

$$Pt(s) + O_2(g) \rightleftharpoons PtO_2(g)$$

has a ΔG_f given by (Allcock and Hooper, 1960):

$$\Delta G = 39270\ (\pm 340) - T(0.93 \pm .21)$$

This value may be used to predict the rate of loss of platinum metal by assuming that the rate for the back reaction is determined strictly be the surface collision frequency of PtO_2 molecules striking the Pt surface (decomposition probability = 1; $PtO_2(s)$ is completely unstable). The rate of platinum loss may therefore be modelled by the rate of mass transfer of the gaseous platinum oxide through the boundary layer arround the Pt wire (Bartlett, 1967; Nowack, 1969).

In conclusion, platinum oxide is thermodynamically stable and should form on platinum surfaces up to about 590°C at 1 atm.. Above this

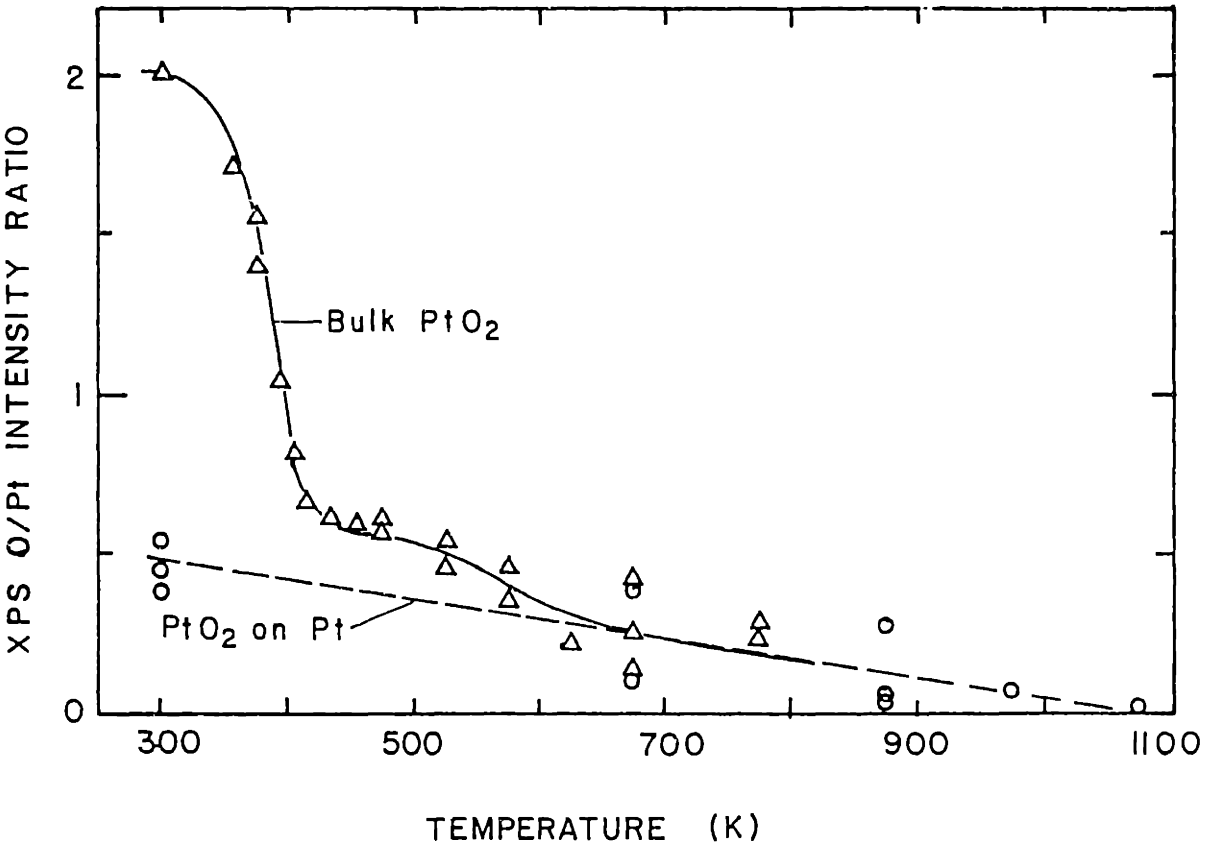

Figure 1.3: Thermal decomposition of bulk and surface PtO_2 versus temperature in UHV (from Peukert and Bonzel, 1984)

temperature, it will decompose and reform platinum and oxygen. At the same time, impurities present in the bulk of the platinum may undergo surface enrichment, and possible oxidation, which confuses the picture. However, whether the oxide forms as a characteristic of Pt, or as a consequence of impurities, oxygen/platinum surface ratios greater than the 0.25 limit observed for chemisorption (Norton, Davies and Jackman, 1982) can be readily obtained.

1.2.3 Solid State Ionics

Solid electrolytes (also known as superionic solids or fast ion conductors) are a group of solids possessing conductivities comparable to those of liquid electrolytes (Etsell and Flengas, 1970). Typically they are ionically bonded crystals which are electronic insulators. They conduct electricity either by ions hopping between point defects in a rigid lattice or by convection of a molten sublattice. The difference between these two is largely in terms of the concentration of the defects. In the former the concentration is about 10^{20} cm^{-3} whereas in the latter it is about 10^{22} cm^{-3}. The primary classification of solid electrolytes is in terms of the ionic species that is conducted (Chandra, 1981):

(i) Alkali metal ion conductors such as α- and β-alumina conduct Li^+, Na^+, K^+ or Rb^+,

(ii) Complexes of silver such as $RbAg_4I_5$ conduct Ag^+ ions,

(iii) Complexes of copper such as Cu_2Se conduct Cu^+ ions,and

(iv) Some transition metal oxides such as zirconia-yttria (ZrO_2/Y_2O_3) which conduct oxygen anions (O^{2-}).

In this thesis, the reactor on which the platinum catalyst is deposited is zirconia-yttria, an oxygen anion conductor. Zirconia-yttria is also are widely used industrially in sensors for O_2, in both gas streams such as automobile exhausts and combustion furnaces (Anderson and Graves, 1982) and in molten metals (Chandra, 1981). They have also been used in laboratory and pilot plant scale experiments as fuel cells using H_2 and CO (Archer, Elikan and Zahradadnik, 1965 and Sverdrup, Warde and Glasser, 1972) and ammonia (Vayenas and Farr, 1980) but have yet to be commercialized. Proposed uses include the decomposition of CO_2 to O_2 in space vehicles, as electrochemical capacitors and as solid state batteries

(Chandra,1981), and in the high temperature electrolysis of steam to hydrogen (Isaacs, Olmer, Schouler and Yang, 1981 and Spacil and Tedmon, 1969).

1.2.3.1 Conduction Mechanisms in Solid Electrolytes

Pure zirconia (ZrO_2) is a brittle ceramic material and undergoes the phase transition (Williams, 1969):

$$\text{monoclinic} \underset{1150^{\circ}C}{\overset{950^{\circ}C}{\rightleftharpoons}} \text{tetragonal}$$

It is stabilized into the cubic fluorite structure (face-centered cubic packing of the zirconium cations (Zr^{+}) with the O^{2-} anions filling all of the tetrahedral sites (Worrel, 1977) by the addition of di- or tri-valent cations such as Y^{3+}, Ca^{2+}, Sc^{3+} or La^{3+}. Figure 1.4 shows the conductivities of a number of these materials and the effect of temperature (Choudary, Maiti and Subbarao, 1980).

Intrinsic conduction in solid electrolytes is either by electrons or ions (Chandra,1981):

1. Thermal excitation of electrons from the valence band to the conduction band results in p- or n-type conduction (electrons or holes):

$$0 \rightleftharpoons e^{-} + h^{\cdot} \qquad K_1=np\ \exp(-E_g/kT) \qquad (4)$$

2. At high partial pressures of oxygen, p-type conduction results from:

$$1/2O_2(g) \rightleftharpoons O_i'' + 2h^{\cdot} \qquad K_3=[O_i'']p^2/P_{O2}^{1/2} \qquad (5)$$

where O_i'' are interstitial oxygen atoms, using Kroger-Vink notation (Worrel, 1977). This conductivity is proportional to $P_{O2}^{1/4}$.

3. At low parial presures of oxygen, n-type conduction results from:

$$O_o \rightleftharpoons 1/2O_2(g) + V_o^{\bullet\bullet} + 2e^- \qquad K_4=[V_o^{\bullet\bullet}]n^2P_{O2}^{1/2} \qquad (6)$$

where O_o is an oxide oxygen and $V_o^{\bullet\bullet}$ are oxygen vacancies in the lattice. This conductivity is proportional to $P_{O2}^{-1/4}$.

4. The movement of ions either interstitialy, or through vacancies arising from the intrinsic Frenkel defects results in ionic conduction:

$$O_o \rightleftharpoons V_o^{\bullet\bullet} + O_i'' \qquad K_2=[V_o^{\bullet\bullet}][O_i''] \qquad (7)$$

1.2.3.2 Effect of Dopant on Conductivity

When a cation of lower vacancy is substituted for the framework cation, for example Y^{3+} for Zr^{4+}, the number of oxygen anion vacancies increases and the number of interstitials decreases:

$$Y_2O_3 \longrightarrow 2Y + 3O_o + V_o^{\bullet\bullet} \qquad (8)$$

i.e. one additional vacancy results for each yttria molecule incorporated. This decreases the concentration of O_o'' by mechanism 4 above, increasing the number of holes by mechanism 2 above, and decreasing the concentration of electrons by equilibrium 3 above.

1.2.3.3 Ionic Transfer Coefficients

The ionic transfer coefficient is a measure of the efficiency of the solid electrolyte for ionic conduction, when compared electronic conduction. When the conductivity of an electrolyte is expressed as:

$$\sigma = \sigma_{ion} + \sigma_{electron} \qquad (9)$$

Then the ionic transfer coefficient is defined by:

$$t_{ion} = \sigma_{ion}/\sigma_{electron} \qquad (10)$$

The ionic transfer coefficient can then be determined experimentally using:

$$E_{meas} = t_{ion}E_{theor.} \qquad (11)$$

by measuring the cell voltage at different oxygen partial pressures and

comparing them to those expected from the Nernst equation (which is discussed in more detail in the next section):

$$E_{theor.} = RT/4F \ln(P_{O2}(inside)/0.21) \quad (12)$$

For an efficient solid electrolyte, the ionic transfer number must be > 0.99; as a general rule these materials have band gaps greater than 300/T eV (Chandra,1981). This is the case over the range of oxygen concentrations and temperatures of interest for zirconia-yttria and those materials shown in Figure 1.4.

1.2.3.4 Theory of Ionic Conductivity

The ionic conductivity can be expressed as (Harding, 1980):

$$\sigma = \sum_i n_i \mu_i (z_i e) \quad (13)$$

For an ideal lattice with independent, mobile ions moving in a completely random walk fashion, the mobility can be expressed as:

$$\mu_i^{(\lambda)} = Z_i e/2kT \quad C_i \sum_\alpha G'_\alpha \chi_\alpha^2 \quad (14)$$

where C_i= mole fraction of defects responsible for conduction and G'_α =jump frequency for jumps of a type α having a projected displacement of χ_α along the λ axis. For a cubic lattice with one jump of one ion, the displacement is the inter-ionic distance r and the conduction equation reduces to:

$$\sigma = nc/6kT \ (ze)^2 \ G' \ r^2 \quad (15)$$

where c is the total concentration of defects. The jump frequency, G' can be determined by assuming a quasi-harmonic hopping model where ions spend most of their time in random vibrations around a lattice site and from time to time jump to a neighbouring site according to:

$$G' = \nu_{eff} \exp(-E_m/kT) \quad (16)$$

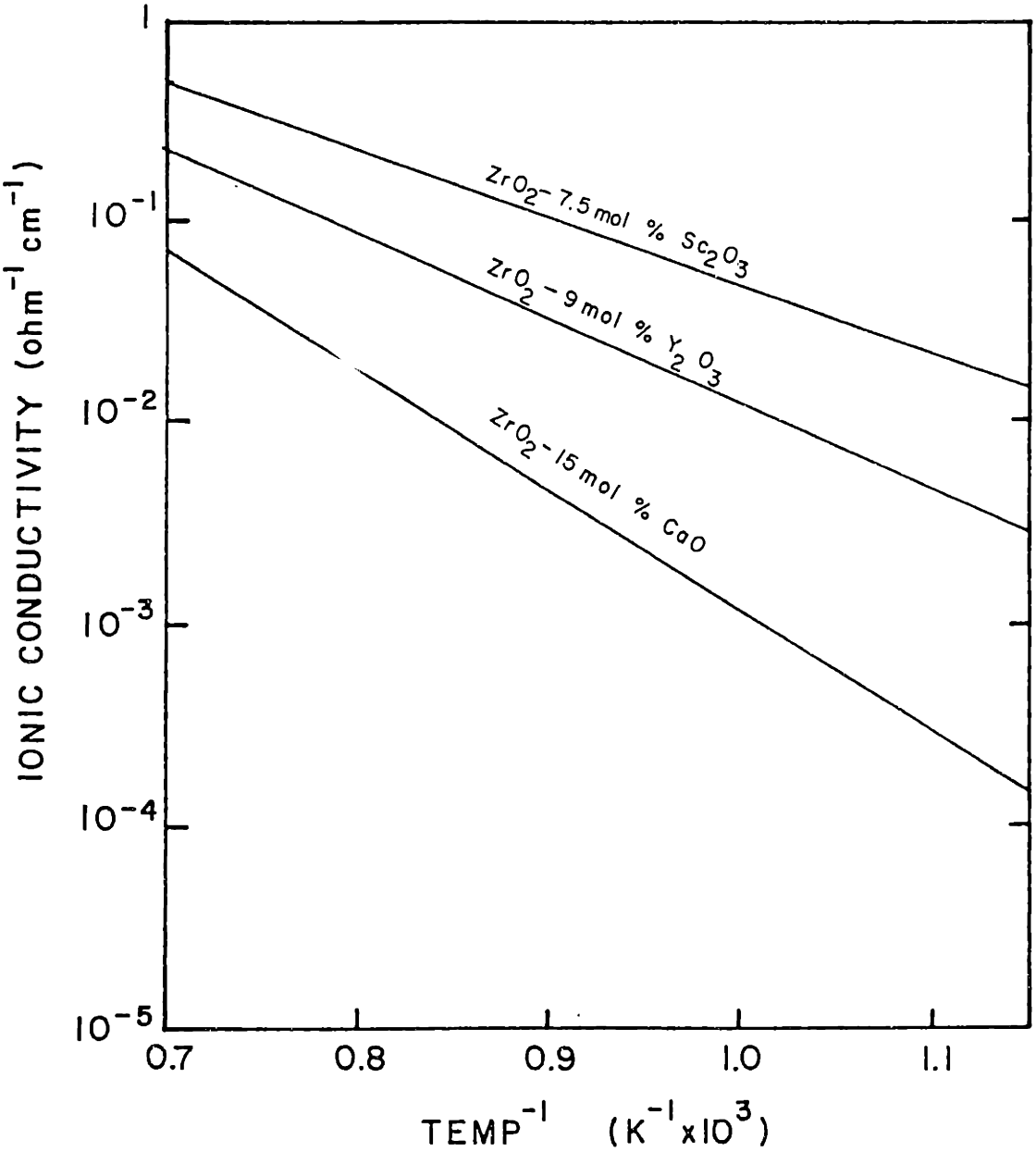

Figure 1.4: Conductivity versus 1/temperature for various oxide electrolytes (from Choudary, et al., 1980)

where E_m is the difference in potentials of the two sites and may be obtained theoretically from static lattice calculations. The frequency of hopping ν_{eff} is related to the entropy for the jumps, $\Delta S_m^{\ddagger}$. For certain cases this can be evaluated by considering the partition function for the quasi-harmonic approximation, leading to:

$$\nu_{eff} = \nu^* \exp(\Delta S_m^{\ddagger}) \tag{17}$$

where ν^* is the reaction coordinate and involves the Debye, or hopping, freqency, and the probability of an adjacent site being vacant.

In summary we can express the conductivity as (Kilner and Brook, 1982):

$$\sigma = A/T \exp(-E_m/kT) \tag{18}$$

where $A = 6nC\nu^* z^2 e^2 r^2/k \exp(\Delta S_m^{\ddagger})$ i.e. the conductivity is a function of the entropy for hopping and E_m, the energy for hopping. The energy for hopping is itself composed of the enthalpy for migration and the enthalpy of association, for the trivalent cation that substitutes into the zirconia-yttria framework.

Considering this theory we can rationalize the behavior of the conductivity, σ, versus concentration for added dopant (figure 1.5). As the intrinsic concentration increases we see a linear increase in the conductivity from increasing C in the pre-exponential factor. ΔH_m depends only on the lattice structure itself and so is independent of dopant concentration. ΔH_a however increases with the concentration due to the occurence of associations between the defects hence decreasing the conductivity at high concentrations of dopant.

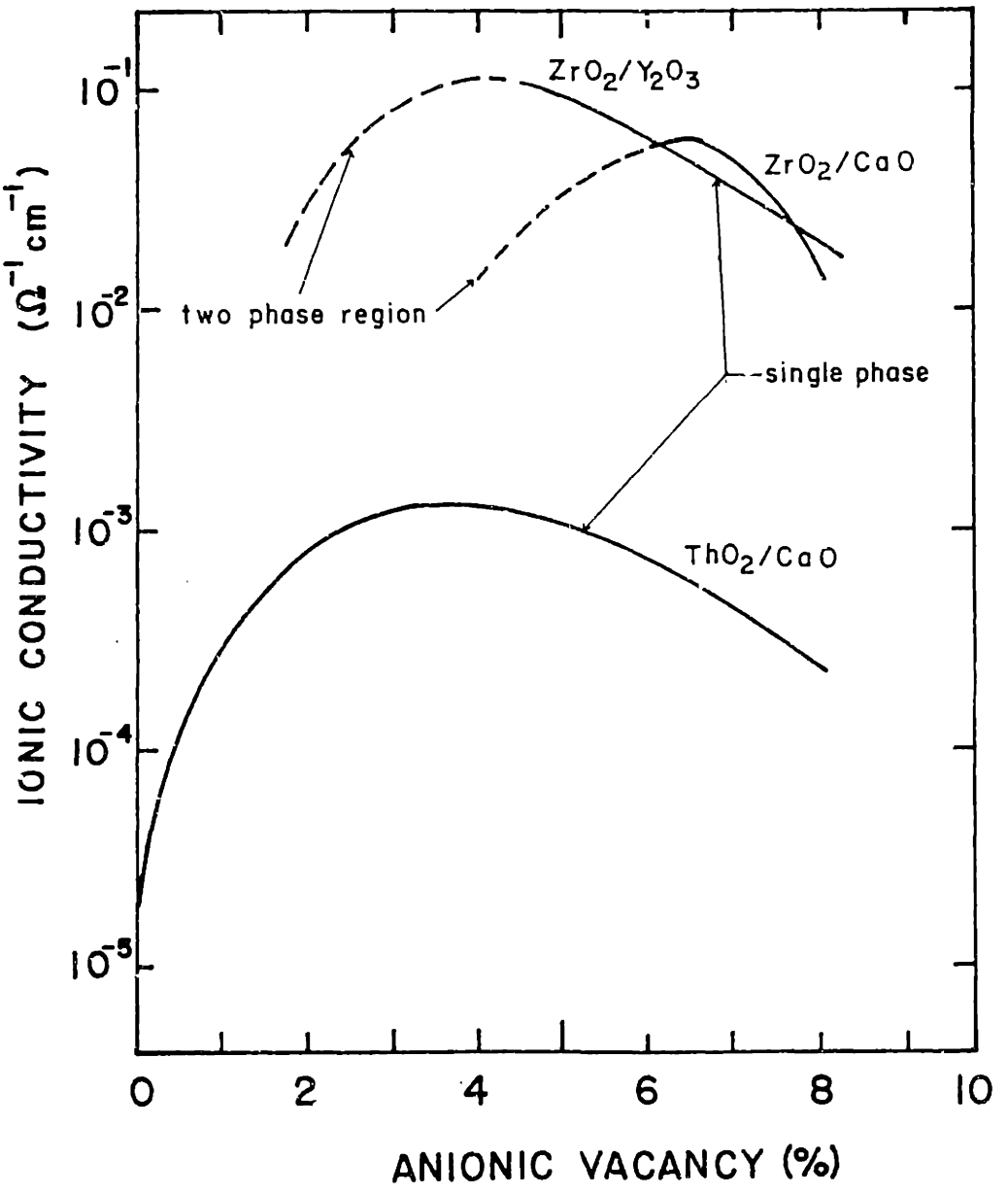

Figure 1.5: Ionic conductivity versus anionic vacancy for various oxide electroytes (from Choudary at al., 1980)

1.2.4 Thermodynamics Electrochemical Cells

1.2.4.1 Nernst Equation

For cells that are at equilibrium, the voltage across the electrochemical cell is a fundamental value and derivable from classical thermodynamics.

The electrochemical potential for an ionic species, j, is μ_j and is given by (Hope 1971):

$$\mu_j = \mu_j^o + RT \ln a_j + z_j F \phi + PV_j \qquad (19)$$

where μ_j^o is the chemical potential in a standard state, R the gas constant, T the temperature in K, a_j the activity of the ion species j, z_j the valency (with sign), F the Faraday constant, ϕ the electric potential, P the pressure and V the partial molar volume. For an electrochemical cell with constant pressure on both sides of the electrolyte, the PV_j term can be ignored. The classical chemical potential is given by the first two terms in equation (19).

The force X_j acting on the ions is proportional to the negative of the gradient of μ_j:

$$\begin{aligned} X_j &= -\text{grad } \mu_j \\ &= - d(\mu_j^o)/dx - RT\ d(\ln a_j)/dx - z_j F\ d\phi/dx \end{aligned} \qquad (20)$$

where x is the distance through the cell from the bulk phase on one side to that on the other. The velocity of ions subjected to this force is the mobility multiplied by the force, i.e. $v_j X_j$, and the flux ϕ_j in the x-direction is the velocity times the concentration:

$$\begin{aligned} \phi_j &= (v_j X_j) c_j \\ &= -v_j c_j \{ d(\mu_j^o)/dx + RT\ d(\ln a_j)/dx + z_j F\ d\phi/dx \} \end{aligned} \qquad (21)$$

For specific cases this equation can be integrated as a function of x. However for the case of equilibrium, the flux is zero, therefore:

$$z_j F\ d\phi/dx = -\{ d(\mu_j^o)/dx + RT\ d(\ln a_j)/dx \} \qquad (22)$$

or

$$\int d\phi = - \int d(\mu_j^o) - RT/z_jF \int d(\ln a_j) \quad (23)$$

When this equation is integrated from the outside, o, to the inside, i, of the cell, and considering that:

$$z_jFE_o = \mu_j^o(o) - \mu_j^o(i) \quad (24)$$

then:

$$E_{rev} = \phi_o - \phi_i = E_o + \frac{RT}{z_jF} \ln\left(\frac{a_i}{a_o}\right) \quad (25)$$

Equation (5) is the general description for any electrochemical cell in equilibrium, and is known as the Nernst Equation.

1.2.4.2 Application of the Nernst Equation for oxygen measurement

For the case of a zirconia-yttria electrochemical cell with both electrode surface exposed to different partial pressures of oxygen, the equilibria involved are:

electrode surfaces	$O_2(g) + 2$ sites	$\rightleftharpoons$	$2O(a)$
electrode/electrolyte interface	$2\{O(a) + 2e^-$	$\rightleftharpoons$	$O^{2-}\}$
through electrolyte	$2\{O^{2-}$(inside)	$\rightleftharpoons$	O^{2-}(outside)$\}$
overall	O_2(inside)	$\rightleftharpoons$	O_2(outside)

There is no chemical change in this "reaction" and, therefore the standard cell voltage, E_o, is zero. When these values are inserted into equation (25) and since the valence of the oxygen ions is 2, the voltage is given by:

$$E_{rev} = RT/2F \ln (a_{O,i}/a_{O,o}) \quad (26)$$

if equilibrium exists between the gas phases and the surface, and air is used as the reference gas on the outside:

$$E_{rev} = \frac{RT}{4F} \ln \left(\frac{P_{O2,inside}}{0.21}\right) \quad (27)$$

Thus it is possible to use a zirconia-yttria electrochemical cell as an oxygen gauge, simply by measuring the cell voltage.

1.2.5 Kinetics of Electrochemical Cells - the Butler-Volmer Equation

As described, the cell voltage is given by the difference in the potential between the two electrodes of an electrochemical cell. When the external circuit of a cell is closed and current flows, following sequence of steps occurs (see figure 1.6).

1. Diffusion of O_2 from the gas phase to the surface of the electrode and in the pores.
2. Adsorption on the electrode.
3. Diffusion along the surface of the electrode, through the bulk or the grain boundaries of the electrode to the intersections between the gas phase, the electrode and the electrolyte (the "three phase boundaries") where the electrochemical reactions occur.
4. Dissociation of molecular O_2 to atomic O (this may occur during adsorption).
5. Reaction with vacancies in the electrolyte:

$$O(a) + V_O^{\bullet\bullet} + 2e' \rightleftharpoons O_O^{2-} \qquad (28)$$

6. Transfer of the anions through the electrolyte.
7. Either the reverse of the above sequence on the inner half of the cell producing O(ads) species which may desorb as O_2 or direct interaction between O_O^{2-} and adsorbed reactants yielding different products depending on the nature of the catalyst.

When current flows, each of the steps contributes to the decrease in potential of each electrode, or an "overpotential" (or "overvoltage"), specifically:

(i) Gas film overpotential - from the resistance to transfer of reactants

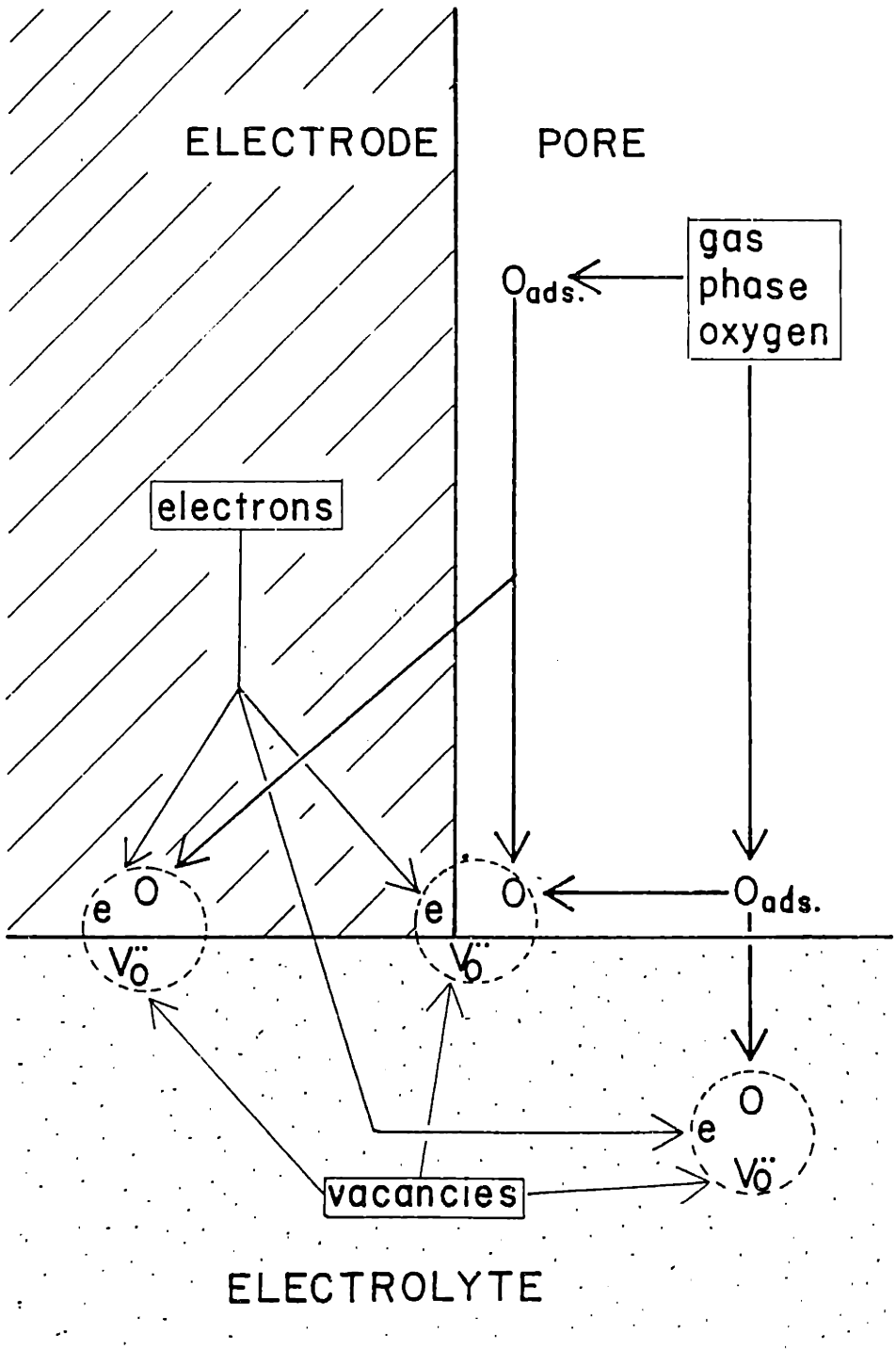

Figure 1.6: Structure of the three phase boundary (after Pizzini, 1973)

from the bulk to the exterior surface of the electrode; the overpotential depends on the size of the resistance and the current (or flux) through the cell.

(ii) Pore diffusion overpotential - from the resistance of the reactants to diffusion through the pores of the electrode to the electrode surface, and vice versa for products.

(iii) Surface adsorption overpotential - from the activation required to adsorb reactants on the electrode surface.

(iv) Surface diffusion overpotential - from diffusion of the adsorbed reactants on the surface of the electrode to the electrode/electrolyte interface.

(v) Ionization or activation overpotential - from conversion of adsorbed reactants into ionic species that can migrate through the electrolyte.

(vi) Electrical resistance overpotential - from the product of the current with the resistance of the electrolyte. The resistance arises because migration of ions through the electrolyte is an activated process (see equation (18)).

The first two and fourth terms are mass transfer mechanisms and may be conveniently be grouped into a "concentration overpotential" term, η_c. The magnitude of η_c is linearly dependent on the concentrations of reactants and the flux, or current, through the cell. The third and fifth terms may be grouped into an "activation overpotential" term, η_a (Liebhafsky and Cairns, 1969). The cell voltage can then be expressed as (see figure 1.7):

$$V_{cell} = E_{rev} - (\eta_c + \eta_a)_{anode} - (\eta_c + \eta_a)_{cathode} - iR_{electrolyte} \quad (29)$$

At large current densities, in dilute concentrations and/or in fluids with low diffusion coefficients such as liquids, it is possible for the predominantly mass transfer controlled η_c to predominate. However, in

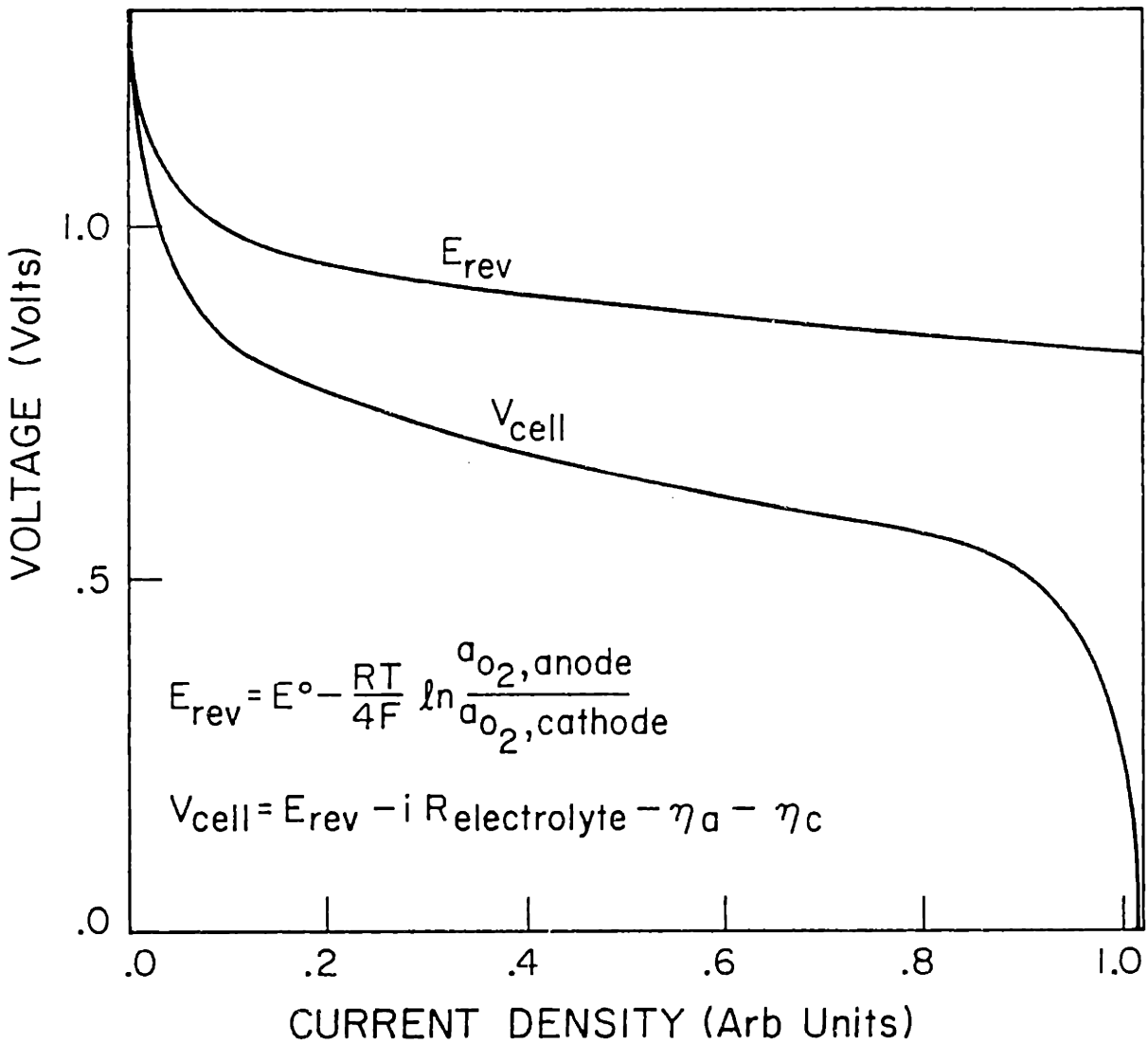

Figure 1.7: Cell voltage versus current for an idealized fuel cell

high temperature electrochemical cells with gases as the fluid this is unlikely to arise (Steele, 1976). Therefore η_c can be neglected, and the cell voltage becomes:

$$V_{cell} = E_{rev} - \eta_a(anode) - \eta_c(cathode) - iR_{electrolyte} \quad (30)$$

The activation overpotentials, η_c and η_a, are themselves complex functions of a large number of variables, and can be expressed by the Butler-Volmer equation (which is derived in Appendix A):

$$i = i_o \exp(\alpha_a F\eta_a/RT) - \exp(-\alpha_c F\eta_c/RT) \quad (31)$$

where i_o is the exchange current density (mA/cm^2) and α_a and α_c are the anodic and cathodic "transfer coefficients".

The transfer coefficients are themselves related to the total number of electrons transfered in the electrochemical reaction, r, the number of times the rate determining electrochemical step occurs, ν, the total number of steps in the multistep transformation, n, and the number of steps assumed to be in equilibrium before the rate determining electrochemical step, g:

$$\alpha_a = n - g/\nu - r\beta \quad (32) \quad \text{and} \quad \alpha_c = g/\nu + r\beta \quad (33)$$

where is the "symmetry factor" which relates the position of the transition state to the thickness of the electron transfer region. It is frequently assumed to be 0.5 (see Appendix 6.1). Therefore by determining the transfer coefficients, it is possible to model the mechanism of the electrochemical step in terms of the number of electrons transfered, etc.

1.2.5.1 High Overpotential Approximation

When the overpotential, η, is large and negative, the reaction is far from equilibrium then:

the rate for the forward reaction >> rate for backward reaction

therefore:

$$i_f = i_o \exp\{-\alpha_f F\eta/RT\} \quad (34)$$

or

$$\ln i_f = \ln i_o - \alpha_f \eta/RT \quad (35)$$

and similarily, when the overpotential is large and positive:

$$\ln i_b = \ln i_o + \alpha_b F\eta/RT \quad (36)$$

Plots of log current versus overpotential are known as "Tafel plots". From the slope of the Tafel plots it is theoretically possible to determine the forward and backward (anodic and cathodic) transfer coefficients, α_f and α_b. When these are known it is possible to hypothesise a number of mechanisms for the electrochemical reaction in terms of the number of electrons transfered, the number of electrochemical steps, etc. (see equations (32) and (33). It is not possible to determine a priori the electrochemical sequence, however judicious examination of the physics of the process will eliminate a number of the mechanisms, hopefully leaving only a single possibilty.

An assumption built in to the Butler-Volmer equation (31) is that it is possible to separate the electrochemical reaction into independent electrochemical and chemical reactions. The pre-exponential, i_o, the exchange current density reflects the chemical reaction and the exponent reflects the effect of the overpotential. Reliable, and linear, Tafel plots require the pre-exponential exchange current density to be independent of the applied overpotential. If the electrochemically transferred ion does not diffuse from the three phase boundary sufficiently quickly, then a build-up of ions will occur, inhibiting the further transfer of ions and resulting in a "limiting current". Increasing the overpotential above the value at which the limiting current occurs will have no effect on the current whatsoever. In some cases, the poor

diffusion of ions from the three phase boundary can prevent linear Tafel plots ever being obtained.

1.2.5.2 Low Overpotential Approximation

When the net overpotential is low, the exponent term in the Butler-Volmer equation can be expanded using a Taylor series. When the second order and above terms are neglected equation (31) becomes:

$$i = i_o [1 + \alpha_b F\eta/RT - (1 - \alpha_f F\eta/RT)$$

$$= i_o F/RT \ (\alpha_b + \alpha_f) \eta \qquad (37)$$

Therefore if $(\alpha_b + \alpha_f)$ is known from the high field approximation, it is possible to determine the exchange current from the slope of a plot of current versus overpotential. This could also have been obtained from the intercept of the Tafel plot, but as described above, linear Tafel plots are not always obtained and the low field approximation requires less data and involves less error.

The exchange current can be readily determined at various temperatures, oxygen or reactant pressures, etc.

All the terms in equation (37) above are constants, therefore a plot of i versus η will be linear and pass through 0. It can therefore be alternatively represented as:

$$i = C_i \eta \qquad (38)$$

where $C_i = (i_o F(\alpha_a + \alpha_c)/RT)$ is the "interface conductance". It is possible therefore to determine the interface conductance of the cell, and its variation with temperature and oxygen pressure, without knowing the transfer coefficients or anything else of the mechanisms.

2 EXPERIMENTAL

2.1 FLOW SYSTEM AND ANALYTICAL METHODS

2.1.1 Flow System

The flow system is shown in figure 2.1. Premixed standards of each gas, prediluted in helium passed through two-stage stainless steel regulators and in-line disposable filters to remove trace imputities. The gases were independently metered through pre-calibrated rotameters, mixed and passed through a 6-port stainless steel valve to the reactor. From the reactor the products passed through the same 6-port valve to the gas chromatograph (GC) for analysis, then back via the 6-port valve to vent. Alternatively, by switching the 6-port valve, the reactants could have been directed via the GC to the reactor and the products vented directly. The use of a 6-port valve ensured that the reactants or products could be analysed without interuption of the flow of reactants to the reactor. Between the 6-port valve and the vent, the gases passed through a dispersive infra-red CO_2 analyser (for details of equipment model numbers see Appendix 6.2). The analyser was used for monitoring purposes; when a change was made in the reactor conditions, it was not assumed to be at the new steady state condition until the CO_2 output had stabilized.

The tubing and valves were leak tested to 85 psig.

2.1.2 Reactor and Recycle Pump

Two types of reactors were used in the studies presented here: a "closed-end" tube reactor and an "annular" reactor.

The closed-end tube reactor, shown in figure 2.2, was a 6" x 3/4" tube of zirconia stabilized with 8 mol% yttria. It was seated on a machined Macor ceramic base and capped by a water-cooled stainless steel

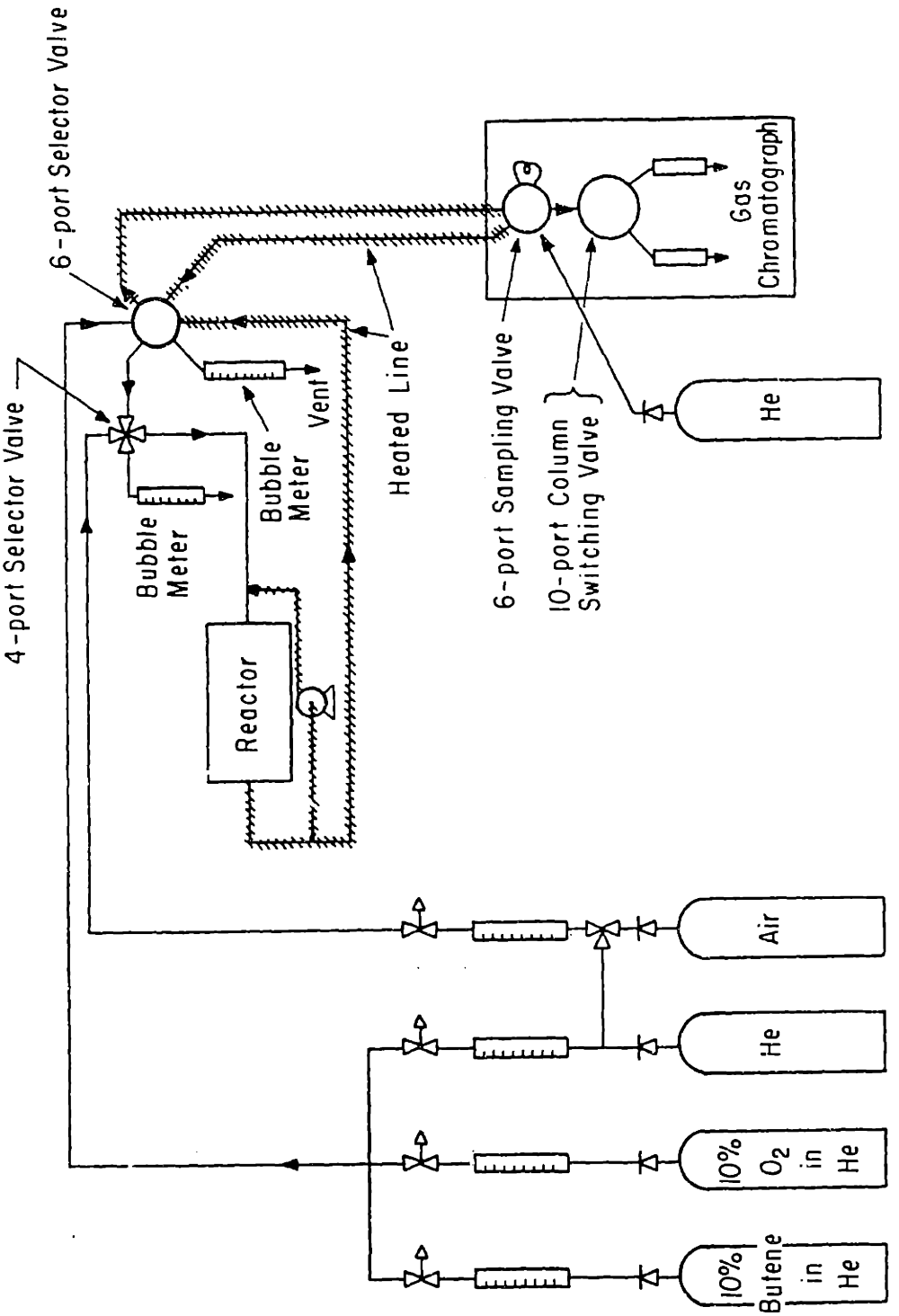

Figure 2.1: Schematic of apparatus

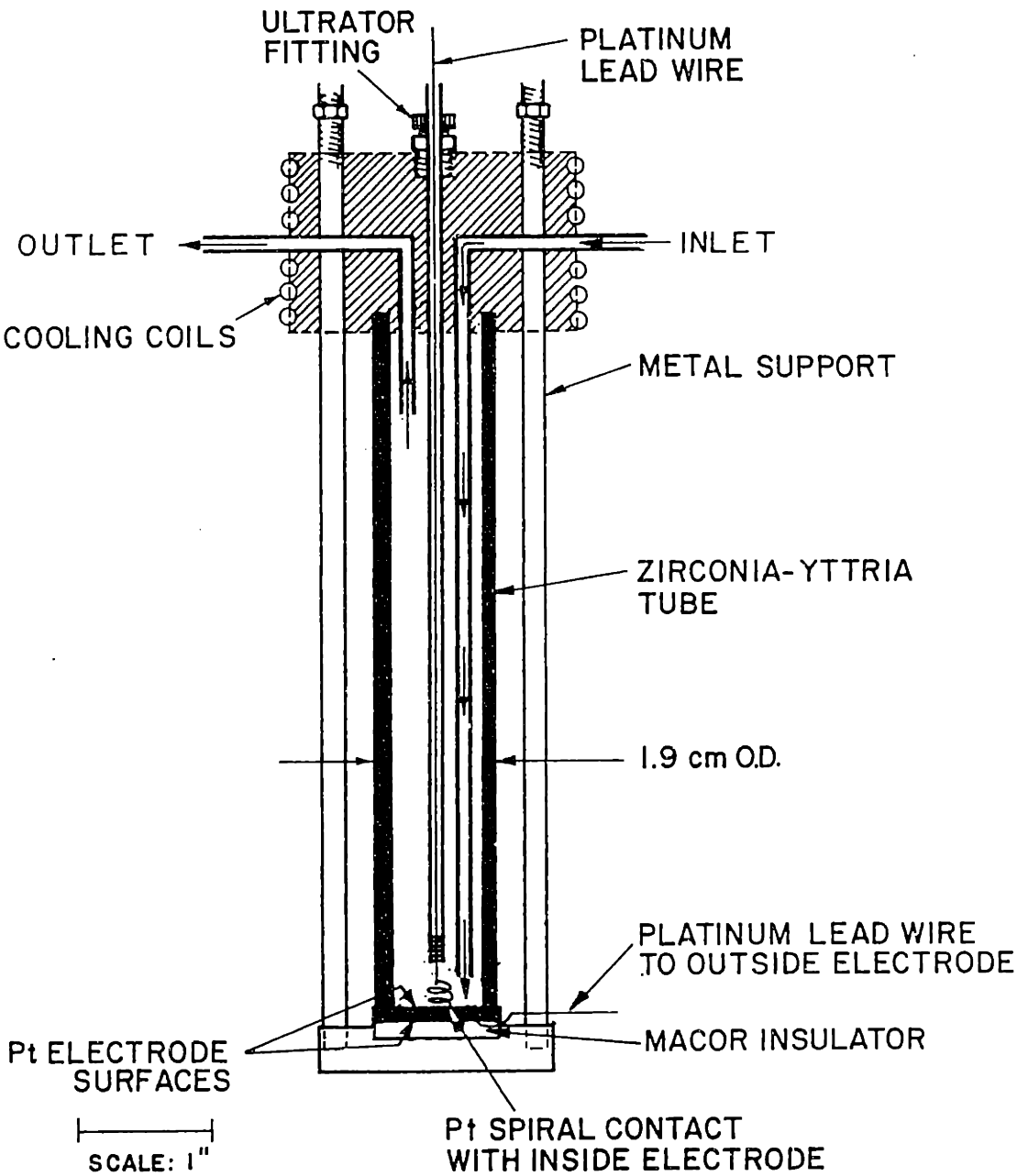

Figure 2.2: Schematic of closed-end tube reactor

head. The head was specially machined with a groove for a silicon rubber washer. The tube, base and head were clamped together forcing the tube to seal against the washer. Gases were fed through quartz feed tubes, since it had been found that stainless steel feed tubes could themselves become catalytic.

In the annular reactor (figure 2.3) gases passed between the outside of an 18" long X 3/4" O.D. tube of zirconia stabilized with 8 mol% yttria and the inner surface of a 1" O.D. quartz tube. The end fittings were fabricated from 3/4" and 1" Ultratorr fittings with appropriate cutting and rewelding, to create a 1" to 3/4" Ultratorr reducing union. The resulting fitting was bored to permit the 3/4" zirconia-yttria tube to pass all the way through. A 1/4" hole was placed in the side of both fittings and lengths of 1/4" stainless steel welded in place for feed, to and, from the annulus.

A metal bellows pump was used with both reactors to provide an external recycle to the reactor. It was connected to the reactors with short lengths of teflon tubing. Teflon tubing was used to eliminate vibrations from the pump disturbing the reactor. The flowrate through the recycle loop was controlled by throttling the flow with a valve and was monitored by a rotameter. A recycle ratio of at least 20 was used throughout, this causes both reactors to behave as CSTRs, while preventing excessive cooling of the reactor (see Appendix 6.3 for details). Since the reactors behaved as CSTRs, the rates of reaction are simply the algebraic difference between the concentrations of the reactants and products. All lines after the reactor were heated with heating tapes to about 50°C to prevent adsorption of water on the lines.

The reactor, pump and lines were additionally leak tested at the pump's maximum pressure of 10 psig. No decrease in the pressure was

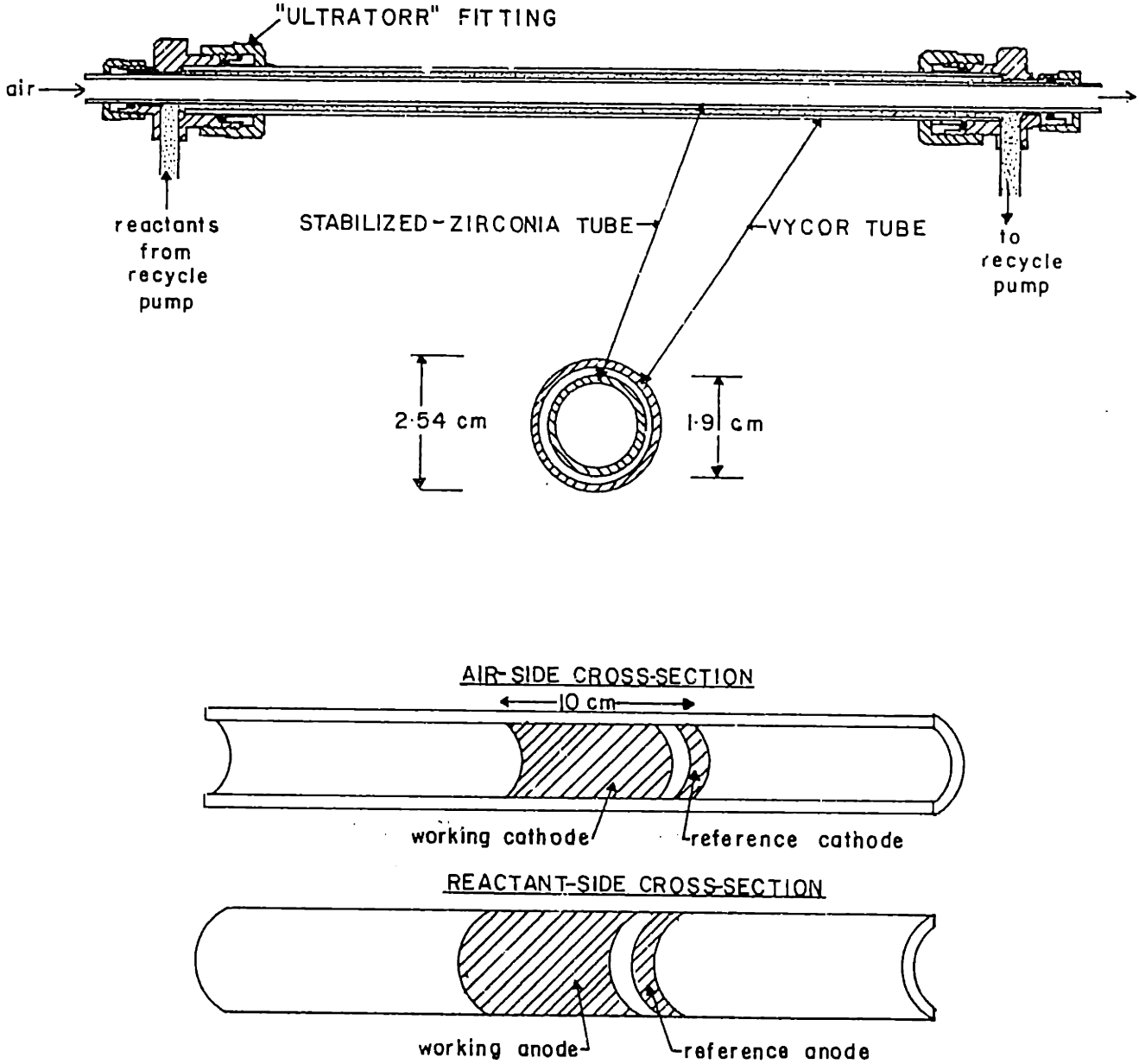

Figure 2.3: Schematic of annular reactor

observed in an hour. The gases used were diluted in helium and so the presence of N_2 in the products (as determined by gas chromatograph, see below) was used to indicate a leak into the reactor. All leaks were sealed prior to data acquisition and no N_2 was determined during experiment.

The flowrate of gases from the reactor was determined using a bubble meter on the exit of the CO_2 analyser. Total flowrates used were typically 120ml/min and the minimum and maximum possible ranges were 30 and 500ml/min respectively.

2.1.3 Preparation and Pretreatment of the Reactor

2.1.3.1 Closed-end tube reactor

The closed-end tube reactor was prepared by initially cleaning a 6" x 3/4" zirconia-yttria tube extensively with aqua regia, deionized water and solvents followed by pre-calcination, to 1000°C, of the empty tube to remove any residues. When cool, both the inner and outer surfaces of the tube were painted with a platinum ink (Engelhard #3788A). The tube was dried in air at 110°C and then fired to 850°C in air at a controlled heating rate of about 60°C/hour. The resistance of the films were measured using a multimeter. Two coats were sufficient to provide films with resistances of less than one ohm.

Contact with the outer electrode was obtained by seating the tube on a small sheet of platinum gauze to which a platinum lead wire had been spot welded. Contact to the inner electrode was by a length of 0.040" platinum wire encases in an 1/8" SiO_2 sheath. The wire was bent into a spiral at the base to provide a spring contact. The quartz sheath and Pt wire were sealed together at the top with silicone glue. The quartz sheath was sealed to the reactor head by a 1/8" Ultratorr fitting.

2.1.3.2 Annular reactor

An 18" x 3/4" zirconia-yttria tube was pre-treated in a similar manner to the closed-end tube. Both the inner and outer surfaces were painted with an unfluxed platinum ink (Engelhard Corp., U.S. part # A-4338, International part # SC6012) in specific paterns to produce an 8 cm long "working" electrode and a 0.5 cm long "reference" electrode (see figure 2.2). The total length of the electrodes was limited to about 10 cm, for the catalyst/electrodes to be isothermal in the tubular furnace used to heat the reactor. isothermality of the furnace (see Appendix 6.5).

The inner electrodes were prepared by using masks of single weight graph paper and by painting with an elongated, bent paintbrush. The surfaces were dried by placing the entire tube in an oven at about 110°C for at least an hour, prior to removal of the paper masks. The quality of the films was inspected using a small mirror and faults, where the ink had diffused under the paper masks, were removed with cotton tipped applicators dipped in ethyl acetate. When visually satisfactory electrodes had been obtained, the reactor was fired in a stream of air to 1000°C at a controlled rate of 1°C per minute using the temperature programer. The resistance of the electrode films was measured across, along and between the electrodes using a multimeter. In all cases the resistance between separate electrodes was infinite indicating no short circuits were present. Two coats were sufficient to reduce the resistance along the length of the electrodes to less than 3 ohms.

Prior to applying the external electrodes, about 3 feet of 0.010 inch platinum wire was wound arround each of the reference and working electrode areas in a spiral of about 1 cm between loops (for the working electrode). The areas to be covered were delineated with masking tape. The electrodes

were painted over the wire and zirconia-yttria and dried, the masking tape removed, and fired as above. This caused the electrode to fuse to the connecting Pt wire and provided stable contacts.

When satisfactory inner and outer electrodes had been prepared, they were further treated using the method suggested by Ehrhardt, Häfele, Lintz and Martins (1984) to remove any possible surface impurities, flux materials from the ink, etc.: Both surfaces were heated in vacuum to 700°C for 2 hours using a mechanical vacuum pump. After cooling, the reactor was treated in boiling 2N HNO_3 for 5 minutes, then washed with doubly distilled water. The zirconia-yttria tube with painted electrodes on both surfaces was then placed inside the 1" O.D. quartz tube and the Ultratorr end caps fitted so that the wires fused to the outer electrodes passed through the 1/4" stainless steel tube and then out one leg of a Swagelock union tee, via a septum. Reliable connections to the outer electrodes were thus achieved. The reactor was sealed and was found to be leak-tight at 6 psig, showing no discernable decrease in pressure within an hour.

Contact was made to the inner electrodes by wrapping futher lengths of 0.010 inch Pt wire around a 1/4" quartz rod. The rod was then placed inside the zirconia-yttria tube so that the Pt wire touched the inner electrode (which was always exposed to air). Separate rods were used for the working and reference electrodes. A few turns of high temperature (Glasscol) tape wrapped arround each rod at the exit of the zirconia-yttria tube served to elevate the ends slightly and so maintain reliable contacts to the electrodes.

Prior to use, unless otherwise noted, the reactor was heated in air to 727°C (1000 K), held there for two hours, and cooled to the operating temperature in air. The reactor was then flushed with helium for two to

four minutes and exposed to the reaction mixture, and the data taken at the appropriate partial pressures of oxygen and butene.

2.2 ANALYSIS

Analysis of all of the products was performed by a gas chromatograph (GC) equipped with a thermal conductivity detector, and a numerical integrator for area determination. Gas samples of 0.5 ml were taken from the line and injected into the GC using a gas sampling valve. The tubing leading to the valve was kept at 110°C as was the sample valve itself, which was placed in one of the injection ports of the GC. There were therefore very short lines between the valve and the GC columns, eliminating problems with dispersion of the sample in the lines. No condensation of water was found to occur. Futhermore, no cooling of the loop occurred irrespective of the gas flowrate, resulting in constant injection sizes.

CH_4, CO_2, C_2H_4, C_3H_6 and H_2O were determined using a 6ft x 1/8" stainless steel column of 80/100 mesh Poropak Q held isothermally at 110°C (method 3). A typical output is shown in figure 2.4, and the retention times are shown in table 2.1. Analysis of O_2, N_2, CO, butene and its isomers were performed by injection on to a 8ft x 1/8" O.D. stainless steel column of 0.19% Picric acid on 80/100 mesh Carbopack C in series with a 6ft x 1/8" column of 120/140 mesh Carbosieve S, temperature programed from 30°C to 110°C at 15°C per min (method 1). After 1.1 minutes, when light gases had eluted from the picric acid column on to the Carbosieve S column, the order of the columns was reversed using an 8-port valve. This caused the butenes to elute from the columns to the detector before O_2, N_2, CO and later CO_2. In some instances, when large amounts of water were formed, the

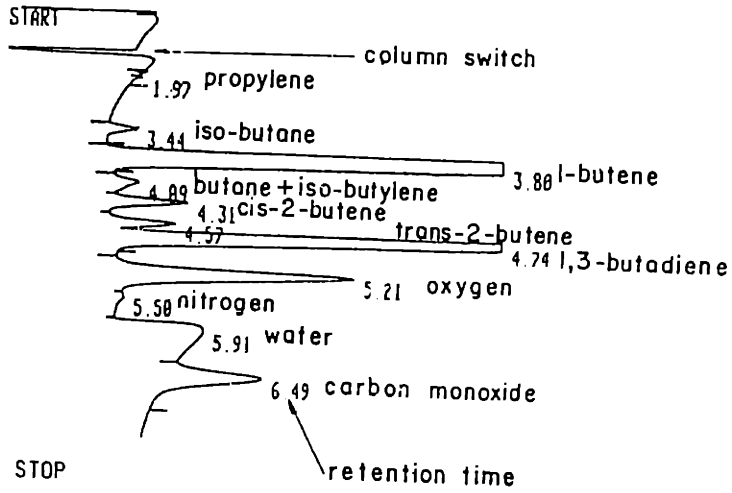

"METHOD 1"

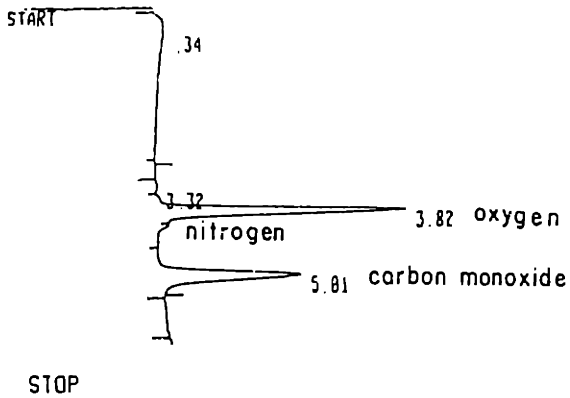

"METHOD 2"

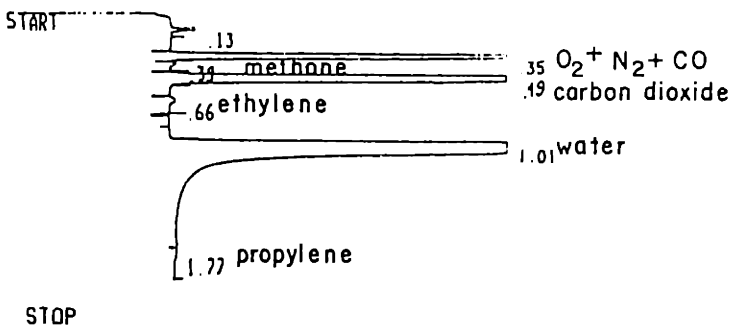

"METHOD 3"

Figure 2.4: Typical gas chromatographic spectra

water eluted simultaneously with CO. In this case the CO and light gases were re-determined by direct injection on to the Carbosieve S column in series with the picric acid column at 80°C and temperature programming at 15°C up to 110°C (method 2).

Components were identified by their retention times. The specific retention times and relative response factors for each component were measured by means of calibrated standards. The response factors were normalized to 1-butene being 81, the value published by Dietz (1967). Measured response factors were similar to those published by Dietz, see table 2.1.

Very small quantities of methane, ethylene and propylene were also observed (figure 2.4). These are the products of thermal cracking. All experiments were conducted under conditions where the rate of thermal cracking was at least an order of magnitude slower than the rates of the catalytic reactions (see Appendix C).

Table 2.1 Experimental retention times and response factors, and data from Dietz (1967).

Component	Symbol	Retention Time (min) Method Number (1)	(2)	(3)	Experimental Relative Response Factor	Dietz's Relative Response Factor
oxygen	O_2	5.29	3.03	0.35	38.76	40
nitrogen	N_2	5.54	3.28	-	46.60	42
carbon monoxide	CO	6.57	4.04	-	39.49	42
methane	CH_4	11.45	8.54	0.44	35.27	35.7
carbon dioxide	CO_2	19.20	15.67	0.58	52.48	48
ethylene	C_2H_4	28.49	-	0.87	-	48
ethane	C_2H_6	35.00	-	0.95	-	51.2
propylene	C_3H_8	2.06	-	1.81	76.90	64.5
iso-butane	i-C_4H10	3.53	-	-	-	82.0
1-butene	1-C_4H_8	3.88	-	5.90	81.00	81
butane	C_4H_{10}	4.16	-	-	-	85
iso-butylene	iso-C_4H_8	4.22	-	-	80.03	82
cis-2-butene	c-2-C_4H_8	4.39	-	-	77.41	87
trans-2-butene	t-2-C_4H_8	4.64	-	-	79.49	85
butadiene	C_4H_6	4.83	-	-	75.11	80
cis-2-pentene	2-C_5H_{10}	6.84	-	} 6.72	109.87	104
trans-2-pentene	2-C_5H_{10}	7.12	-			
water	H_2O	(14.61)	-	1.22	26.76	33

Absolute response factors were determined periodically throughout the experimental program by repetitive measurement of the 10% 1-butene in He used (Matheson calibrated standard). The absolute response factor of the detector increased slightly with time at first, then stabilized, as shown in table 2.2. The changes in the absolute response factor was taken into account in calcuating the molar flowrates.

Table 2.2 Absolute response factors for 1-butene determined throughout experimental program

date	moles per integrator area unit ($x10^{12}$)
4/4/83	4.138
6/2/83	4.728
7/17/83	4.932
9/22/83	5.307
11/29/83	5.704
2/16/84	5.790
11/26/84	5.411
5/8/85	5.823

The integrated areas, absolute and relative response factors, temperature, measured voltages, current and flowrates were entered into a Fortran 5 program (see Appendix 6.4) for conversion to molar flowrates and reaction rates. Mass balances for oxygen and carbon were also determined and were randomly distributed about 100%. Hydrogen could not be analysed with the current equipment, however calculated hydrogen balances were also distributed about 100% indicating that there was probably no free H_2

produced.

The rate of reaction of each component was determined by the difference in the flowrate of that component in the reactants and in the products. This calculation was performed because the reactants contained impurities that appeared as products, although, at concentrations too low to interfere with the reactions.(see table 2.3)

Table 2.3 Impurities in the 1-butene feed

Component	Concentration (%)
iso-butane	0.0404
1-butene	99.149
butane }	0.589
iso-butylene	
trans-2-butene	0.0563
butadiene	0.0892
oxygen	0.0352
nitrogen	0.0406
total	100.00

The rate of butene consumption was determined both by the difference between the reactants and the products and also from the rates for the individual components. When the consumption of butene was low, calculating the rate by difference between the reactants and the products involved taking the difference between two very large GC areas which resulted in details tending to be lost in the random noise of the sampling technique. Calculating the butene rate based on the individual rates assumes perfect mass balance closure. However, the mass balance closures were randomly

distributed and therefore using this method introduced no systematic error.

2.3 METHODS OF TAKING DATA

2.3.1 Platinum oxygen system

The annular reactor with platinum electrodes was used to determine the mechanism of incorporation of oxygen into the electrolyte (see equations (1.32) and (1.33) and Section 1.2.5), and also the effect of oxygen partial pressure and temperature on the exchange current density. Both the electrochemical reaction and the effects of temperature and oxygen partial pressure involve measurements of the cell overpotential related to the cell current. To determine the overpotential, it was first necessary to determine the resistance of the electrolyte (equation 1.30). Further, the exchange current densities could only be determined once the transfer coefficients were known (equation (1.37).

2.3.1.1 Electrolyte Resistance

The resistance of the electrolyte of the annular reactor was measured by imposing a current across the electrochemical cell, interrupting the current and recording the decay in the voltage signal with time. Experimentally, the current interrupt was performed by imposing a current in the form of a square wave at 1000 Hz. This was achieved by imposing a square voltage wave through a resistor in series with the cell (see figure 2.5. The instantaneous change in the current that the cell experiences was calculated by dividing the instantaneous voltage change, as measur on one channel of a two channel oscilloscope, by the size of the resistor (see figure 3.1. The decay of the voltage across the cell, between the

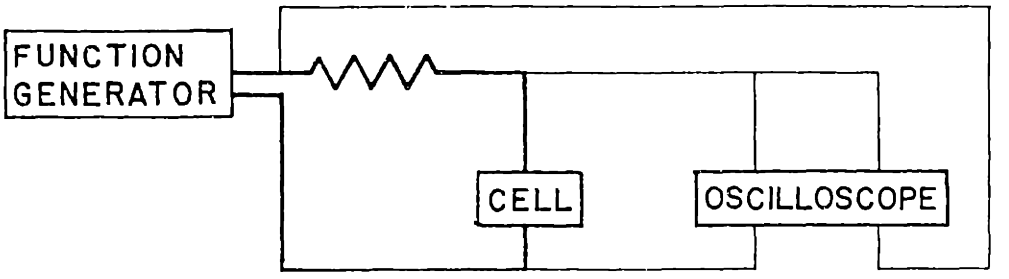

Figure 2.5: Wiring diagram for electrolyte resistance measurement

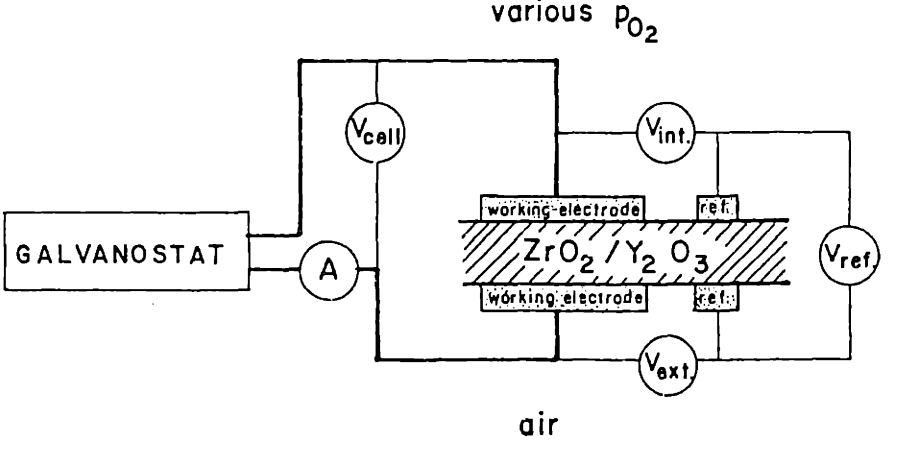

Figure 2.6: Wiring diagram for overvoltage measurements

working electrodes and between the working electrode and reference electrode on each side of the electrolyte, was measured on the other channel of the oscilloscope. The resistance of the electrolyte was measured for currents between 1 and 100 mA.

2.3.1.2 Overpotential Measurements

The reactor was pretreated by exposure to air overnight at 513°C. A current was applied between the inner and outer working electrodes by the galvanostat. The voltage was recorded on a chart recorder until a steady state value was obtained; this usually took several hours. When a steady voltage had been obtained, the voltage difference between the working electrodes was measured as well as the voltage differences between the working and reference electrodes on each side of the zirconia-yttria electrolyte (figure 2.6) The overpotentials were calculated by subtracting out the voltage drop due the electrolyte alone:

$$\eta_i = V_i - iR_{electrolyte,i} \qquad (1)$$

where i refers to either the inside or outside surface of the electroyte.

The current was varied between zero and 40mA, at which current the overvoltage on the air electrode was approaching 2.5 volts. The overvoltage was kept below this value to prevent reduction of the zirconia-yttria by:

$$ZrO_2 \longrightarrow Zr + O_2 \qquad (2)$$

which has an equilibrium constant of $10^{61.4}$ at 800 K (JANAF tables). This is equivalent to a voltage of 2.44 volts using the thermodynamic manipulations:

$$\Delta G = -nFE_o \quad \text{and} \quad \Delta G = -RT \ln K_p$$

therefore:

$$E = RT/4F \ln K_p \qquad (3)$$

2.3.1.3 Interface resistance

The resistance of the platinum-oxygen-zirconia yttria interface was measured at temperatures from 477-677°C (650-850 K) and at oxygen partial pressures from 10^{-6} to 1.0 atm O_2 in helium. The reactor/catalyst was pretreated by calcining in air to 1000°C, as described above. The reactor was then cooled to about 500°C and exposed to the various oxygen pressures and temperatures used, with no particular sequence of p_{O2} and temperature. Prediluted standards of oxygen in helium alone, or further diluted with helium, were passed over the platinum electrode in the annular region of the reactor. A small current was applied using a galvanostat (a constant current scource) to the working electrodes. The current was sufficiently small that the voltage drop did not exceed about 8 mV. The voltage difference between the working and reference electrodes on the same zirconia-yttria surface was measured (see figure 2.6). This could be divided by the current to measure the interface resistance, since for the small currents used, the voltage-current behavior follows the linear, low overpotential, limitation of the Butler-Volmer equation (1.31).

2.3.2 Oxygen desorption kinetics by surface titrations

The kinetics of desorption of oxygen which had been pre-adsorbed on the platinum electrodes were determined by titrating the oxygen adsorbed on the surface with CO or ethylene; the ethylene or CO reacts with the oxygen to form CO_2 which was measured by the in-line CO_2 analyser.

Two sets of surface titration data were taken. The first were performed only at 477°C over a platinum surface on the base of the closed-end tube reactor. The second set used the annular reactor in an attempt to determine the activation energy for desorption from the platinum surface. The methodology used for titrating the surface was identical for both data

sets and was as follows (the outputs are shown schematically in figure 2.7):

1. The reactor was pretreated in 2.17% ethylene in helium to reduce the platinum and remove any adsorbed oxygen.
2. The reactor was flushed with helium for two minutes to remove gas phase ethylene and to avoid forming an explosive mixture.
3. The platinum surface was oxidized in prepurified air for a specified number of minutes (t_{air}), between 1 and 100, at a flowrate of about 150 ml/min.
4. The ambient gas was then changed to helium at a high flowrate of about 360 ml/min, causing some of the adsorbed oxygen to desorb and be swept from the reactor.
5. After a specified number of minutes in helium (t_{He}, between 1 and 6) the gas was switched back to ethylene which reacted with oxygen, that had not desorbed from the platinum, to form CO_2.
6. The amount of CO_2 released was measured using the in-line dispersive infra-red CO_2 analyser, which had been pre-calibrated with a standard of 2.5% CO_2 in helium to give an output of 1000 mV. The output from the analyser was recorded versus time on a chart recorder.
7. The area under the CO_2 versus time peak was integrated numerically using Simpson's rule to yield an area count. The area count was converted into the number of moles of CO_2 released by using the ideal gas law and considering the gas flowrate, the chart speed and the response of the CO_2 analyser.

Occasionally, samples of the CO_2 peak were re-directed to the gas chromatograph by the in-line sampling valve to determine whether incomplete

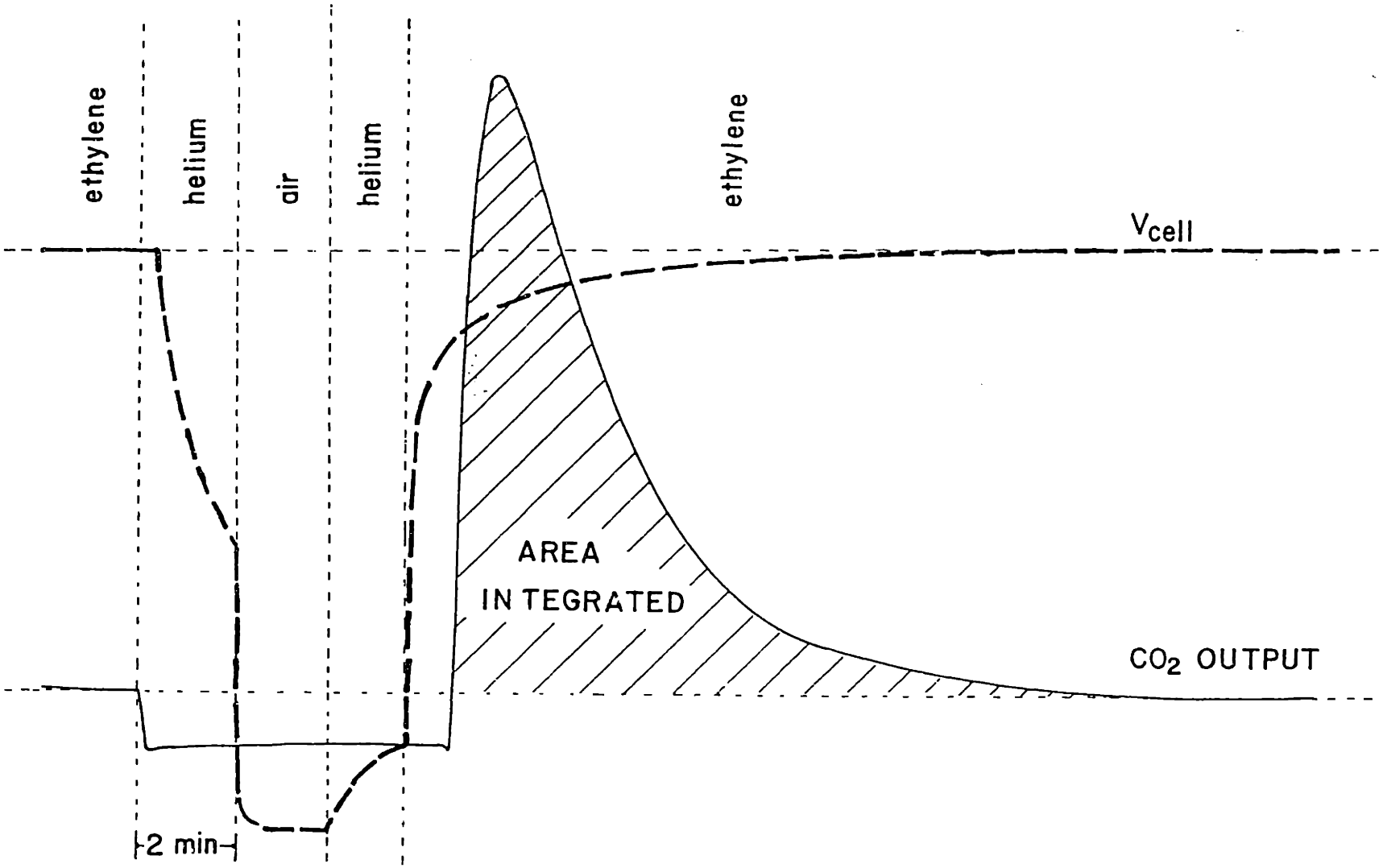

Figure 2.7: CO_2 output and cell voltage during surface oxygen titration

combustion to CO had occurred, or whether molecular oxygen had desorbed from the surface. The only components detected by the GC were CO_2 and ethylene. No CO or O_2 were observed.

The reactor volume was 30.2 ml (for the closed-end tube). At a flowrate of 360ml/min, the residence time was about 5 seconds. Allowing ten residence times to completely change the gas, the minimum time to completely remove all oxygen from the reactor was fifty seconds. The minimum time used to flush oxygen from the reactor, before attempting to measure the surface oxygen, was one minute.

The cell voltage was about 1 V when exposed to ethylene, 200 mV when exposed to helium at a flowrate of 360 ml/min (using the Nernst equation (1.31), this corresponds to an oxygen partial pressure of about 8.8×10^{-7} atm) and 0 V when exposed to air. The cell voltage was recorded and used to measure the oxidation and desorption times by noting the distinct changes that occurred in the voltage at the switch between each gas. The cell voltage gave a more precise measure of the oxidation and desorption times than the times when the valves were switched, since these ignored lag times due to tubing and reactor dead volumes.

A second set of titrations were performed using the annular reactor described in section 2.1.2 above, both with and without the recycle pump. With the recycle pump, the reactor behaives as a CSTR and therefore has similar characterisics to the closed-end tube with the external recycle pump. With no recycle pump, the output was not smoothed with time, as is the case with the recycle pump in place, and therefore the output gives an indication of the rate of reaction between adsorbed oxygen and ethylene, with time in ethylene.

The platinum electrodes for the annular reactor, as described above, were prepared from Engelhard paste #A-4338. The only difference between

paste #A-4338 and #A-3788, as was used in the closed-end tube, is the size of the platinum crystallites (Mahoney, 1986); in #A-4338 they are about 4-5 um, whereas in #A-3788 they are 1-3 um. Titrations were performed in an identical manner to that described above, for the closed-end reactor, except that CO was used to react with the adsorbed oxygen and reduce the Pt surface, rather than ethylene. Titrations were performed at 323, 377, 423, 477 and 523°C. At each temperature, however, only one oxidation time of four minutes in air was used.

2.3.3 Kinetics of butene oxidation to butadiene

Prior to use, the reactor was pre-treated by heating in air to 727°C (1000K), held there for two hours and then cooled to the reaction temperature, also in air. The reactor was then flushed with helium for two minutes to prevent an explosive mixture from being formed.

2.3.3.1 Effect of time on stream

The effect of the time on stream was investigated by measuring the changes in activity and selectivty that occurred when the reactor was exposed to a 2% butene and 0.08% oxygen in helium mixture. The gas composition that the surface was exposed to was kept constant by measuring the output from the reactor and adjusting the input to give the desired output. This was performed iteratively. The activity and selectivity were recorded for up to 700 hours.

At the end of this run, the reactor was cooled to room temperature in the reaction mixture. The gas was then switched to air and the reactor temperature programmed from room temperature to 730°C at about 67°C per hour. This was done to indicate the pre-treatment required to completely remove all carbon from the surface.

The effect of time on stream on the build-up of carbon on the surface was also investigated by measuring the carbon on the surface of the catalyst at the end of each period of taking data. The amount of carbon was determined by first flushing the reactor for two minutes with helium, then exposing the surface to a dilute mixture of oxygen in helium (about 0.5%). Carbon on the surface reacted with the oxygen forming CO_2. The amount of CO_2 formed by this reaction was determined by integration of the CO_2 versus time peak.

2.3.3.2 Effect of recycle ratio

The effect of the recycle ratio on the rates of reaction was investigated by simply measuring the output from the reactor as the recycle rate was increased from the minimum of about 250 ml/min to to pump's maximum rate of 6 l/min. This was performed under conditions where butadiene was the major product and also when CO_2 was the major product.

No effect of pump flowrate was observed above a flowrate of about 1.5 l/min. Below this flowrate, the rates all increased slightly (figure 2.8). Above about 1.5l/min, the reactor behaves as a CSTR and no spikes from the incoming feed, being richer than the average, are observed (see Appendix D). All subsequent data were taken at a recycle rump flowrate of 2.0 l/min, which is equivalent to a recycle ratio of about 17.

2.3.3.3 Effect of butene and oxygen partial pressures

Various data sets were taken between 466 and 544°C and at oxygen partial pressures from zero to about 2% and butene partial pressures from 0.5% to 40%. The required pressures were obtained by mixing and further dilution of pre-diluted standards of butene in helium and oxygen in helium. To cover this range the following standards of each gas were required:

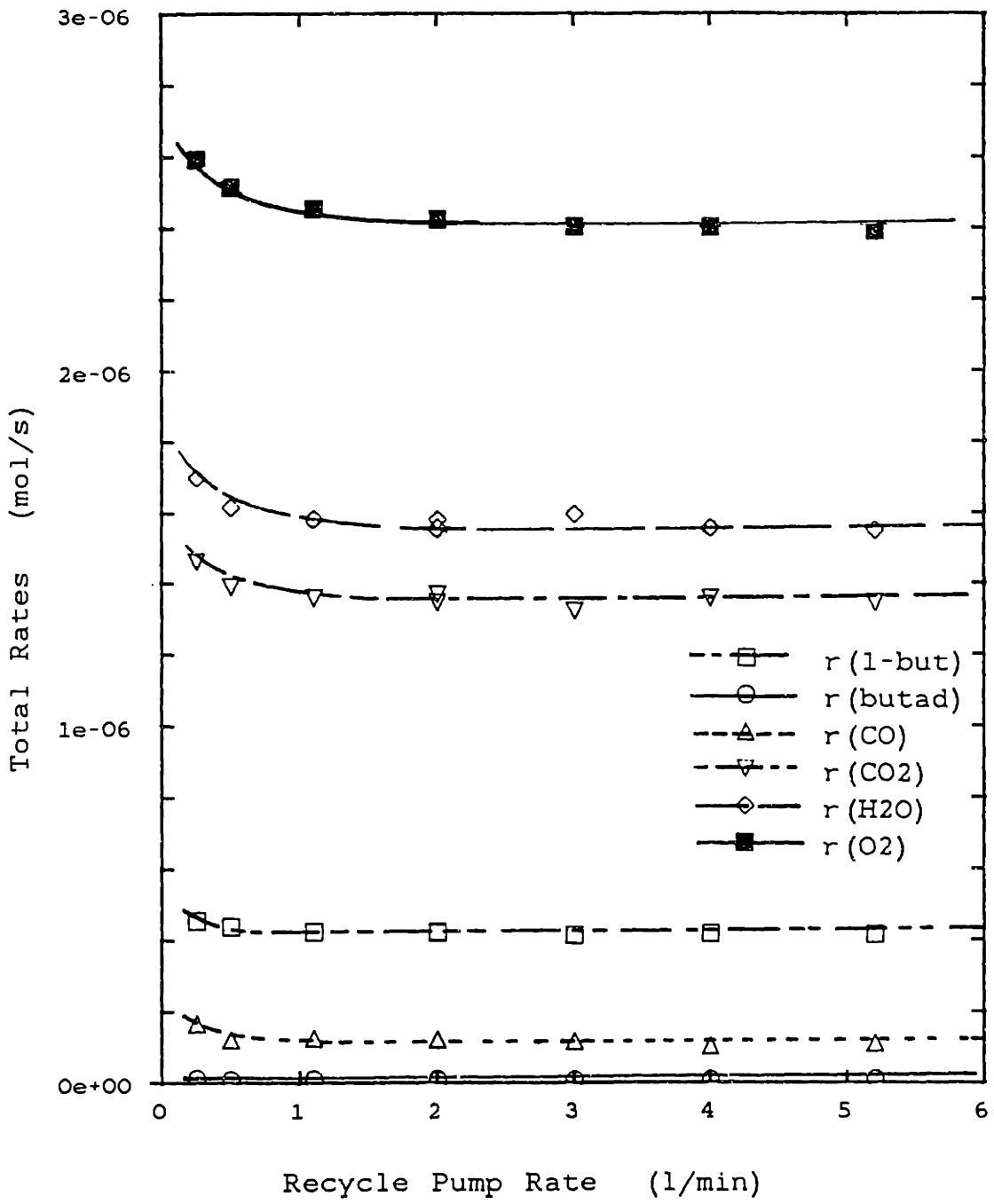

Figure 2.8: Effect of recycle pump rate on reaction rates (State 2 conditions)

0.5%, 2.0% and 10.0% oxygen in helium and 1.0%, 10.0% and 100% butene in helium. The apparatus was fitted with sufficient switching valves such that it was possible to switch between the various standards with no interuption of the flow.

The kinetic data were taken in two sets. The first (the "matrix" set) involved randomly varying the oxygen and butene partial pressures about a standard condition of 2.0% butene and 0.08% oxygen. The butene partial pressures used were 0.61%, 0.125%, 0.25%, 0.5%, 1.0%, 2.0% and 4.0%. At each butene partial pressure the reactor was exposed to 0.04%, 0.08%, 0.16% and 0.32% oxygen. At each condition, the exit from the reactor was measured, at the feed to the reactor changed to give the desired output. This was done iteratively until the required condition was obtained. These data were only taken at 513°C.

The second set of data were taken by cycling the butene feed to the reactor while keeping the exit oxygen concentration constant, and vice versa (see table 2.4). After pre-treatment by calcining in air to 727°C and cooling in air, the reactor was exposed to (say) 0.08% oxygen and the minimum concentration of butene that the gas chromatograph could detect (about 0.05%). While keeping the oxygen concentration constant, the butene concentration was then gradually increased up to 40% (the gas chromatograph's maximum detection for butene). The reactor was left at 40% butene overnight and then the butene was gradually decreased back to the initial starting conditions.

A similar scheme was used for oxygen. After pretreatment in air, the reactor was exposed to the desired concentration of butene and the maximum concentration of oxygen possible and still remaining in the non-explosive regime (Zabetakis, 1965). The oxygen concentration was then decreased until the GC's minimum detectability for oxygen was reached (about 0.01%).

After a night at these conditions the oxygen was increased up to the starting conditions again.

Table 2.4: The specific butene and oxygen partial pressures and reactor temperatures used were as follows:

Temperature(°C)	P_{butene}	P_{oxygen}
464	1.0	cycled
"	cycled	0.18
513	0.4	cycled
"	1.0	"
"	1.8	"
"	cycled	0.04
"	"	0.08
"	"	0.32
544	1.0	cycled
"	cycled	0.32

2.3.3.4 Effect of Step Changes in the Butene Partial Pressure

The effect of step changes in the butene partial pressure was investigated a set of experiments whereby the reactor was pre-oxidized to 727°C to remove any carbon deposits, then cooled to 544°C in air. The feed to the reactor was then switched to provide an exit composition of 0.25% butene and 0.25% oxygen. After the switch, the reactivity of the catalyst changed slowly with time and so it was necessary fine tune the feed to the reactor to maintain the exit composition constant at the desired concentration.

After 24 hours at 0.25% butene and 0.25% oxygen, the feed of oxygen and butene to the reactor was changed in the following exit compositions:

1. 2.00% butene; 0.25% oxygen for 24 hours;
2. 40.0% butene; 0.25% oxygen for 24 hours, then back to:
3. 2.00% butene; 0.25% oxygen for 24 hours, then finally back to:
4. 0.25% butene; 0.25% oxygen for a final 24 hours.

This sequence mimics the data taken at 544°C when cycling the butene partial pressure, but instead of measuring the reactivity with semi-continuous changes in the butene concentration, the reactivity was recorded at only the three gas compositions.

2.3.3.5 "Spiking" the feed

A limited amount of data were taken to aid in the elucidation of the reaction mechanism by "spiking" the feed. The exit concentrations of butene and oxygen were kept constant and then increasing (and decreasing) amounts of ssible reaction intermediates were added to the reactor, including: carbon monoxide, carbon dioxide, hydrogen, butadiene and water. The first four components are gases at room temperature and therefore could be added to the reactor feed in place of diluent helium. In the case of water, a separate diluent stream of helium was used which was saturated with water using a gas sparger. If the component effected the rates of reaction, the oxygen and butene feed rates were adjusted to keep them constant at the desired values.

2.3.3.6 Electrokinetic experiments

The effect of current on the rates of butadiene formation and deep oxidation were investigated by applying a voltage across the working electrodes of the cell. Experimentally, the voltage was not controlled, the current being drawn from the cell, or being driven through the cell was

controlled by a galvanostat, which provides a constant current irrespective of the cell voltage. By definition, the voltage on the inside of the cell was positive. Therefore, when applying a current, the "current" flows from high potential side to low potential side of the cell, or ,in reality, O^{2-} ions pass from the reference, air, side to the reactant side of the electrolyte. The exit concentration from the reactor was kept constant at 2.0% butene and 0.08% oxygen while the current from the galvanostat was varied from 0 to 60 mA. The current was also varied from 0 to -60 mA. When applying negative currents, the exit concentration of oxygen in the exit from the reactor dropped and the feed of oxygen had to be increased to compensate.

2.4 SURFACE ANALYSIS OF PLATINUM ELECTRODES

The surface of the platinum electrode was analysed both before and after use, and after several pretreatments. The surface was analysed by scanning electron microscopy, X-ray photoelectron spectroscopy and by Auger electron spectroscopy.

2.4.1 Scanning Electron Microscopy (SEM)

SEM was used to view the physical shape of the platinum electrodes, both as prepared, and after use, to qualitatively view the effect of use on the electrodes. It was used in conjunction with energy dispersive analysis of X-rays (or EDAX) which analyses the composition of a volume of 1.5 μm diameter by 1.5 μm deep, and as such measures the bulk composition of the sample. SEM photographs were taken at 2000X and at 20000X on an AMR model

1000A scanning electron microscope, equipped with a Tracor Northern model TN2000 X-ray analyser (which uses a 20 keV beam and analyses for 25 seconds).

Samples of the catalyst/electrode surface were taken before use, by preparation of a small film in an identical manner to that used for the reactor. After the catalyst had been used, samples of the surface were removed, from the cooled reactor, by prying small areas of the film from the zirconia-yttria surface with a razor blade. Care was taken in handling the film to avoid contamination.

The samples were mounted with double sided tape and grounded with silver paint. When the surface was to be analysed, the samples were viewed as mounted. However, higher contrast images could be obtained by coating the sample a thin film (about 200 A) of gold to prevent charging of the surface. Analysis of the bulk is still possible, however, Pt and Au overlap extensively in their X-ray spectra. The gold film was applied by the standard technique of vacuum deposition from a heated scource (Edwards, Model E306A).

2.4.2 Auger Electron Spectroscopy and X-Ray Photoelectron Spectroscopy

Auger electron spectroscopy (AES) and X-ray photoelectron spectroscopy (XPS) were used to analyse the surface composition of the catalyst after various pretreatments.

In XPS, the sample is bombarded with x-ray photons and the kinetic energy of electrons emitted from the core levels is analysed. The kinetic energy (KE) of the emitted electrons is given by:

$$KE = h\nu - BE - \phi_s \qquad (4)$$

where $h\nu$ is the energy of the photon, BE is the binding energy of the atomic orbital from which the electron originates, and ϕ_s is the work

function of the spectrometer. The KE is therefore specific for each particular element and is also sensitive to the valence of the atom. When a photoelectron is emitted, Auger electrons are also emitted due to the relaxation of the energetic ions left after the emission. Typically, for optimal sensitivity, different instruments are used for each technique.

When either photoelectrons or Auger electrons are emitted, only the electrons in the top 4 to 10 Å (depending on the specific electron energy) are able to escape from the sample and be detected. Both techniques are therefore extremely surface sensitive. Whereas the sample beam for XPS is about 1 cm square, the sampling beam in AES is typically about 1 μm in diameter. AES is therefore also sensitive to inhomogeneities across the surface.

Both techniques were used in an attempt to independently analyse the effect of butene and oxygen partial pressures on the relative amounts of oxygen, carbon and platinum exposed on the surface and also to analyse for the presence of impurities which may be present on the surface, but not the bulk. The surface composition was correlated with the activity of the catalyst at the time the sample was taken. The catalytic activity and selectivity of the reactor were determined by GC analysis of the product stream (see section 2.2). The surface composition of the catalyst was determined both by surface analysis and also by depth profiling.

2.4.2.1 Sample preparation

All the samples discussed below taken from the annular reactor (prepared using Engelhard Pt 4338A platinum ink), which had been pretreated prior to use (see section 2.1.3.2) to remove any impurities that may have been present in the ink. The reactor was exposed to a particular butene and oxygen partial pressure, for a specific amount of time, and the

catalytic activity and selectivity measured. The reactor was then cooled to room temperature, in the same gas mixture. The reactor was cooled as quickly as possible, effectively at about 500°C per hour, by switching off the furnace, and opening it slightly. The furance could only be openned slightly to prevent thermally shocking the zirconia-yttria, and cracking it.

When cool, the reactor was dis-assembled, exposed to air, and samples removed from the surface by gently prying them from the surface using a razor blade. The samples were only handled with tweezers, to prevent contamination, and were stored in air.

For Auger spectroscopy, the samples were mounted on the spectrometer sample holders physically by screws and clamps. No adhesive, glues, tape or any possible contaminant was used to mount the samples. Therefore, the Auger spectra obtained came only from the platinum surface, and that Pt surface was the same one as used for the kinetic experiments.

XPS, however, requires a sample area of about 1 cm square, whereas, the samples pried off the surface were always smaller than this. Several pieces were glued to coupons of silver with either silver paint or carbon paint, to achieve the required area. This meant that there were problems of contamination from the mounting procedure, and XPS could therfore only be used qualitatively.

2.4.2.2 Pre-treatment of Samples

Prior to the specific pretreatment used, the reactor was calcined to 727°C (1000 K) in air and kept there for two hours. At p_{O2}=0.21 atm, platinum oxide is unstable (see section 1.2.2.3) and therefore treatment at this temperature and atmosphere should clean the platinum surface, removing any carbon deposits but not depositing any oxide. The pre-treatments used

for sample analysed by Auger spectroscopy are shown in table 2.5.

Table 2.5: Preparations used for Auger samples

Sample Number	Partial pressures butene (%)	O_2 (%)	Time (hrs)	Comment
1	0	0	16	Cooled in 10.0% H_2 in He from 727°C to room temperature at 67°C/min
2	0	0.21	16	In air for > 2 hrs at 513°C
3	0.15	0.25	16	After re-oxidation at 727°C
4	2.0	"	1/2	After reheating to 513°C
5	2.0	"	16	" " " "
6	40.0	"	16	" " " "
7	2.0	"	1/2	" " " "
8	2.0	"	16	" " " "
9	1.0	0	16	After re-oxidation at 727°C
10	-	-	-	polcystalline Pt foil - for reference

The rate of depth profiling was estimated to be about 100 Å per minute. This was calculated by sputtering away a film of Ta_2O_5, that that had been electrochemically grown to a depth of 1000 Å on a tantalum cystal, under identical sputtering conditions, to those used for Pt.

XPS spectra were taken of samples 2 (oxidized in air), 5 (2.5% butene and 0.25% oxygen), 9 (reduced in 1.0% butene in helium) and 10 (the polycrystalline Pt foil) only.

2.4.2.3 Analysis conditions - Auger electron spectroscopy

Auger spectra were taken on a (Perkin-Elmer) Physical Electronics Model 590 Scanning Auger Microprobe upgraded with computer interfacing, to a Digital PDP-11/04 microcomputer running MACS (Multiple-technique Analytical Computer System) software, for computerized data acquisition and instrument control.

Analyses were performed using a beam voltage of 5 keV and a beam current of 100 μA. Survey spectra of the surfaces were taken both in spot model and when the electron beam was rastered over the surface. When the analysis is performed in the spot mode, the sampling area is approximately 1 μm in diameter. As discussed in the results section, some non-uniformity of surface composition was found and more representative surface analysis results were obtained by rastering the electron beam at a magnification of 2000X; in this case, analyses were taken over an area of about 50 μm.

After survey spectrum had been obtained, the surface composition was determined by multiplexing (repeatedly measuring) the platinum, carbon and oxygen peaks (at 64 eV, 238 eV and 512 eV, respectively) for ten minutes. The peak-to-peak heights were converted to atomic concentrations by the software, using the sensitivity factors listed in table 2.6.

The depth profiles of Pt, C and O were determined by depth profiling. The surfaces were sputtered with argon ions at an ion current of 60 μA and ion gun voltage of 4.5 kV, rastered over an area of 1.0 mm X 1.5 mm (PHI model 04303). The surface was sputtered for 15 seconds and the peak-to-peak heights of the Pt, C and O signals measured and signal averaged for sufficient time to give reasonable signals, typically 10 times for platinum and carbon and 20 times for oxygen. The surface was then sputtered for a further 15 seconds, etc., for a total of 5 minutes.

2.4.2.4 Analysis Conditions - X-Ray Photoelectron Spectroscopy

XPS spectra were taken on a (Perkin-Elmer) Physical Electronics Model 548 spectrometer which had been similarily upgraded with computer interfacing to a Digital PDP11/04 microcomputer, also running MACS software for digital data acquisition and control. The system pressure was always less than 1×10^{-8} torr.

All spectra were obtained using non-monochromatized Mg K-α radiation as the excitation scource, operating at 15.0 keV and 300 watts. Survey spectra were obtained using a cylindrical mirror analyser (PHI model 15-255G) operated at 100 eV with a 4mm slit. The binding energy was varied between 0 and -1000 eV and the signal averaged 4 times. No charging of the surface was observed, and all binding energies are reported as received, and have not been corrected.

Table 2.6 Relative Atomic Sensitivity Factors for XPS and AES.

Element	XPS		AES	
	Line	Relative Area Sensitivity Factor	Electron Energy (eV)	Peak-to-peak Rel. Sens. Factor
Platinum	$4f_{7/2}$	4.6	64	0.28
Carbon	1s	0.25	272	0.14
Oxygen	1s	0.67	512	0.40
Silicon	-	-	92	0.28
Iron	$2p_{3/2}$	3.00	703	0.128
Silver	$3d_{5/2}$	3.00	356	0.97

3.PLATINUM OXYGEN SYSTEM

3.1 RESULTS

3.1.1 Electrolyte Resistance

The voltage drop versus time was recorded on an oscilloscope, when a square wave of 50mV at 1000Hz, having passed through a resistor, was applied between the two working electrodes. The voltage across the cell dropped instantaneously within the first 5 μs and then decreased more slowly, figure 3.1. The voltage drop within the first 5 μs was assumed to be due to the electrolyte and that beyond 5 μs due to the electrode reactions. The voltage drop within 5 μs is plotted versus various currents in figure 3.2, on log-log scales for T=578°C. The straight lines have a slope=1, indicating that the resistance of the electrolyte obeys Ohm's law, V=iR. The resistance between the working electrodes was 9.3 ohms, between the working and reference electrodes on the external surface of the tube was 5.90 ohms and between the working and reference electrodes of the inner surface was 2.58 ohms.

3.1.2 Transfer Coefficients

The overvoltage, η, was determined by subtracting the product of the electrolyte resistance and the current, from the voltage drop between the working and reference electrodes on each side of the zirconia-yttria electrolyte:

$$\eta = V_{meas} - iR - V_0 \qquad (1)$$

where V_0 was the voltage at zero current. This was typically close to zero (about 2 mV) and probably arose from minor temperature variations. The log of the current was plotted against the overvoltage (Tafel plot) as shown in figure 3.3, in accordance with the high overpotential approximation of the Butler-Volmer equation (equations 1.35 and 1.36). It was necessary to

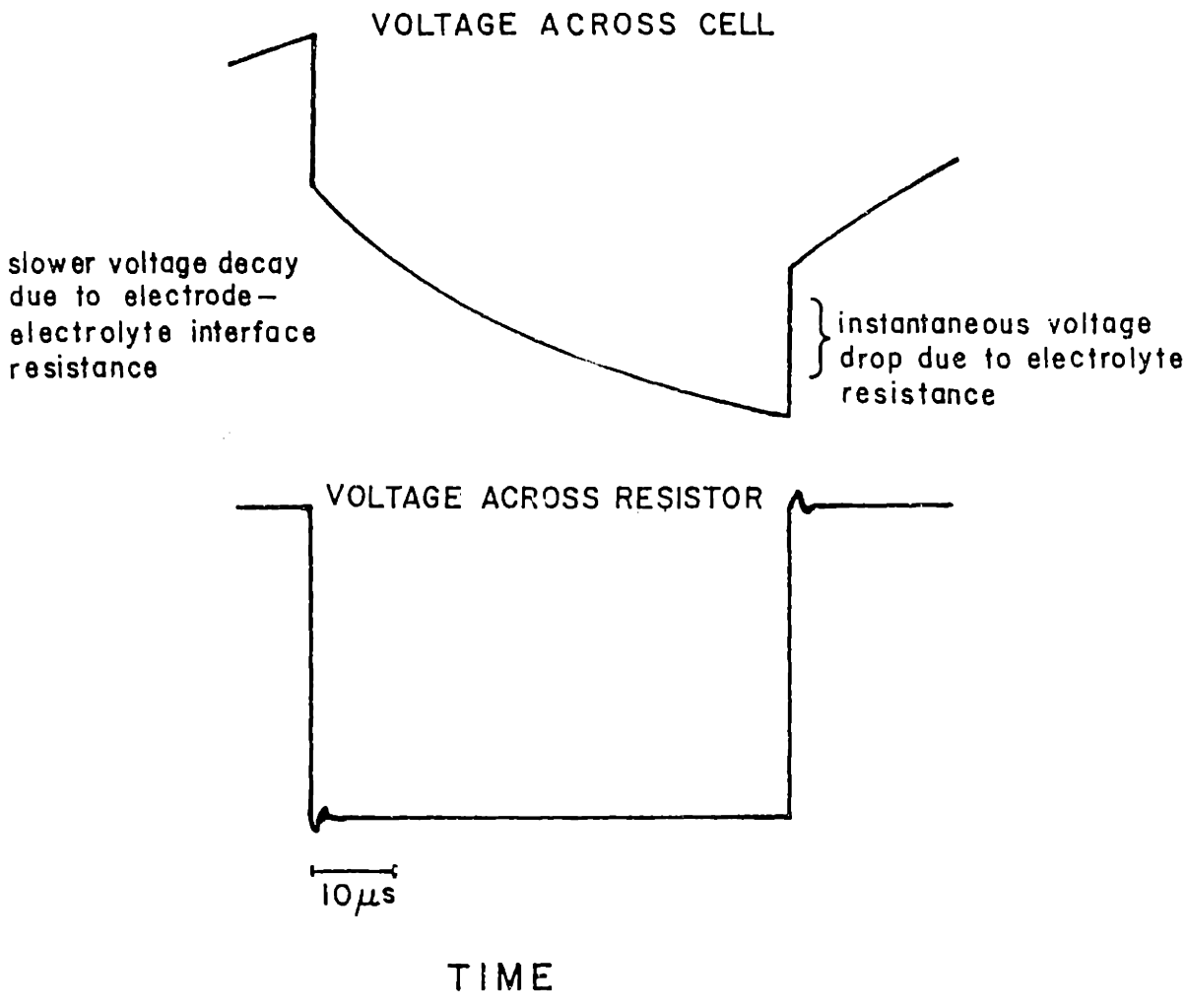

Figure 3.1: Schematic response of cell to a current square wave at 1000 Hz

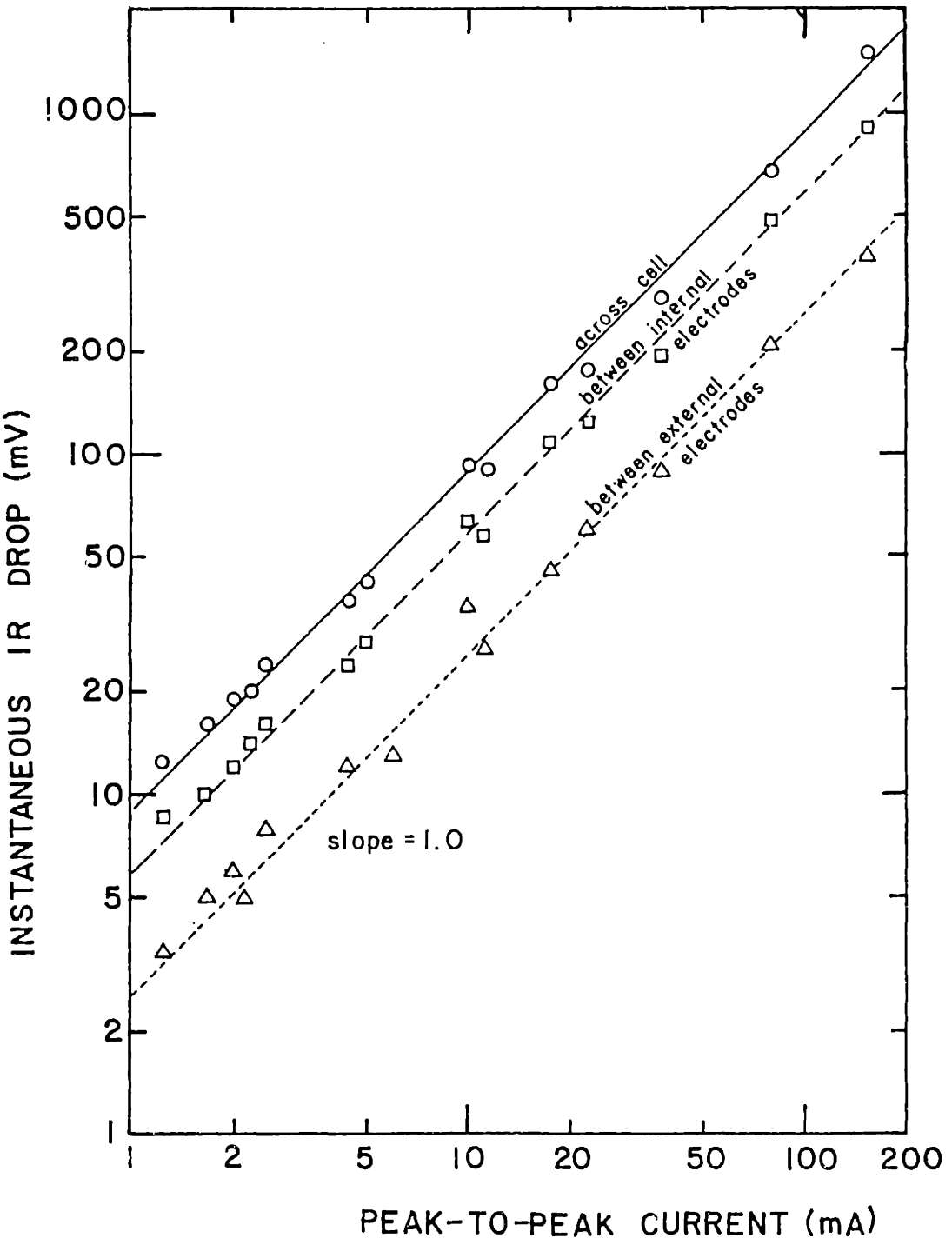

Figure 3.2: Electrolyte resistance at 578°C

leave the cell at each current for several hours for the voltage to reach steady state. When increasing the current, the voltage tended to drift up and when decreasing the current, the voltage tended to drift down.

The least squares fit for the linear regions of the Tafel plots (at overpotentials between 0.05 and 0.4 volts, figure 3.3) gave slopes of 13.25 and 13.40 which, since F, R and T in equations (1.35) and (1.36) are known, correspond to values of α_a=0.97 and α_c=1.05. The lines drawn on the figure are the theoretical slopes for α_c=α_a=1.0.

Also, as shown in figure 3.3, at currents greater than 12 mA (0.24mA/cm^2), the overpotential increased rapidly and the curve assymptoted to a "limiting current". Under these conditions the mechanism for the charge-transfer reaction must have changed from that controlling when α_c=α_a=1.0, and is probably controlled by mass transfer limitations.

3.1.3 Electrode-Electrolyte Interface Resistance

When a small current was applied to the electrochemical cell, the voltage was initially linear with current up to about 0.040 V and then deviated upwards, as expected from the Butler-Volmer equation. When the overvoltage was kept below 10mV, the overvoltage-current plot was linear, with zero intercept, under all conditions; figure 3.4 is typical. After it had been ascertained that the response was always linear, the entire curve was not recorded, but only the overvoltage for two or three currents. The exchange current density was calculated from the overvoltage assuming that the low η approximation of the Butler-Volmer equation applies, and that α_a=α_c=1.0. The exchange current density versus temperature at different oxygen partial pressures is shown in figure 3.5. At high temperatures and/or low oxygen partial pressures, it is proportional to $p_{O_2}^{1/4}$ and at low temperatures and/or high oxygen partial pressures, the conductance is

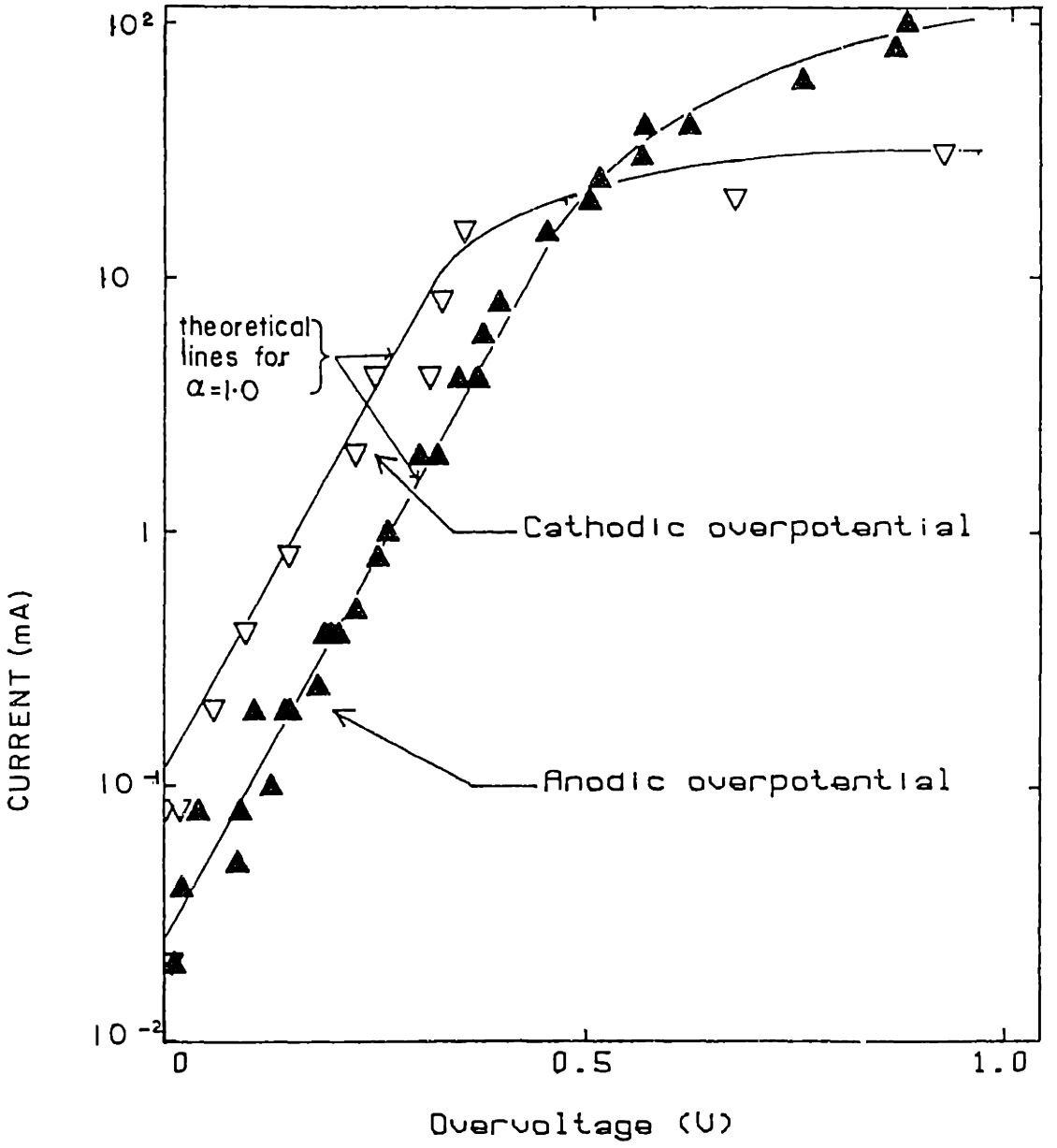

Figure 3.3: Tafel plot for Pt electrodes exposed to air, at 578°C

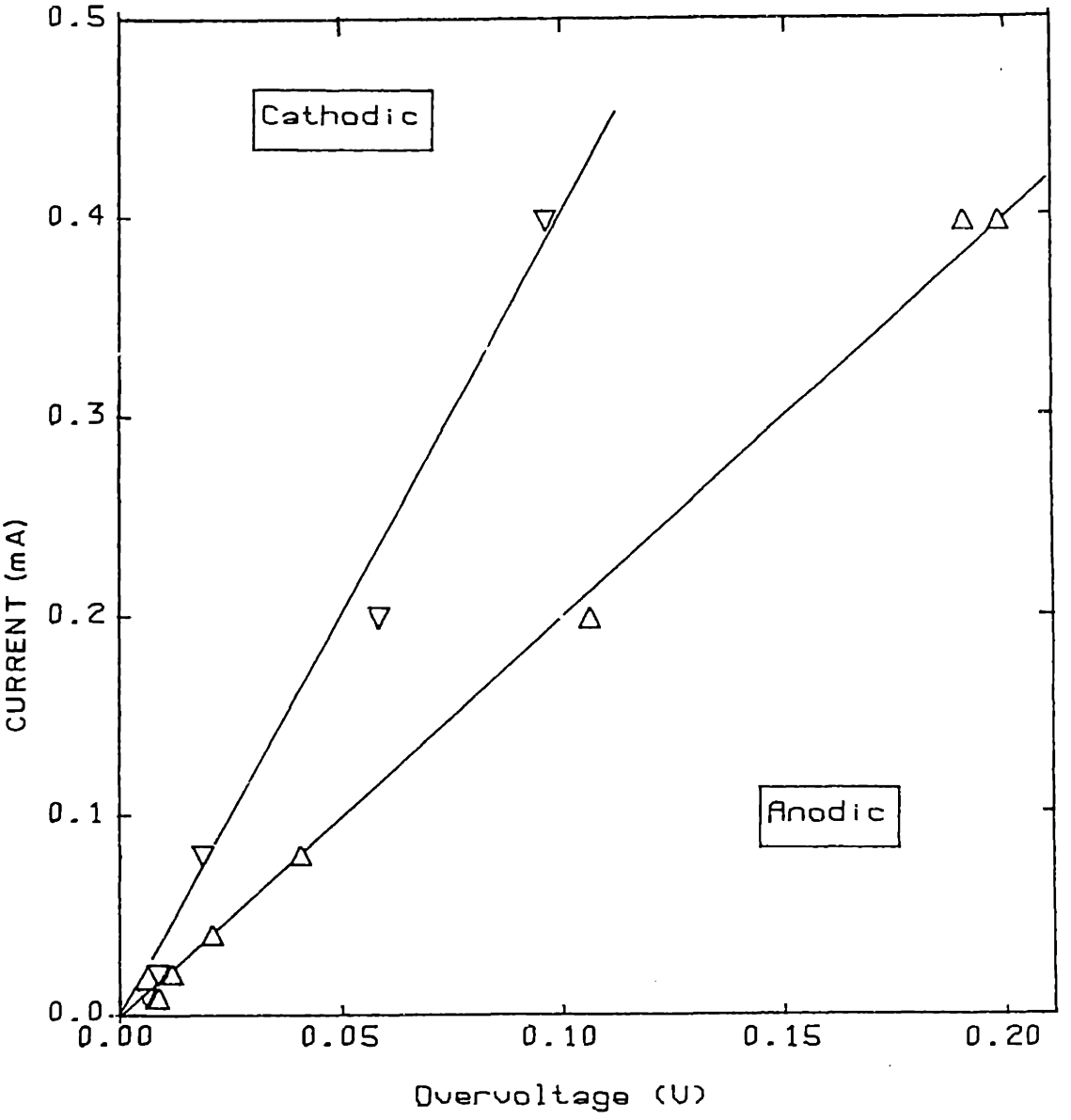

Figure 3.4: Typical response of Pt electrode to a small overvoltage ($T=578^{o}C$)

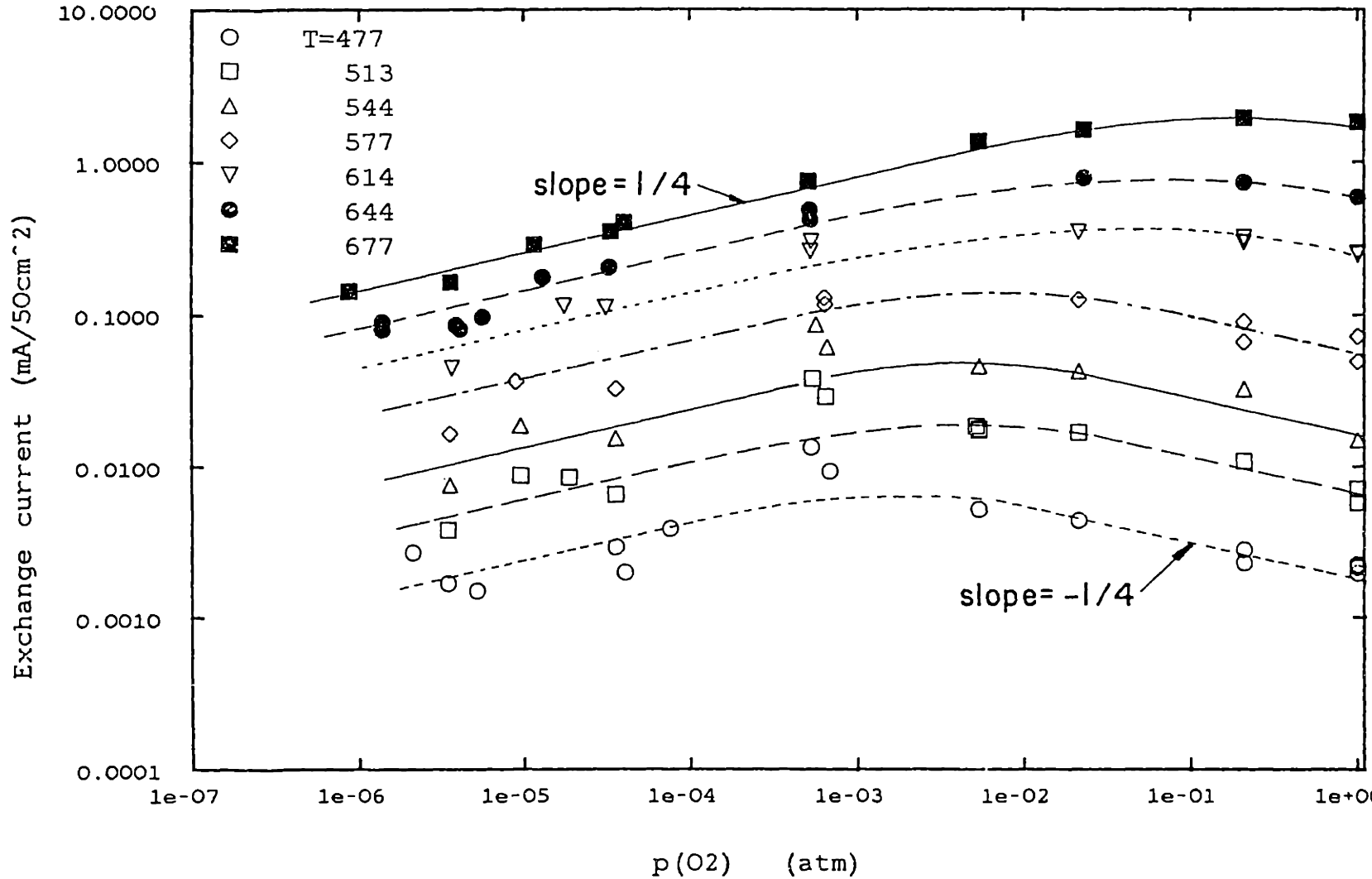

Figure 3.5: Exchange current density versus oxygen partial pressure

proportional to $p_{O2}^{-1/4}$. Under the latter set of conditions, the data were far more erratic, and the values tended to drift downwards with time.

3.2 DISCUSSION

3.2.1 Transfer Coefficients

The value of both of the transfer coefficients being 1.0 agrees with the values determined by Wang and Nowick (1983) using similar electrodes but coated on ceria-doped-calcia solid electrolytes and with Isaacs et al.(1981) who used a similar cell to that used here. The rationalization of the values of the transfer coefficients, below, is an extension of the arguement presented in the work of Wang and Nowick (1983).

As discussed in section 1.2.3.2 above, the value of the transfer coefficients are related to the number of electron transfer steps before and after the electrochemical rate determining step (ERS), γ_b and γ_a, the number of electrons transfered in the ERS, n, the frequency of the ERS, ν, and the symmetry factor, β. Assuming that the symmetry factor is 0.5, equations (1.32) and (1.33) apply:

$$\alpha_a = n - \gamma_a/\nu - 0.5r \tag{2}$$

and

$$\alpha_c = \gamma_a/\nu + 0.5r \tag{3}$$

which imply:

$$\alpha_a + \alpha_c = n/\nu \tag{4}$$

and

$$n - \gamma_b - r\nu = \gamma_a \tag{5}$$

From the physics of the system, it is known that zirconia-yttria conducts oxygen anions as O^{2-} species, and that oxygen exists as O_2 molecular species in the gas phase. For an electrochemical reaction to occur, the number of electrons, n>0 and there must be an integral number of steps. With these conditions it is possible to determine sets of combinations of γ_a, γ_b ,n and ν that yield $\alpha_a = \alpha_c = 1.0$ (table 3.1).

Table 3.1 Possible mechanisms for the electrochemical reaction at the electrode-electrolyte interface; combinations of γ, n, r and ν that yield $\alpha_a = \alpha_c = 1.0$

Mechanism #	r electrons transfered in ERS	ν times ERS step occurs	n total of e trans	γ_b steps before ERS	γ_a steps after ERS	comment
1	0	1	2	1	1	possible
2	0	2	4	2	2	possible
3	0	3	6	3	3	wrong # e^-
4	1	2	4	1	1	O_2 transferred
5	1	4	8	2	2	too many e^-
6	2	1	2	0	0	possible
7	2	2	4	0	0	O_2 transferred

Only rows 1, 2 and 6 in table 3.1 are feasible because all other sequences either require the transfer of too many electrons, or the transfer of molecular oxygen through the interface into the electrolyte. Oxygen cannot exist as a molecular species in the zirconia-yttria. The sequences corresponding to the permitted rows 1, 2 and 6 are:

Row 1 $O_2(g) \rightleftharpoons 2O(a)$

$$O(a) + e \rightleftharpoons O^-(a) \xrightarrow{rds} O^-_{oxide} \overset{+e}{\rightleftharpoons} O^{2-}_{oxide}$$

Row 2 $$O_2(g) \rightleftharpoons O_2(a) \overset{+e}{\rightleftharpoons} O_2^-(a) \overset{+e}{\rightleftharpoons} 2O^-(a) \xrightarrow[\text{twice}]{rds} 2O^-_{oxide}$$

$$\overset{+e^-}{\rightleftharpoons} O^-_{oxide} + O^{2-}_{oxide} \overset{+e^-}{\rightleftharpoons} 2O^{2-}_{oxide}$$

Row 6 $$O_2(g) \rightleftharpoons 2O(a) \xrightarrow[+2e^-]{rds} 2O^{2-}_{oxide}$$

In row 1 the electrons are added sequentially to dissociatively chemisorbed oxygen and the ERS is the incorporation of a singly charged oxygen atom from the platinum side of the three phase boundary (the zirconia-yttria/platinum/gas interface, figure 1.6) into the electrolyte side, followed by the further addition of an electron to the singly charged oxygen atom, see figure 3.6. Row 2 differs from row 1 only in that the addition of the first electron occurs to molecularily adsorbed oxygen molecule prior to its cleavage into atomic oxygen. Row 6 differs in that the ERS involves a concerted reaction involving the simultaneous addition of two electrons at the same time as incorporation into the oxide.

It is not possible to differentiate between these three mechanisms on the basis of the exchange current density measurements alone. However row 6 would probably be unlikely from statistical reasoning since it requires a three body collision (of two electrons and an oxygen atom) occuring at the three phase boundary. Molecularly adsorbed oxygen is not observed on platinum surfaces at temperatures above about 150 K (Gland, Sexton and Fisher, 1980) and therefore it is unlikely that it will be sufficiently stable for the mechanism in row 2 to predominate. On transition metals oxygen frequently adsorbs as O_2^- or O^- species, which act as the electrophilic reagents in the oxidation and partial oxidation of olefins and hydrocarbons (Bielanski and Haber, 1979). Atomic oxygen existing as

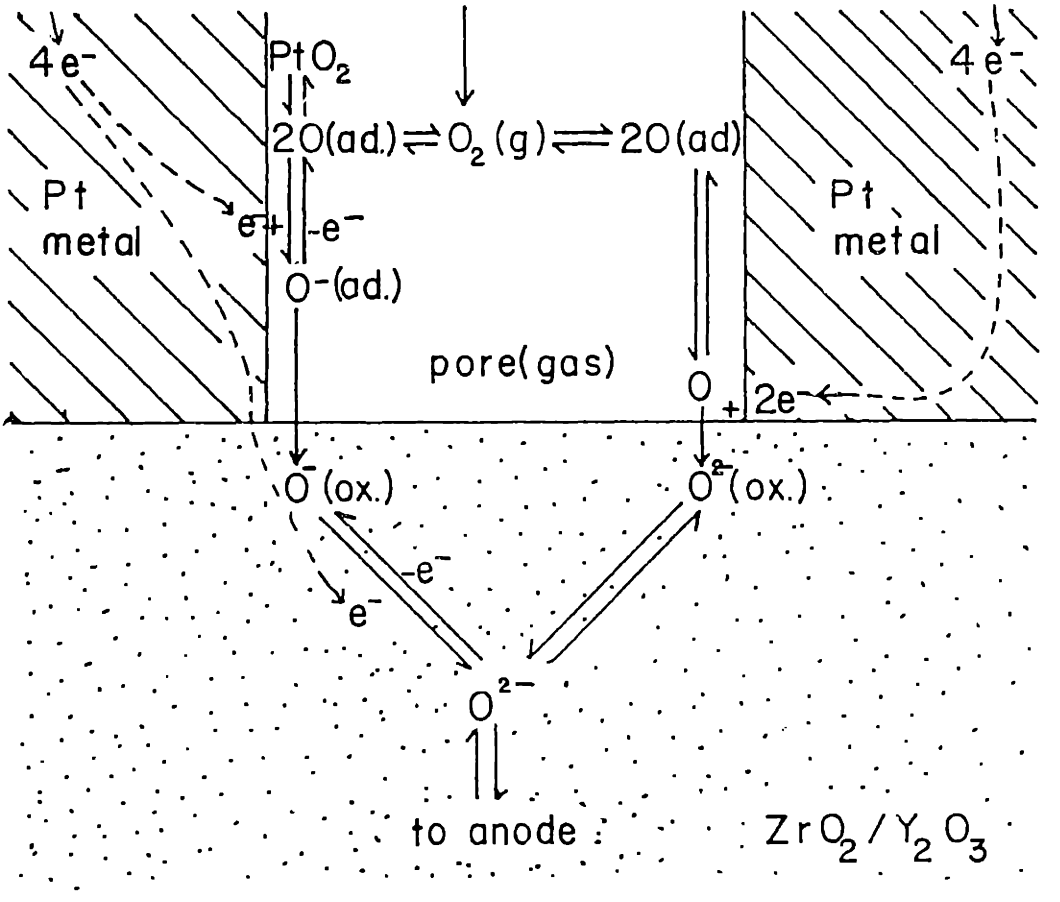

Figure 3.6: Schematic of three-phase boundary, based on experimental data

singly charged species on the platinum surface would tend to confirm the proposed mechanism of row 1.

3.2.2 Exchange Current Density of the Interface

The exchange current density, at various temperatures and oxygen pressures, was calculated from the slope of overpotential versus current plots. These are the low η approximation of the Butler-Volmer equation (1.31):

$$i = i_o F (\alpha_c + \alpha_a) / RT$$

It should be noted that the relationship between the conductance of the interface and the exchange current density is given by:

$$C = i_o (\alpha_a + \alpha_c)/RT \qquad (6)$$

In other words, "exchange current density" is a measure of the conductance of the interface, and the two parameters differ only by the value of the constants $(\alpha_c + \alpha_a)/RT$. This permits us to compare these experimental exchange current density measurements to literature data, which have been published in terms of interface resistance, interface conductance or exchange current density.

The observed dependence of the interface conductance on oxygen partial pressure of 0.25 at low p_{O2} and -0.25 at high p_{O2} agrees with data published by Okamoto, Kawamura and Kudo (1983) where they observed the dependence of 0.2 at low p_{O2} and -0.2 at high oxygen pressure, using a similar system of platinum electrodes on zirconia-yttria. Wang and Nowick (1983), using calcia doped ceria solid electrolytes, the same study as discussed above on calcia doped ceria, also observed dependences on oxygen pressures of 0.25 and -0.25 at low p_{O2} and high p_{O2} conditions, respectively. This similarity would be expected since Fabry and Kleitz (1974) found that changing the nature of the electroyte had no qualitative

effect on the behavior of the interface.

In all of the above studies, the positive and negative slopes were observed in separate experiments. In the experiments presented here, the positive and negative slopes and maxima between the two were observed in the same experiments. This permits us to extend the theory of Wang and Nowick (1983) to calculate adsorption equilibrium parameters and to evaluate the model quantitatively.

3.2.2.1 Modelling the Exchange Current Density versus Oxygen Pressure

According to single crystal ultra high vacuum studies of oxygen adsorbed on platinum (Engel and Ertl, 1979) oxygen adsorbs dissociatively at temperatures above 100 K. If oxygen is the only species adsorbing on the surface and it adsorbs according to a Langmuir-Hinshelwood mechanism then:

$$O_2 + 2 \text{ sites} \rightleftharpoons 2O(a) \tag{7}$$

and

$$(K_{O2}\ p_{O2})^{1/2} = \frac{\theta_O}{(1 - \theta_O)} \tag{8}$$

or

$$\theta_O = \frac{(K_{O2}\ p_{O2})^{1/2}}{(1 + (K_{O2}\ p_{O2})^{1/2})} \tag{9}$$

The charge transfer reaction is:

$$2\{O(a) + 2e^- + V_{oo} \rightleftharpoons O^{2-}_{oxide} + V\} \tag{10}$$

where V_{oo} is a vacancy in the oxide.

The rate for the forward reaction may be expressed as a current:

$$i_{o,forward} = 2Fk^{o}_{cath}\ \theta_O \exp(-\alpha_c F \eta / RT) \tag{11}$$

and

$$i_{o,back} = 2Fk^{o}_{an} (1-\theta_0) \exp(\alpha_a F\eta/RT) \quad (12)$$

if $\alpha_a=\alpha_c=1.0$ then

$$i_o = (i_{o,for}\ i_{o,back})^{1/2} = 2Fk_r \{\theta_0(1-\theta_0)\}^{1/2} \quad (13)$$

where: $k_r = (k^{o}_{an}\ k^{o}_{c}$

$$= 2Fk_r \{[\ \frac{(K_{02}\ p_{02})^{1/2}}{1+(K_{02}\ p_{02})^{1/2}}\ ]\ [\ \frac{1}{1+(K_{02}\ p_{02})^{1/2}}\ ]\ \}^{1/2} \quad (14)$$

i.e.

$$i_o = 2Fk_r \frac{(K_{02}\ p_{02})^{1/4}}{1 + (K_{02}\ p_{02})^{1/2}} \quad (15)$$

This equation has two limiting cases:

at low p_{02}: $\quad 1 >> (K_{02}\ p_{02})^{1/2}$

therefore: $\quad i_o \approx (K_{02}\ p_{02})^{1/4} \quad (16)$

at high p_{02}: $\quad 1 << (K_{02}\ p_{02})^{1/2}$

therefore: $\quad i_o \approx (K_{02}\ p_{02})^{-1/4} \quad (17)$

These limiting cases were observed experimentally.

Also, the maximum of the i_o vs p_{02} curve is given by $di_o/dt = 0$. When equation (15) is differentiated:

$$K_{02}\ p_{02} = 1$$

or

$$K_{02} = 1\ /\ p_{02},\ \text{at max io}$$

or, when applying equation (9):

$$\theta_0 = 0.5,\ \text{at max } i_o$$

The exchange current density versus p_{02} data were fitted according to equation (14) using the FIT FUNCTION subroutine in the RS1 software program (BBN Research Systems) as shown in figure 3.7. This gave more reliable values than reading the p_{02}, at max io from figure 3.7. The values for K_{02} and k_r obtained from the fit are plotted as Van't Hoff and Arrhenius plots,

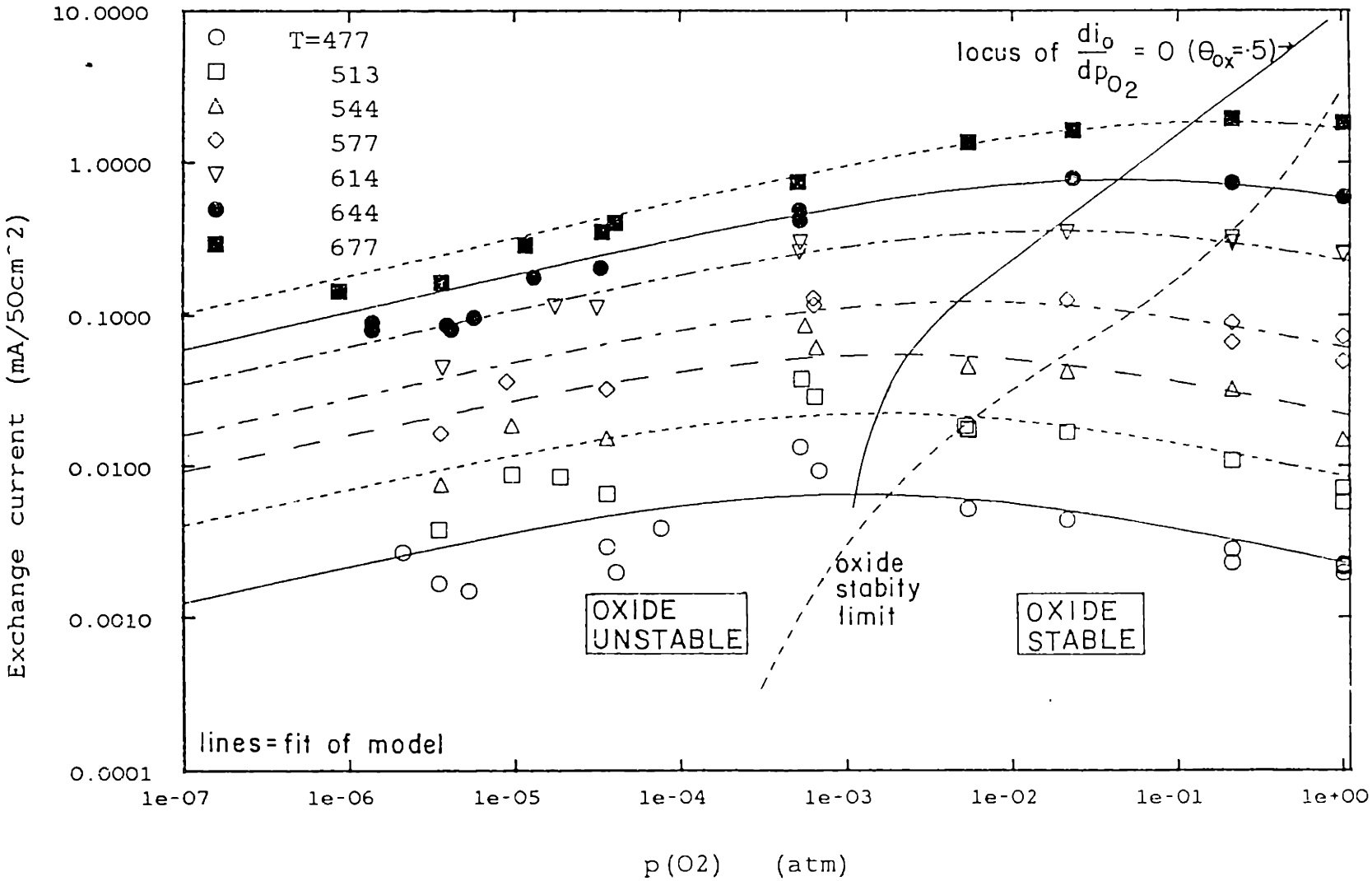

Figure 3.7: Exchange current density versus oxygen partial pressure.

Fit of model to data

respectively, in figure 3.8, where the error bars are the standard deviations of the fit. The activation energy for k_r, the root mean square average for the oxidation/reduction of oxygen atoms, was 41.6 kcal/mole, which agrees extremely well with the value found by Wang and Nowick of 40.3 kcal/mole (1.75 eV).

At temperatures above 545°C, the Van't Hoff plot for the adsorption of oxygen on the platinum surface is linear and indicates an enthalpy for adsorption/desorption of 53.1 (±5) kcal/mole. At temperatures less than 545°C the van't Hoff plot for oxygen adsorption on the platinum deviates from a straight line and the error bars for the fit of the data to the model become excessively large, indicating that the simple Langmuir-Hinshelwood model proposed above does not fit the data in these temperature regimes (see section 3.2.2.2, below)

There have been several determinations of the adsorption/desorption equilibrium constant in the literature with which the value of 53.1 kcal/mole agrees reasonably well. Gur, Raistrick and Huggins (1980a) reviewed the literature and found values between 53 and 70 kcal/mol. They also measured the activation energy of the interface resistance of platinum electrodes on ZrO_2-Sc_2O_3 in regimes where oxygen adsorption/desorption is rate controlling. They used AC admittance measurements and found an activation energy of 56 kcal/mol, whereas, Sasaki, Mizusaki, Yamauchi and Fueki (1981) using a similar method for platinum on zirconia-yttria found 48 kcal/mole. Okamoto, Kawamura and Kudo (1983) performed, what appears from their paper, to be an eye-ball fit to analagous exchange current vs p_{O2} data and found an activation energy of 43 kcal/mole, having fortuitously assumed transfer coefficients $\alpha_a=\alpha_c=1.0$. In contrast, Verkerk, Hammink and Buggraf (1983) using similar measurements

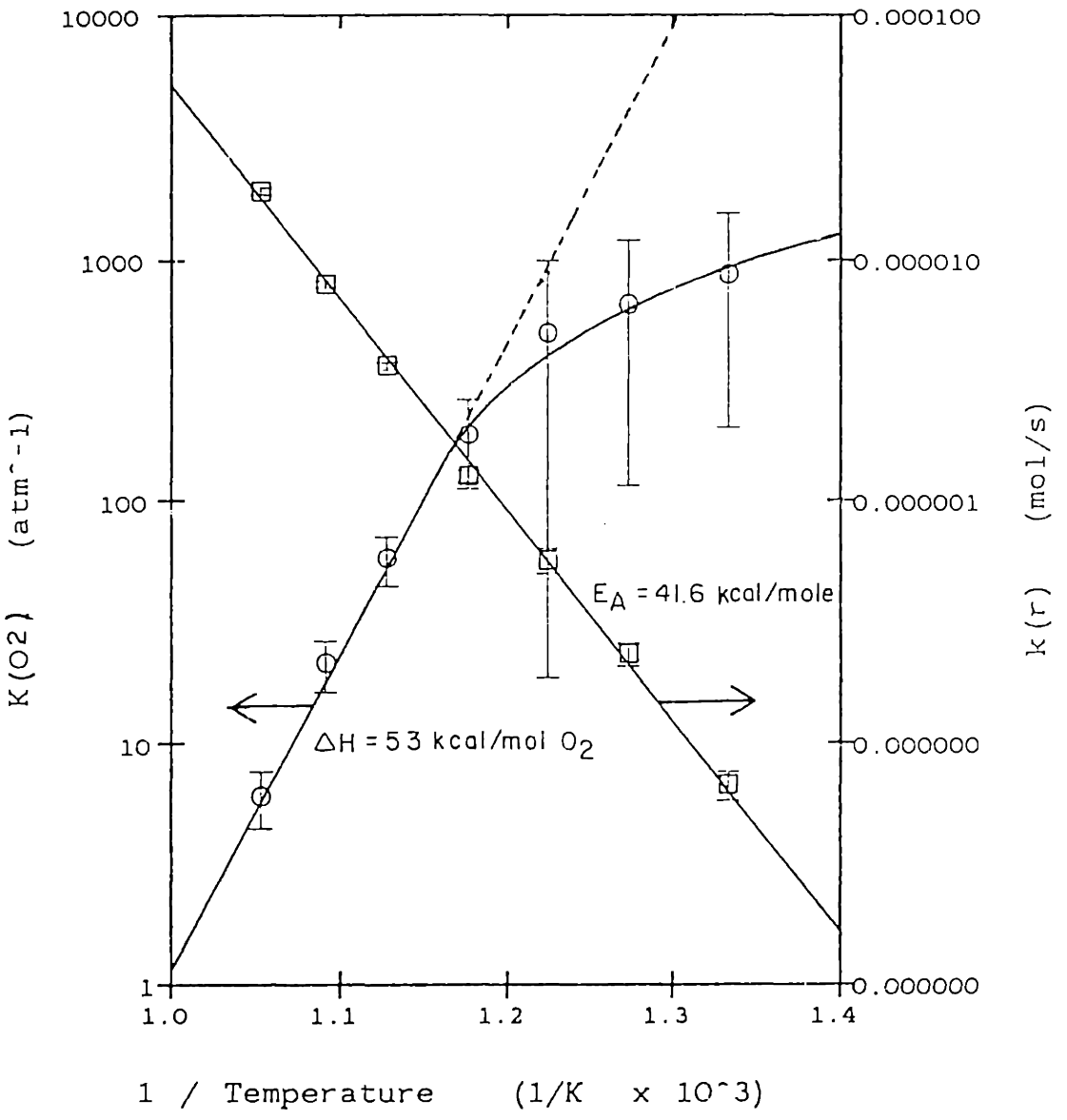

Figure 3.8: Van't Hoff plot for adsorption/desorption of oxygen on platinum electrode/catalyst, and Arrhenius plot for k_r, the rate constant for the electrochemical oxidation/reduction at the electrode/electrolyte interface.

found that $i_o = p_{02}^{1/2}$ and an activation energy of 38 kcal/mole. However, this activation energy is probably for surface diffusion rather than oxygen adsorption/desorption.

3.2.2.2 The Exchange Current Density at Low Temperatures

The Arrhenius plot of rate constant for the electrochemical reaction, k_r (figure 3.9), did not deviate from a straight line, indicating that the mechanism for the electrochemical reaction apparently did not change with decreasing temperature. Assuming that this is correct, a possible explanation for the failure of the model is a decrease in the area available for oxygen adsorption/desorption on the platinum surface, possibly by the build-up of a layer of oxide. If an oxide were to form, the fractions of adsorbed species on the surface would change from $\theta_O + \theta_v = 1$ to $\theta_O + \theta_v + \theta_{oxide} = 1$.

According to section 3.2.1 above, oxygen is transfered across the electrode/electrolyte interface as an O^- species. Previous studies of platinum oxide (Berry (1978)) indicate that the oxide exists as PtO_2, not PtO. As such, it would be inactive for the electrochemical reaction. The fraction of the platinum surface available for the charge transfer would, therefore, be reduced by that fraction occupied by the oxide, θ_{oxide}. This would then in turn reduce i_o as follows:

If oxygen adsorbed dissociatively and reversibly only on the platinum surface and the oxide acted only to block adsorption sites, then equation (8) would become:

$$(K_{02}\ p_{02})^{1/2} = \theta_O \ / \ (1 - \theta_O - \theta_{oxide}) \qquad (18)$$

or:

$$\theta_O = \frac{(K_{02}\ p_{02})^{1/2}}{(1 + K_{02}\ p_{02})^{1/2}} \ (1 - \theta_{oxide}) \qquad (19)$$

and following the same algebra as in equations (10)-(14), equation (15), the expression for the effect of oxygen partial pressure on exchange current density, i_o, would become:

$$i_o = 2Fk_r \left\{ \frac{(K_{O2}\ P_{O2})^{1/4}}{1 + (K_{O2}\ P_{O2})^{1/2}} \right\} \quad (1 - \theta_{oxide}) \tag{20}$$

or:

$$\frac{i_o}{i_{o,\ no\ oxide}} = (1 - \theta_{oxide}) \tag{21}$$

Therefore the values for i_o measured in the presence of oxide would be lower than those in the absence of oxide. If i_o is lower than expected, the model proposed would not be applicable because, at high p_{O2}, $K_{O2} \approx i_o^{1/4}$ (from equation 16), and at low p_{O2}, $K_{O2} \approx i_o^{-1/4}$ (from equation 17). The observed effect would be for the error bars for the fit of the model to the data to explode, as occurred in figure 3.8 at lower temperatures.

3.2.2.3 Oxide Model Evaluation

As discussed in the literature review section there has been controversy in the surface science literature over the existence or otherwise of platinum oxide, however the consensus seems to be in favor of its existence (see section 1.2.2.3). Berry (1978) used high precision electrical resistance measurements of Pt wire to determine ΔH_f=-41.9 kcal/mole and ΔS^o=-49 cal/mol K. Vayenas and Michaels (1981) determined the stability limits for the oxide formed during ethylene oxidation reactions to be described by ΔH_f=-46 kcal/mole and ΔS=-45 cal/K mol O_2. Vayenas and Michaels used a similar experimental system of a platinum sponge electrode on a zirconia-yttria solid electrolyte which would correlate better with the system used in this study than Berry's smooth wires. Vayenas and Michaels' data correspond to a equilibrium oxygen

partial pressure for oxide formation given in table 3.2.

Table 3.2 Equilibrium partial pressures for oxide formation, from data of Vayenas and Michaels (1982): $\ln P_{O2} = 25.0 - 24000/T$

Temperature C	$P_{O2,crit}$ atm
477	.000912
511	.00365
544	.0126
577	.0393
612	.1202
643	.3009
677	.769

When these values are superimposed on the data of figure 3.7, only a small fraction of the data taken at 577°C and above fall in the regime where the oxide would be stable. Above 577°C, the fit of the Langmuir-Hinshelwood model to the data was good. At temperatures below 544°C, however, an increasing fraction of the data were taken at oxygen pressures above the stability limit of the oxide at that temperature. Under these conditions the fit of the Langmuir-Hinshelwood model to the data was poor, as indicated by the large sized of the error bars in figure 3.8. It would be anticipated, furthermore, that the deviations of the data from the model would become more significant with decreasing temperature since more of the data would fall into the stable oxide regime, as was observed experimentally.

Similar behavior was observed by Gur, Raistrick and Huggins (1980b) in their study of the limiting current of $Pt/ZrO_2-Y_2O_3$ cells where the

limiting current disappeared above 700°C, indicating a change in the mechanism for the reaction at the electrode/electrolyte interface. Above this temperature, platinum oxide is unstable and its decomposition would therefore decrease the interface resistance (increase the exchange current density, see equations 3.20, 3.21), causing the limiting current to dissappear.

In conclusion, the model for oxygen adsorption on the platinum electrodes accounts for the exchange current density versus oxygen partial pressure data; the heat of adsorption/desorption of oxygen on the platinum electrode used in this study was about 53 kcal/mole; and at temperatures below about 600°C, platinum oxide probably formed on the surface inhibiting the reactions at the electrode/electrolyte interface.

3.3 SURFACE TITRATIONS

3.3.1 Results

The results for the first set of data taken at 477 C on platinum prepared from Engelhard #A-3788 are shown in figure 3.10. The reactor was exposed to air for 1, 2, 5, 10, 50 or 100 minutes and then flushed with helium for 1 to 6 minutes. After switching to ethylene, the concentration of CO_2 released by reaction between the gas phase ethylene and the oxygen adsorbed on the surface was recorded continously by the CO_2 analyser (see figure 2.7). The amount of CO_2 formed by the reaction was determined by integrating the peak with respect to time over a thirty minute period, the time required for all of the CO_2 to be released. The amount of CO_2 formed decreased exponentially with time of flushing in helium (figure 3.10). When the y-axis of moles of CO_2 released was converted to a log basis, linear plots of $\log(CO_2)$ versus flushing time in helium were obtained (figure 3.11). The rate of the decrease (the slope of the $\log(CO_2)$ versus time lines) also decreased inversely with the time of exposure to air.

The volume of the reactor was 30.2 mls and the flowrate was about 360 ml/min, resulting in a residence time of about 5.0 seconds. Assuming that the reactor behaived as a CSTR, 95% of the gas would change in three residence times, or 15 seconds, and complete turnover of the gas (99.995%) would occur in ten residence times or 50 seconds. One minute therefore constituted the minimum time required to completely flush the reactor. The amount of CO_2 that would have been formed had it been possible to not flush the reactor with helium was found by extrapolation back to zero time. Irrespective of the oxidation time used, this amount was about 8.05×10^{-6} mols.

Gas chromatographic analysis of the gas eluting from the reactor during the CO_2 peak showed there to be only CO_2 and ethylene in the diluent

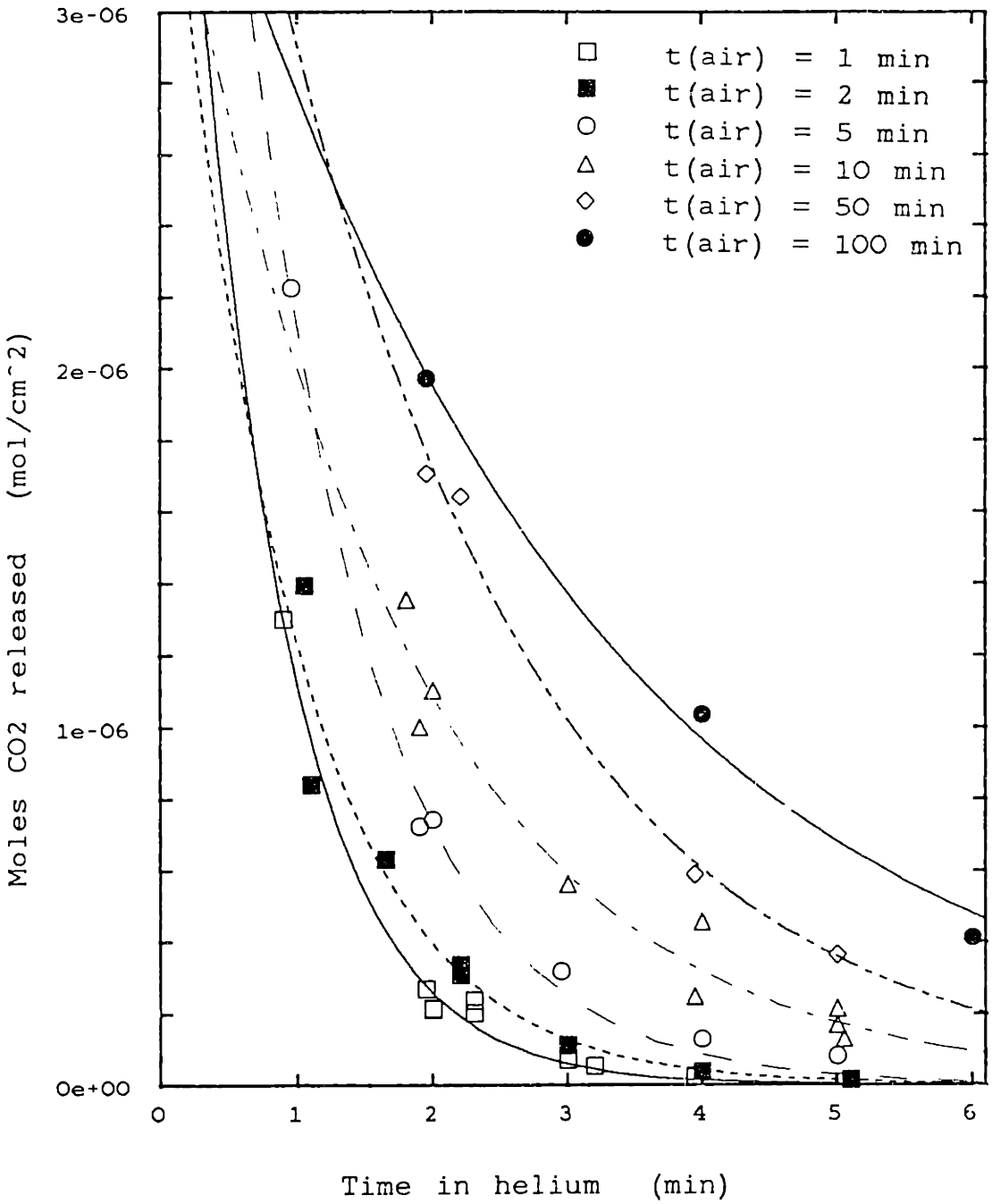

Figure 3.10: Titration of surface oxygen with ethylene, versus time for flushing surface in helium; closed-end tube reactor, T=477°C

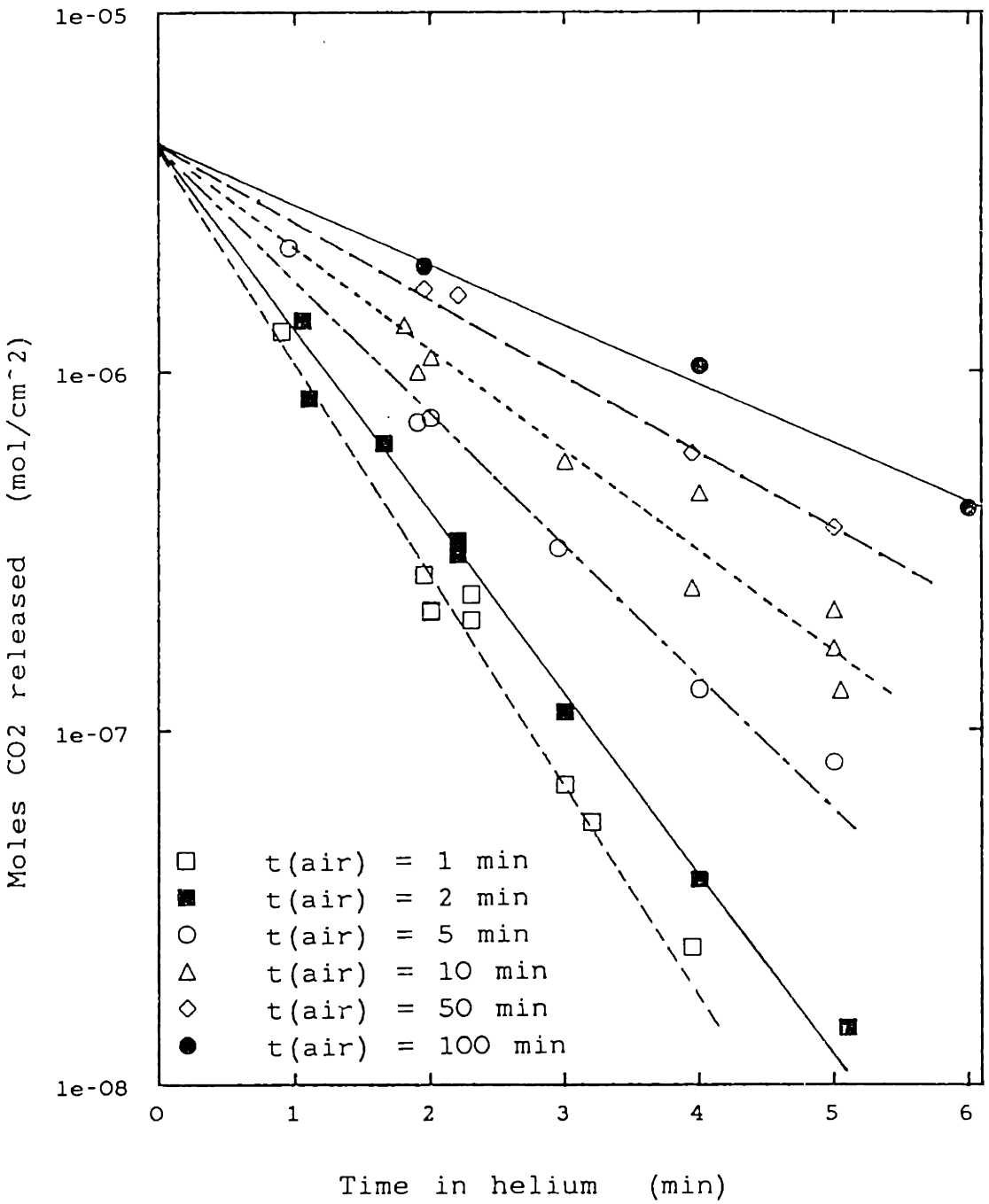

Figure 3.11: Titration of surface oxygen with ethylene (replot)

helium. No CO, which would have formed from partial combustion of the ethylene, was observed. No molecular oxygen was observed, indicating that once exposure to ethylene had occurred, no further desorption of oxygen occurred.

There is some scatter in the data of figures 3.10 and 3.11. The scatter in the y-axis, the amount of CO_2 released, arose from the difficulty of re-establishing the exact location of the base line of the CO_2 output after the peak, since it approached zero output assymptotically. Minor variations in the base-line would produce significant errors over the thirty minute integration period. Some scatter was also present in the times for oxidation and desorption because of lag time between switching the valves and complete flushing of the old gas from the reactor. Although the initial change in the cell voltage, which occurs when the gases are switched, was used to indicate the change of gas (see figure 2.7), some irreproducibility ($\pm$0.2 min) was still present in the times, because the initial change may not necessarily have coincided with complete removal of the displaced gas.

The shape of the CO_2 elution peak was not identical throughout these experiments. When the reactor was exposed to air for only a short time, the CO_2 eluted faster than when longer oxidation times were used (figure 3.12). The rate of CO_2 elution was quantified in terms of the width of the CO_2 peak at one half of its maximum height (PWHM). This was independent of the time used to flush the reactor with helium but increased with the time of oxidation of the surface in air from 2.17 minutes for 1.2 minutes pre-oxidation to about 2.9 minutes for ten or more minutes oxidation. Specifically, the PWHM's were: 2.17 ($\pm$0.12), 2.43 ($\pm$0.07), 2.52 ($\pm$0.08), 2.90 ($\pm$0.14), 2.88 ($\pm$0.11) and 2.88 ($\pm$0.28) minutes for 1.2, 2.0, 5.0,

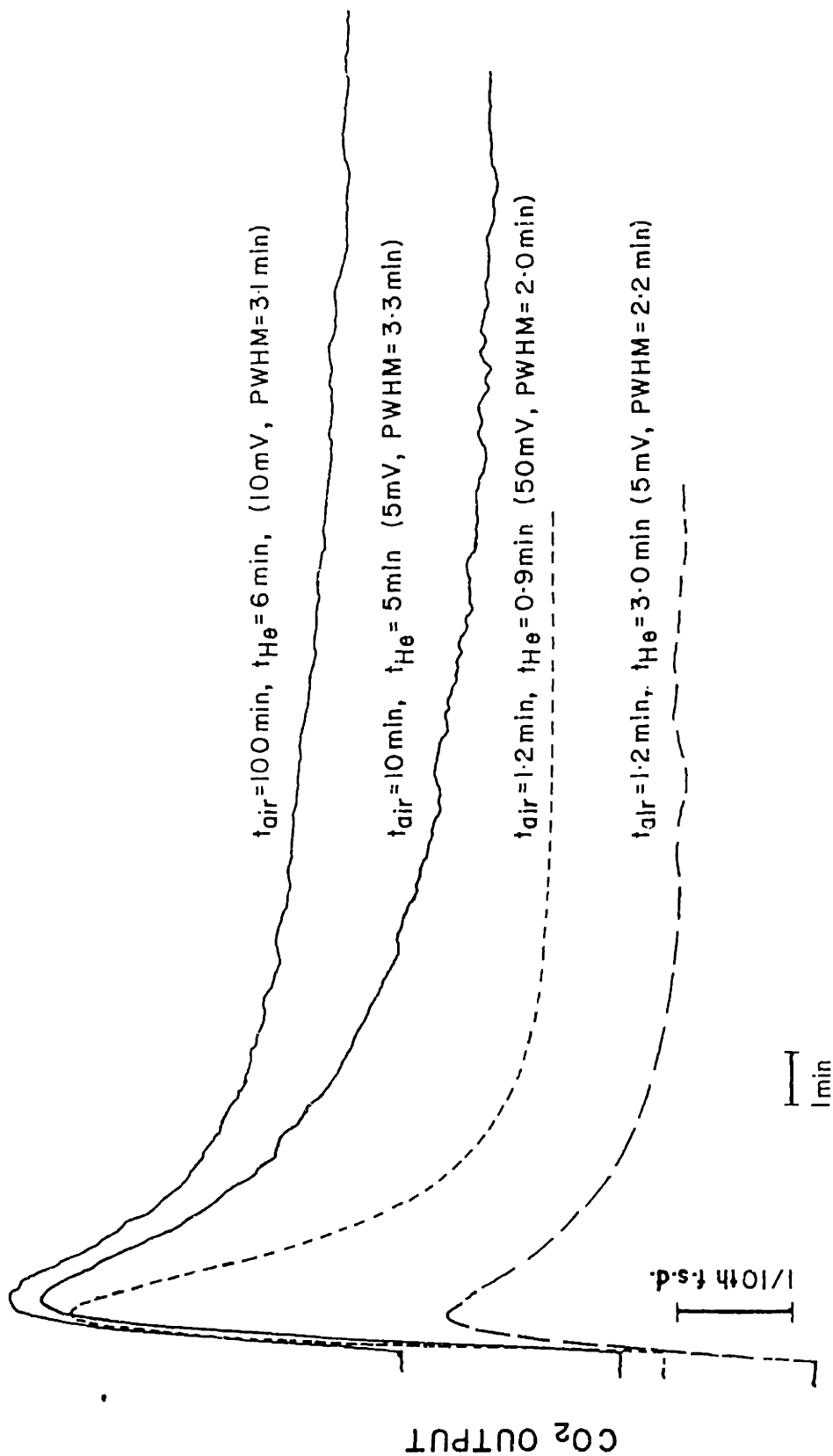

Figure 3.12: CO_2 elution peaks for different pre-oxidation times, different He flushing times, T=477°C

10.0, 50.0 and 100 minutes pre-oxidation in air, respectively.

The second set of titration data were taken with the annular reactor and using CO as the reducing gas. The raw data are shown in figure 3.13. When plotted on $\log(CO_2)$ versus linear flushing-time in helium basis, the data for 423, 477, 523 and 577°C all have linear responses, but with different y-axis intercepts (figure 3.14). The y-intercept increases from 423 to 523°C and then decreases slightly for 577°C. When the annular reactor was operated without the recycle pump, two peaks were observed in the CO_2 output from the reactor (figure 3.15). The first apparently being narrow and the second eluting more slowly and tailing significantly.

3.3.2 Discussion

According to Vayenas, Lee and Michaels (1980), the oxidation of ethylene in the presence of oxygen occurs by an Eley-Rideal mechanism between dissociatively adsorbed oxygen and gas phase ethylene. In the first data set, using ethylene as the reducing gas, gas chromatographic analysis showed no other components besides CO_2 and ethylene in the CO_2 product peak. It seems reasonable to assume that all the oxygen that had been adsorbed on the platinum surface was converted into carbon dioxide and water according to:

$$6\ O(a) + C_2H_4(g) \longrightarrow 2\ CO_2 + 2\ H_2O \qquad (22)$$

Therefore 1 mole of CO_2 would have formed for every three moles of O that had been on the surface, and it is possible to convert the y-axis of figure 3.10 to moles of oxygen on the surface by simply multiplying each number by three.

Irrespective of the oxidation time used, the amount of oxygen that was on the surface at zero flush time in helium was the same, about 2.4×10^{-5} mols. According to Engel and Ertl (p7, 1979), the density of surface atoms

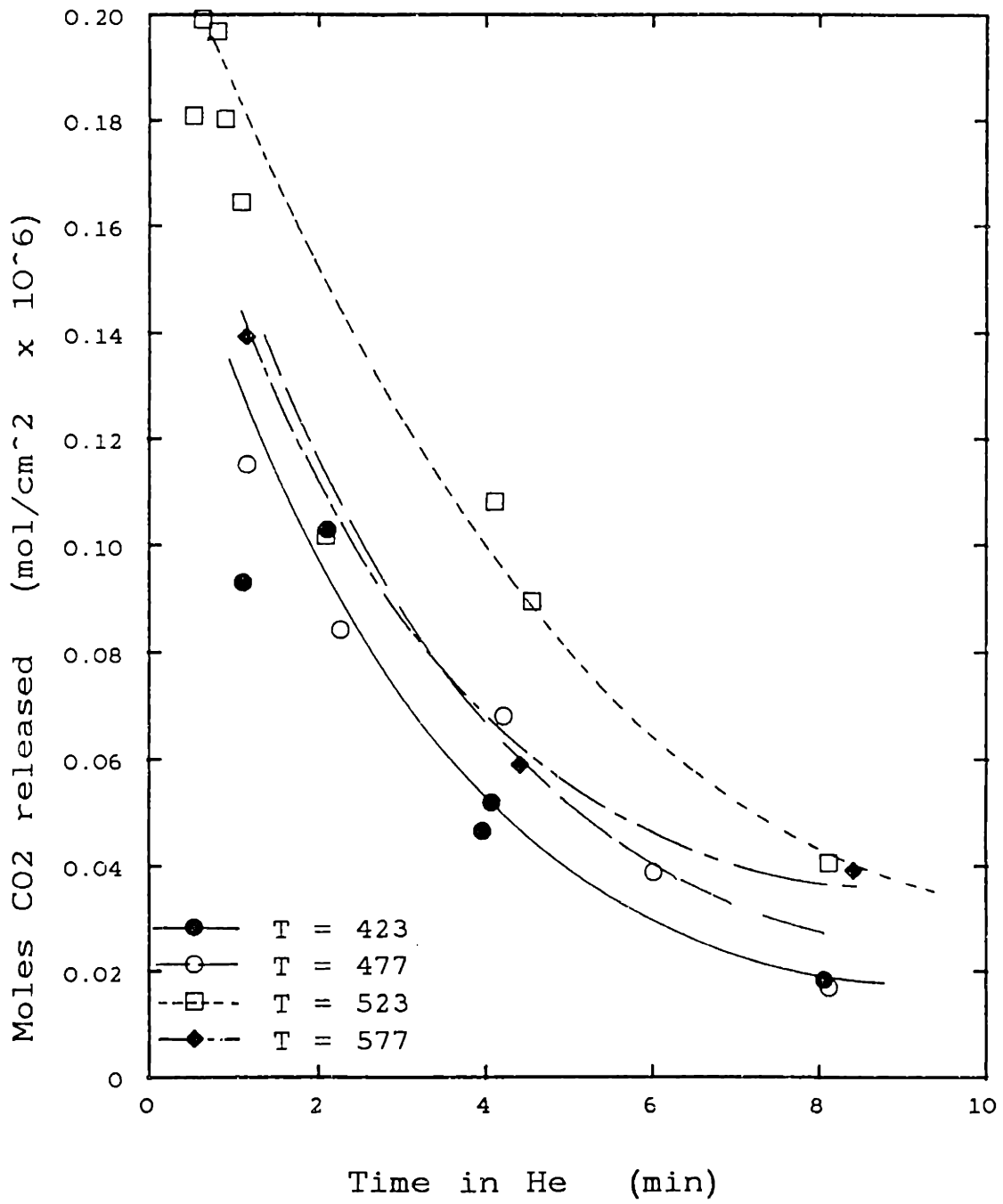

Figure 3.13: Titration of surface oxygen with CO versus helium flushing time for surfaces pre-oxidized for 4 min.; annular reactor

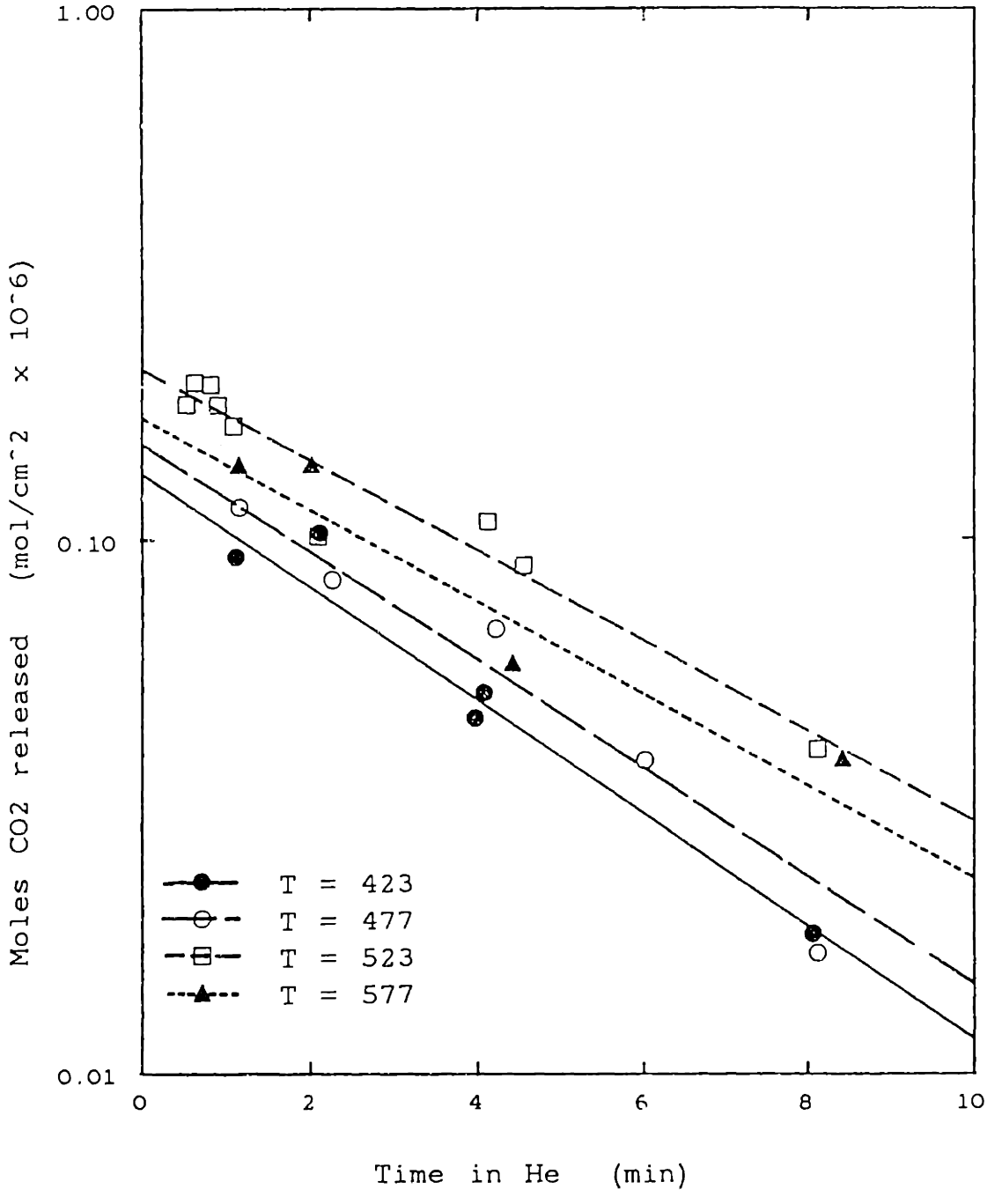

Figure 3.14: Titration of surface oxygen with CO (replot)

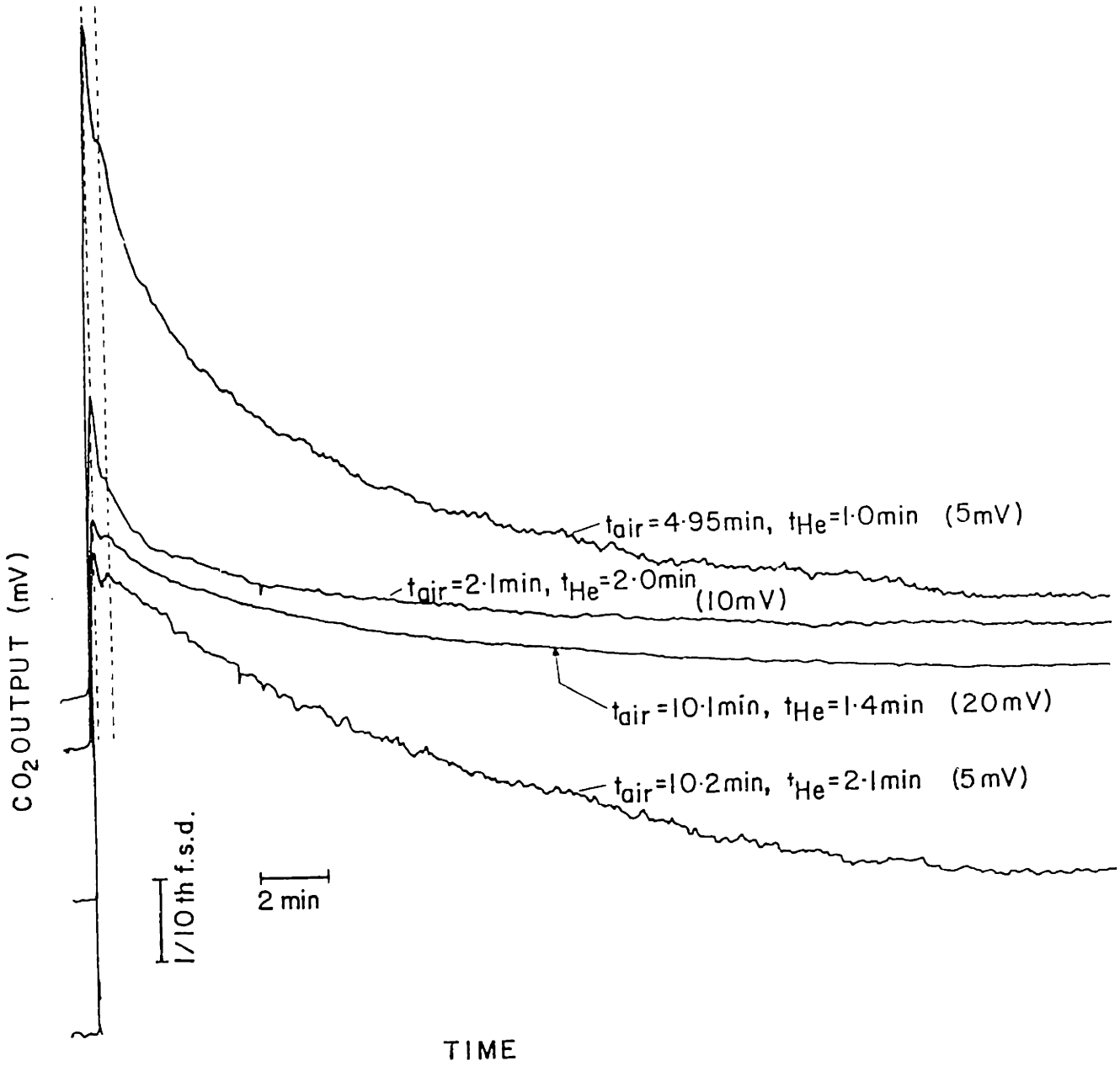

Figure 3.15: CO_2 elution peaks for annular reactor without recycle pump; T=477°C (voltage in brackets=mV full scale; 1000mV=2.5% CO_2)

for the Pd (111), (100), (110), (210) and (311) faces are 1.53, 1.33, 0.94, 0.80 and 0.53 x 10^{-15} cm^{-2} respectively. Assuming that there is one oxygen atom per Pt atom, that the surface density of platinum is similar to that of palladium and that 1.0 x 10^{-15} cm^{-2} is a reasonable average value, the surface area of this reactor was about 2.9 m^2.

3.3.3 Modelling the Desorption

Above 100 K oxygen adsorbs dissociatively (Gland, Sexton and Fisher, 1980):

$$O_2(g) + 2 \text{ sites} \underset{k_d}{\overset{k_a}{\rightleftharpoons}} 2\ O(a) \qquad (23)$$

If the data in figures 3.10 and 3.13 were due simply to the reverse of this reaction, then the rate of desorption would have been proportional to the square of the amount of oxygen on the surface:

$$\frac{d[O(a)]}{dt} = k_d\ [O(a)]^2 \qquad (24)$$

or, upon integration:

$$1/[O(a)] = 1/[O(a)]_i - k_d t \qquad (25)$$

Experimentally, equation (25) implies that $1/CO_2$ versus flush time in helium should have been linear; not log CO_2 versus time, as was observed. Furthermore, according to this model, the slope of the desorption curve would not be dependent on the pre-oxidation time. It therefore appears that the controlling mechanism is not, exclusively, the desorption of oxygen from the surface.

3.3.3.1 Model Hypothesis

In terms of the equilibrium for oxide formation (figure 1.1), at 477°C and one atmosphere air (21 kPa oxygen), platinum oxide should be stable and

would therefore be expected to form on the Pt electrode. When the gas is switched to helium, the oxygen partial pressure dropped to about 10^{-8} atmospheres. Under these conditions, the oxide is unstable and would be expected to decompose.

It may be hypothesised that after the reactor had been exposed to air for long periods of time, that the CO_2 released on exposure to ethylene came from the reaction of ethylene with oxygen that had been adsorbed on the surface in the form of an oxide. When flushing with helium, the rate controlling step would have been the reverse of the oxide formation reaction, with the oxide decomposing back to chemisorbed atomic oxygen, which in turn desorbed rapidly. In contrast, when the reactor had been exposed to air for only short periods of time, the CO_2 may have come from oxygen dissociatively chemisorbed on the surface. During flushing with helium, the rate controlling step would then be the desorption of chemisorbed oxygen.

This hypothesis would explain the doublet observed in the CO_2 output for the annular reactor with no recycle pump, since the first peak would have come from the chemisorbed oxygen and the second from the oxide decomposition. It is likely that chemisorbed oxygen would desorb more rapidly than oxygen in the form of an oxide.

The increase of the "peak width at half maximum" (PWHM) with increasing oxidation time for the closed-end tube reactor would also be explained by this hypothesis. In this reactor, all the data were taken with the recycle pump in place, therefore if two CO_2 peaks had been released, they would have been summed together. However, for short pre-treatment times in air, the CO_2 output would have contained a greater fraction of the chemisorbed oxygen (with its faster kinetics for reaction

with oxygen) and therefore exhibit a smaller PWHM value. When the reactor was exposed to oxygen for longer periods of time, the majority of the CO_2 output would have been due to the oxide (with its slower kinetics for reaction with ethylene) and therefore exhibit a larger PWHM value. Experimentally, the PWHM value increased from 2.17 min for 1.2 minutes pre-treatment in air to about 2.9 mins for pre-treatment in air for 10 or more minutes. Since the PWHM remained constant for oxidation for more than ten minutes, it would appear that there is only a negligble amount of chemisorbed oxygen on the surface for these longer times.

As mentioned above, in the closed-end reactor at 477°C, different oxidation times all give the same concentration of oxygen on the surface when extrapolated back to zero flush time (zero minutes flushing in helium). This implies that equilibrium between oxygen in the gas phase and that adsorbed on the surface was probably reached in less than one minute, resulting in complete saturation coverage, either as chemisorbed oxygen or as an oxide. Further, the oxide formed is equivalent to that of the saturated coverage of adsorbed oxygen, irrespective of the oxidation time. One minute was the minimum time required to flush the gas phase oxygen from the reactor completely.

This is in agreement with the findings of McCabe and Schmidt (1976). They measured the saturation density of clean and oxidized platinum and found that although increasing the fraction of the surface that was oxidized decreased both CO and H saturation coverage on clean Pt, the **total** saturation coverage (from both the clean and oxidized Pt) remained constant. In other words, oxide formed on the same sites that had adsorbed CO and H and formed at the expense of the clean sites, while the total number of sites did not change.

3.3.3.2 Model Assumptions - oxidation in air for > 2 minutes

A model which is consistent with the titration data for pretreatment in air for long periods of time, has been developed and has the following assumptions:

(i) Oxygen adsorbs dissociatively on the platinum surface, and occupies a fraction of the surface, θ_O.

(ii) The adsorption/desorption of oxygen on the platinum surface is rapid and therefore the gas phase oxygen molecules and dissociatively adsorbed oxygen atoms are in thermodynamic equilibrium.

(iii) Pre-treatment in air occurs for a time t_{air}.

(iv) During pre-treatment in air, there is an excess of oxygen present and two adsorbed oxygen atoms react to form a platinum dioxide surface moiety, which consumes one site for oxygen adsorption, and a vacant site, which can be reused for oxygen adsorption; the fraction of surface occupied by oxide is θ_{oxide}.

(v) Flushing the reactor with helium occurs for a time t_{He}.

(vi) During desorption in helium, oxygen that has desorbed does not re-adsorb.

3.3.3.3 Model Formulation - oxide decomposition

The model based on these assumptions is formulated as follows:

adsorption/desorption

$$O_2(g) + 2 \text{ sites} \rightleftharpoons 2\ O(a) \tag{26}$$

if at equilibrium:

$$K_O P_{O2}^{1/2} = \theta_O/(1-\theta_{oxide}-\theta_O) \tag{27}$$

or:

$$\theta_O = \frac{K_O P_{O2}^{1/2}}{1 + K_O P_{O2}^{1/2}} (1 - \theta_{oxide}) \tag{28}$$

During pretreatment in air, platinum oxide forms on the surface:

$$2\ O(a) \xrightarrow{k_x} \theta_{oxide} + site \qquad (29)$$

When flushing the reactor with helium, the oxide that had formed during pretreatment in air decomposes by the reverse of equation (29):

$$\theta_{oxide} + site \xrightarrow{k_R} 2O(a) \qquad (30)$$

i.e.

$$\frac{d\theta_{oxide}}{dt} = - k_R\, \theta_{oxide}\, \theta_{vacant\ sites}$$

$$= - k_R\, \theta_{oxide}\, (1 - \theta_{oxide} - \theta_0)$$

applying equation (27):

$$= - k_R'\, \theta_{oxide}\, (1 - \theta_{oxide}) \qquad (31)$$

$$\text{where:} \quad k_R' = k_R \frac{1}{1 + K_0 P_{O2}^{1/2}} \qquad (32)$$

$$\approx k_R \text{ at low } p_{O2}$$

integrating:

$$\ln \frac{\theta_{oxide}}{(1-\theta_{oxide})} = - k_R' t + \text{const.} \qquad (33)$$

boundary condition: $t=0,\ \theta_{oxide} = \theta_{oxide,i}$

therefore:

$$\ln \frac{\theta_{oxide}}{(1-\theta_{oxide})} = \ln \frac{\theta_{oxide,i}}{(1-\theta_{oxide,i})} - k_R' t \qquad (34)$$

The data from figure 3.11 were converted from mols CO_2 to moles of oxygen on the surface (using equation (22), above) and plotted according to equation (24) (figure 3.16). As can be seen, the model fits the data well for oxidation times in air of 5 minutes and more, all having the same slope and with increasing intercepts with oxidation time.

The value of k_R' is given by the slope of the lines in figure 3.16 and

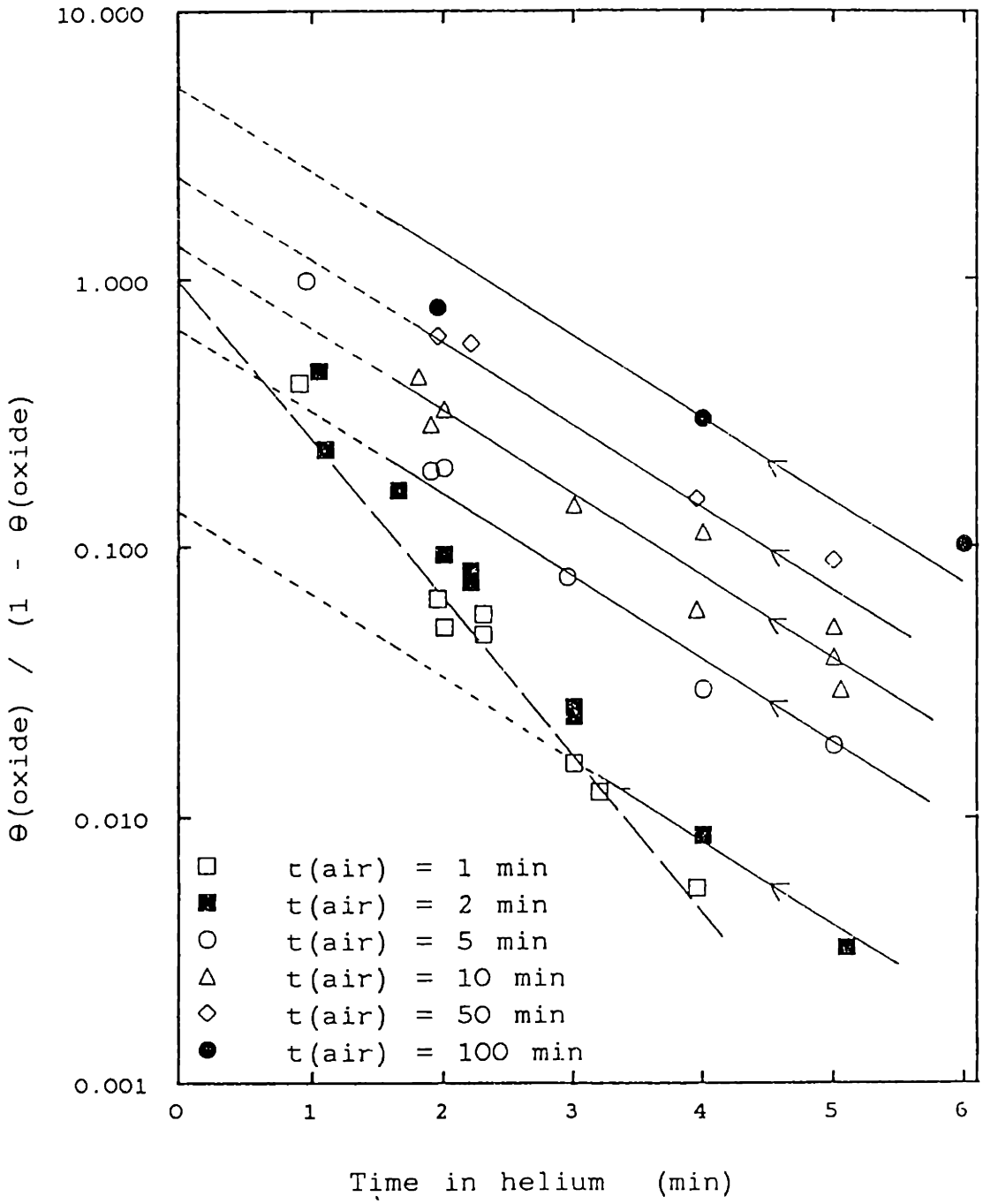

Figure 3.16: Replot of surface titration data according to oxide decompostion model. Closed-end tube reactor, T=477°C

is 0.72 min^{-1}. At low p_{O2} $k_R' \approx k_R$ and therefore the rate constant for oxide decomposition is about 0.72 min^{-1}.

The validity of this approximation was ascertained by flushing the reactor with helium for over 100 minutes, until a steady state voltage, of 0.209 volts, was reached between the inner and outer electrodes. Since there are no interfering gases, the cell voltage can be related to the oxygen partial pressure by the Nernst Equation (1.31):

$$V_{cell} = \frac{RT}{4F} \ln \frac{p_O^2}{0.21} \qquad (1.31)$$

This voltage therefore corresponds to an oxygen partial pressure of 5.1 x 10^{-7} atm. This residual oxygen concentration probably arose from imputities in the helium or from leaks into the reactor. The equilibrium constant for adsorption/desorption of oxygen, K_O, on similar platinum sponges was determined in section 3.2 (by extrapolation of figure 3.8) to be about 118.3 $atm^{-1/2}$ at 477°C. Therefore according to equation 11, above:

$$k_R' = 1/(1 + K_O p_{O2}^{1/2})\, k_R$$

$$= 0.922\, k_R$$

therefore the rate constant for oxide decomposition is about 8% higher than for k_R', or 0.78 min^{-1} or 1.30 x 10^{-2} s^{-1}.

This value for the rate of oxide decomposition agrees reasonably well with the data of Turner and Maples (1984). They measured the weight gain by platinum powders in a Cahn balance when oxidized at temperatures between 160 and 360°C. When their data are extrapolated to 477°C (the temperature used here), their data would indicate an oxide formation rate constant of about 7.3 x 10^{-3} s^{-1}, which compares reasonably well with the value reported here of 1.30 x 10^{-2} s^{-1}.

3.3.3.4 Analysis of Experimental Observations

This model can also explain the original plot of the data (figure 3.11) of linear $\log(CO_2)$ versus time, with decreasing slopes for increasing oxidation times, because the figure may be expressed mathematically as:

$$\ln CO_2 = [\ln CO_2]_{t=0} - k_2 t \tag{35}$$

Now, assuming that the CO_2 arose from the oxide and adsorbed oxygen (equation 22), and that at zero flush time there is complete coverage of all of the surface sites, then equation (35) becomes:

$$\ln(\theta_0 + \theta_{oxide}) = [\ln(\theta_0 + \theta_{oxide})]_{t=0} - k_2 t$$

$$= k_2 t \tag{36}$$

For t_{air}>2.0 minutes, chemisorbed oxygen contributes negligibly, therefore equation (36) becomes:

$$\ln (\theta_{oxide}) \approx k_2 t \tag{37}$$

Equation (37) is the integrated form of the differential equation:

$$\frac{d\theta_{oxide}}{dt} = - k_2 \theta_{oxide} \tag{38}$$

with the boundary condition that θ_{oxide}=1 at t=0.

If equation (38) for the experimental data is compared with equation (21) from the model, then k_2 can be expressed as:

$$k_2 = k_R' (1 - \theta_{oxide}) \tag{39}$$

Since θ_{oxide} increases with pre-treatment time in air (equation (29), then, according to equation (39), k_2, the slope of the experimental $\log(CO_2)$ versus time plot, must decrease with pre-treatment time. This was observed in figure 3.11.

The plots in figure 3.11 are linear because although θ_{oxide} changes more than an order of magnitude, $(1-\theta_{oxide})\approx 1$ and so remains constant and can therefore be incorporated in the constant k_2.

3.3.3.5 Desorption after oxidation of less than two minutes

In figure 3.16, the data for an oxidation time of 1.0 minute has a different slope from the other data and has a y-intercept of 1.0. The behavior is distinctly different from that at other oxidation times indicating that a change of mechanism must occur between the short and longer oxidation times. Thus the model described above would not apply to this data.

For an oxidation time of two minutes, the data (in figure 3.16) fit the oxide model, and have the required slope, only for helium flushing times above three minutes. For times less than three minutes, the data fall on to the same curve as the one minute oxidation data, i.e. for short oxidation times, the desorption is independent of oxidation time.

This result is consistent with the observations of Wilf and Dawson (1977) and McClellan, McFeely and Gland (1983) where they both reported TPD data indicating 2nd order desorption of oxygen at low coverages and 1st order at high coverages, over Pt(110) and Pt(321), respectively. Wilf and Dawson discussed the kinetics in terms of occupation of nearest neighbour sites; that when nearest neighbour sites are occupied desorption is 1st order. However, when the adsorbed oxygen is obliged to migrate across the surface, as is the case at low coverages, desorption is 2nd order.

3.3.3.6 Model Formulation - Oxidation of the platinum surface

An extension of the model for oxide decomposition describes the formation of the oxide layer during the pre-treatment in air. This model uses the same assumptions as the model for the oxide decomposition, except that it is assumed that under these conditions, the rate of oxide decomposition (equation 30) is many times slower than the rate for oxide

formation (equation 29) and therefore may be ignored.

Oxide formation, given by equation 29, is given by:

$$\frac{d\theta_{oxide}}{dt} = k_x \theta_0^2$$

applying equation (27):

$$= k_x \left(\frac{K_0 P_{O2}^{1/2}}{(1 + K_0 P_{O2}^{1/2})} \right)^2 (1 - \theta_{oxide})^2$$

integrating:

$$\frac{1}{(1-\theta_{oxide})} = k_x \left(\frac{K_0 P_{O2}^{1/2}}{(1 + K_0 P_{O2}^{1/2})} \right)^2 t_{air} + \text{const.}$$

boundary condition: $t_{air} = 0$, $\theta_{oxide} = 0$, therefore const.= 1

Using this boundary condition and rearranging:

$$\theta_{oxide} = \frac{k_x \left(\frac{K_0 P_{O2}^{1/2}}{(1 + K_0 P_{O2}^{1/2})} \right)^2 t_{air}}{1 + k_x \left(\frac{K_0 P_{O2}^{1/2}}{(1 + K_0 P_{O2}^{1/2})} \right)^2 t_{air}} \qquad (40)$$

or inverted:

$$\frac{1}{\theta_{oxide}} = 1 + \{1 / k_x \left(\frac{K_0 P_{O2}^{1/2}}{1 + K_0 P_{O2}^{1/2}} \right)^2 t_{air}\} \qquad (41)$$

The values for θ_{oxide} at zero helium flushing times were determined from the y-axis intercepts of figure 3.16 and are plotted according to equation (41) in figure 3.17. Again, the data for oxidation times greater than 5 minutes ($1/t_{air} \leq 0.2$ min^{-1}) fit the model well, being linear in time. Since oxide formation is probably not the rate determining step for exposure to air for only 1 and 2 minutes, the data for these times do not fit the model.

The rate constant for platinum surface oxidation can be determined from the slope of figure 3.17 and applying equation (41). If we assume

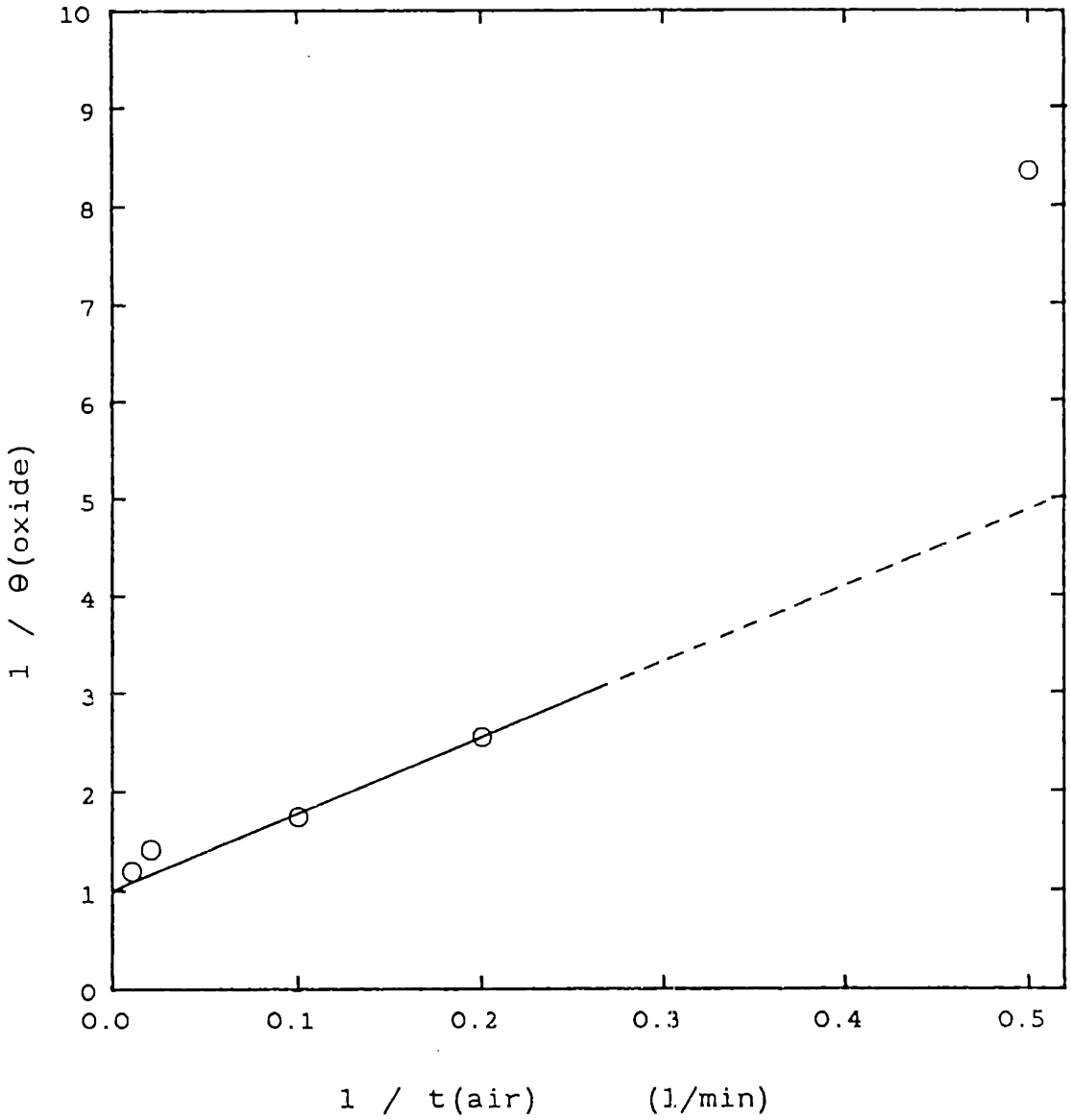

Figure 3.17: Oxide formation of Pt on exposure to air; closed-end tube reactor, T=477°C

that $K_0P_{O2} >> 1$ (K_0 was found to be about 118 $atm^{-1/2}$ above and p_{O2} is 0.21 atm) then the rate constant for oxide formation is about 0.135 min^{-1} or 2.25×10^{-3} s^{-1}.

3.3.4 Activation Energy for Desorption

A second set of desorption data were performed using a reactor prepared with Pt ink #A-4338. These data were taken over a limited number of oxidation times, but over a wider temperature range, from 276°C to 523°C. Above 423°C the data followed linear log(CO_2) versus linear time curves similar to figure 3.11 (see figure 3.14). This is an important result because it indicates that the same behavior (of log CO_2 versus t_{He}) is observed in both the closed-end tube and annular reactors. This implies that this behavior is not an artifact of the reactor geometry or the platinum ink used (#3788-A versus #4338-A). However, the data for 423, 477, 523 and 577°C each had different intercepts with the y-axis. This implies that at zero flushing time, the surface concentration of oxide increased with temperature.

Below 423°C, log CO_2 versus time behavior was not linear, indicating that surface oxide formation, at least as described by the model above, is not the rate controlling mechanism. The data for temperatures below 423°C exhibited considerable scatter and no clear trend was discernable.

Assuming values for surface platinum density and O/Pt ratios as used for the data from the first set, the y-intercepts of figure 3.14 correspond to surface areas of 0.82, 1.04 and 1.33 m^2 for T=423, 477 and 523°C, respectively. These values are lower than that for the platinum surface prepared from ink #A-3788 (2.9 m^2) probably because of the larger particle size used in the second preparation, but also because a thinner film was

used (less coats of ink were applied). The increase in oxygen coverage, with temperature, before flushing with helium, taken from the y-intercepts of figure 3.14 has an apparent activation energy of 5.6 kcal/mole (figure 3.18). The model above is unable to account for this observation. A possible explanation is the formation of multilayers of oxide on the surface, or an increase in the solubility of oxygen in the platinum, near the surface.

Niehus and Comsa (1980) prepared samples of both chemisorbed and oxided platinum on a Pt(111) crystal in an ultra-high vacuum system. They confirmed the difference between the two states by shifts in the Auger spectra and their stability to heat treatment. When they performed low energy ion scattering, the spectrum for the oxidized Pt surface was identical to the clean Pt surface, with no oxygen observable. This, they concluded indicated that the first layer of the "oxide" surface consisted only of Pt atoms, and that the oxidation of the surface had led to oxygen atoms adsorbed beneath the surface platinum atoms. If this were to be the case then it would be reasonable to expect the amount of sub-surface oxygen to be temperature dependent and to increase with temperature, as observed.

Using the values for initial oxygen coverage obtained above, the application of the oxide decomposition model, equation (34), to this data yield a similar response for log $\theta_{oxide}/(1-\theta_{oxide})$ versus flushing time (figure 3.19), which lead to rate constants for the decomposition of the oxide of 0.401, 0.461 and 0.458 min^{-1} at 423, 477 and 523 C respectively. This implies an activation energy of only 1.6 kcal/mole (figure 3.18). The small size of this activation energy is somewhat surprising, but it does agree well with the data of Turner and Maples (1984) where they observed an activation energy for the reduction of platinum oxide by CO at a much lower temperature of 150-200°C, of also 0 ± 1 kcal/mole.

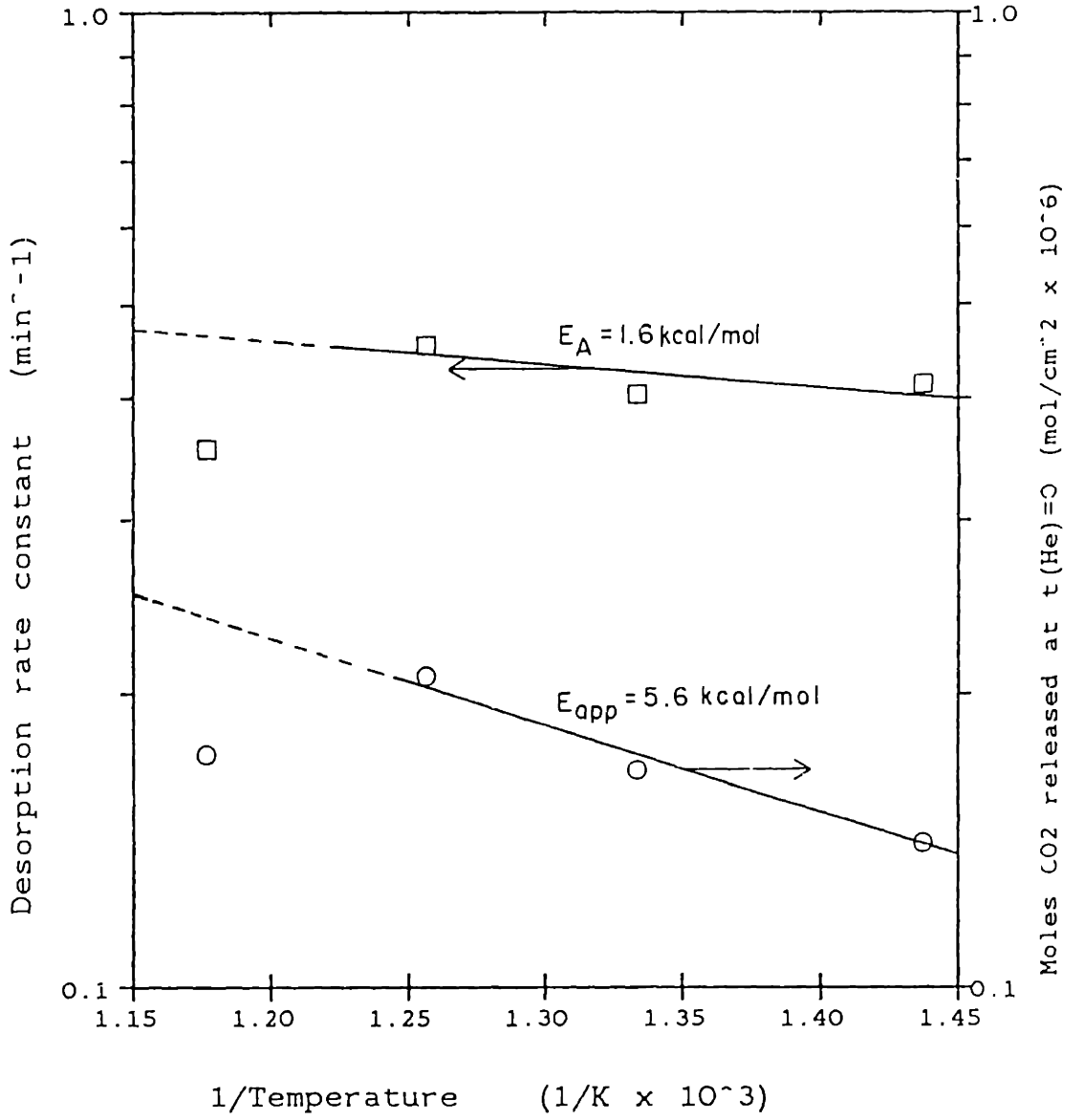

Figure 3.18: Arrhenius plot for oxide decomposition, and for amount of CO_2 released after zero time flushing reactor in He.

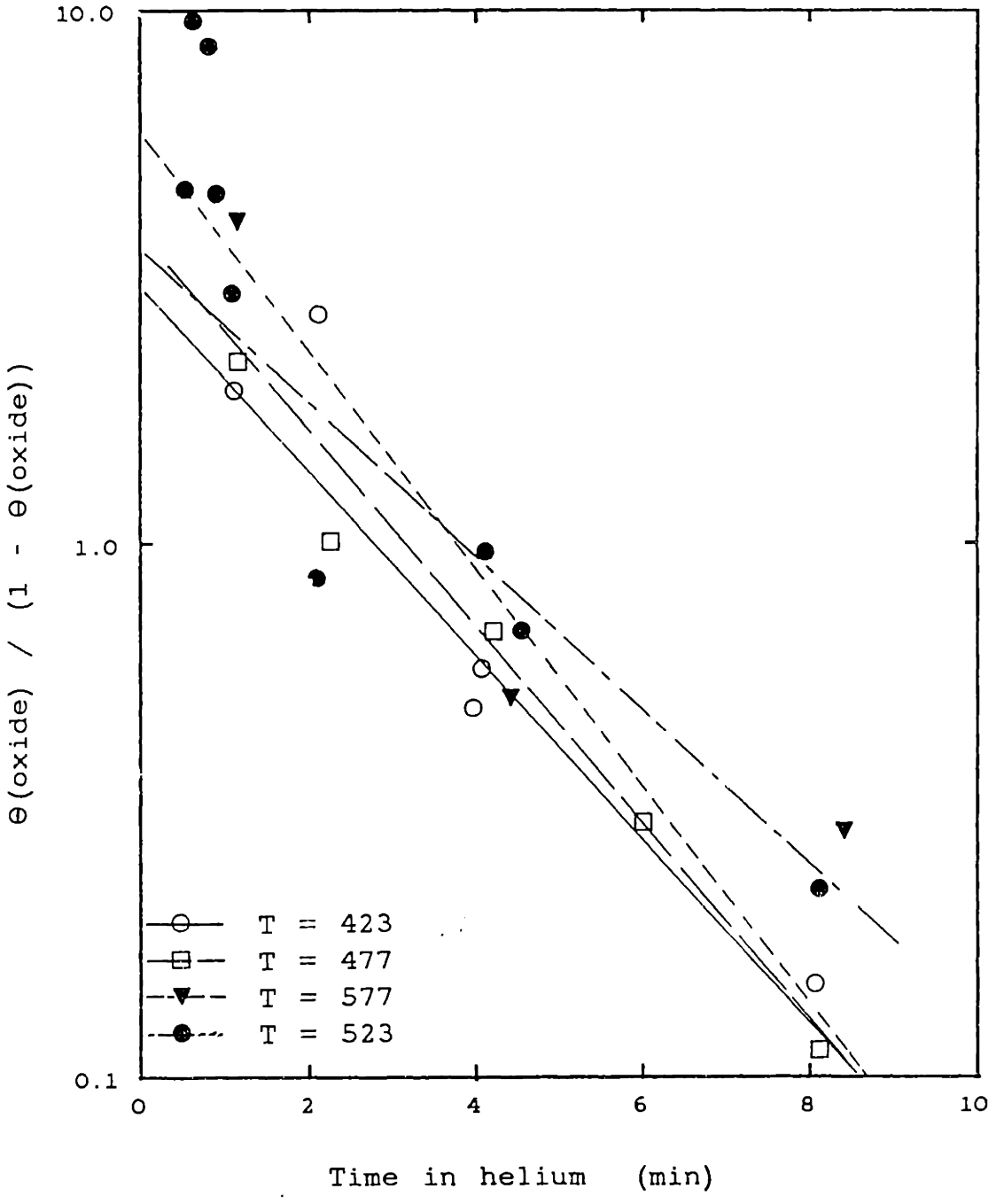

Figure 3.19: Replot of surface titration data according to oxide decomposition model; annular reactor, 4 min pre-oxidation.

3.4 CONCLUSIONS

3.4.1 Electrochemical Experiments

The **transfer coefficients** for the Tafel plot, log current versus applied current, of the zirconia-yttria electrochemical cell with platinum electrodes exposed to oxygen are 1.0 for reaction in both the forward and back directions. These values were used to model the electrochemical reaction of transfer of oxygen anions between the electrode and the electrolyte. Oxygen adsorbs dissociatively on the platinum electrode and acquires an electron form the Pt. The rate controlling step is the transfer of the O^- anion from the electrode into the electrolyte. Once in the electrolyte, the anion readily acquires a further electron to become O^{2-}, the stable anion in the electrolyte. At the anode, the reverse process occurs.

The **exchange current density** of the interface varied with $p_{O2}^{1/4}$ at low oxygen partial pressures and high temperatures. At low temperatures, high p_{O2}, it varied as $p_{O2}^{-1/4}$, which was in agreement with other reports in the literature. This behavior was modelled in as a Langmuir-Hinshelwood adsorption of oxygen on the platinum surface. The data were fitted to the model and yielded an enthalpy of adsorption of oxygen on the surface of 53± 5 kcal/mole (literature values vary between 48 and 68 kcal/mole).

At low temperatures, the exchange current density data deviated from the simple Langmuir-Hinshelwood model, probably because of the formation of a platinum oxide on the surface which would reduce the area available for oxygen adsorption.

3.4.2 Surface Titrations

After the platinum electrode had been pre-oxidized in air at 477°C, the reactor was flushed in helium for a specified time and then the oxygen remaining on the surface was determined by titration with ethylene or CO. During the helium flush, oxygen that had been adsorbed on the surface, desorbed by a first order mechanism, the rate of which decreased with increasing pre-oxidation times. This indicated that under these conditions the rate controlling step was not recombination of the oxygen molecule, since this would be a second order desorption process (as is observed in ultra high vacuum experiments). The desorption was successfully modelled by the decomposition of an oxide layer that would have been stable, and formed, during pre-oxidation, but unstable when flushing the reactor with helium. The rate controlling step for desorption being the reaction between an oxide moeity and a vacant site.

The decomposition was found to be approximately independent of temperature (activation energy=0±1 kacl/mole), whereas, the initial coverage of oxygen prior (found by extrapolation back to zero time for flushing the reactor in helium) increased with an apparent activation energy of about 6 kcal/mole. It is possible that oxygen exists as a sub-surface species, the concentration of which may increase with temperature.

4. OXIDATION OF 1-BUTENE OVER PLATINUM

4.1 RESULTS

4.1.1 Effect of Time on Stream

The activity and selectivity of the platinum catalyst in the annular reactor were recorded versus time on stream when exposed to 2.0% butene and 0.08% oxygen in helium (figure 4.1). The activity of the catalyst, for butadiene formation, increased during the first ten hours, was stable between ten and about one hundred hours, and then decreased beyond one hundred hours. In contrast, although the selectivity increased during the first ten hours, it remained constant beyond one hundred hours, even when the activity had decreased by more than 50%.

At the end of this run, the reactor was cooled to room temperature in the butene/oxygen/helium mixture. The gas was then switched to air and the reactor was temperature programed from room temperature to 730°C at about 67°C per hour. Above about 400°C, oxygen from the air reacted with carbon adsorbed on the platinum surface to form CO_2. The concentration of CO_2 in the effluent was recorded continuously using the in-line infra-red CO_2 analyser. The temperature was simultaneously recorded and is shown in figure 4.2 with the CO_2 concentration. The majority of the CO_2 was released between 460 and 560°C with the maximum at 520°C. By time the reactor had reached 700°C, the CO_2 released had decreased almost back to zero (figure 4.2). When the reactor was re-exposed to a gas mixture of 2.0% butene and 0.08% oxygen in helium, the same activity and selectivity as before were reached after a further 10 hours on stream. Over the course of the study, the catalyst was reactivated about 20 times with no net loss of catalytic activity.

On the basis of the above effects, all experimental data were taken

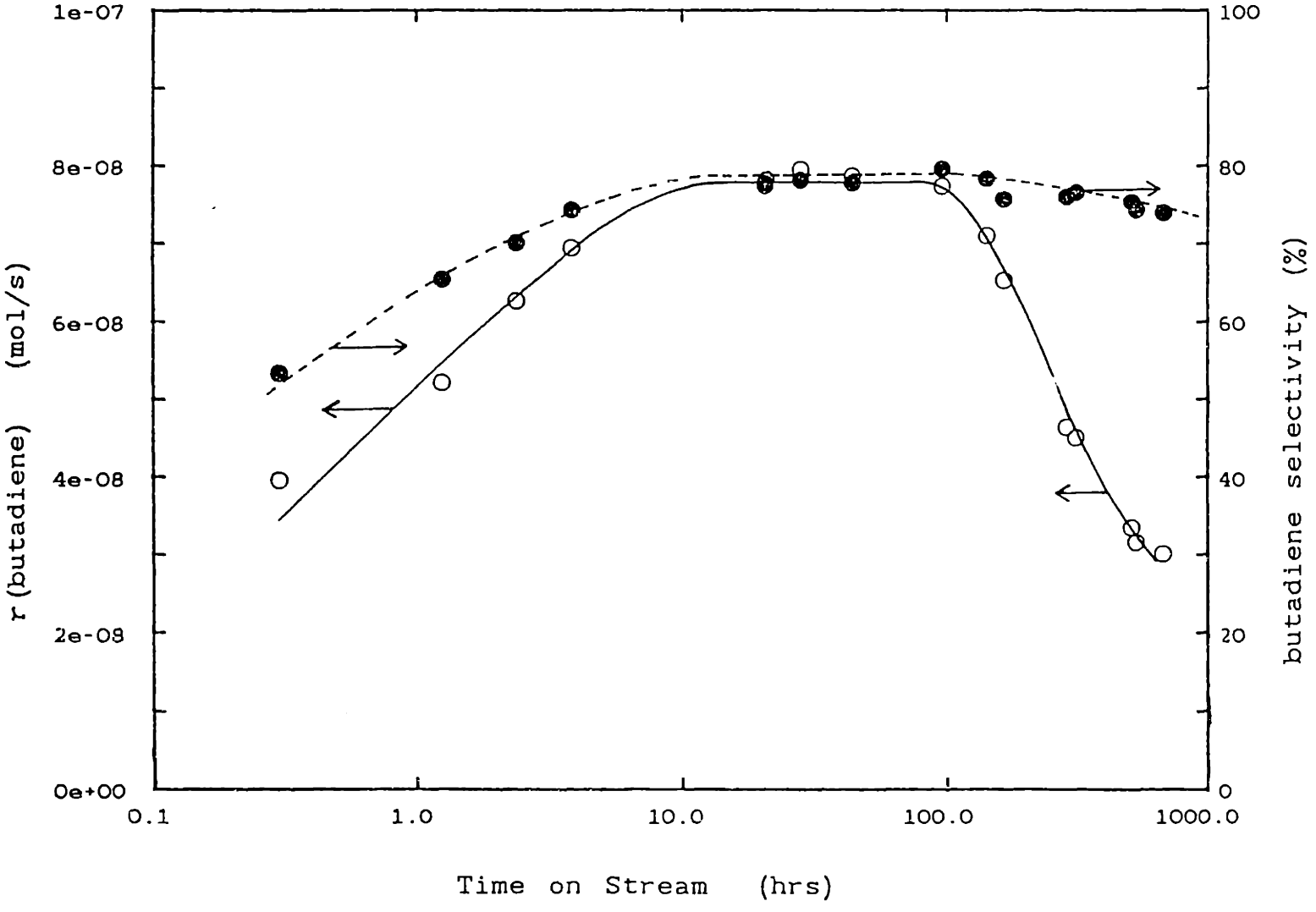

Figure 4.1: Effect of time on stream on activity and selectivity; annular reactor, T=513°C, p_{butene}=0.02 atm, p_{O2}=0.008 atm oxygen, τ=2.65 s

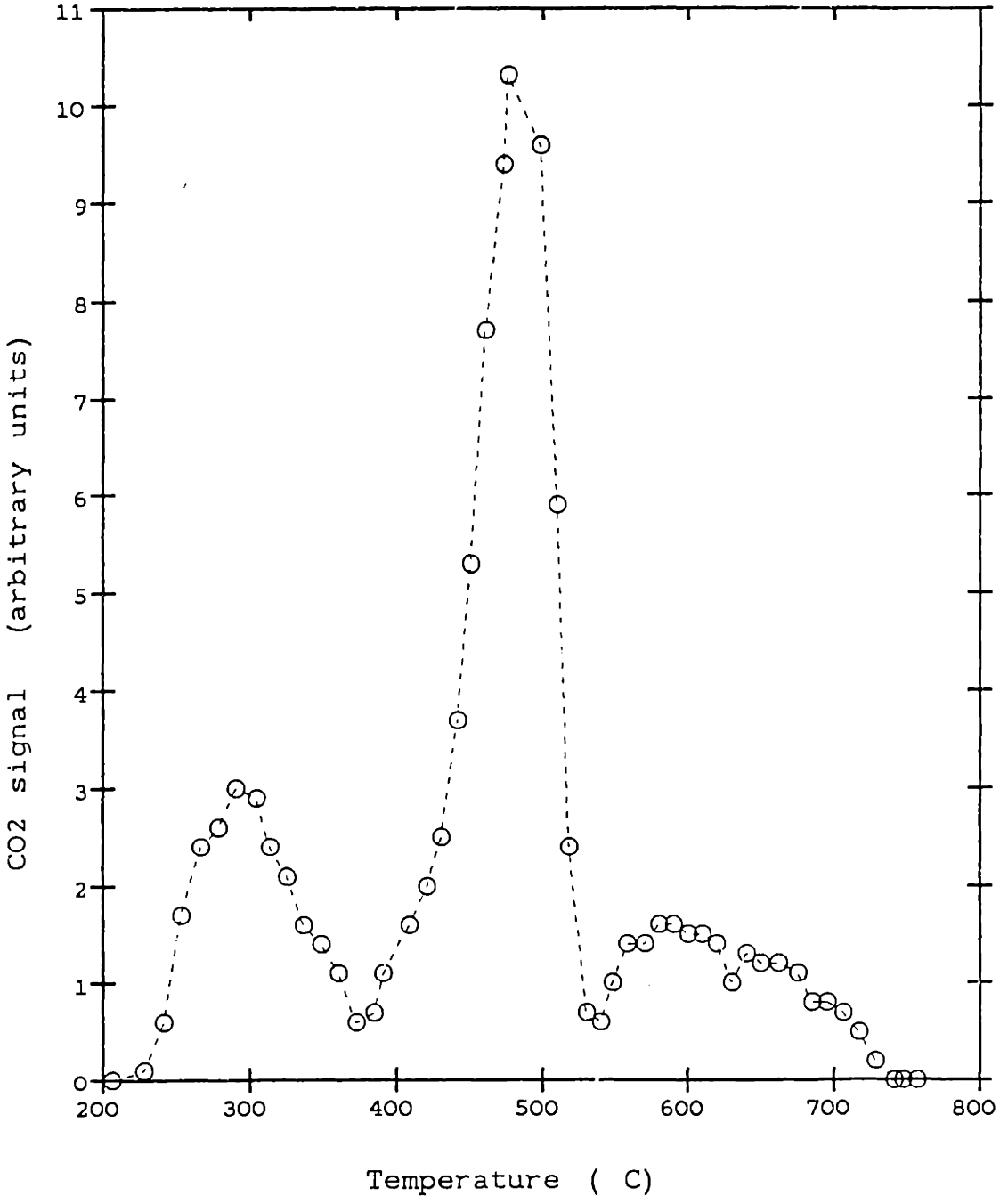

Figure 4.2: Temperature programmed oxidation of surface carbon

within one hundred hours of pre-treatment. Pre-treatment involved heating the reactor to 727°C (1000 K), in air, keeping it there for about two hours, then cooling it to the reaction temperature (466-544°C) in air before exposure to the reaction mixture. Also, all data, unless otherwise mentioned, were taken after the reactor had equilibrated in the reaction mixture for at least ten hours (and after less than one hundred hours on stream).

At the end of each period of taking data, the reactor was flushed with helium for two minutes to clear the reaction mixture from the reactor. The reactor was then exposed to a dilute stream of oxygen in helium (about 0.5%), causing carbon adsorbed on the surface to react with the oxygen forming CO_2, which was measured by integration of the CO_2 versus time peak. When the CO_2 response had returned to zero, the gas was switched to air and any extra CO_2 released was similarily measured and added to the previous amount. The amount of CO_2 released on exposure to oxygen increased primarily with the time the reactor had been on stream (figure 4.3), but also varied slightly with the particular reactor conditions at the end of the run. Thus, experiments in which the gas mixture had been particularily rich in oxygen had somewhat lower CO_2 outputs, and vice versa. Overall, the amount of CO_2 released increased in the first few hours on stream, remained approximately constant up to 100 hours and then increased linearly with time beyond this point.

Several samples of the CO_2 peak were redirected to the gas chromatograph for analysis. These samples contained only oxygen and CO_2, no desorbing hydrocarbons were detected, nor were any incompletely combusted products, such as CO, found.

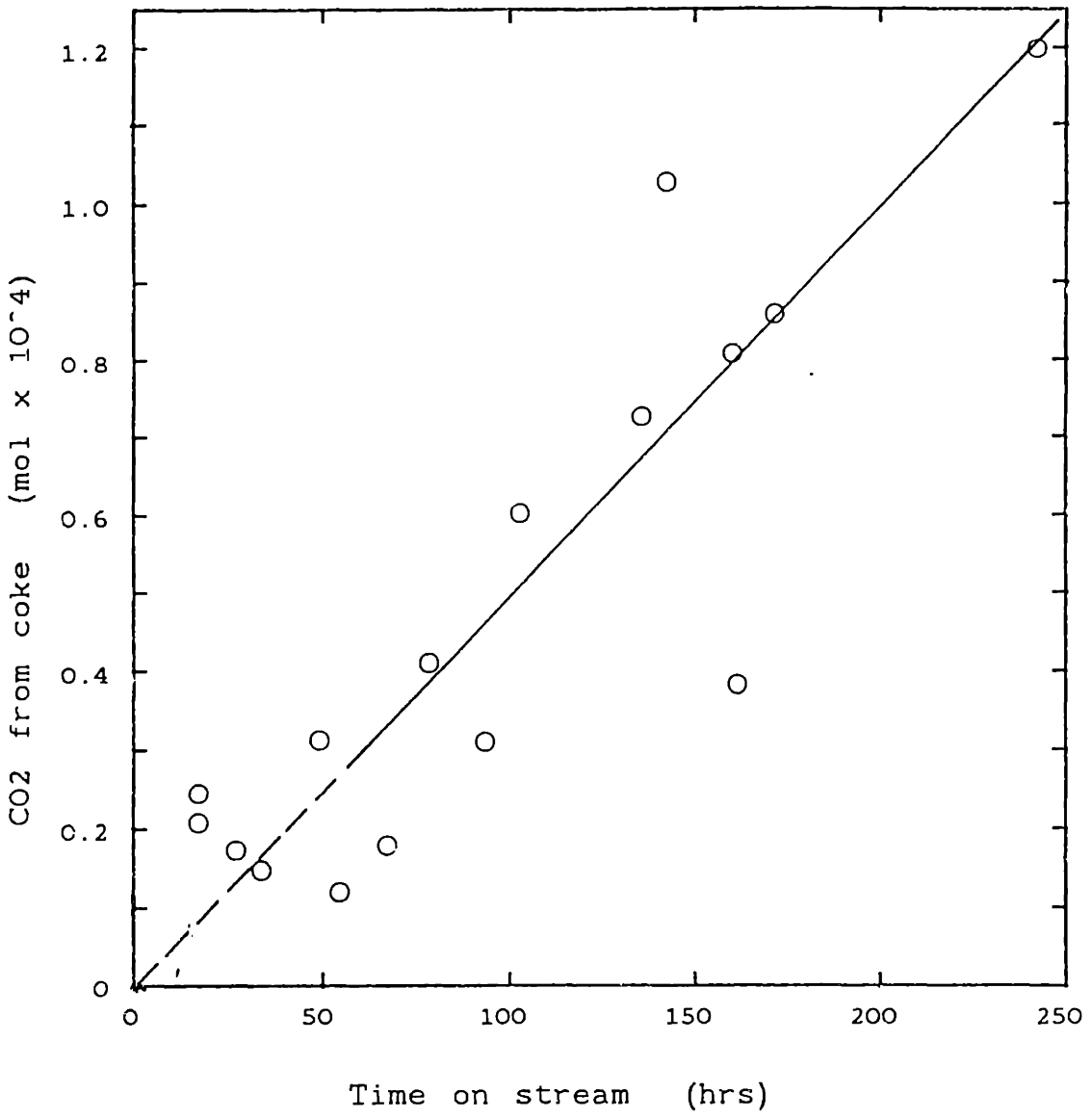

Figure 4.3: CO_2 formed from oxidation of surface carbon, versus time on stream.

4.1.2 Oxidation of Butene in a High Temperature Fuel Cell

The effect of using the reactor as a fuel cell for the oxidation of butene was investigated by applying a voltage across the cell and driving oxygen anions from the air, reference, side of the electrolyte, through the electrolyte to the inside where they could react with the butene over the platinum electrode/catalyst. The flow of oxygen anions in this direction is defined as a positive current.

When the reactor was at 477°C, and the reactor was fed with 1% butene in helium (no gas phase oxygen), application of a positive current caused the rate of deep oxidation (oxidation to CO and CO_2) to vary linearly with current (figure 4.4) At zero current, there was a slight dehydrogenation of butene to butadiene. Application of a current caused the rate of butadiene production to increase about 20% before becoming zero order in current. The rates of butene conversion, CO and CO_2 formation all varied linearly with current (flow of O^{2-} anions). Similar behavior was also observed at 513°C when using a similarily low concentration of oxygen in the gas phase (figure 4.5).

When the partial pressure of oxygen in the gas phase was increased and held constant at about 0.75%, when no current flowed, the rates of butadiene, CO and CO_2 production all more than doubled (figure 4.6). When current flowed in this case, a smaller increase in the rate of butadiene production was observed at low currents, but at high currents the rate of butadiene production was negative order, i.e. butadiene was consumed. The rates of CO and CO_2 production, which have been summed as a rate of "deep oxidation" in figure 4.6, still increased linearly with current. The rate of butene conversion, in this case, was not effected by the current.

When the current was reversed, and O^{2-} anions pumped from the electrode exposed to the butene-oxygen mixture to the air electrode, the

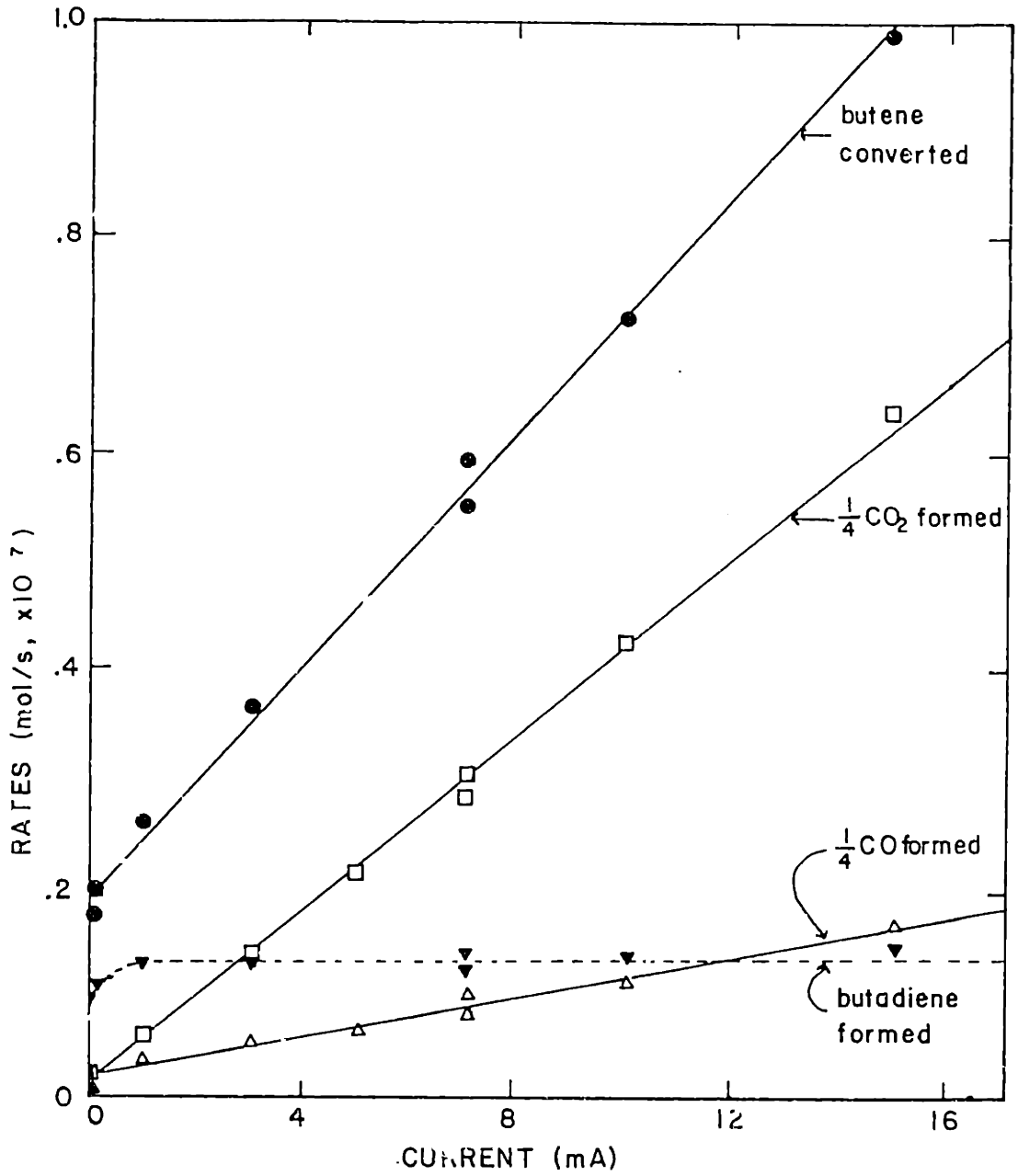

Figure 4.4: Rates of reaction versus applied current, P_{butene}=0.011 atm, P_{O2}=0, T=477°C

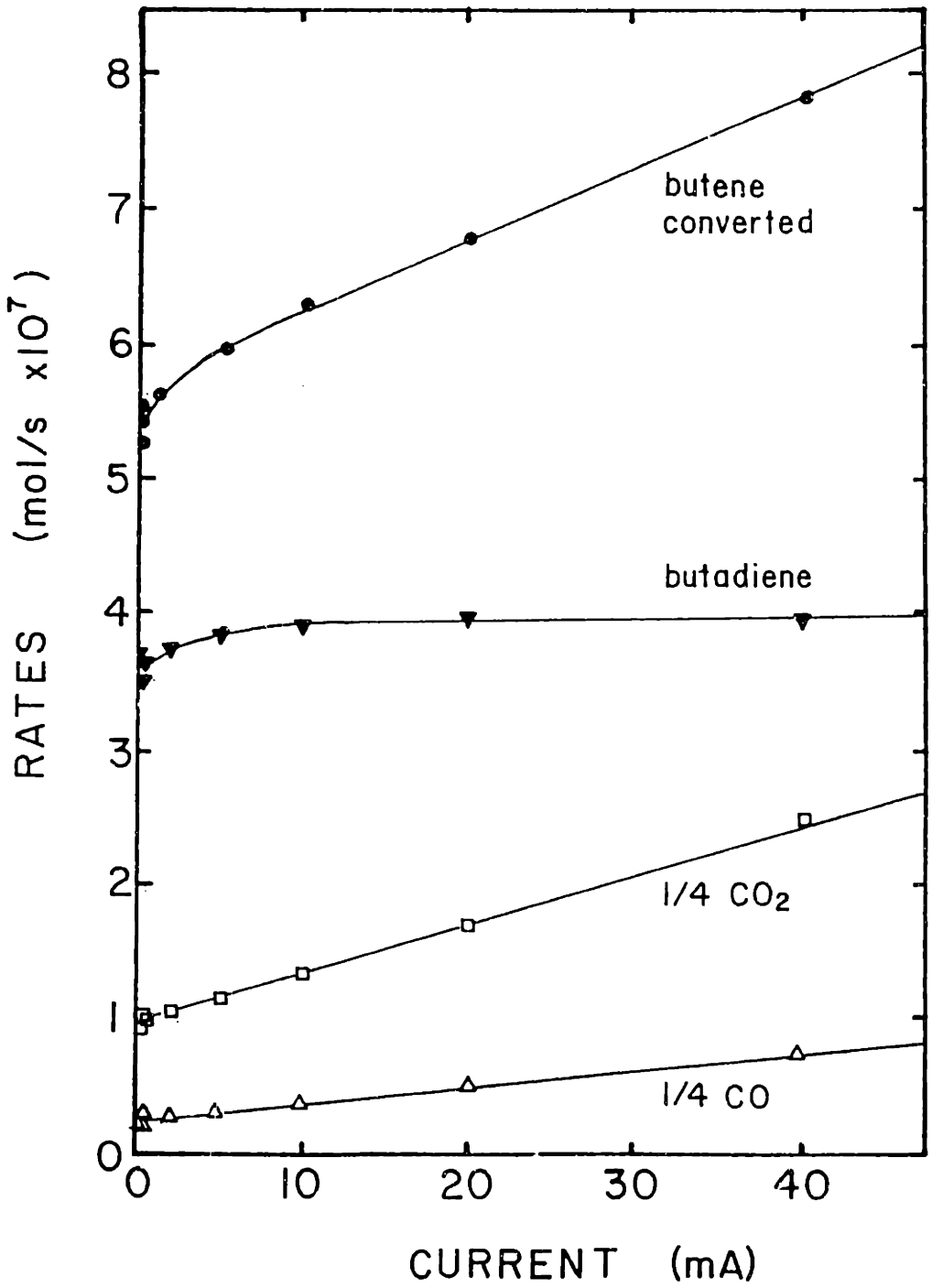

Figure 4.5: Rates of reaction versus applied current, p_{butene}=0.02 atm, p_{O2}=0.0015 atm, T=513°C

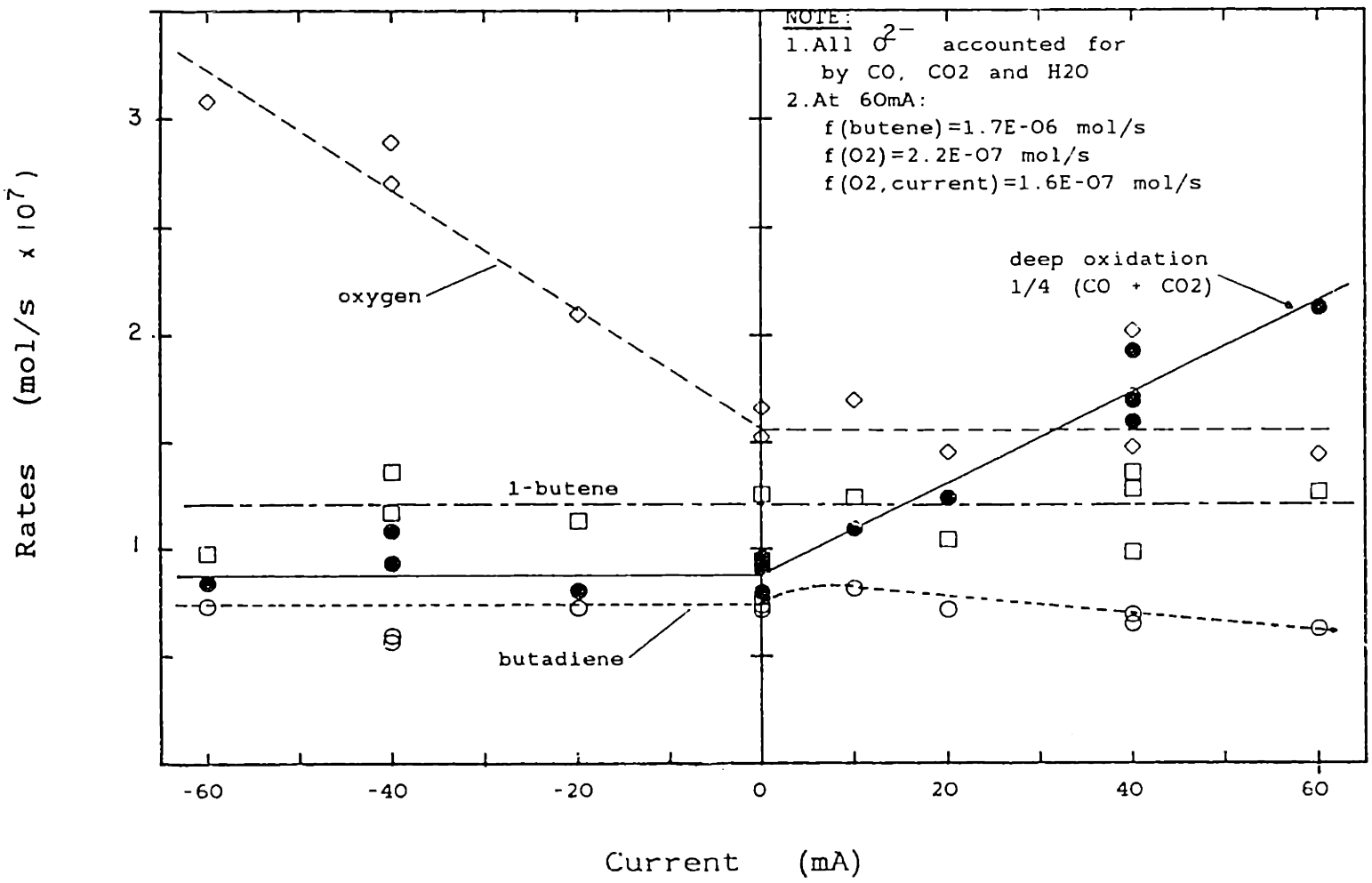

Figure 4.6: Rates of reaction versus applied current, P_{butene}=0.02 atm, P_{O2}=0.008 atm, T=513°C

rates of butene consumption and butadiene, CO and CO_2 production were all uneffected. Under these conditions, the partial pressure of oxygen in the exit stream decreased, and the feed of oxygen to the reactor had to be increased to maintain the exit conditions constant. The difference between the amount of oxygen fed to the reactor and the amount in the exit stream (the rate of oxygen consumption, since the reactor is a CSTR) was found to vary linearly with current.

Oxygen balances for the application of current are shown in table 4.1.

Table 4.1: Oxygen balances when current flows through electrochemical reactor; T=513°C, p_{O2}(gas phase) = 0.0075atm

Current (mA)	$f_{O2,\ elect.}$ x10^7 mol/s	r_{O2} x10^7 mol/s	ΣO_2 in prods	Δ (ΣO_2 in prods) / $f_{O2,\ elect.}$	Δ (r_{O2}) / $f_{O2,\ elect.}$
0	0	1.526	1.475	-	-
-20	-0.517	2.100	1.428	-.004	1.078
-40	-1.036	2.702	1.470	-.04	1.120
-60	-1.554	3.082	1.351	+.05	0.989
0	0	1.479	1.345	-	-
20	0.517	1.454	1.995	1.091	-0.17
40	1.036	1.477	2.449	0.984	-0.63
60	1.556	1.444	3.085	1.064	-0.63

$f_{O2,electr.}=ni/F=4i/96487$ (mol/s); $r_{O2}=f_{O2,feed}-f_{O2,exit}$ (mol/s)

$\Sigma O_{2,\ in\ prods} = r_{CO2} + r_{H2O}/0.5 + r_{CO}/0.5$ (mol/s);

Δ (value) = (value at i=0)-(value at i=i).

The flux of oxygen was related to the current via:

$$f_{O2,electrical} = n\ i\ /\ F \qquad (1)$$

where n is the number of electrons transfered per molecule (4 in the case of O_2), i is the current and F is Faraday's constant (96487 coulombs/equivalent). Columns 5 and 6 in table 4.1 are the oxygen balances for the cases of positive and negative currents, respectively. Their values are disributed about 1.0 indicating that all the oxygen that came through the electrolyte was accounted for and no free oxygen was produced (see discussion).

4.1.3 Effect of Oxygen and Butene Partial Pressures - "Matrix" Data

The partial pressures of butene and oxygen were, initially, varied only slightly about a median value, with p_{butene}>0.5%, and the effects on the rates were observed.

The oxygen and butene partial pressures were varied about a median value of 2% butene and 0.08% oxygen in helium. The partial pressures used were oxygen: 0.04, 0.08, 0.24 and 0.32% and butene: 0.5, 1.0, 2.0 and 4.0%. For each set of conditions, the output from the reactor was analysed and the input corrected and the output re-analysed, the input re-corrected, etc. until the required output conditions were obtained. No particular order of p_{O2} and p_{butene} were used.

4.1.3.1 Butadiene Production

The effect of oxygen partial pressure on the production of butadiene is shown in figure 4.7. The rate of production of butadiene is positive order in oxygen, and the rates decrease with increasing butene partial pressure. When p_{butene} was decreased from 0.5% to 0.061%, the rate of butadiene production decreased precipitously (deep oxiadtion products CO and CO_2 were the major products). Under these, "state 2" conditions, after the catalyst had been exposed to low butene partial pressures, the rate is

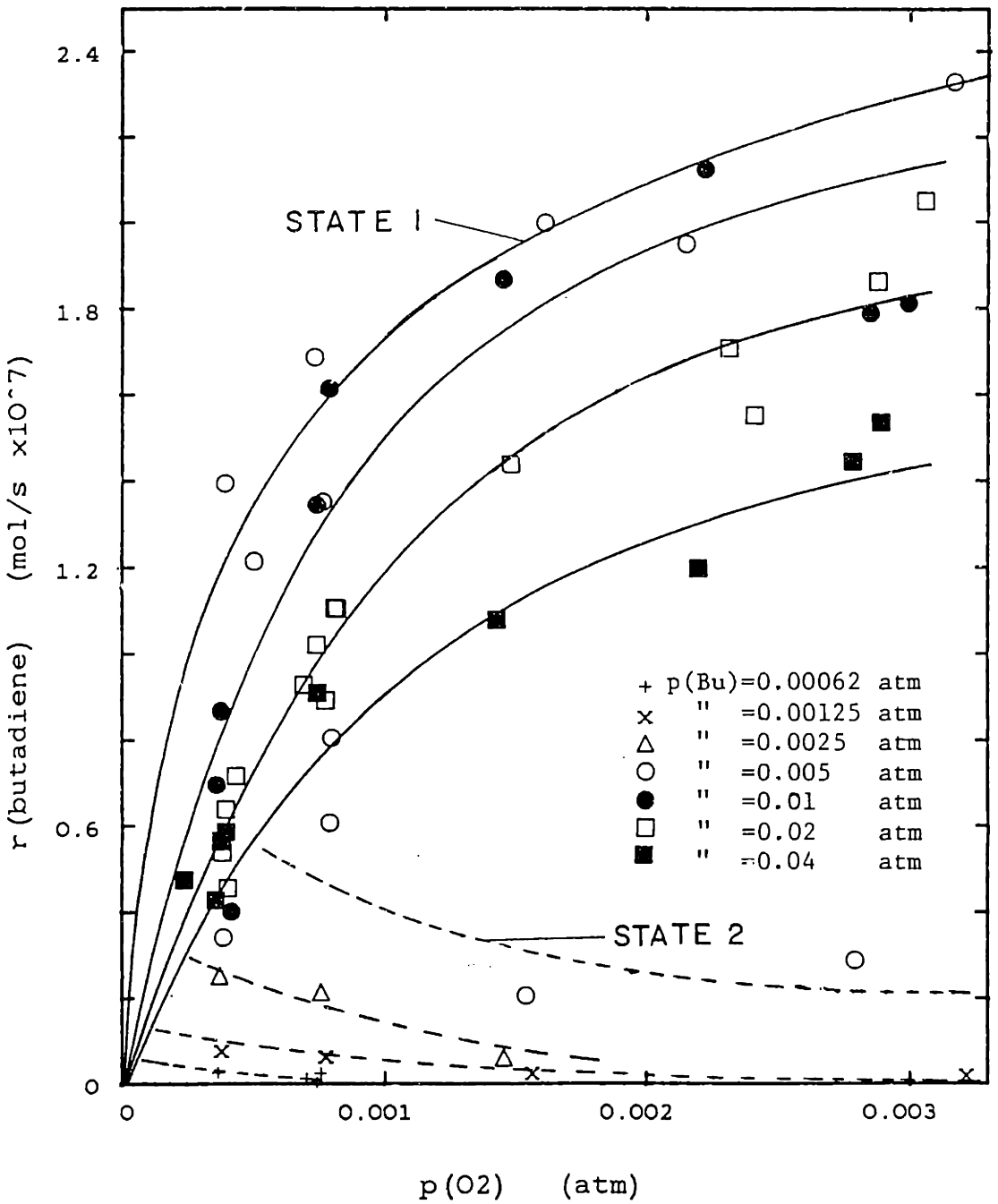

Figure 4.7: Rate of butadiene formation versus p_{O2} at fixed p_{butene}, T=513°C

zero order or slightly negative order in oxygen, and, in contrast to the state 1 data, the rate increases with butene partial pressure. Only data for p_{butene}=0.5% were taken under both sets of conditions. The p_{butene}=0.5% data that fit in state 1 were obtained when decreasing the p_{butene} from higher values. The data in state 2 were obtained when increasing the p_{butene} from the low values.

These trends are also shown in the cross-plot of the data, at constant p_{O2} and varying the p_{butene}, figure 4.8. When the p_{butene} was kept above 0.5% (0.005 atm), the rate of butadiene production was negative order in butene. After the p_{butene} had been lowered below about 0.5%, the reaction order changed to positive order. The conditions for each state are shown diagramatically in Table 4.2.

Table 4.2 States that exist for each oxygen and butene partial pressure

p_{O2}	p_{butene}(%)						
(%)	0.61	.125	0.25	0.5	1.0	2.0	4.0
.04	2	2	2	1/2	1/2	1	1
.08	2	2	2	1/2	1/2	1/2	1
.16	(2)	2	2	1/2	1*	1*	1*
.32	(2)	(2)	(2)	1/2	1/2	1*	1*

* indicates data only taken when p_{butene}>0.5%

(2) indicates the rate of deep oxidation too high to obtain data - total conversion of butene occurred under these conditions, so unattainable.

4.1.3.2 Deep Oxidation of Butene

The rates of formation of CO and CO_2 were combined into a rate of "deep oxidation" for convenience. The amount of CO formed was always less than 20% of that of CO_2, and it therefore it did not seem expedient to

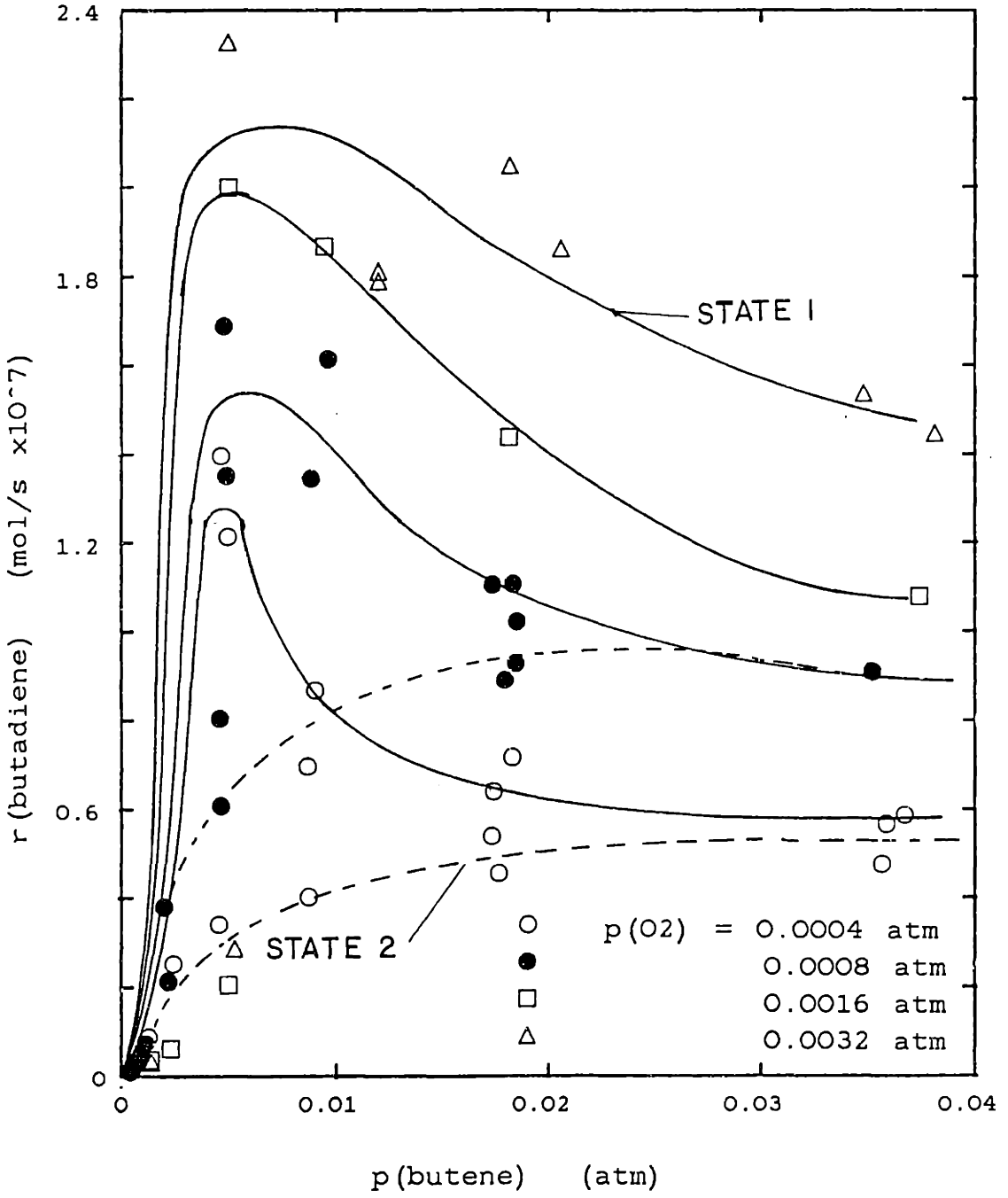

Figure 4.8: Rate of butadiene formation versus p_{butene} at fixed p_{O2}, T=513°C

analyse it separately.

The rate of deep oxidation corresponding to the butadiene data discussed above are shown in figures 4.9 and 4.10. In state 1 conditions (where butadiene was negative order in butene and positive order in oxygen) the rate of deep oxidation followed similar behavior to that of butadiene, with respect to both oxygen and butene partial pressures, although not as strongly effected as the butadiene. The rate of deep oxidation under state two conditions differed dramatically from the rate of butadiene production. Whereas the rate of butadiene production was negative order in oxygen, the rate of deep oxidation was first order in oxygen (the rate versus p_{O2} is linear in figure 4.9), and with respect to p_{butene}, the rate in strongly negative order relative to butene, instead of positive order (figure 4.10).

4.1.3.3 Other Products

Some cis- and trans-2-butene isomers were observed, however, the rate of isomerization was always about an order of magnitude lower than the rates of butadiene formation or deep oxidation and had neglegible effect on the rate of butene converted. This is not unexpected since oxygen is a poison for the isomerization reaction (Ragaini, 1974). The isomers were ignored from further analysis.

Retention times in the GC columns were also recorded for furan, formaldehyde and acrolein using standard compunds. During reaction, no GC peaks were observed at these retention times, also, the overall mass balances were randomnly distributed about 100%, indicating that no significant unaccounted side reactions occurred.

As discussed in section 4.1.1 (effect of time on stream) carbon was deposited on the catalyst surface in significant quantities after 100 hours on stream. After 180 hours on stream, approximately 10^{-4} moles CO_2 were

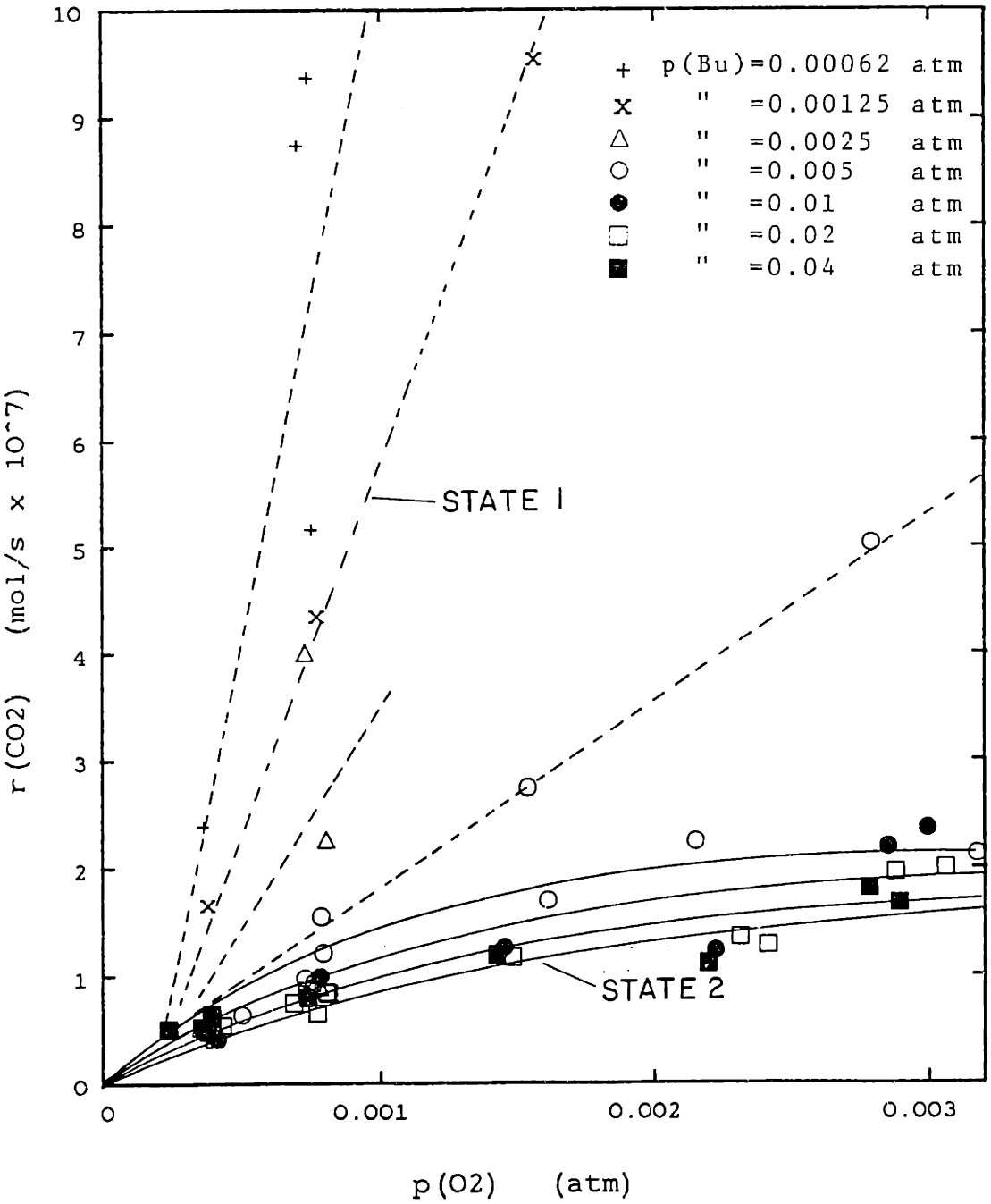

Figure 4.9: Rate of CO_2 formation versus p_{O2} at fixed p_{butene}, T=513°C

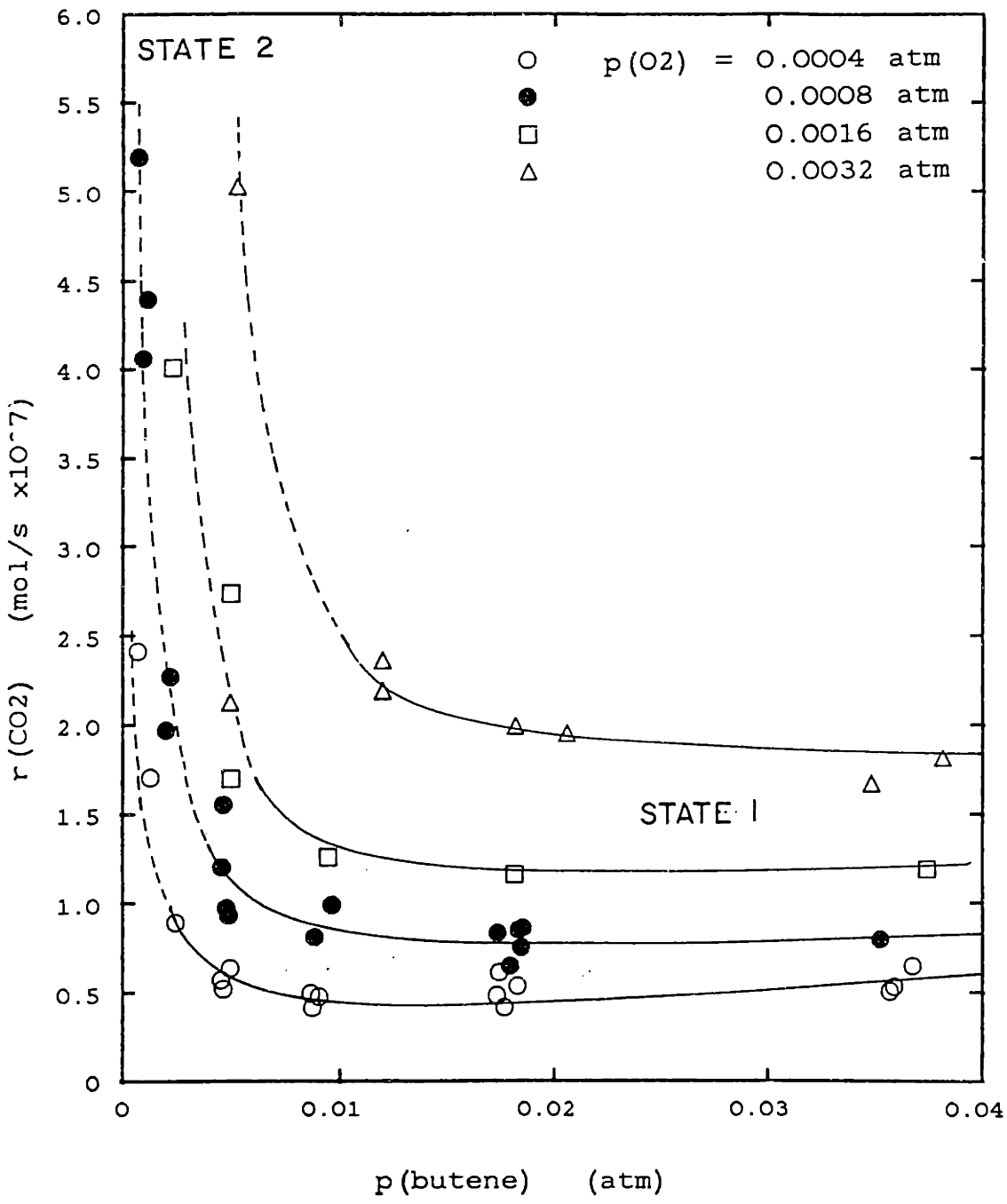

Figure 4.10: Rate of CO_2 formation versus p_{butene} at fixed p_{O2}, T=513°C

realeased on oxidation of the surface carbon (figure 4.3). Assuming typical rates of reaction of $r_{butadiene} \sim r_{deep\ oxid.} \sim 10^{-7}$ mol/s than approximately 0.065 moles butene would have reacted to butadiene, 0.016 moles to CO and CO_2 and 2.5×10^{-5} (1/4 of 10^{-4}) to carbon on the surface, i.e. carbon deposition had a negligible effect on the mass balances.

4.1.4 Cycling Butene and Oxygen Partial Pressures

With the dissimilarity of the data from states 1 and 2, it was decided to change the method of taking data from a random matrix method to cycling the butene (or oxygen) partial pressure between wide limits while keeping the oxygen (or butene) partial pressure constant, in an attempt to move smoothly between the two states.

It should be noted that the oxygen and butene partial pressures were each varied over two to three orders of magnitude. This is larger than is typically used in catalytic studies, and enables us to observe the entire spectrum of the oxidation kinetics and to account for the partial order kinetics that are observed here, and that have been reported in the literature.

The reactor was pretreated by calcining to 727°C in air to burn off any carbon that was on the surface. It was then cooled to the reaction temperature and exposed to butene at the minimum concentration detectable by the gas chromatograph (0.05%). The oxygen concentration was held constant at a desired value (0.04, 0.08, 0.16 or 0.32%). The concentration of butene was then increased up to the gas chromatograph's maximum detectability of about 40% butene. The reactor was left overnight at these conditions. The butene was then decreased slowly back to the initial value, recreating the initial conversion and selectivity results.

A similar scheme was used for oxygen cycling. After pretreatment in

air, the reactor was exposed to the desired butene concentration (1, 2 or 4%) at a high oxygen concentration. The oxygen concentration was then decreased until the gas chromatograph's minimum for oxygen concentration of 0.01% was reached, left at these conditions overnight, before increasing up to the starting conditions again. The data taken with cycling of butene or oxygen are shown in table 4.3.

Table 4.3 Conditions used for cycling butene (oxygen) at constant oxygen (butene) partial pressure, their corresponding figures and the approximate butene and oxygen partial pressures at which the change from state 1 to state 2 behavior occurs.

Figure #	P_{O2} (%)	P_{butene} (%)	Temperature (°C)
4.11	cycled	1.0%	464
4.12	0.18%	cycled	"
4.13	cycled	0.4%	513
4.14	"	1.0%	"
4.15	"	1.8%	"
4.16	0.04%	cycled	"
4.17	0.08%	"	"
4.18	0.32%	"	"
4.19	cycled	1.0%	544
4.20	0.32%	cycled	"

It should be noted that both the x and y axes in figures 4.11to 4.20 are log scales and therefore the slopes of these lines correspond to the

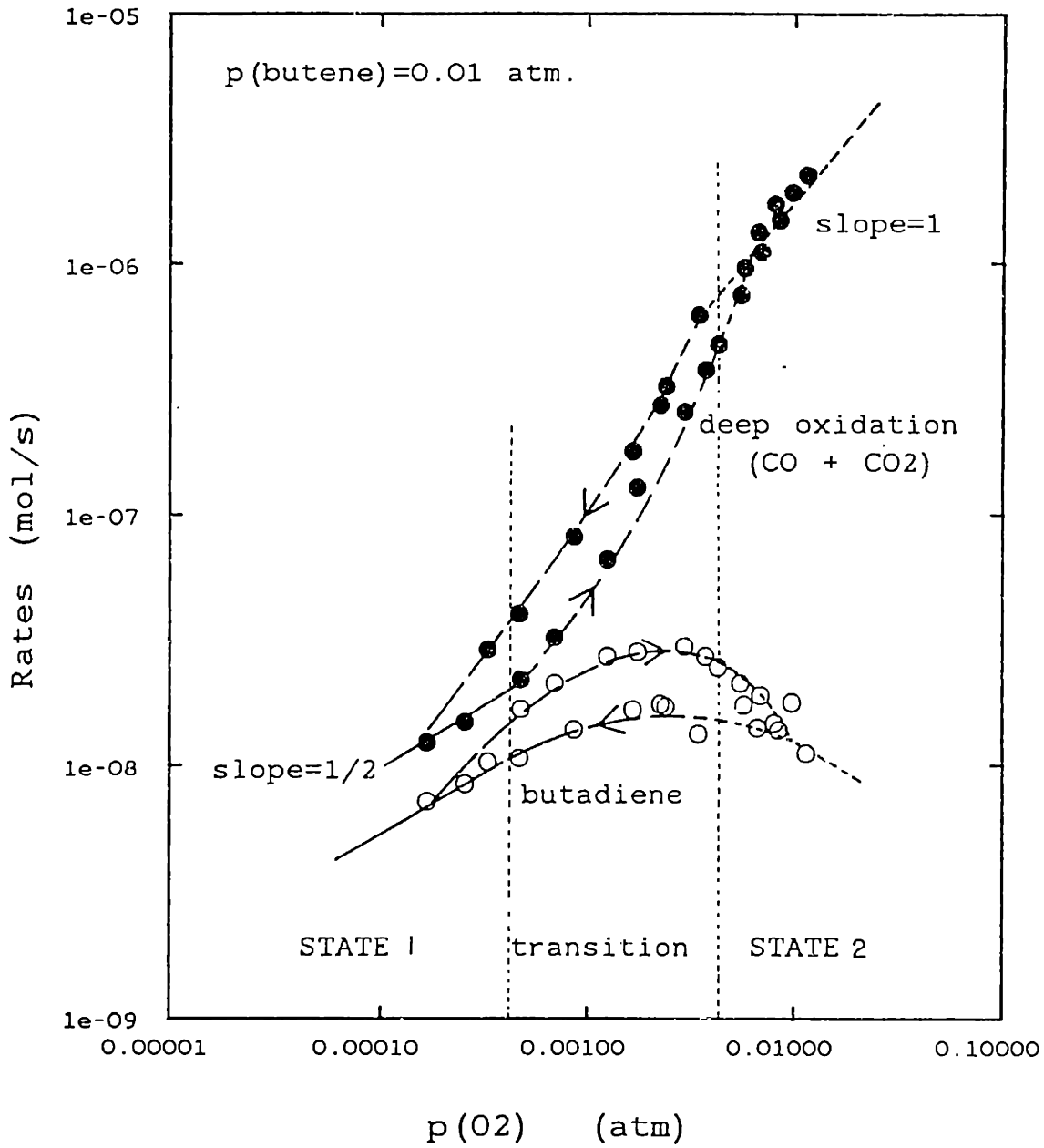

Figure 4.11: Rate of butene oxidation versus p_{O2} at p_{butene}=0.01 atm, T=466°C

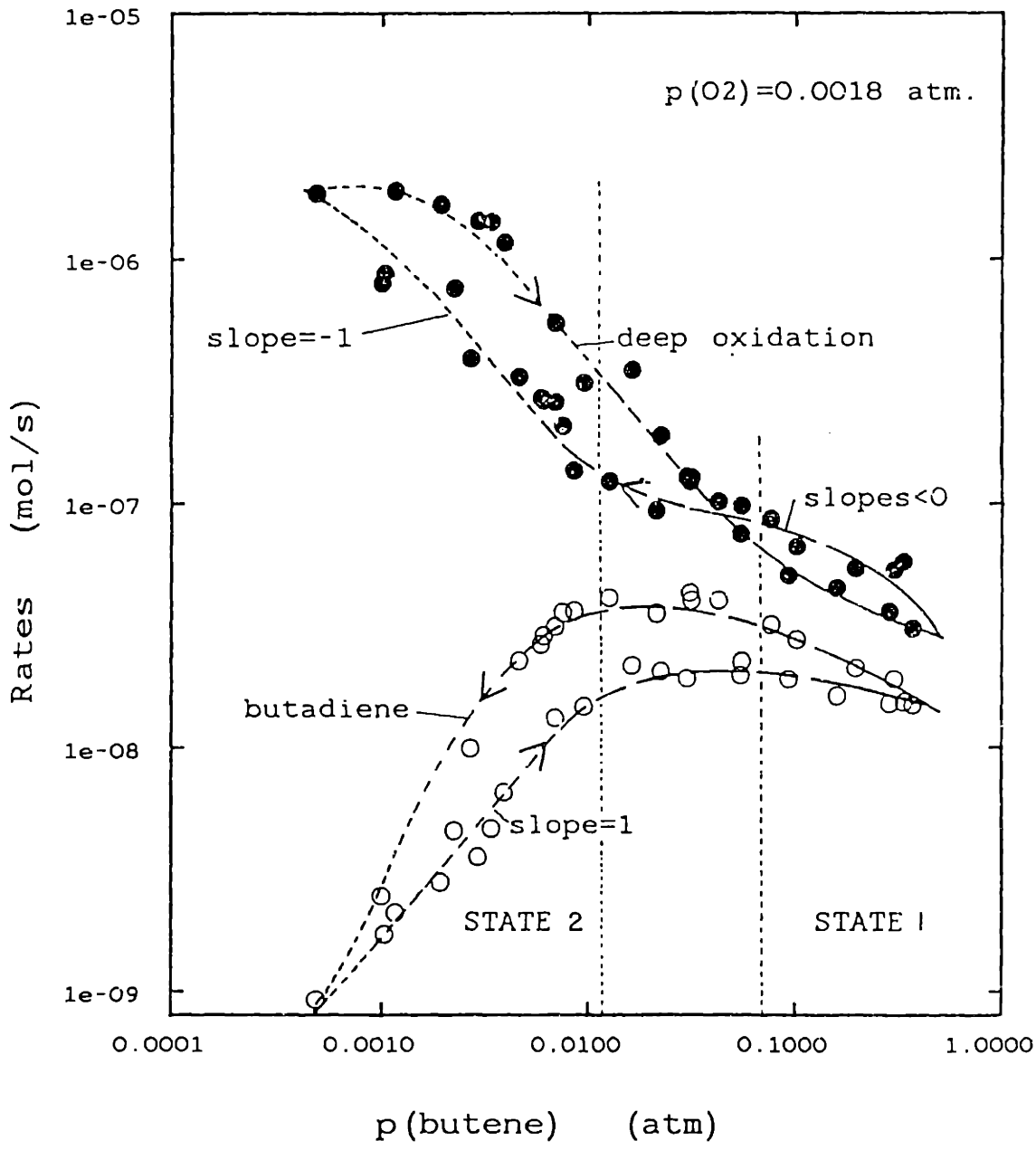

Figure 4.12: Rate of butene oxidation versus p_{butene} at p_{O2}=0.0018 atm, T=466°C

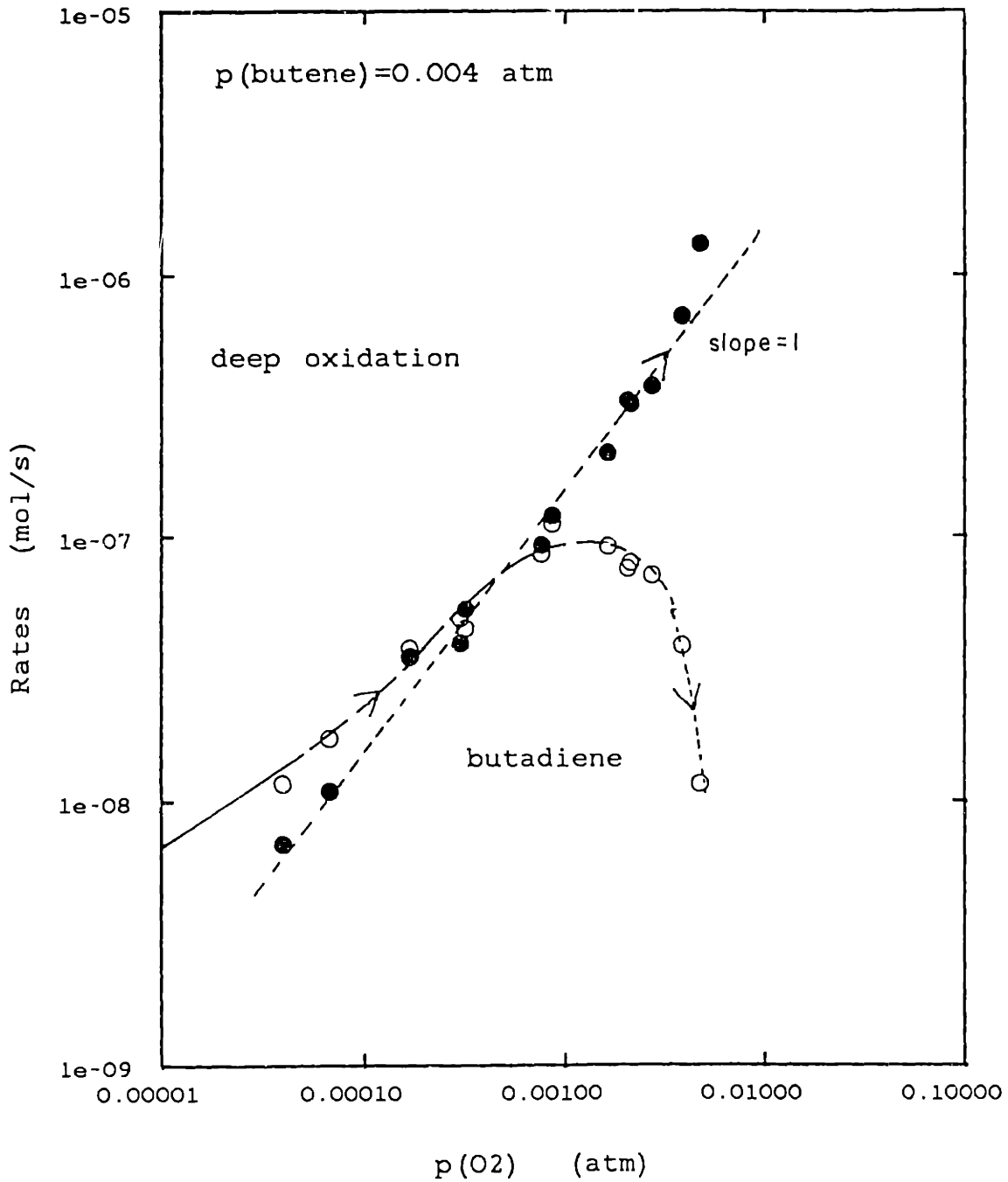

Figure 4.13: Rate of butene oxidation versus p_{O2} at p_{butene}=0.004 atm, T=513°C

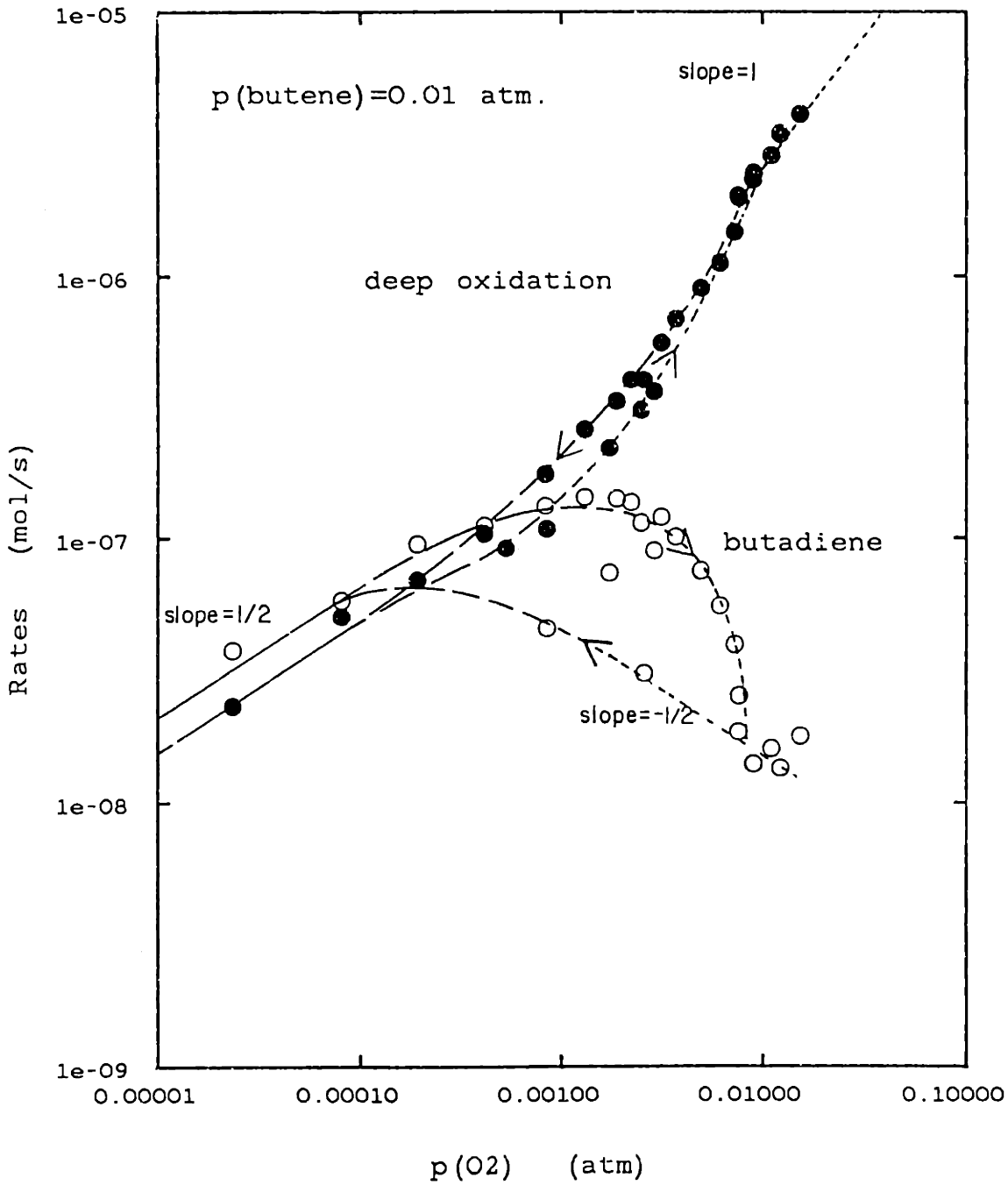

Figure 4.14: Rate of butene oxidation versus p_{O2} at p_{butene}=0.01 atm, T=513°C

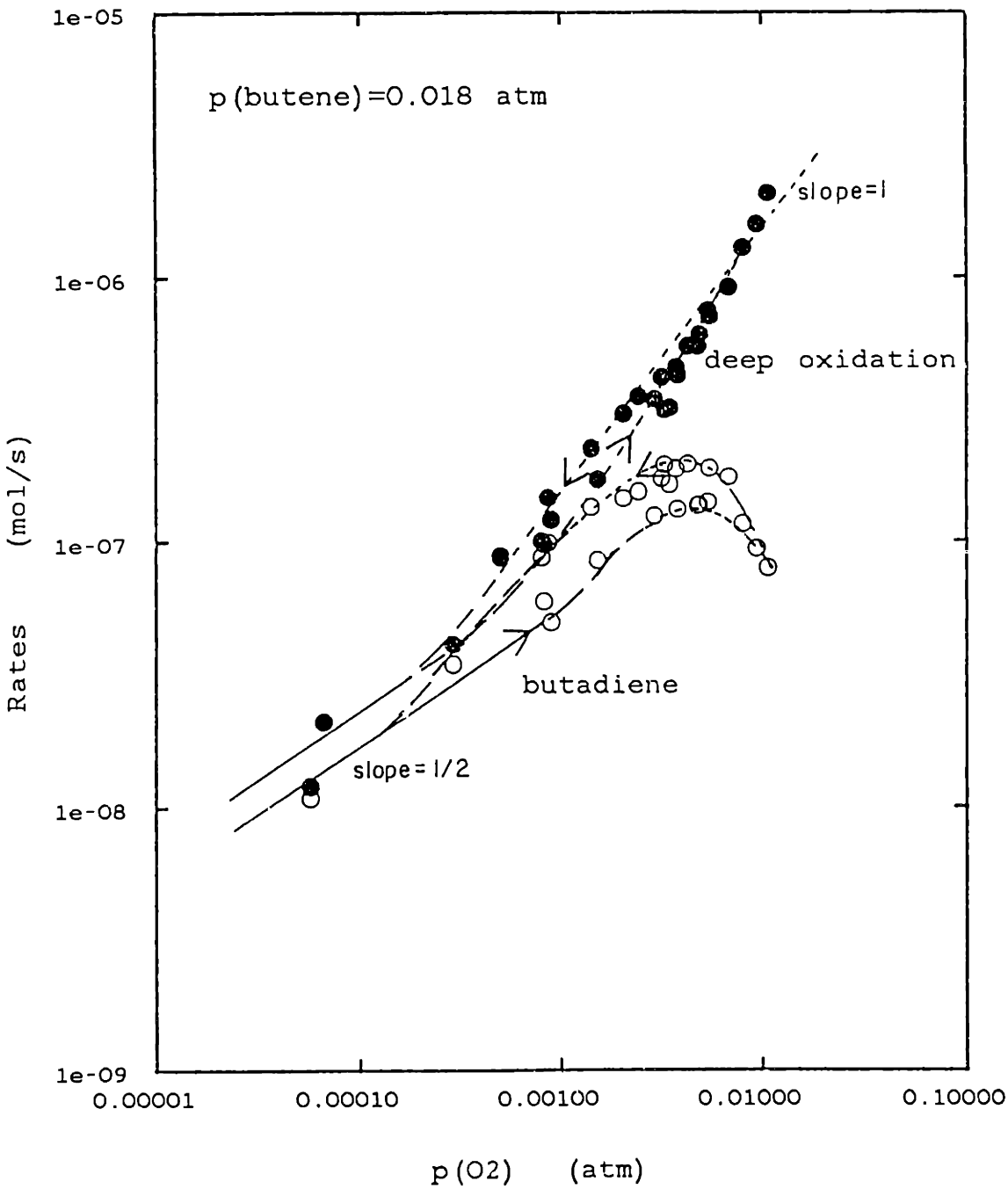

Figure 4.15: Rate of butene oxidation versus P_{O2} at P_{butene}=0.018 atm, T=513°C

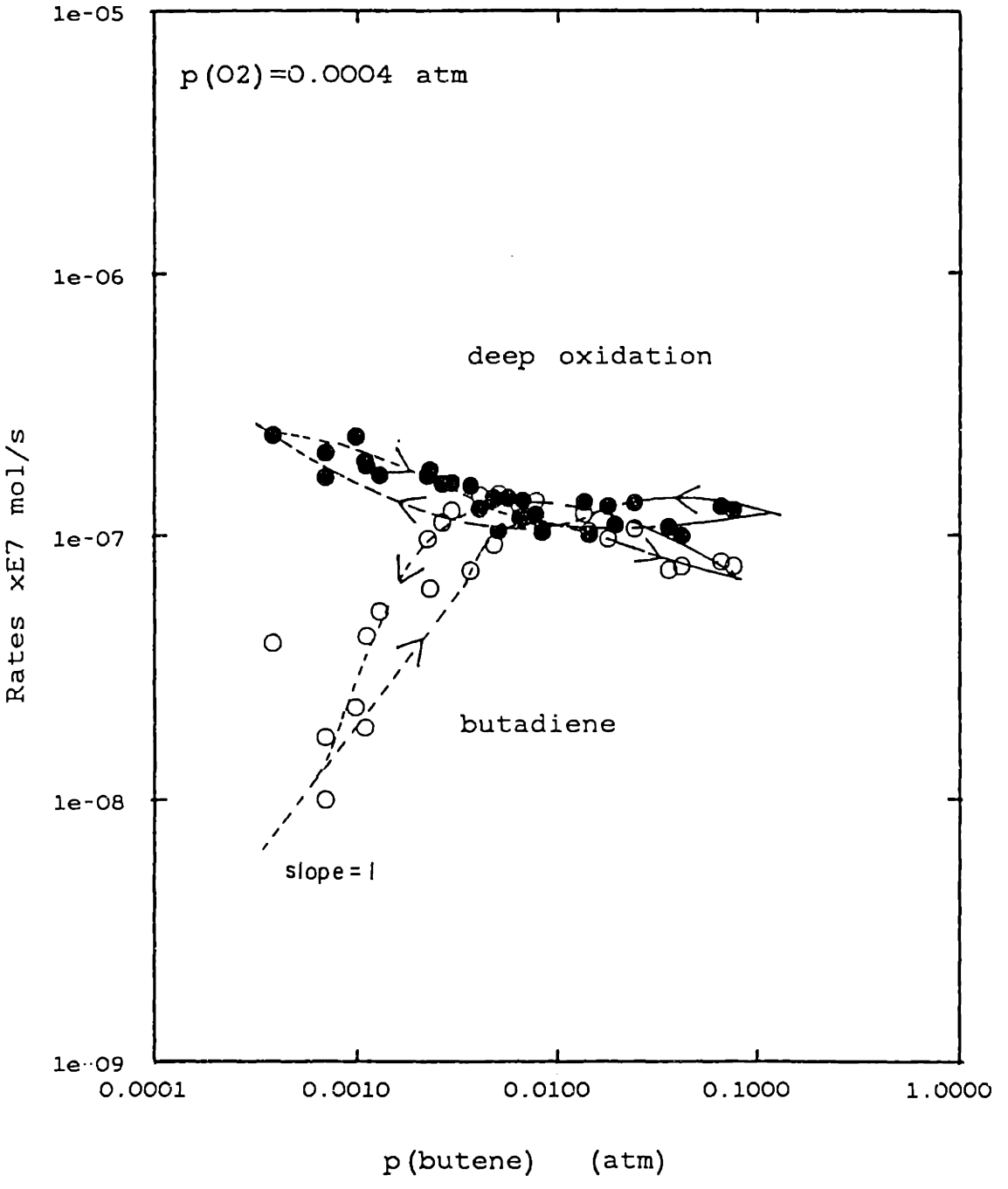

Figure 4.16: Rate of butene oxidation versus p_{butene} at p_{O2}=0.0004 atm, T=513°C

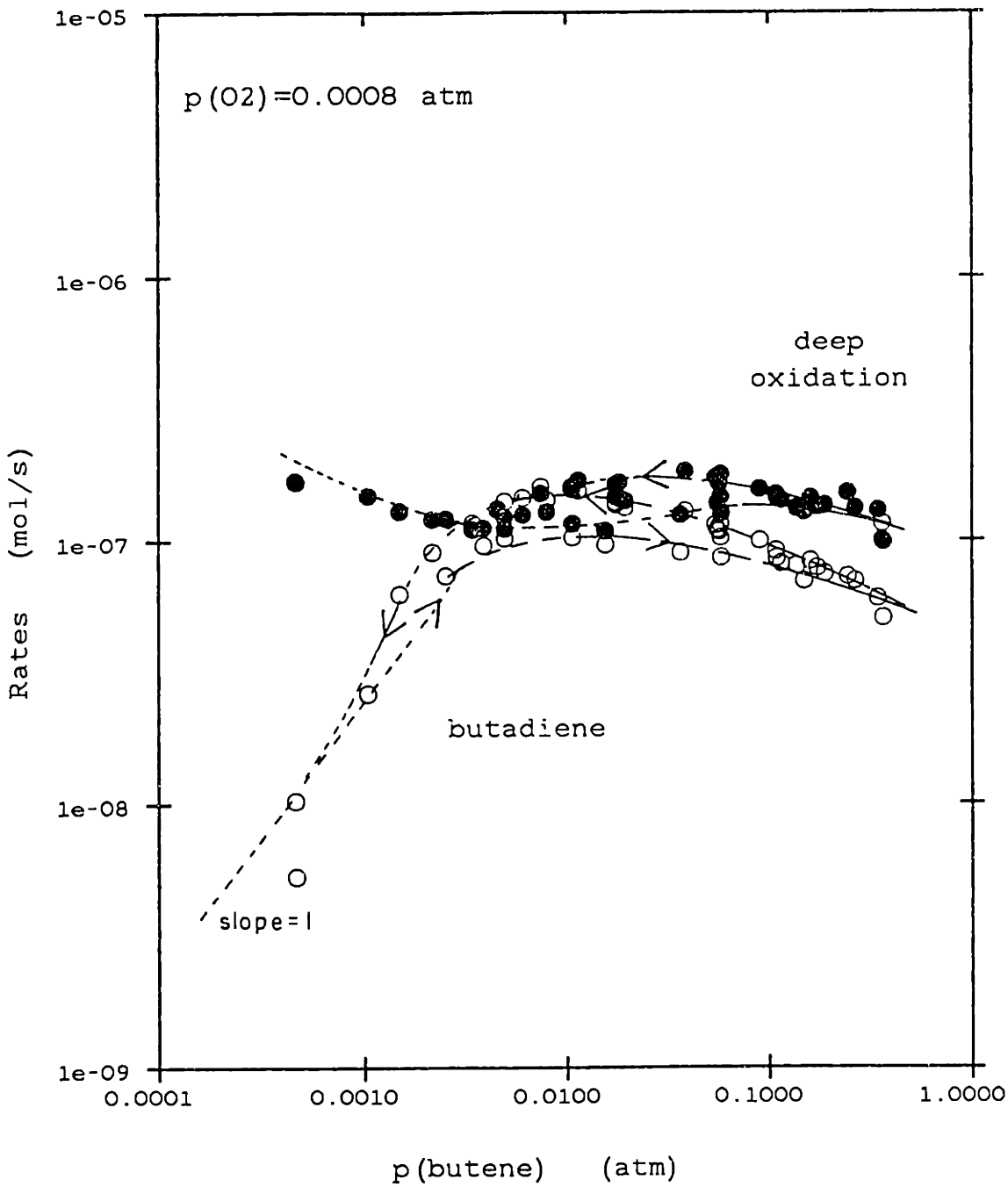

Figure 4.17: Rate of butene oxidation versus p_{butene} at p_{O2}=0.0008 atm, T=513°C

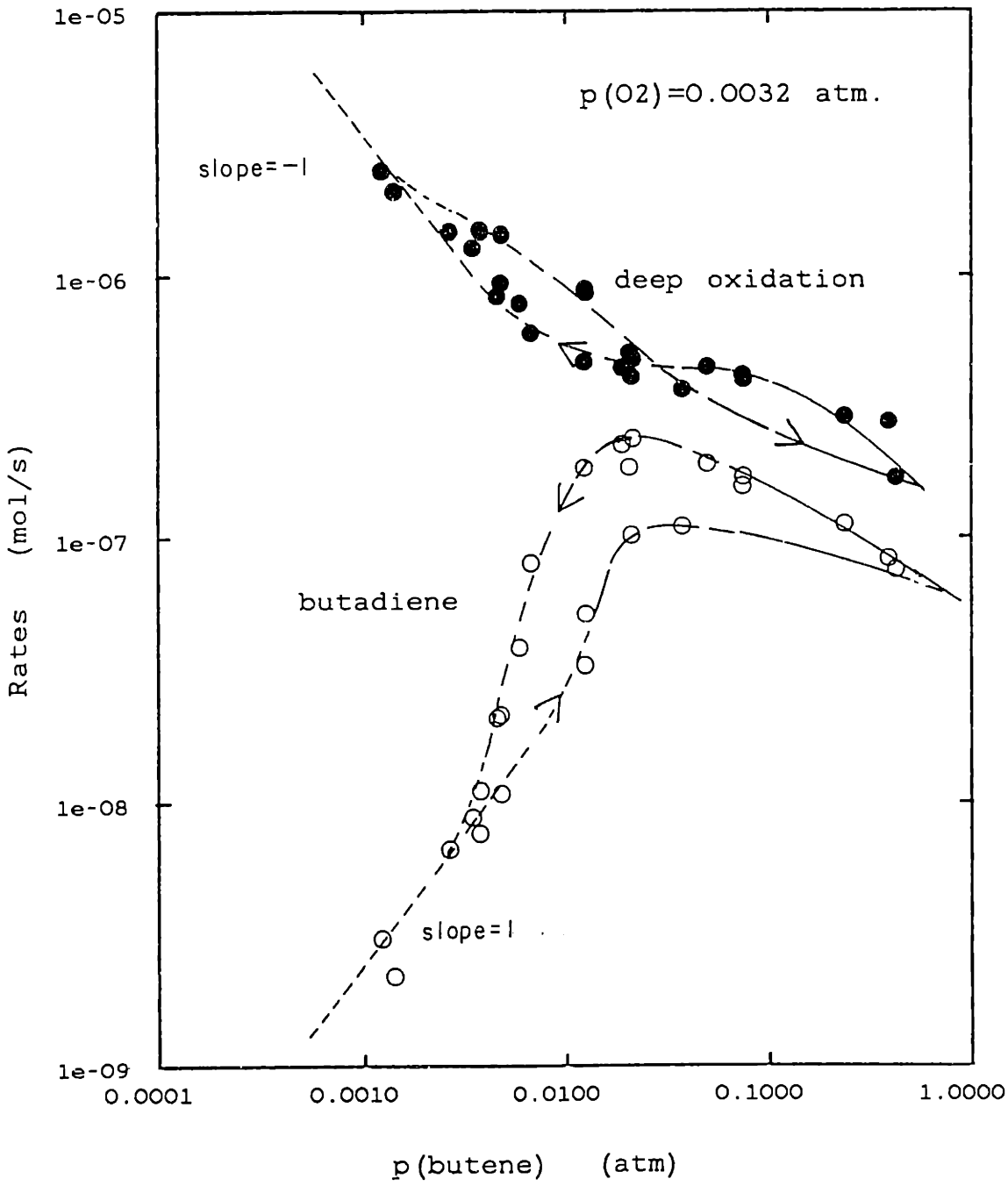

Figure 4.18: Rate of butene oxidation versus p_{butene} at p_{O2}=0.0032 atm, T=513°C

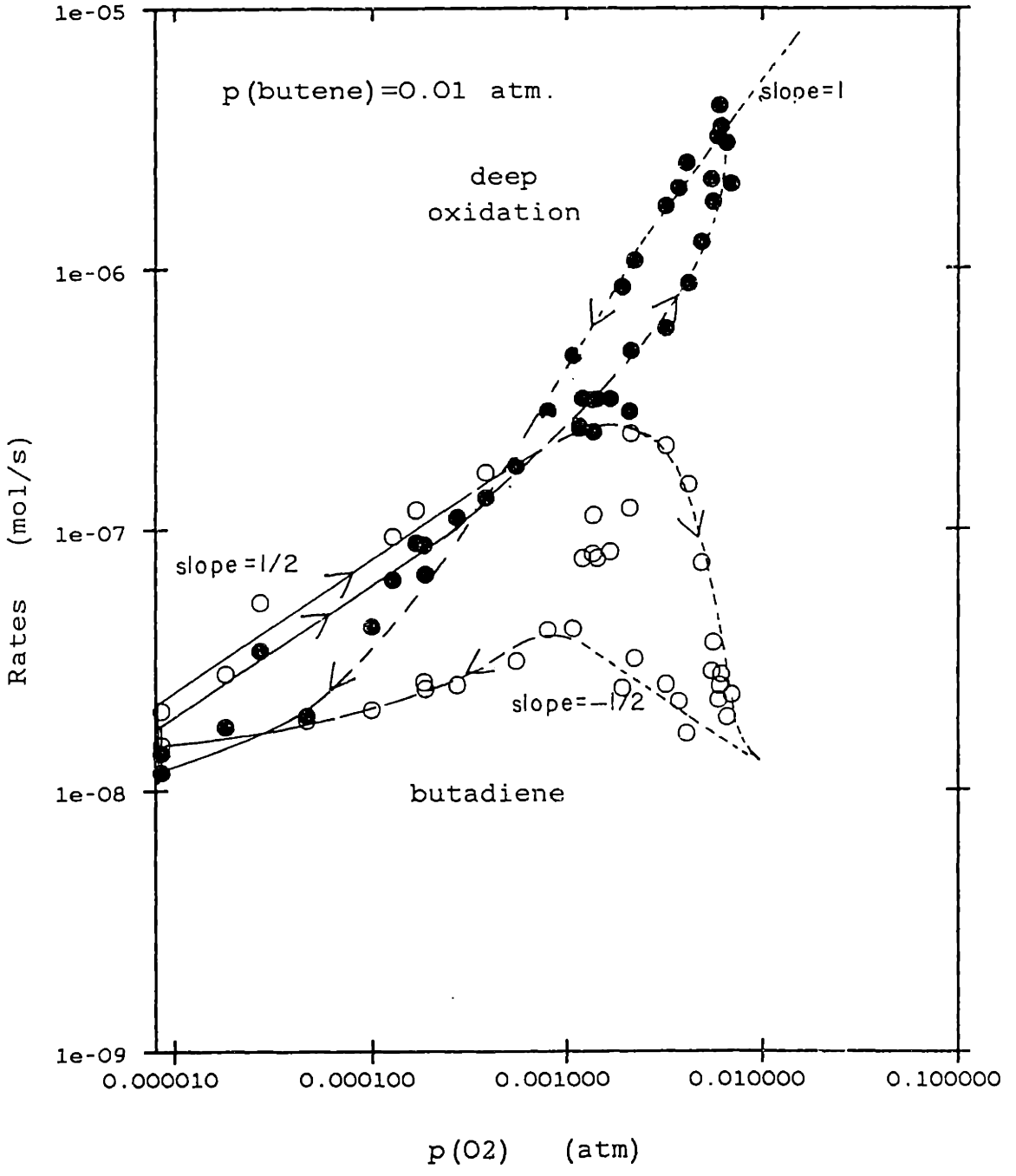

Figure 4.19: Rate of butene oxidation versus p_{O2} at p_{butene}=0.01 atm, T=544°C

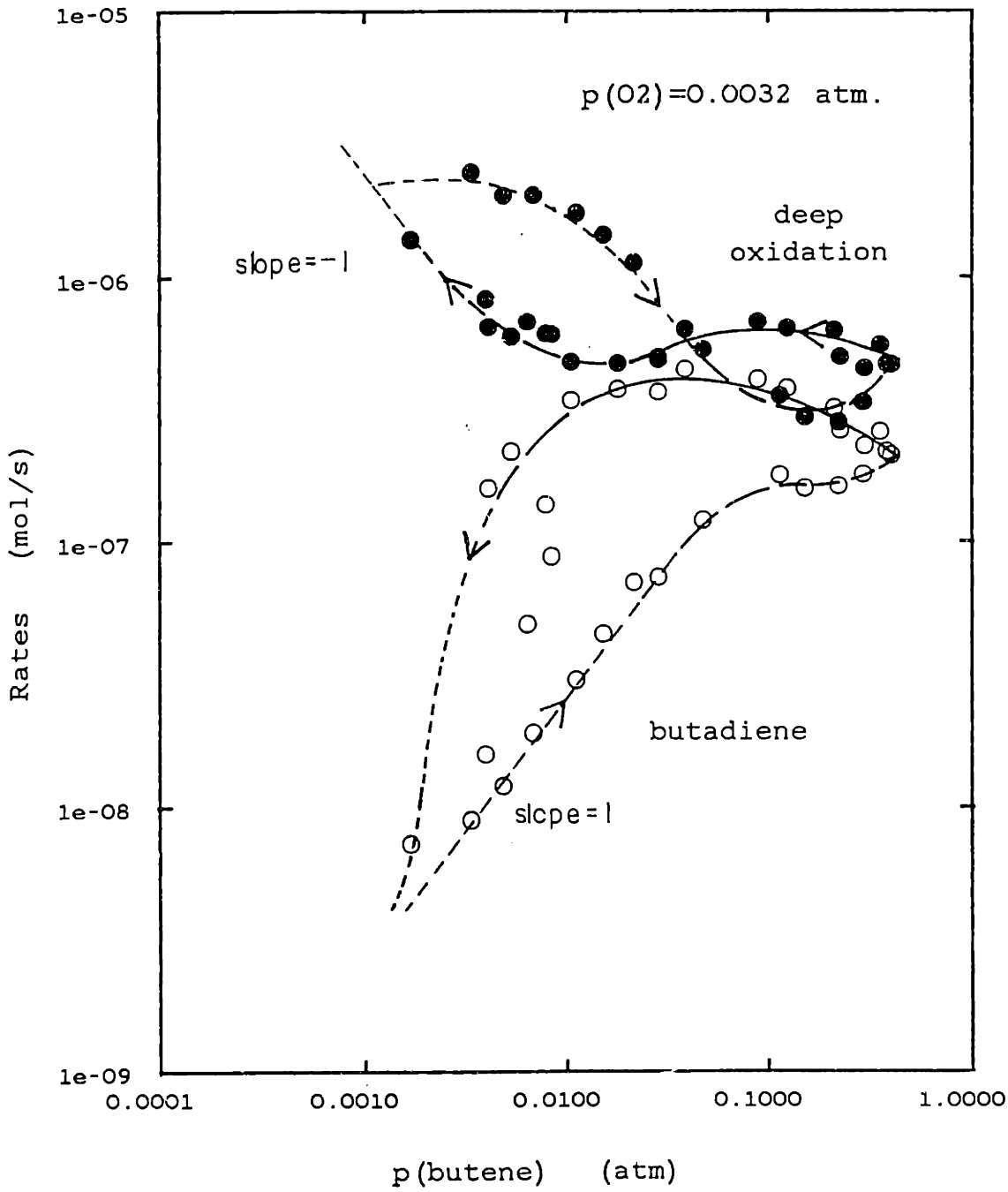

Figure 4.20: Rate of butene oxidation versus p_{butene} at p_{02}=0.0032 atm, T=544°C

order for the rate of butadiene production, or deep oxidation, relative to the x-axis parameter of butene or oxygen partial pressure.

The data presented in figures 4.11 to 4.20 can also be described in terms of the two states used to describe the matrix data. "State 1" occurred under high butene and low oxygen partial pressures, and "state 2" under low butene and high oxygen partial pressures. The cyclic data were taken under steady state gas conditions, but before the slower transition mechanism that drives the mechanism between the two states, possibly due to changes in the surface, had come to a steady state (see section 4.1.4 below); each data point was taken, typically, about 45 minutes after the gas composition had been changed the small amount from the previous data point.

The cyclic data reflect the kinetics for butadiene and CO and CO_2 formation under the extreme states and in the intermediate region where contributions from both states occur. It is only near the extremes of each cycle, when the slow mechanism causing the switch between the two states (thought to be cuased by the catalyst surface composition) ceases to function, that the orders of reaction can be readily discerned, and which agree with the matrix data. In the central region of each cycle, the specific rate of reaction depends on the previous history of the catalyst, whether it had been exposed to an excess of butene or of oxygen. When the gas was left at a single composition until the reactor reached steady state (as discussed below) the rates from each curve moved to values midway between the two curves shown in the figures. This implies that the curves in the data indicate envelopes of activity and that the equilibrium, steady state activity lies in between. The rate of the slow mechanism governing the switch between the two states is itself dependent on the concentrations of butene and oxygen and this results in transient orders of

reaction of up to ± 3 that are observed.

The order of the reactions under steady state conditions may be seen at the extremes of butene and oxygen partial pressures. Under state 1 conditions of high butene and/or low oxygen partial pressures, at 466°C, for example (figure 4.11), the order of the reaction for both the production of butadiene and for deep oxidation is one half order with respect to oxygen at oxygen partial pressures up to .001 atm (when increasing the oxygen partial pressure). Relative to butene partial pressure, figure 4.12, the rate of both butadiene formation and deep oxidation is negative order, less than -1, at butene partial pressures greater than 0.01 atm.

"State 2" conditions prevailed under high oxygen and low butene partial pressures. Refering to figure 4.11 again, rate of production of butadiene was negative order with respect to oxygen for $p_{O2} > 0.005$ atm, and the limited data near the maximum p_{O2} approach a slope of -1/2, and with respect to butene (figure 4.12), the rate was first order in butene (at $0.006 < p_{butene} < 0.01$ atm). For deep oxidation, the orders are positive order in oxygen (about +1 at $p_{O2} > 0.08$ atm in figure 4.11) and negative one order with respect to butene ($p_{butene} < 0.01$ atm in figure 4.12).

Similar behavior is observed, more or less distinctly, in all the figures from 4.11 to 4.20. It should be further noted that when the hysteresis exists, the data for the higher butadiene leg coincide with the lower deep oxidation leg, and vice versa. There is an exception to this rule occurs when the rate of deep oxidation crosses itself (see figure 4.12 at $p_{butene} > 0.03$ atm.). Under these conditions, the rate of deep oxidation exhibits very similar behavior to the butadiene reaction, and at times even becomes positive order in butene (figure 4.20, $0.001 < p_{butene} < 0.013$ atm.).

The data from cycling the butene and oxygen feeds therefore duplicate qualitatively the data seen when taking the data in a matrix fashion. It should be noted, however, that the matrix data were taken over a smaller range of oxygen and butene partial pressures and therefore some trends discernible in the cycled data would not be seen in the matrix data. Also, in the matrix data study, the change between states 1 and 2 was abrupt and did not show the transitions that were seen when the concentrations were cycled.

Similar complexities in the reaction order were observed by Yao (1984) for the oxidation of propylene and hexene over platinum wire catalysts that had been pre-oxidized in 1% oxygen in He at 500°C. He observed reaction orders of 1.3 to 2 with respect to oxygen partial pressure and -0.6 to -2 with respect to butene partial pressures. However, he used a differential reactor and so was restricted to conversions of less than 20% (which is high for a differential reactor). He therefore observed data over a far more limited range than was observed here using a CSTR.

4.1.4.1 Cell Voltage at Open Circuit

The platinum catalyst acts as one electrode of an electrochemical reactor, the other is exposed to the air and acts as a reference electrode. The voltage of the reactor was measured in every experiment. The behavior was, however complex and is difficult to explain quantitatively. The variation with butene and oxygen partial pressures that correspond to figures 4.19 and 4.20 are shown in figures 4.21 and 4.22. The cell voltage data corresponding to figures 4.11 to 4.18 are included in the appendix.

When the butene partial pressure was kept constant, and the oxygen partial pressure cycled (figure 4.21), the cell voltage varied according to:

$$V_{cell} = RT/2F \ln p_{O2} + \text{constant} \qquad (2)$$

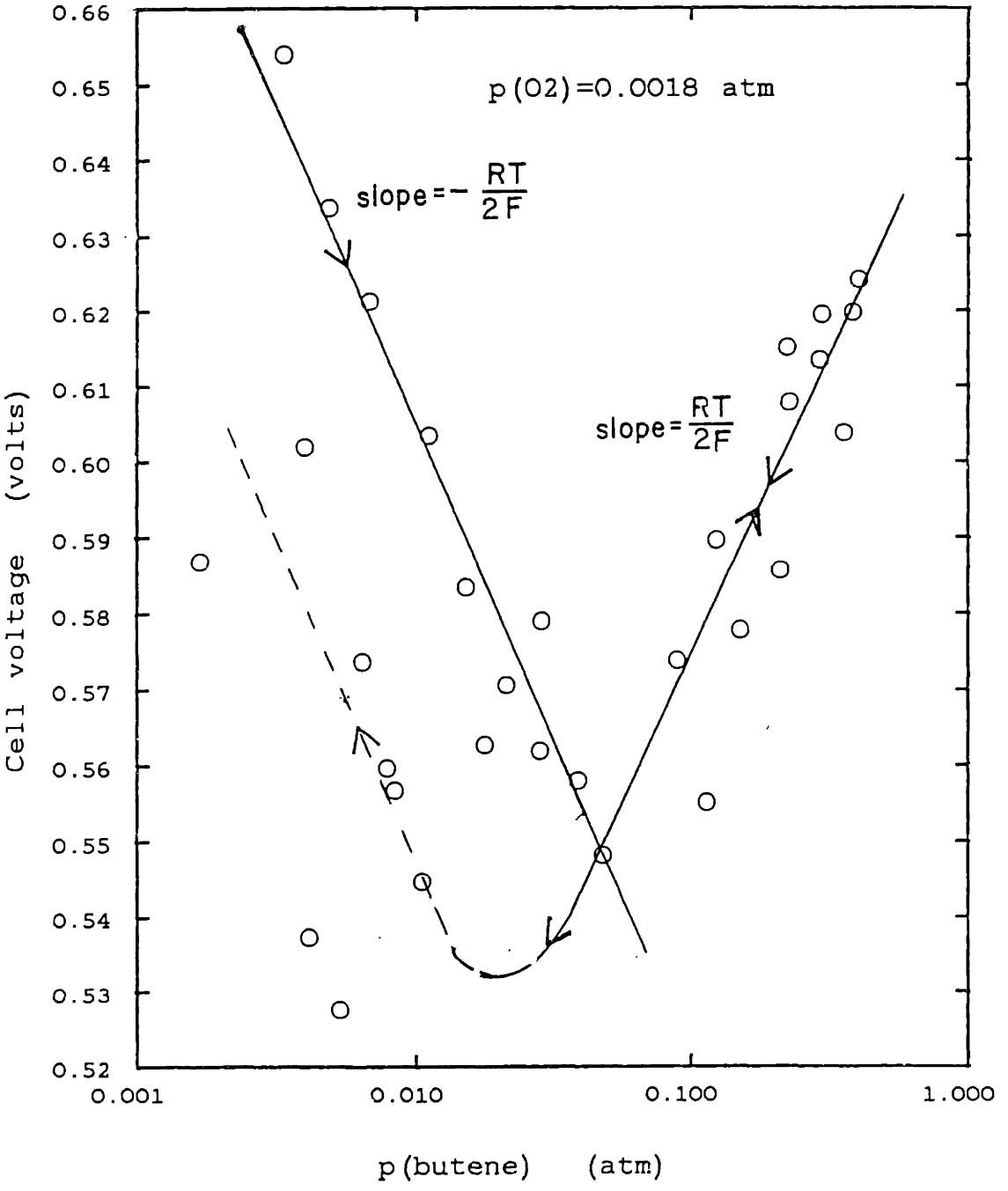

Figure 4.21: Cell voltage versus p_{butene} at p_{O2}=0.0032 atm, T=544°C

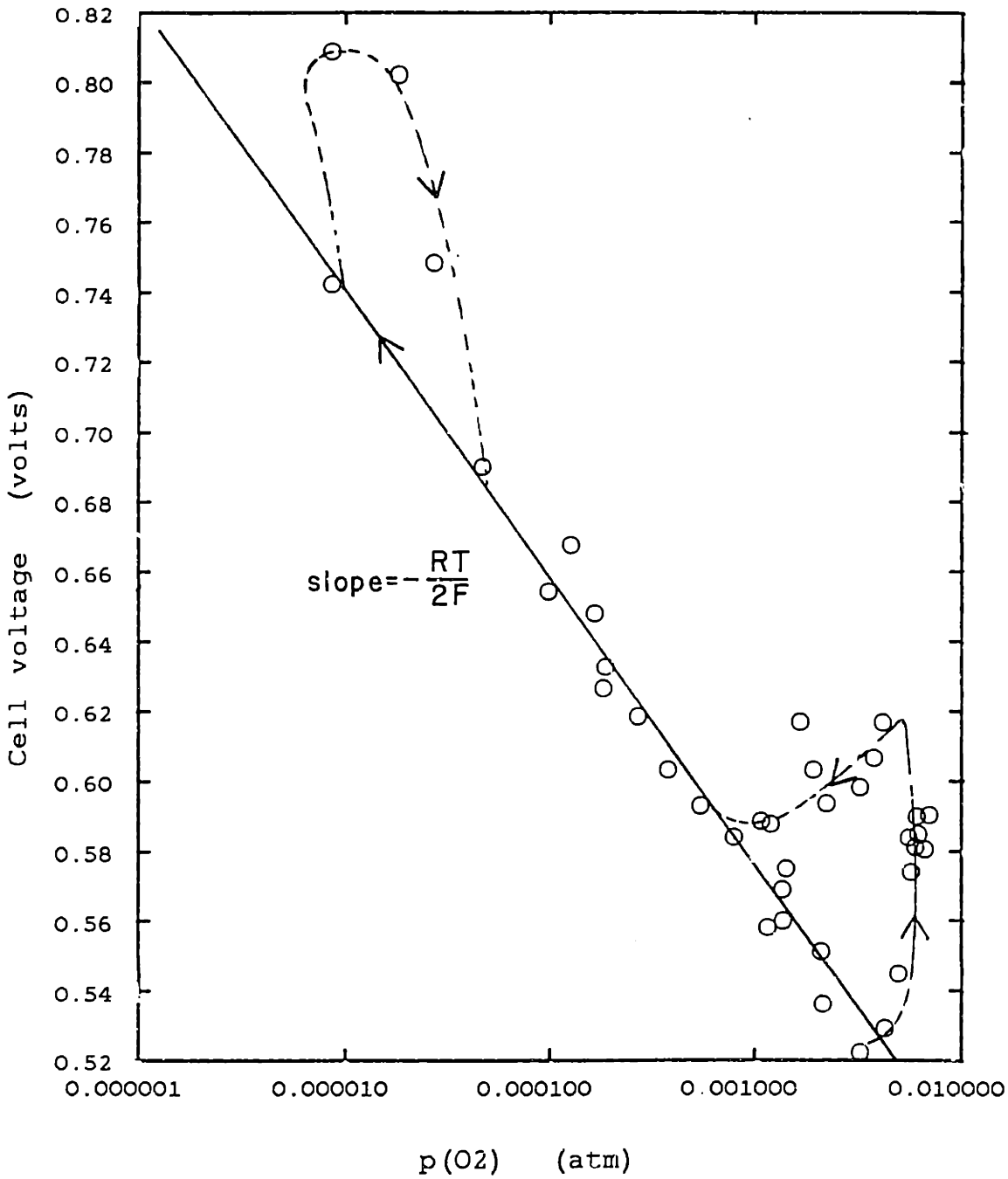

Figure 4.22: Cell voltage versus p_{O2} at p_{butene}=0.01 atm, T=544°C

from the minimum p_{O2} used up to about 0.005 atm, which is the oxygen pressure at which the butadiene rate decreased rapidly (figure 4.19). This contrasts with the cell voltage when no butene is present, which obeys the Nernst equation (1.31):

$$V_{cell} = \frac{RT}{4F} \ln \frac{p_{O2}}{0.21} \qquad (1.31)$$

where 0.21 is the partial pressure of oxygen in the reference gas, air, and 4 is the number of electrons transfered per oxygen molecule.

When the oxygen partial pressure was kept constant and the butene partial pressure cycled, the cell voltage was again V-shaped, with a minimum at about 0.08 atm. (figure 4.22) and increasing at both lower and higher butene partial pressures. Below 0.08 atm. the cell voltage varied according to:

$$V_{cell} = -RT/2F \ln p_{butene} + \text{const.} \qquad (3)$$

When the butene partial pressure was decreased to a point where there was no butene in the exit, i.e. all the butene had been oxidized to CO and CO_2, then, the cell voltage dropped precipitously to about 0.0812 volts (not included in figure 4.22). Using the Nernst equation, this corresponds to an oxygen partial pressure of 2.08×10^{-3}atm. Experimentally, as measured by the gas chromatograph, the oxygen partial pressure was 2.00×10^{-3}atm., i.e. the same within experimental error. Therefore, when there is no butene in the exit stream, the cell voltage measures the oxygen partial pressure.

4.1.5 Effect of Previous History

The effect of the previous history on the catalytic activty was investigated by pretreating the catalyst at 544°C at the minimum p_{butene}

used in figure 4.20, of 0.5% and at p_{O2}=0.3% (region A of figure 4.23). The concentration of butene in the gas phase was then increased to 2.5%, while keeping the oxygen concentration constant (region B of figure 4.23). The rates of butadiene production and of deep oxidation were recorded versus time for 26 hours, until steady state was reached (figures 4.23 and 4.24). The rate of butadiene production doubled from 0.8 x 10^{-7} mol/s to 1.6 x 10^{-7}mol/s, while the rate of deep oxidation decreased from 7.1 x 10^{-7} to 2.8 x 10^{-7}.

The p_{butene} was then increased to 40% (p_{O2} still 0.3%, region C) for 16 hours, and then decreased back to the original 2.5% (region D). The rates were again measured versus time and are also shown in figures 4.23 and 4.24. The rate of butadiene production decreased from 4.8 x 10^{-7} mol/s back to the same value found at the end of the previous run, about 1.7 x 10^{-7} mol/s. The rate of deep oxidation also decreased, from about 6 x 10^{-7} to the same value as reached previously, 2.8 x 10^{-7}. This would indicate that the deep oxidation reaction had been positive order in butene, which agrees with the data when butene was cycled (figure 4.20). Finally, the partial pressure of butene was decreased back to 0.3% and the rates of deep oxidation and butadiene productionreturned to values similar to those maesured initially.

4.1.6 "Spiking" the Feed

The exit gas composition from the reactor was kept constant at 2.0% butene and 0.08% oxygen and, in turn, CO, CO_2, H_2, butadiene and water were added to the feed (spiked) to test their effects on the reactions occurring. It should be noted that the reliability of these data are less than for the conversion data. For the results discussed above, the rate of reaction for each component is the difference between the flowrate of that

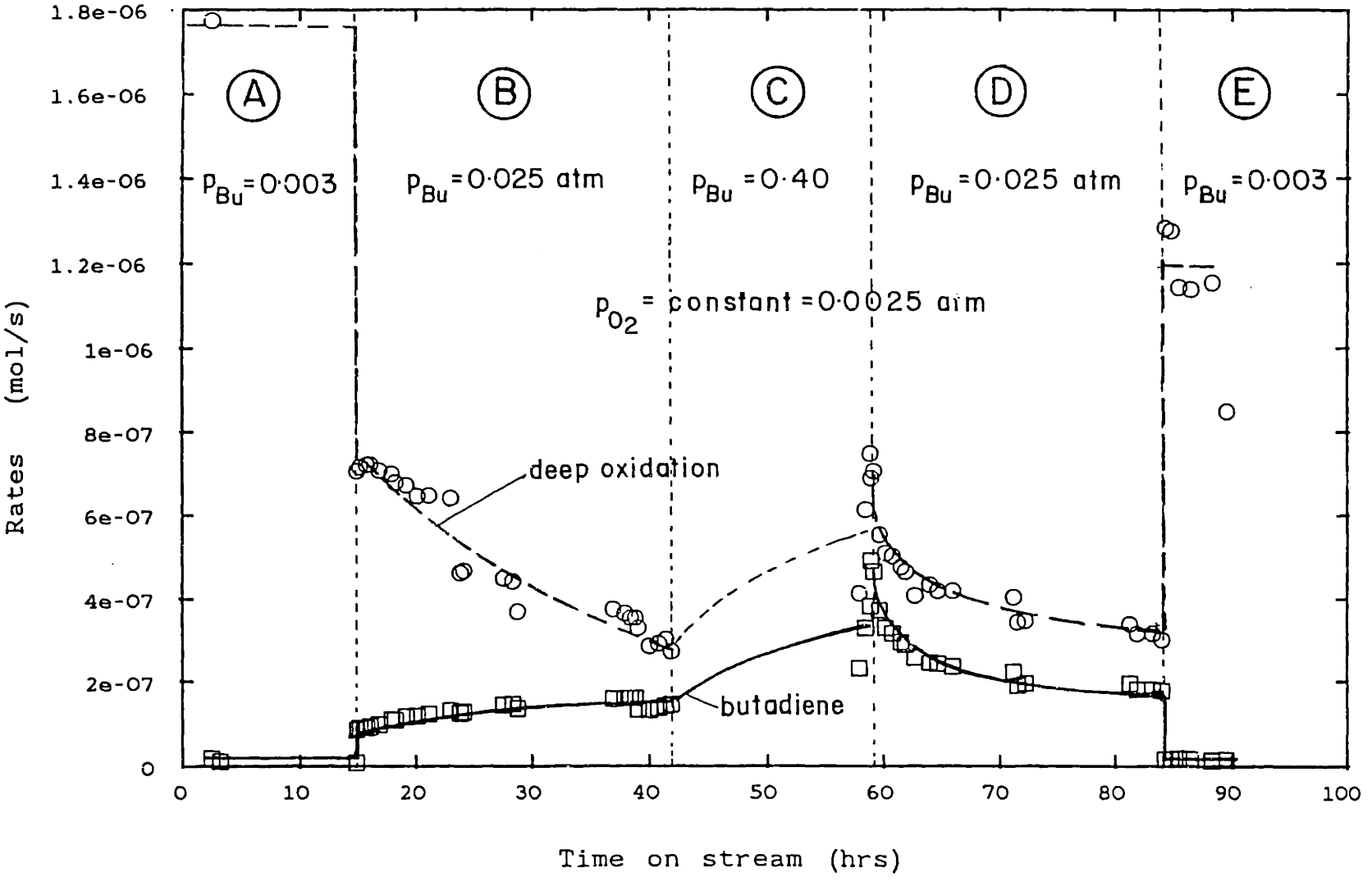

Figure 4.23: Effect of changing ambient gas on reaction rates,

P_{butene}=0.0247 atm, P_{O2}=0.003 atm, T=544^{o}C

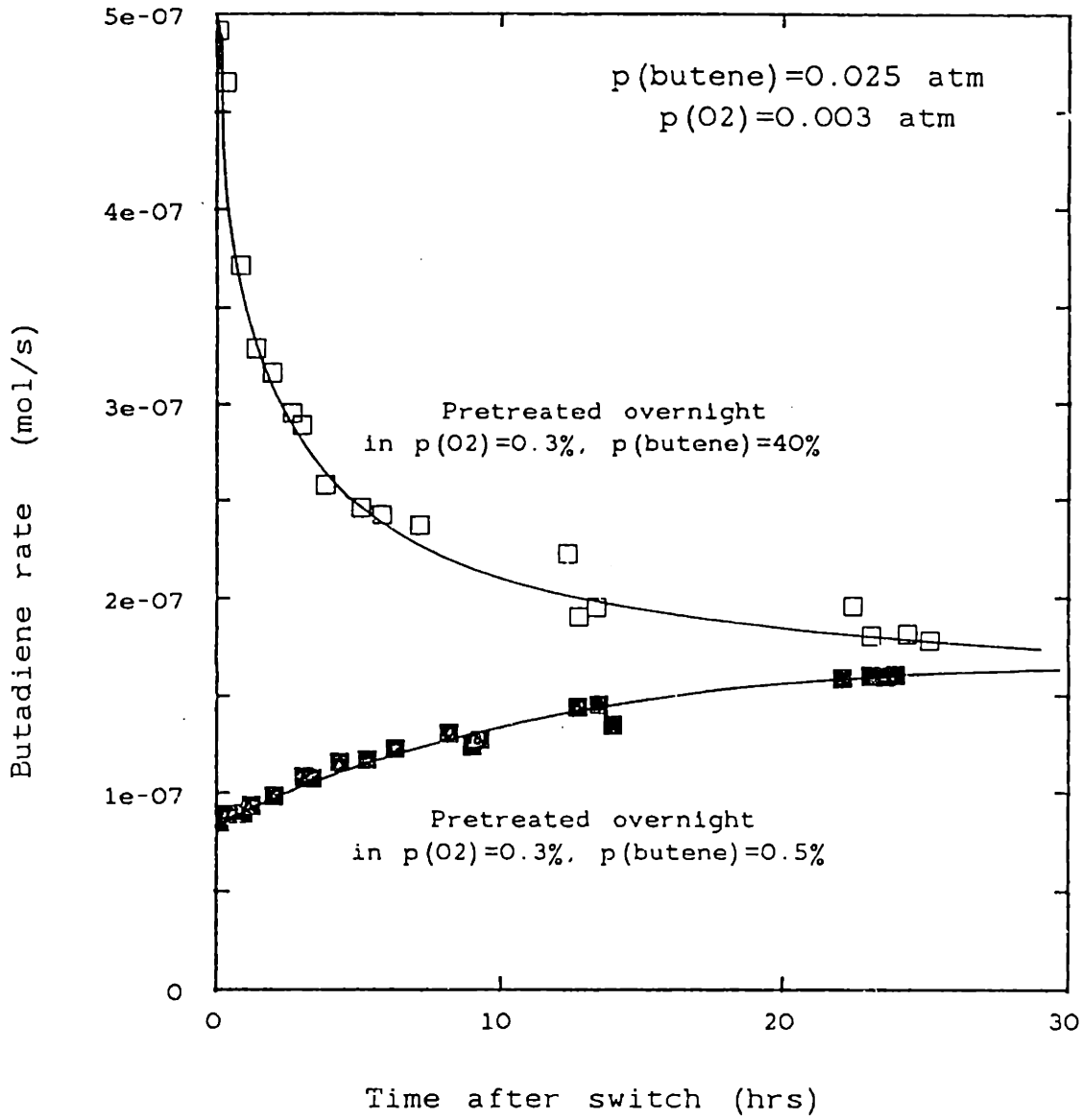

Figure 4.24: Effect of time on stream after different pre-treatments, P_{butene}=0.00247 atm, P_{O2}=0.003 atm, T=544°C

component in the feed (usually zero) and that in the product stream. When the feed is spiked with a component that is also a product, the rate is now the difference between two large numbers (rather than between a small number and zero). This introduces errors and therefore the rates for the spiked component may become erratic, particularily when added at concentrations greater than about 5%.

Spiking the feed with **carbon monoxide** has no effect on the rate of butene consumption, nor on the rate of butadiene production (figure 4.25). The only effect is that CO is further oxidized to CO_2 in a first order process.

Spiking the feed with **carbon dioxide** has no effect on any of the rates whatsoever (figure 4.26).

Spiking the feed with **water** also has no effect on any of the rates (see figure 4.27).

Spiking the feed with **hydrogen** has no effect on the rate of butadiene production (figure 4.28). However, under state 1 conditions, it does appear to initially decrease the rate of CO_2 production by about 50% when it is first added, but then it has no further inhibiting effect. The rate of water production was approximately linear in concentration of hydrogen fed to the reactor. It appears as if the oxygen that would otherwise have been used for CO_2 production is consummed by the hydrogen and forms water.

Under state 2 conditions, where the exit concentrations of butene and oxygen were 1.0% and 1.4% respectively, only one data point was taken, because of limitations in attainable flowrates with the gases available and safety concerns. Nonetheless, adding 0.52% hydrogen to the feed caused the rates of butadiene production and deep oxidation to change almost negligibly (decrease by about 6% each, which is within experimental accuracy for the spiking experiments), whereas the rate of water production

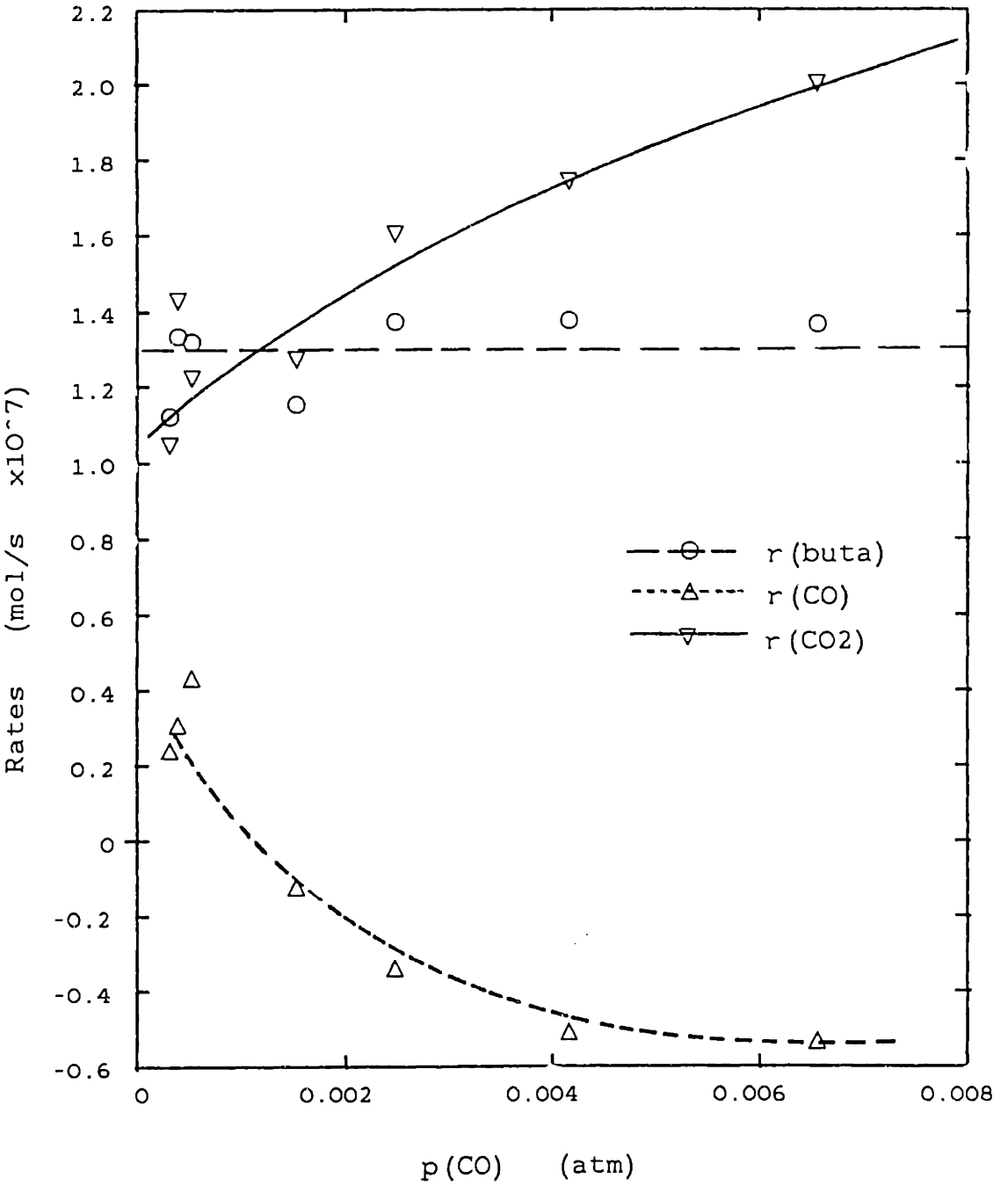

Figure 4.25: Effect of "spiking" the feed with CO, T=513°C

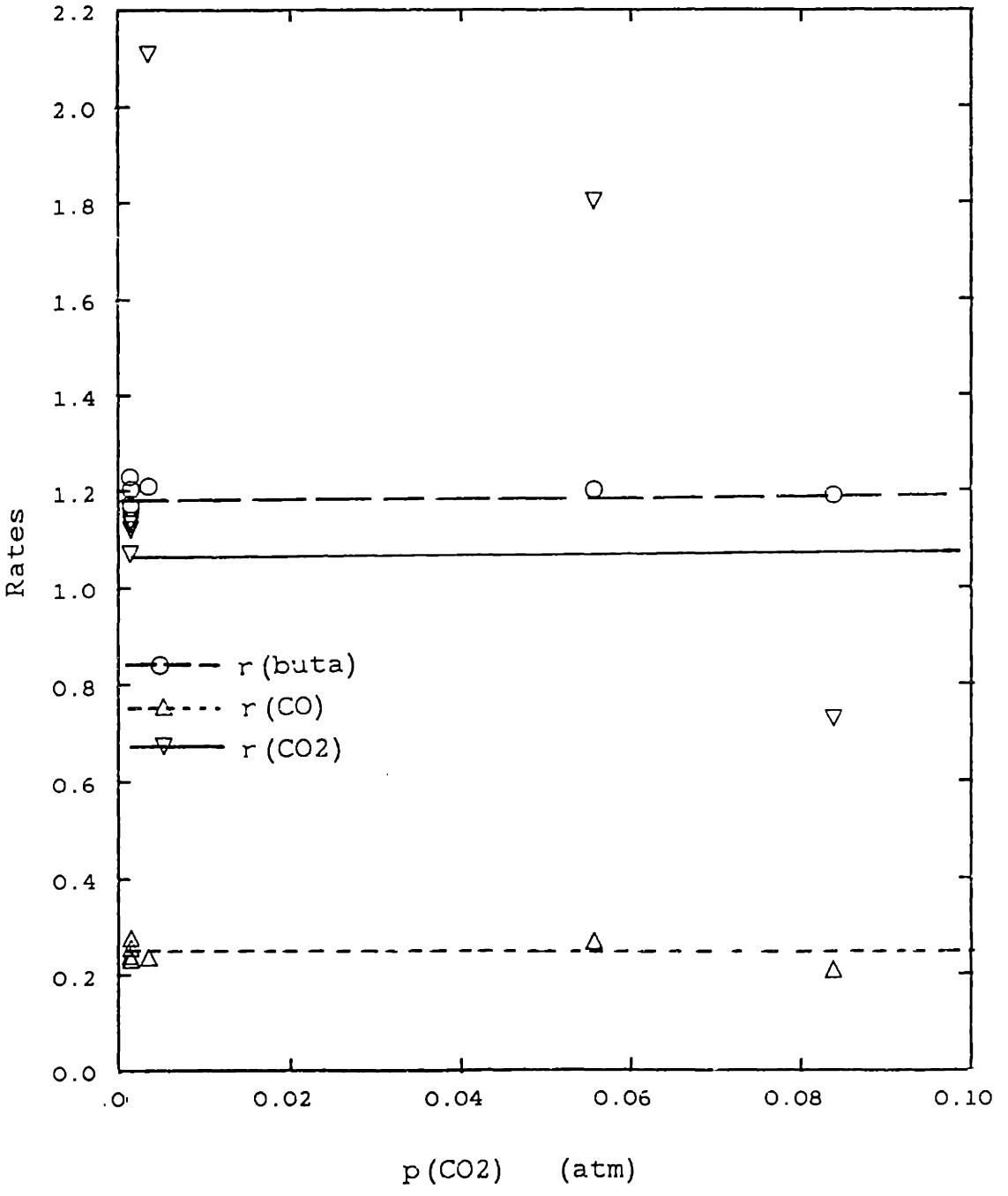

Figure 4.26: Effect of "spiking" the feed with CO_2

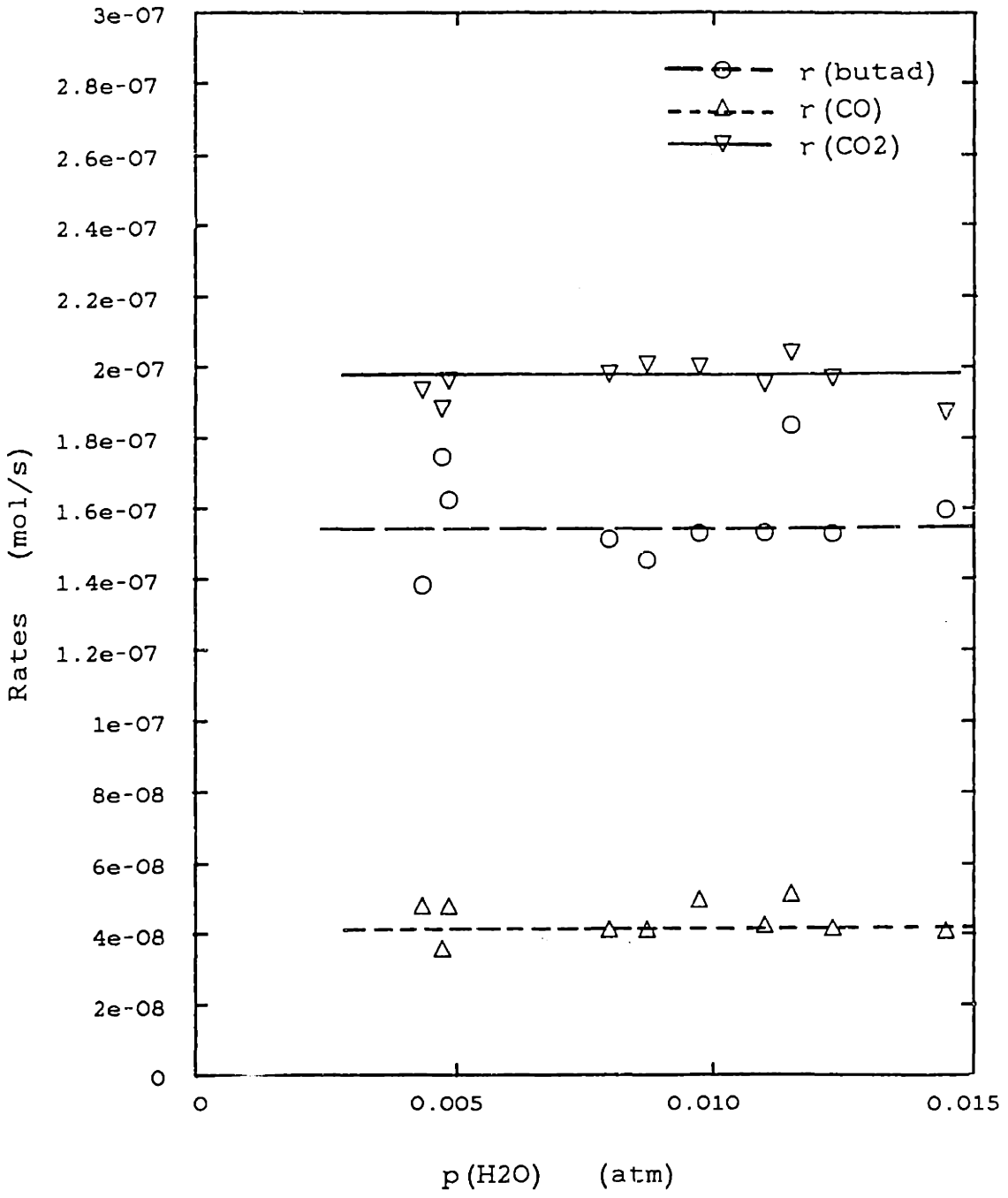

Figure 4.27: Effect of spiking the feed with water

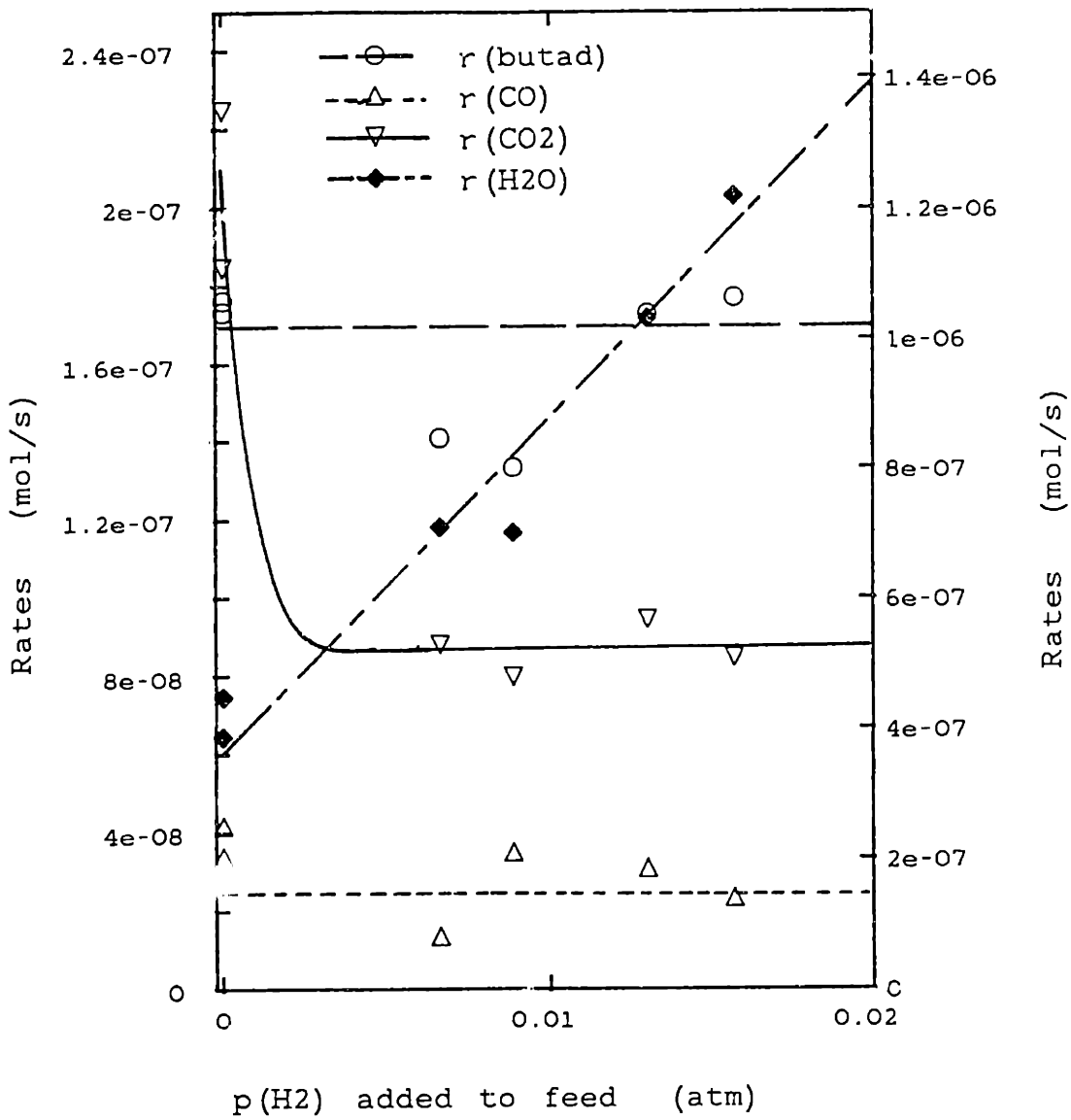

Figure 4.28: Effect of "spiking" the feed with H_2

increased by about 6%.

The effect of **butadiene** on the rates is more significant than for any of the other components (figure 4.29). It appears that at high concentrations of butadiene (above 1%) that the butadiene inhibits the conversion of butene to butadiene, while having almost no effect on the rate of deep oxidation.

4.1.7 Surface Analysis

4.1.7.1 Scanning Electron Microscopy

Scanning electron micrographs of the platinum electrodes before use are shown in figure 4.30. Their corresponding EDAX (energy dispersive analysis by x-rays) spectra showed that both catalyst films prepared from Engelhard Pt 4338-A ink and from Pt 3788-A ink contained no impurities that could be detected by this x-ray analysis. Both appear as sponges and there is little difference between the two samples. The sponge prepared from Pt 3788-A has pores of avout 2-4 m whereas the crystallites formed from Pt 4388-A are about 3-4 m in diameter.

The micrographs of the surface prepared form Pt A-4338 ink is shown in figures 4.31 after use. There is little difference between the before and after photographs. In the photographs taken before use, the faces of the platinum crystals that made up the sponge are visible (the edges between the crystalline faces appear as lines on the photograph). After use, the edges between the individual face have become blurred and the sponge has a more rounded appearance.

Although the surface was predominantly platinum, occasional aberations were observed, as shown in figure 4.33a. The marked area by arrow 1, in this figure, had an EDAX spectrum (figure 4.33d) which was predominantly

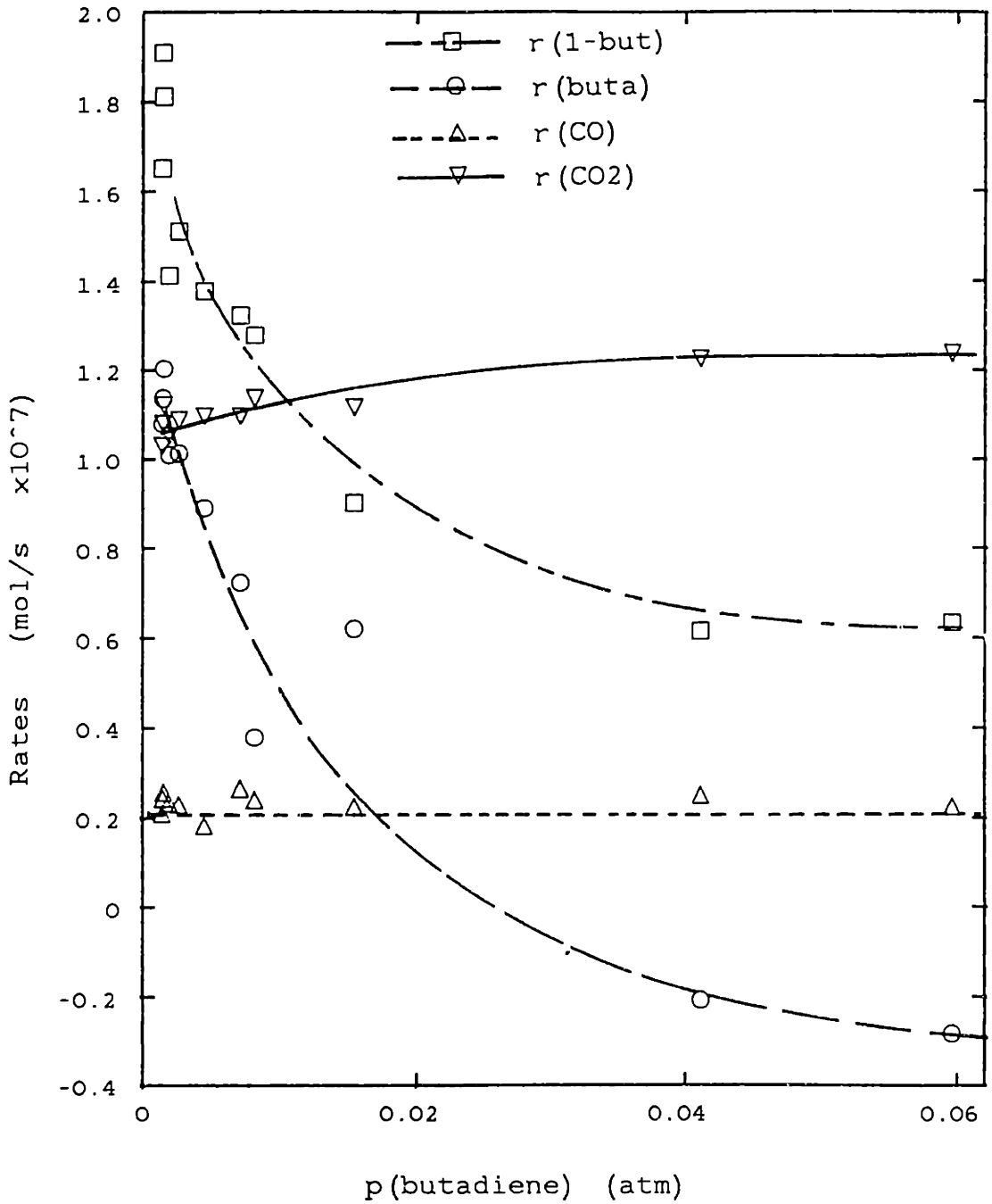

Figure 4.29: Effect of "spiking" the feed with butadiene

(a) Pt (from ink # A-3788)

(b) Pt- (from ink # A-4338)

1 μm

Figure 4.30: Scanning electron micrographs of Pt surface before use, magnification = 20000X

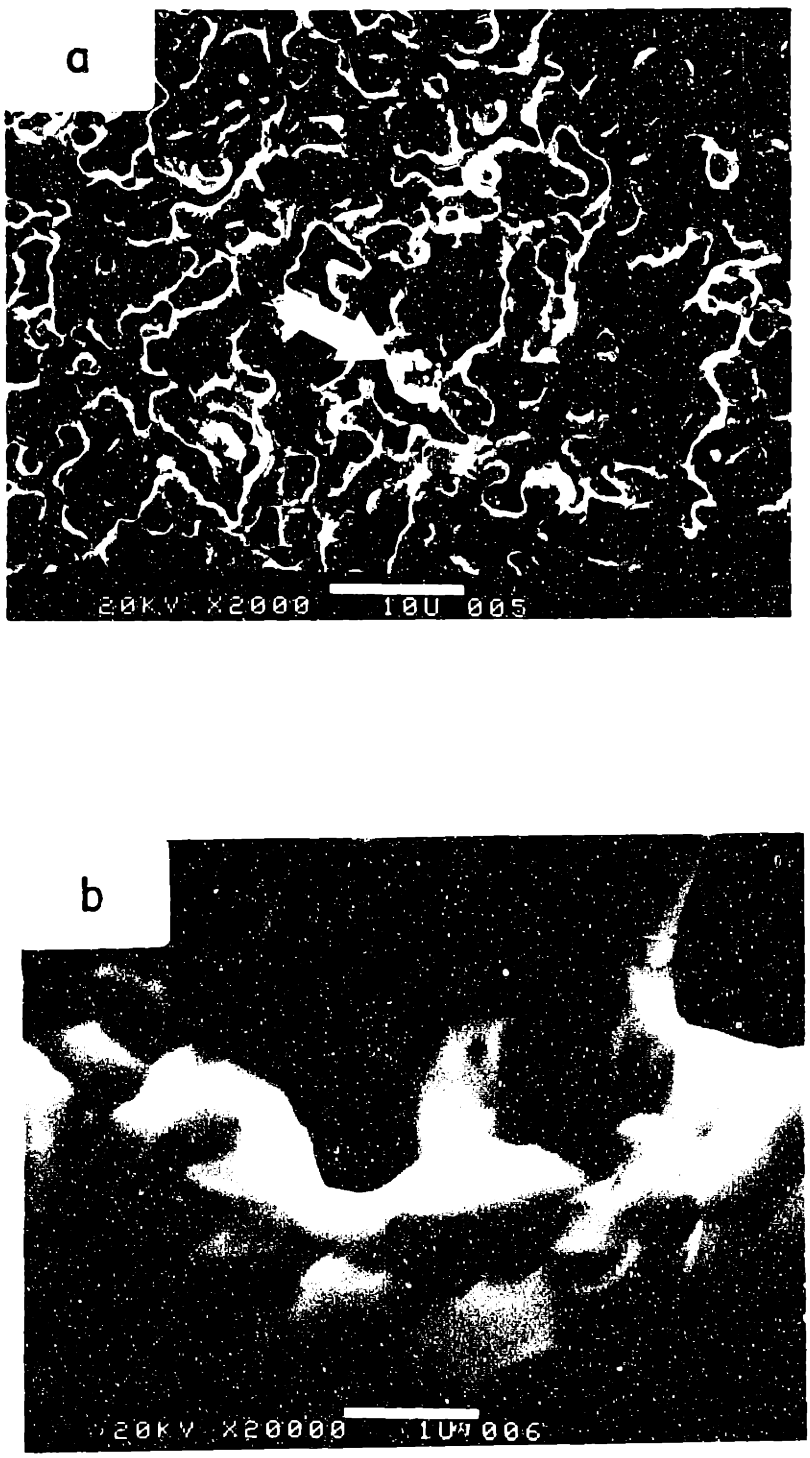

Pt, after use (from ink # A-4338)

Figure 4.31: Scanning electron micrographs of Pt surface after use: (a) 2000X, bar indicator is 10 μm, occlusion indicated by arrow is Ie impurity; (b) 20000X, indicator is 1 μm

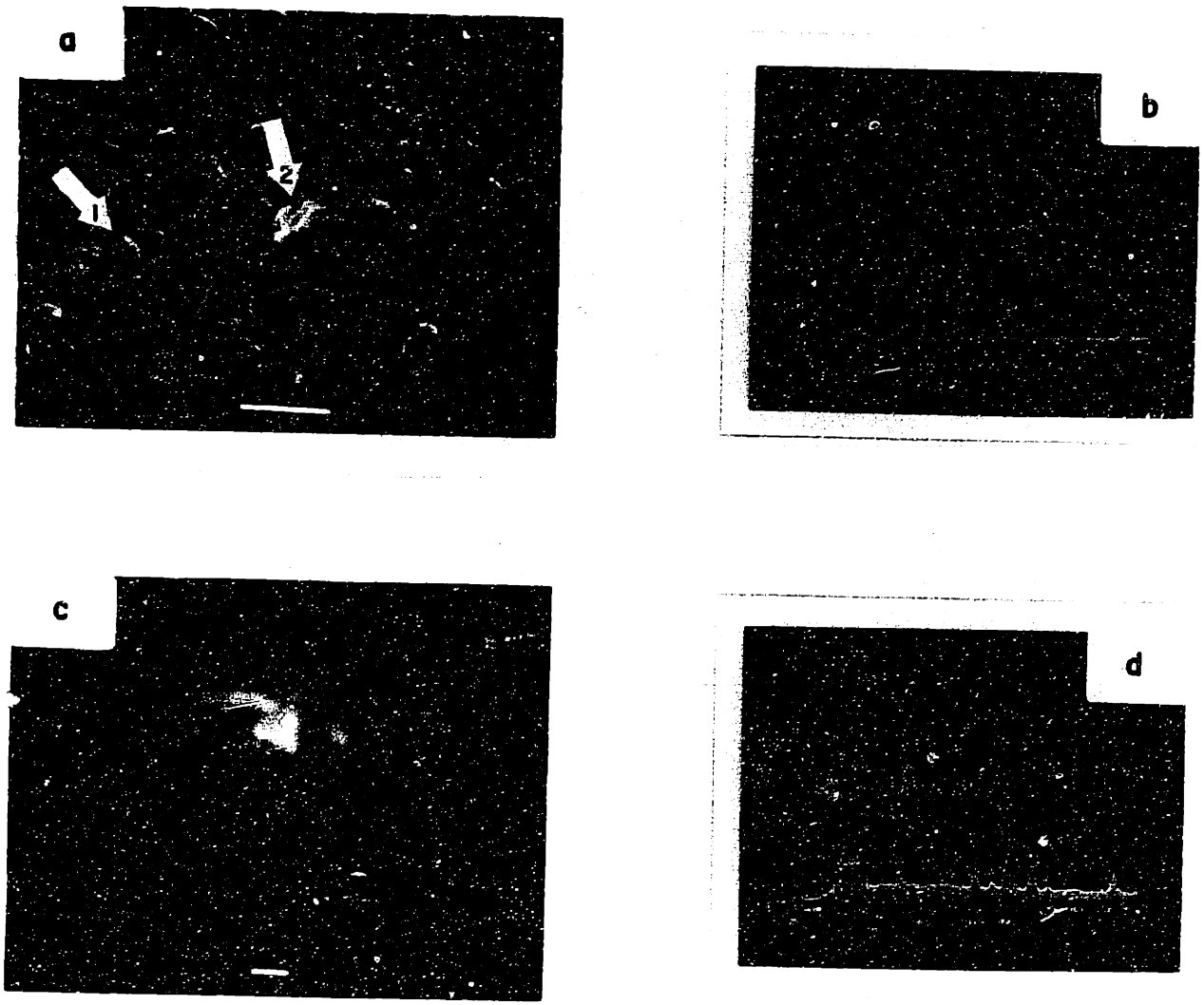

Figure 4.33: Scanning electron micrographs of Pt surface after use: (a) bar indicator is 10 μm (b) EDAX of entire surface shown in (a), (c) increased magnifaction of arrow 1 in (a) (d) EDAX of (c), i.e. an Fe impurity; arrow 2 is agglomerated Pt

that of impurities, specifically Fe, Cr, Ni and Si. This spot had a different, more "fuzzy" appearance than the sponge (figure 4.33c). When an analysis of the entire region of figure 4.33a was performed (figure 4.33b), the relative concentration of iron was considerably lower, indicating that most of the imputity signals came from the aberation, that it was an aberation, and that with the exception of the aberation, the surface was predominantly platinum. These spots were comparatively rare and only seen on the sponge that had been pretreated in air. When the sponge was pretreated in hydrogen, no such impurities could be found on the surface.

4.1.7.2 X-Ray Photoelectron Spectroscopy

A limited number of XPS spectra were taken of samples taken from the surface of the annular reactor after it had been exposed to air, 1.0% butene in He, and 2.0% butene with 0.25% oxygen in He. A mosaic of the small samples was made in order to obtain an area of about 1 cm square large enough for XPS analysis. Spectra were also taken of a polycrystalline platinum film for reference purposes.

The survey spectra of the foil, taken from 0 to -1000 eV, are shown in figure 4.34a before the surface was sputtered with Ar ions to remove the surface layers, and in figure 4.34b after the surface was so sputtered. After sputtering, the polycrystalline platinum foil (figure 4.34b) contains no impurities that can be detected by XPS (with the exception of an extremely small carbon peak at 285 eV, which must have arisen from re-adsorption of carbon from the UHV) and all the peaks belong to platinum and correlate with standards (Physical Electronics, 1976).

The spectra for the surfaces without sputtering (figure 4.36) are similar to the Pt foil spectrum, except that the oxygen and carbon peaks are considerably larger. There are however some minor surface impurity

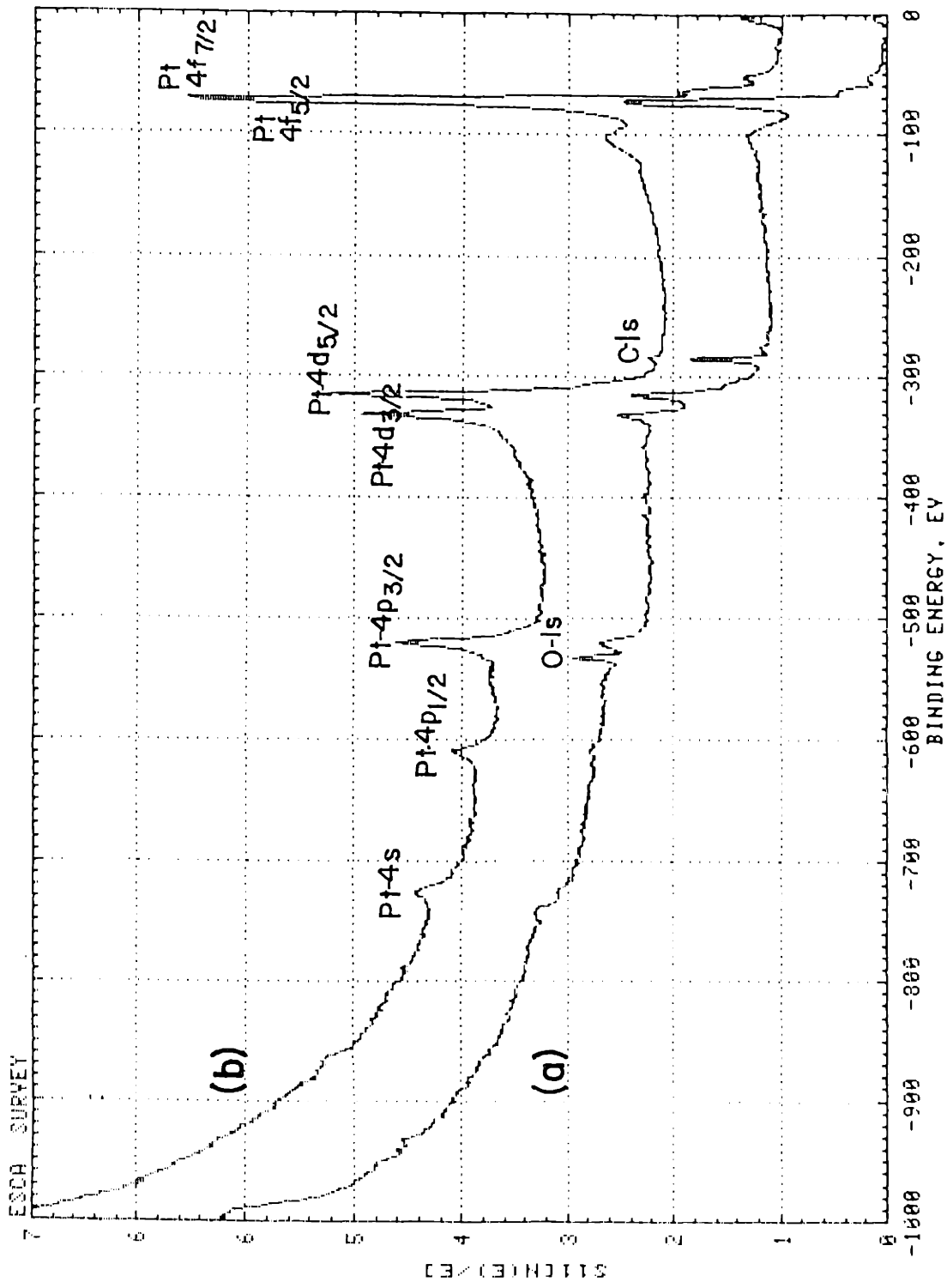

Figure 4.34: XPS spectra of polycrystalline Pt foil (for reference); (a) as received, (b) after sputtering with Ar ions for 5 minutes.

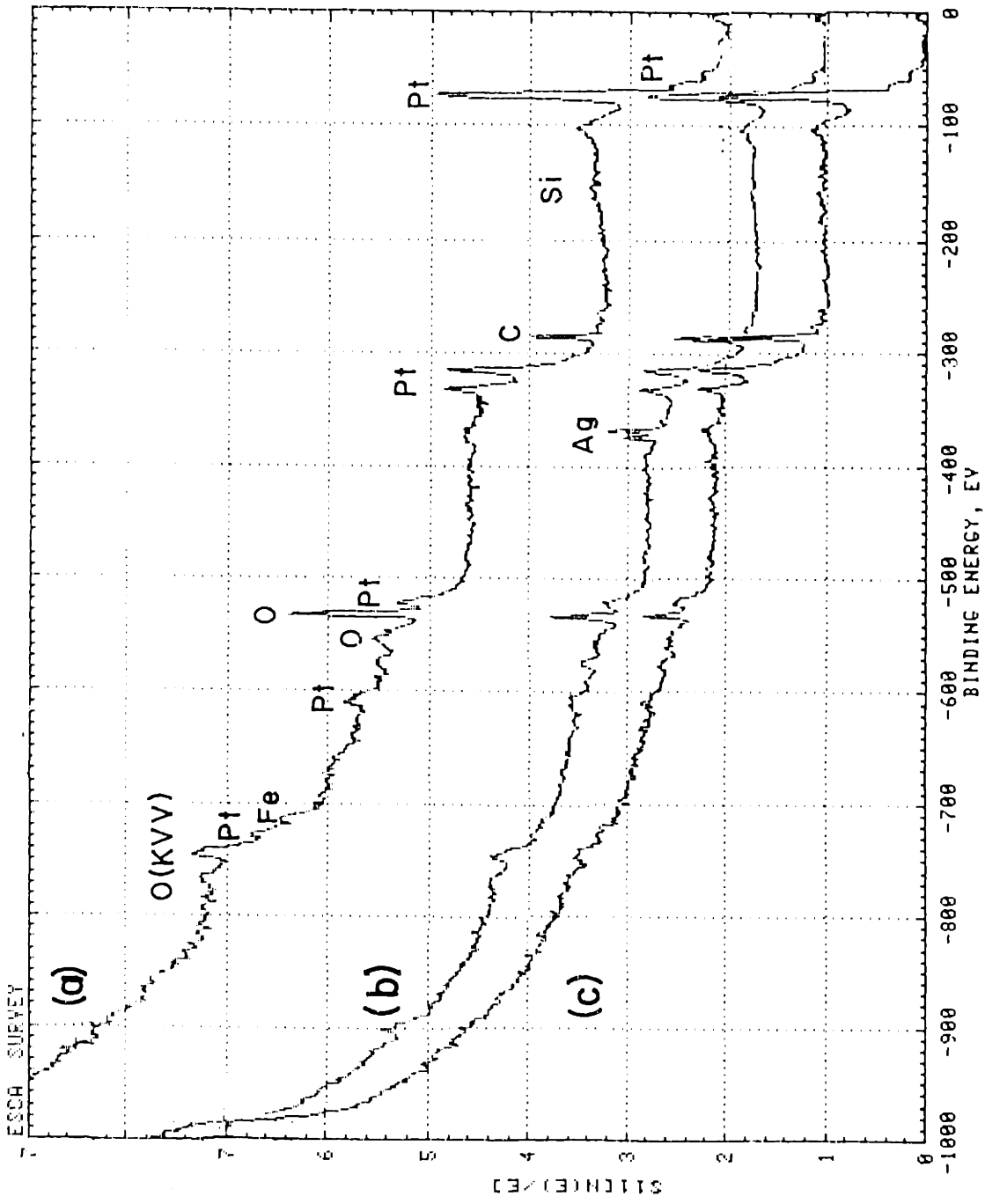

Figure 4.36: XPS spectra of Pt electrode/catalyst after use and pretreatment in (a) air, (b) 0.025 atm butene and 0.0025 atm O_2 (mounted using Ag) and (c) 0.01 atm butene, no r

peaks which are almost at the detectability limit of the instrument: in figure 4.36a (pretreated in air), there are extremely small peaks at about 150 and 170 eV which could be from Si, 370 and 380 eV possibly from Ag and a small peak at about 715 eV possibly from Fe, all other peaks belong to Pt, C or O. The surface atomic composition was determined (using the sensitivity factors listed in table 2.6) as: 14.7% Pt, 47.7% C, 35.6% O, 1.2% Fe and 0.5% Ag.

In figure 4.36b (pretreated in 2% butene and 0.25% oxygen), the catalyst was mounted with Ag paint and the resulting Ag doublet at 370 and 380 eV is clearly visible, together with the other Ag peaks at 575, 605 and 905 eV. Besides the Pt peaks, no other peaks are visible. In figure 4.36c (pretreated in 1% butene in He), the only non-Pt, -C or -O peak is a small Ag peak at 370-380 eV.

No other peaks are visible in these surveys, specifically none for chlorine (the 2p peak is at 200 eV), aluminum (the 2p peak at 75 eV would have been masked by the Pt peaks, however the 2s peak at 120 eV should have been visible), chromium (the $2p_{3/2}$ peak is at 580 eV) or nickel (the $2p_{3/2}$ peak at 860 eV may have been masked by the O(KVV) Auger peak, but the Ni(LMM) peak is strong and occurs at 405 eV and 490 eV).

4.1.7.3 Auger Electron Spectroscopy

Auger electron spectroscopy requires a smaller sample size and the samples could therefore be mounted directly, i.e. it was easier to use. Consequently, it was used to investigate more thoroughly the effect of various pre-treatements on the surface composition. The sequence of pre-treatment atmospheres used, mimicked the sequence of gas compositions used when investigating the effect of a step change in the butene partial

pressure on the activity and selectivity of the catalyst. As discussed in section 4.1.5, the activity and selectivity of the catalyst changed with time on stream after a step change in butene partial pressure, reflecting a change between the two "states" of the catalyst. Surface analysis was performed to see whether these two states correlated with differences in surface composition.

The activity and selectivity of the catalyst were measured at the time that the furnace power was switched off. Minor changes in the surface composition may have occurred during cooling. Although the activity of the catalyst was measured, it is not possible to correlate it with the data in sections 4.1.4 and 4.1.5 because taking samples involved removing pieces of the catalyst from the reactor and therefore reducing the catalyst surface area.

Survey spectra for sample (9), the polycrystalline foil which has a purity of 99.999% is included for reference purposes and is shown in figure 4.37. Figure 4.37a was taken before the foil was sputtered and besides the peaks for platinum, there are peaks from impurities such as carbon and oxygen and other unknown impurities, the result of handling. After the foil had been sputtered with argon ions to remove the adventitial carbon and other surface impurities (figure 4.37b), a large number of peaks remain, all of which belong to Pt and correspond to the published data (Perkin Elmer Handbook, 1976).

Survey spectra of the surface were taken after sputtering with argon ions and all the spectra resembled that of the sputtered platinum foil, with no impurity peaks present, except some C and O. In survey spectra taken before sputtering, the majority of the peaks are due to Pt, C or O, however, there are some other surface impurities present. The amount and concentration of these impurities varied with sample pretreatment, was not

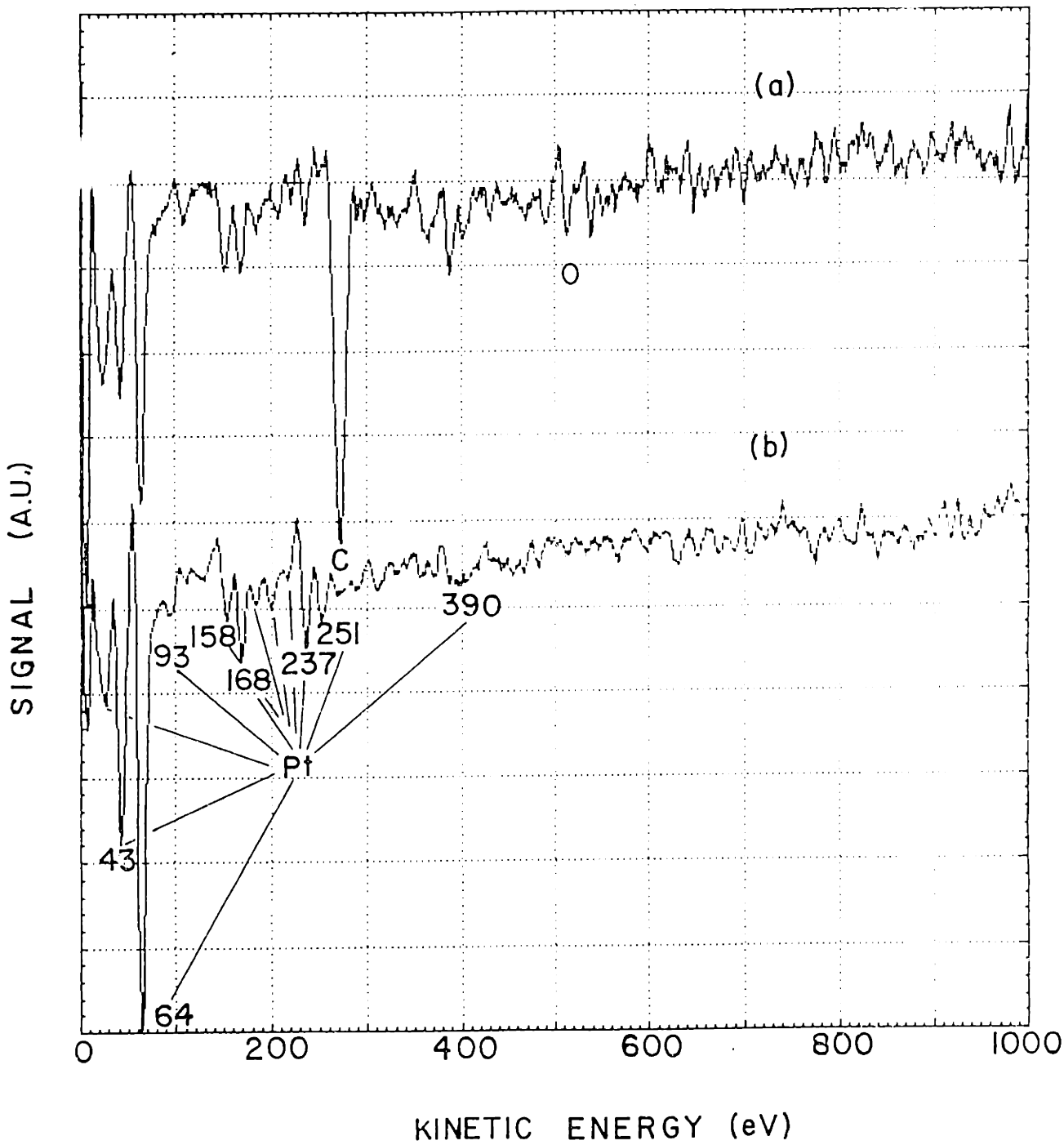

Figure 4.37: AES spectra of polycrystalline Pt foil (for reference); (a) as received, (b) after sputtering with Ar ions for 5 minutes.

homogeneous across the sample surfaces, nor were they consistent between repeat analyses of different samples which had had the same pretreatment.

After pretreatment in 10% H_2 in He (figure 4.38a), besides the expected peaks for Pt, C and O, there appears to be some chlorine on the surface at 150 eV, and silver at 350 eV. Chlorine was not observed in any other spectra irrespective of the pretreatment. When the reactor was pretreated in oxygen, figure 4.38b and 4.39a, iron (a triplet at 598, 650 and 703 eV) was sometimes observed (figure 4.39a) but not at other times (figure 4.38b). There is also a peak at about 80 eV which may be due to Al and an even lower energy peak at about 20 eV possibly from the carbon.

In the absorbed current image of the surface pretreated in 0.15% butene and 0.25% oxygen, regions of lighter and darker complexion were observed. When the electron beam was focussed on a lighter region, it was found to have a high concentration of iron (18.7 atomic % of the surface). On the same surface an adjacent region had an iron concentration of 10.9% and another sample 0 % iron (figure 4.39b).

When pretreated in 1.0% butene in He at 513°C (figure 4.38c), carbon dominated the surface, reducing the sizes of the platinum peaks significantly and also not permitting any other impurities to show. The low energy peak at about 20 eV is probably from the carbon overlayer.

The kinetic energy for the elements were:
Pt: 64.0 - 64.7 eV; C: 270.4 - 271.0 eV; O: 511.0 - 511.5 eV and did not change with pretreatment, nor with sputtering. The atomic concentrations of the surface, before sputtering, as determined by multiple scanning of the specific peaks are shown in table 4.4.

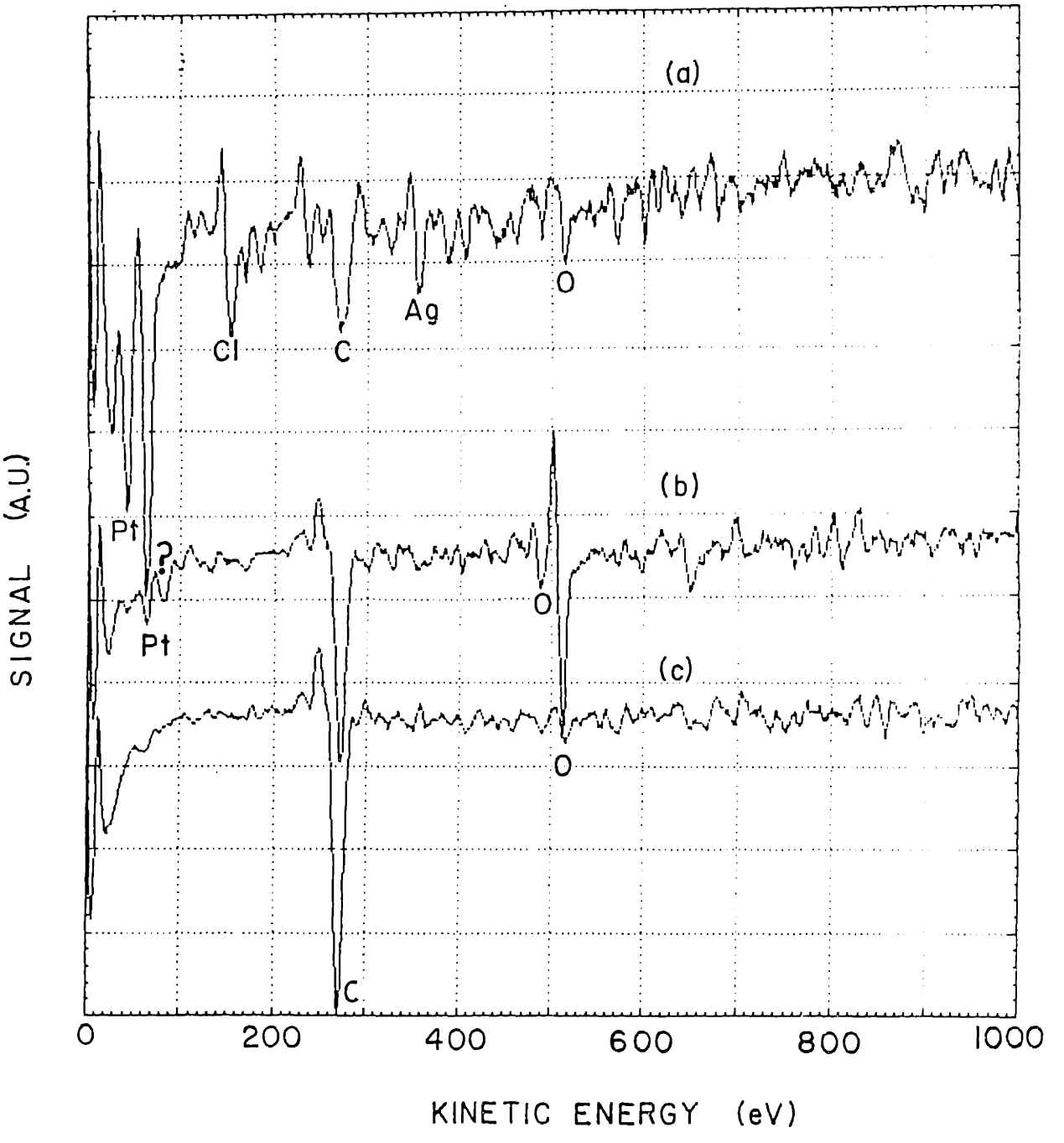

Figure 4.38: AES spectra of Pt electrode/catalyst after pretreatment in (a) 0.10 atm H_2, (b) air, (c) 0.01 atm butene.

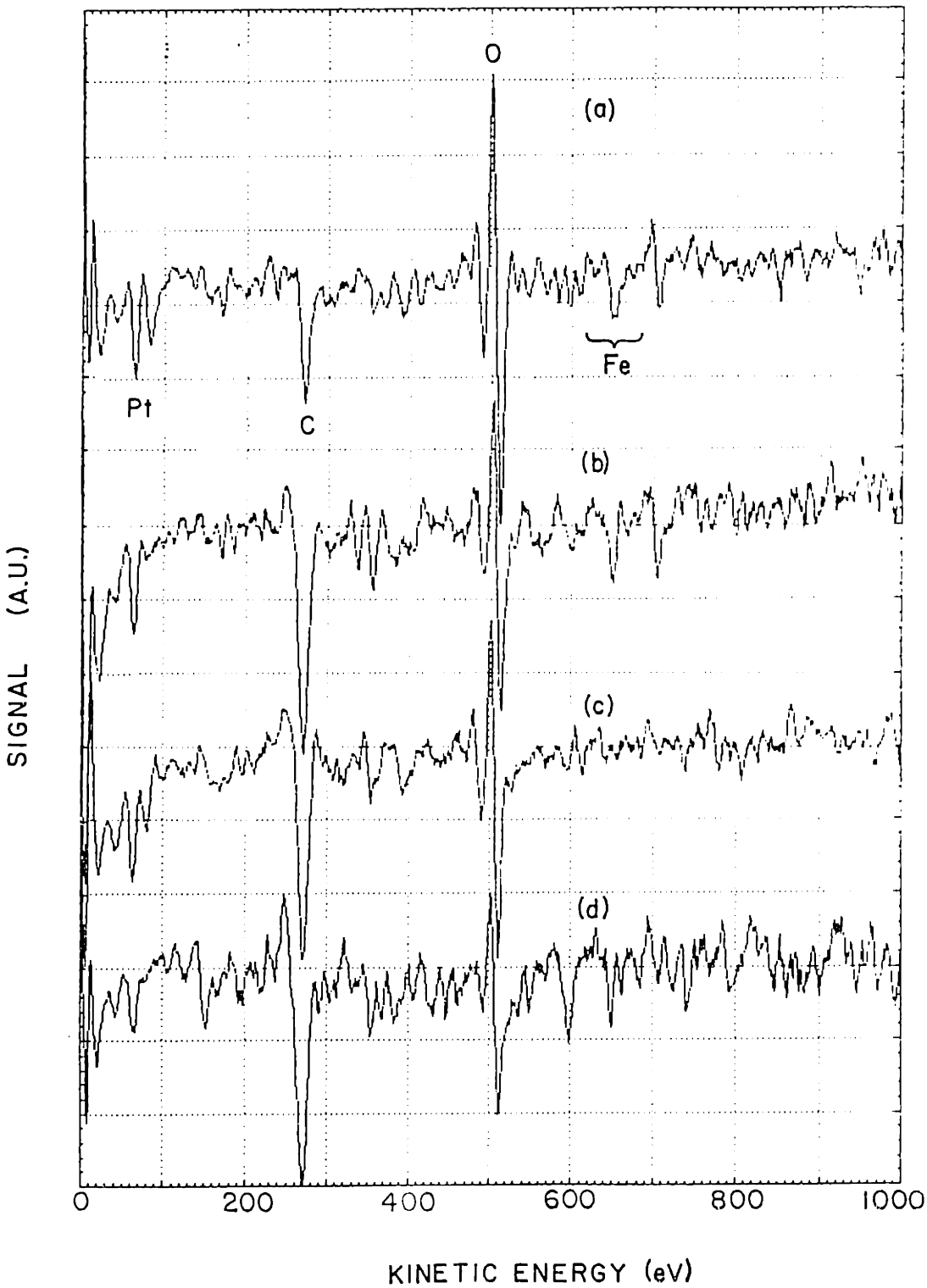

Figure 4.39: AES spectra of Pt electrode/catalyst after pretreatment in (a) air (repeat), (b) 0.0025 atm butene, 0.0025 atm O_2, (c) 0.025 atm butene, 0.0025 atm O_2 for 1/2 hr after 16 hrs in 0.0025 atm butene, 0.0025 atm O_2, (d) 0.025 atm butene, 0.0025 atm O_2 for 16 hrs.

Table 4.4 Atomic concentrations of the surface of the platinum catalyst as determined by Auger spectroscopy

Sample	Pre-treatment Conds.			Surface Composition				
#	[Bu] (%)	[O_2] (%)	time (hrs)	Impurities Observed	Pt (%)	C (%)	O (%)	O/Pt
1	(10.0% H_2 in He)			Cl	58	38	7	0.11
2	0	21	16	Al, Ag, Fe	13	42	45	3.6
3	0.15	0.25	16	Ag, Fe	15	52	35	2.4
4	2.0	"	1/2	Al	16	52	33	2.1
5	2.0	"	16	Fe	9	76	15	1.6
6	40.0	"	16	none	-	~100	-	-
7	1.0	0.0	16	"	18	54	5	0.12
8	Pt foil			"	41	54	5	0.12

The surface of a 1000 A film of tantalum oxide on tantalum was sputtered off using identical sputtering conditions to those used below (figure 4.40 (c)). It took 8.8 minutes to penetrate the film with the ion gun settings of 4.5 kV and 60 A. The time for penetration is calculated assuming that the penetration curve may be modelled as an exponential decay, and that the time of penetration is the decay constant for the curve, or 1/e of the decrease.

The surfaces of the catalyst was sputtered off after the surface analysis was complete. The atomic concentrations of Pt, C and O were recorded versus sputtering time for each pre-treatment used. The sputter profiles for the Pt foil and for the catalyst surface pre-treated in 10% H_2 in He are shown in figure 4.40 (a) and (b). To convert sputter times into depths, even when the rate is known for a standard such as Ta_2O_5, it is

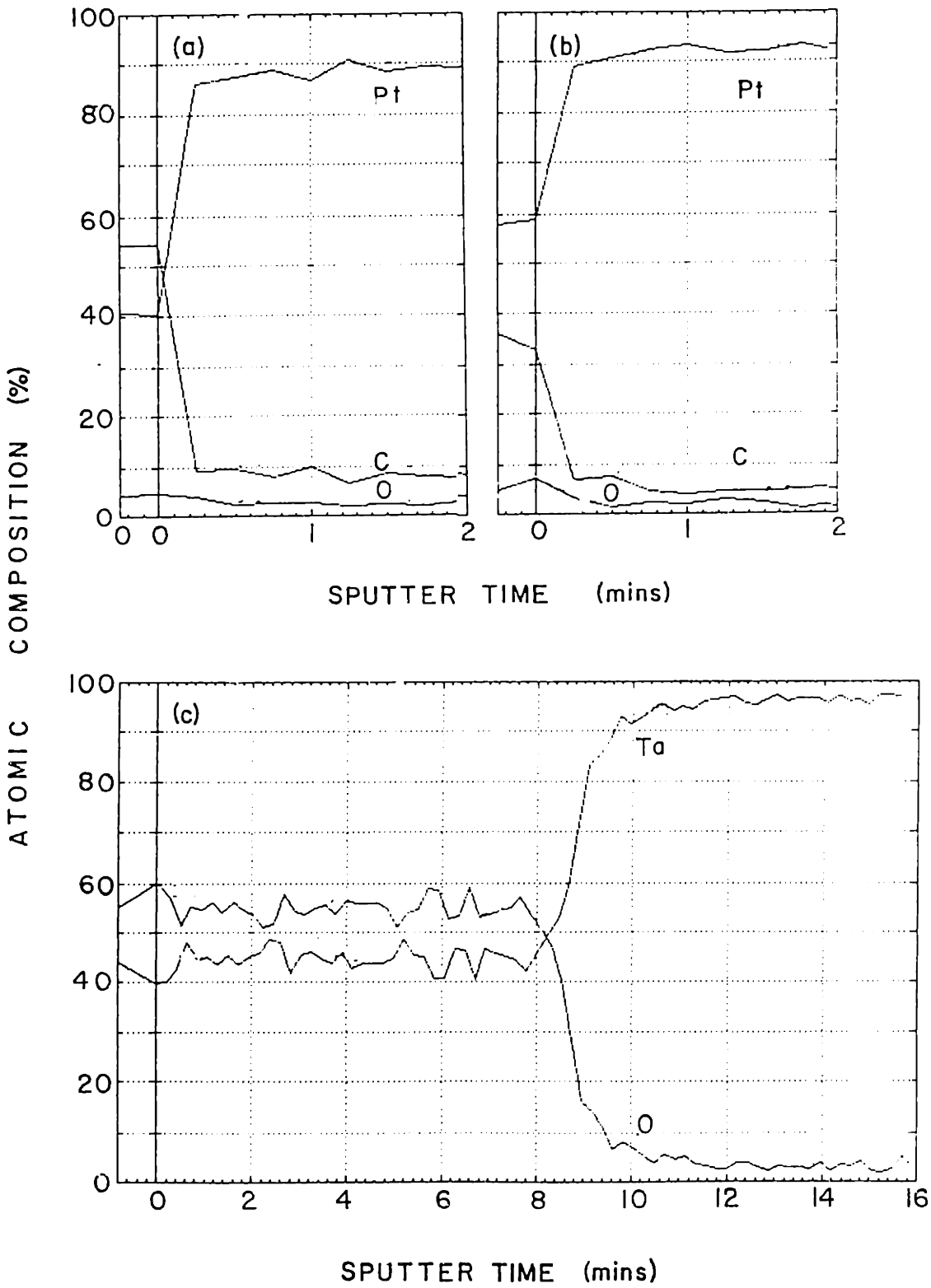

Figure 4.40: Sputter profiles: (a) reference Pt foil, (b) Pt catalyst after pre-treatment in H_2 and (c) 1000 A thick film of Ta_2O_5 on Ta.

necessary to know the sputter yield (in atoms/ion) for the sample under investigation. Sputter yields are known for a few standards, but not for platinum oxide on a platinum surface partially covered with carbon. Platinum metal is sputtered at about 2.2 times the rate of Ta_2O_5, and oxides are typically sputtered at a slower rate than their corresponding metals. However, if the rate is assumed to be identical to that for the Ta_2O_5 standard. a semi-quantitative estimate may be obtained which is probably correct within an order of magnitude.

In figure 4.40 (a) and (b), the carbon was completely removed within 0.25 minutes, which corresponds to a thickness of less than 15 A, and arose from adventitial carbon on the surface. The similarity between the foil and the H_2 pretreated sample confirms that handling the sample in air did not cause significant changes to the surface.

In figure 4.41 (a), the O signal decreased to 0.369 of the initial signal in about 0.38 minutes, which corresponds to approximately 42 A. After exposure to 0.0025 atm butene and 0.0025 atm oxygen, the O/Pt ratio had not decreased significantly, but the thickness of the oxide film decreased to about 20 A (figure 4.41 (b)). The C, O and Pt profiles are indentical in figure 4.41(c) which had been exposed to 0.002 atm butene and 0.0025 atm oxygen for 1/2 hour, but after 16 hours (figure 4.41(d)), the carbon film had increased to about 40 A. After exposure to 0.40 atm butene and 0.0025 atm oxygen, the carbon film had increased significantly and corresponded to about 125 A (figure 4.41(e)) compared to about 80 A after 16 hours in 0.01 atm butene (no oxygen, figure 4.41(f)).

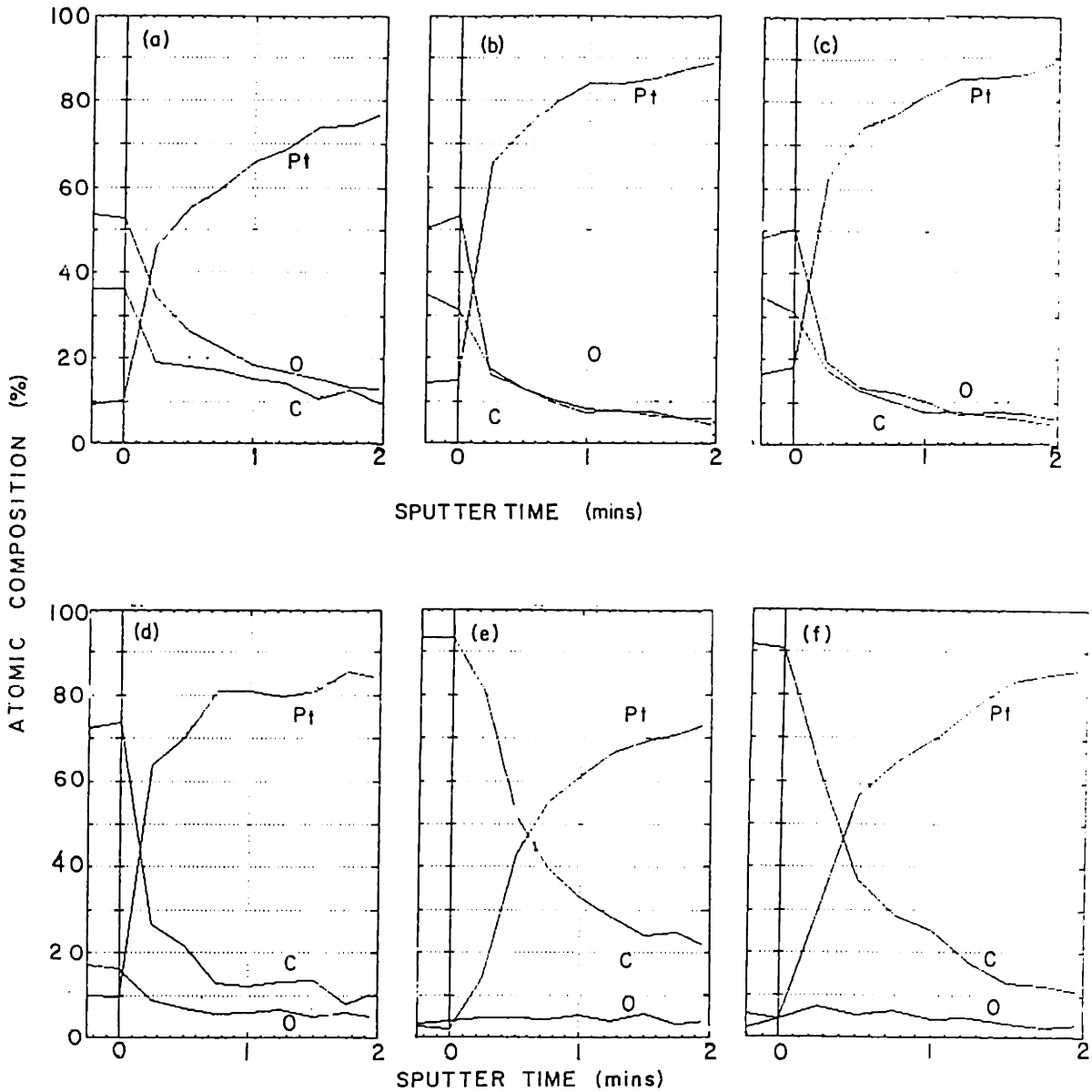

Figure 4.41: Sputter profiles after pre-treatment in (a) air, (b) 0.0025 atm butene, 0.0025 atm O_2, (c) 0.02 atm butene, 0.0025 atm O_2 for 1/2 hr, (d) 0.02 atm butene, 0.0025 atm O_2 for 16 hrs, (e) 0.40 atm butene, 0.0025 atm O_2 and (f) 0.01 atm butene, no O_2

4.2 DISCUSSION

4.2.1 Effect of Time on Stream

The effect of leaving the reactor exposed to the reaction mixture (figure 4.1) was to cause the surface to come to equilibrium over about 10 hours where it remained stable for about 100 hours before the activity slowly decreased.

4.2.1.1 Short Time Reactivity Changes

It should be noted that, in figure 4.1, the selectivity to butadiene increased significantly during the first ten hours, then remained stable, even when the activity was decreasing, beyond 100 hours. It therefore appears that a significant change in the catalyst may have occurred in the first ten hours resulting in the decrease in the deep oxidation rate and increase in the butadiene production rate. The catalyst had been pretreated in air to remove carbon deposits from the surface, and it may be hypothesised that the change in the activity/selectivity is due to the removal of surface oxygen or oxide species on the surface. The time involved, about ten hours, would appear to imply that the change could not have been due to chemisorbed oxygen, since this would have been removed within a few minutes. It would rather imply a slow reaction, probably a solid state reaction, possibly the decomposition of an oxide layer or layers on the platinum surface.

The effects of time on stream on the rates of butadiene production and deep oxidation after various pretreatments appear to bear this out (figures 4.23 and 4.24). After the catalyst had been pretreated in 0.5% butene and 0.3% oxygen, the rate of butadiene formation increased with time when the exit composition was kept constant at 2.5% butene and 0.3% oxygen reaching steady state after about 24 hours. At the same time, the rate of deep

oxidation decreased by a factor of three. The hypothesis is that after pretreatment in a low p_{butene}, the surface was covered with an oxide film, which slowly decomposed, leaving the clean platinum surface. After the catalyst had been pretreated in 40% butene and 0.25% oxygen, the rate of butadiene decreased (figure 4.23) possibly because the formation of oxide was reducing the area available for butadiene formation.

Ostermaier, Katzer and Manogue (1976) found that the rate of NH_3 oxidation at 433°C decreased with time on stream under oxidizing conditions due to the formation of platinum oxide (probably PtO_2) on the surface. This is analagous to the decrease in activity for butadiene production observed in these experiments, with time on stream at high $p_{02}^{1/2}/p_{butene}$ ratios.

A similarily long time scale was observed by Amirnagmi and Boudart (1975) during the decomposition of NO over Pt foil at 1000°C. When O_2 was added to the NO feed, an oxidized surface (of PtO_2) was apparently formed which slowed the reaction rate. It took approximately 1.4 hours for the oxide to form (or decompose) and for a steady state to be obtained.

The concept of a surface platinum oxide film was proposed to explain the kinetics of oxygen desorption as described in section 3.3.3, above. The time required to decompose the oxide in those experiments was considerably less than ten to twenty hours observed here. This difference may be due to the oxidation times and conditions used. In the desorption kinetics measurements, the surface was oxidized for a maximum of only 100 minutes at 477°C, whereas the pretreatments used for this reactor involved at least two hours at 727°C (1000 K) before cooling to the reaction temperature in air and then exposure to air for about 16 hrs. This would have resulted in a far greater degree of surface oxidation, possibly as

multilayers of oxide as was observed by Ostermaier, Katzer and Manogue (1976). Therefore, although the rates may not appear to be the same, the underlying mechanism may be.

4.2.1.2 Long Time Activity Change.

Beyond 100 hours, the activity of the catalyst decreases while the selectivity remain constant (figure 4.1). At the same time, the data of combustion of surface carbon to CO_2 show an increase in the CO_2 released with the length of time that the catalyst was on stream (figure 4.3).

After each set of data had been taken, the reactor was exposed to helium for at least two minutes, which was sufficient time for the reaction mixture to be flushed from the reactor. Therefore, the CO_2 that was released must have come from carbon adsorbed on the surface via:

$$C_nH_m(a) + \text{oxygen (gas or adsorbed)} \longrightarrow nCO_2(g) + m/2H_2O \qquad (4)$$

When comparable experiments were performed to determine the kinetics of oxygen desorption from the surface, no CO_2 was found when switching from ethylene (or CO) to air, via two minutes in helium. This indicates that ethylene had not adsorbed very strongly on the surface and that insignificant amounts of carbon had formed on the surface during the (about) 30 minutes exposure to ethylene.

It seems reasonable to hypothesise that butene would behave similarily to ethylene and not adsorb irreversibly on the platinum surface, and therefore the CO_2 formed arose from carbon on the surface which had arisen from the dehydrogenation, cyclization and aromatization reactions of adsorbed butene. Furthermore, the amount of CO_2 released is about an order of magnitude greater than that formed during the oxygen desorption kinetic runs. From figure 3.14 about 10×10^{-6} mols CO_2 were formed by titration of the monolayer of oxygen adsorbed on the surface. In figure 4.3, the

amount of CO_2 released by combustion of surface carbon in air is about 20 x 10^{-6} mols of CO_2 and increases to about 120 x 10^{-6} mols CO_2 with longer times on stream, or the equivalent of about 2 to 12 monolayers of coke.

Barbier et al. (1985) reported similar behavior for Pt-Al_2O_3 catalysts that had been coked in pentane/nitrogen mixtures. They observed two peaks in the CO_2 output when performing temperature programmed oxidation of pre-coked samples. They associated the lower peak, at 270°C, with carbon on the platinum catalyst, and the higher temperature peak, centered at 450°C, with carbon on the support. All the coke had burned off the surface by about 620°C. During coking, the catalytic activity dropped significantly in the first hour then remained stable. Identical results were observed by Pareara, Figoli and Traffano (1983) during the DSC (differential scanning calorimetric) temperature programed oxidation of coke on Pt-Al_2O_3 catalysts which had been coked in hexane- or methylcyclopentane-hydrogen mixtures at 500°C for 2 hours.

The data presented here with Perera and Barbier et al.'s data appear to confirm the model of a working catalyst proposed by Davis, Zaera and Somorjai (1982, and Davis, Zaera, Gordon and Somorjai, 1985) where they proposed that the surface of a platinum catalyst has a steady state coverage of both "active" and "inactive" carbon (for ethylene hydrogenation) on the surface which may be several molecules high. At the same time however, there are still some uncovered, reactive Pt atoms exposed. From the data presented here, it appears that this steady state probably forms rapidly when the reactor is first brought on stream. Coke then continues to form at a slow rate, not significanlty affecting the butadiene and deep oxidation reactions for the first 100 hours. Beyond 100 hours, the amount of carbon on the surface apparently becomes so great (figure 4.3) that it has an effect such as blocking catalytic sites on the

surface, or blocking the pores and limiting access to the catalyst interior, thereby decreasing the catalytic activity (figure 4.1).

In contrast to the activity, the selectivity is not effected by the carbon deposition. This indicates that either the carbon blocks all sites on the catalyst indiscriminately as was proposed by Davis, Zaera and Somorjai (1982), or the catalytic sites are approximately identical in activity with respect to butadiene formation (at constant p_{butene} and p_{O2}).

In conclusion, after pre-oxidation of the catalyst, the changes in the activity/selectivity that occur after the reactor has been on stream for a short time arise because oxide on the surface is being decompsed, producing more platinum surface, which is favorable for butadiene formation. after long times on stream, the surface becomes covered with carbon which blocks the sites on the platinum surface for both the butadiene formation and the deep oxidation reactions.

4.2.2 Surface Analysis

The elemental composition of the catalyst bulk was determined by EDAX, and the surface composition of the catalyst by XPS and Auger spectroscopy, in an attempt to independently evaluate the hypothesis presented above, that the surface is covered by an oxide film in the presence of excess oxygen, which decomposes in the presence of excess butene. The surface analysis data qualitatively confirm this hypothesis, however, it is necessary to first assess the significance of the impurities seen.

4.2.2.1 Surface Impurities

The catalyst surfaces were made form "inks", which are platinum crystallites dispersed in an organic matrix. When they are fired in air, the organic matrix burns off leaving the Pt crystallites behind, which fuse

to form the sponges seen in figure 4.30. The crystallinity of the fresh samples is visible in the figures. The only difference between these two preparations is the size of the crystallites used, about 2-4 μm for Pt 3788-A versus about 3-4 μm for the Pt 4338-A ink. When micrographs were taken without depositing gold on the surface, surface charging was a problem, preventing high magnification. This would indicate the presence of an insulating film on the surface, possibly due to an oxide.

According to the EDAX analysis of the catalysts, the bulk of the material is platinum (figure 4.33b). There were, however, odd inclusions of Fe, Cr, Ni and Si that were observed both by EDAX (figure 4.33d) and which appeared "fuzzy" in the associated micrograph (figure 4.33c). The "inks" from which the sponges are produced are manufactured by Engelhard, Inc. from platinum black, which is ball-milled in a stainless steel ball mill with stainless steel balls in an attempt to reduce the surface area (Mahoney, 1986). It is possible that the "nodule" of impurity, of about 1 μm that was observed in the micrograph, may have entered the ink in this processing step. The composition of the nodule was predominantly iron with lesser quantities of chromium and nickel. This correlates with the composition of stainless steel; for example, type 304 stainless steel is 1% Si, 2% Mg, 18-20% Cr, 8-12% Ni and the balance, about 68%, Fe (Castle Metals, 1977).

Iron was not observed by either XPS or AES when the surface was pretreated in the presence of butene or hydrogen. When the surface was pretreated in air, iron was sometimes observed, by AES, but not at other times (figure 4.38b versus 4.39a). It is possible that pretreatment in air causes any iron present to oxidize and segregrate to the surface. Also, in Auger spectroscopy the analysis beam is about 1 μm diameter, and if the

iron had arisen as a nodule of about 1 μm from processing (as observed in the SEM), then this would also account for the inhomogeneity and occassional high concentration of iron on the surface, as observed by Auger spectroscopy. In XPS analysis of the surface, an extremely small peak of iron was observed only in the sample that was pretreated in air (figure 4.36a, at 710 eV). XPS is reasonably sensitive to iron (see table 2.6) and this small peak would correspond to a surface concentration of less than 1.2%, this is at the detectability limit of the technique. This compares with 15% for platinum, 47% for carbon, 36% for oxygen and .5% for silver.

It seems likely that the iron impurities arose from processing, exist in small islands (after pretreatment and surface segregration in air) but in sufficiently small quantities that it can be ignored.

Other impurities detected on the surface of the platinum film after various pretreatments include chlorine, aluminum and silver. None of these components was ever detected in the "bulk" analysis by EDAX. Chlorine was only seen on the sample pretreated in hydrogen, and may also have arisen from Engelhard's processing (Mahoney, 1986). The scource of aluminum and silver is not known, although Schmidt and Luss (1971) report observing Ag in Pt/Rh catalyst gauzes and Fe was observed in 99.99% purity polycrystalline platinum foils (Razon and Schmidt, 1986).

Fluxing agents are sometimes added by the manufacturer to decrease the temperature required for firing the films, and still obtain good adhesion. Isaacs and Olhmer (1982) reported the presence of bismuth in fluxed platinum inks which inhibited the performance of the inks as electrodes in oxygen sensors. They proposed using mixtures of platinum black and an platinum organometallic resin to avoid this problem. Erhrardt et al (1984) also reported problems when using catalysts formed from fluxed platinum

inks for the oxidation of CO in oxygen. They found that calcining the reactor in vacuum for two hours followed by washing the reactor in boiling 2N HNO_3 for five minutes removed surface impurities and restored the specific catalytic activity to that of a film that had been calcined at 1200°C until a steady state specific activity had been reached.

Teague (1981) performed Auger analysis of Pt electrodes prepared from a fluxed ink (Engelhard A-3788), the fluxed ink after it had been sintered at 1000°C for 3 hours and an unfluxed Pt-Rh ink (Engelhard 6929). She observed Be, Cl, K and Ag impurities in the electrode prepared from fluxed ink which were not present in either the "sintered" or Pt-Rh preparations.

The Pt ink used for the majority of this study, Engelhard Pt 4338-A, is an unfluxed ink prepared from platinum black suspended in a mixture of cellosolve acetate and terpineol 318, with a platinum content of 65.2-65.7 wt %. It contains only platinum, no fluxing agents are added. Also, although not required, the cleaning technique of Erhrardt et al. was used to remove any (ceramic) impurities that may have been added by processing. Thus, although some impurities were detected by AES, it is felt that their concentrations are sufficiently low that their effects may be ignored.

4.2.2.2 Surface Contamination from Handling

For sample 1, the reactor was pretreated in air to 750°C, then switched to 10% H_2 in He, cooled and the sample taken. It was stored and transported to the spectrometer in air. The surface concentration of oxygen was about 7%, although this number is probably a product of the noise in the instrument (see figure 4.38a). The surface concentration of carbon was significantly higher, about 38%, and this peak is real and results from exposure of the sample to the ambient air. The kinetic energy

of the XPS peak for this carbon was at 284.6 eV, and the Auger peak was at 272 eV, both of these values correspond to "adventitial" carbon. This always arises in exposure of samples, used for XPS of AES, to the ambient air.

The conclusion is therefore that exposure of a clean platinum sponge to the air results in no oxygen adsorption on the surface, but in a significant carbon accumulation (see also discussion of depth profiling, below). In the data for samples pretreated at other conditions, therefore, a surface concentration of carbon of about 40% is not significant, and arises from handling. Any surface concentration of oxygen, however, is significant and indicates the presence of oxygen bound to the surface more tightly than oxygen chemisorbed at room temperature and 0.21 atmospheres. It is hypothesised that this oxygen is in the form of an oxide.

4.2.2.3 XPS Data

The kinetic energy of oxygen in this study was about 532.8 eV. The lowest value found was for the polycrystalline platinum foil which was not pretreated, 532.5, and the highest for the sponge pretreated in air, about 533.0 eV. Under these conditions, the carbon peak appeared at 284.8 eV, with the exception of the Pt foil which appeared at 285.1 eV. Adventitial carbon (or $(CH_2)_n$) occurs at 284.6 eV (Wagner at al., 1979) and this coincides somewhat with the observed value. It therefore appears as if there is only a small surface charge build-up (surface charge build-up causes the peaks to shift). The values for the oxygen peaks found in this study are somewhat higher than expected from the literature. This may be due in part to the XPS spectrometer used here was calibrated with the gold 4d peak at 84.0 eV, whereas other workers have used 83.8 or 83.6 eV.

Peuckert and Bonzel (1984) recently performed temperature programed

desorption of platinum oxide that was formed on the surface of Pt(111) single crystal. They observed that the oxygen signal at 530.2 eV, that they attributed to platinum oxide, dissappeared when heating the sample to about 380°C in the ultra high vacuum. They also reported that the binding energy for oxygen chemisorbed on the surface was indendical to PtO_2, 530.2 eV, and that they were unable to differentiate between the two forms on the basis of the XPS binding energies alone. They observed O/Pt ratios of 0.2 for chemisorbed oxygen and 0.5 for oxide oxygen. Unfortunately, because of mounting problems, it was not possible to compare our data with theirs quantitatively, but the oxygen peak in the sample pretreated in air is considerably larger than when pretreated in butene, probably because the surface has become oxidized.

Legare, Hilaire and Maire (1984) reported XPS binding energies for O on Pt at 530.0 and 531.6 eV. They also analysed the binding energy of O on Pt/Si alloys which had been pretreated in air to cause the silicon to appear at the surface. They concluded that O peaks at 532.1 and 533.4 eV were due to the SiO_2 on the surface. At the same time they observed decreases in the intensity of the Pt peak by a factor of 3 and large Si peaks were observed. It cannot be completely ruled out that the O signal observed here not due to SiO_2, however, very little Si was observed in the XPS spectra (figure 4.36), and under state 1 conditions (high p_{O2}/p_{butene}), where the higher O/Pt surface ratios were observed, the rate of deep oxidation was up to three orders of magnitude greater than the rate of butadiene formation. It is unlikely that SiO_2 would be more active than the Pt surface itself.

4.2.2.4 Effect of Pre-treatment on AES Surface Concentrations

When pretreated in air, the O/Pt ratio, as determined AES, was about 3.6, and decreased slightly to about 2.4 when the catalyst was equilibrated in 0.25% butene and 0.25% oxygen (Table 4.4). When the surface was re-heated in the 0.25% butene/0.25% oxygen mixture, the selectivity of the catalyst had not changed from before cooling, and removing the sample. It therefore appears that cooling and sampling the surface has no effect on the activity/selectivity of the catalyst, if it is already at equilibrium. When the gas above this surface was switched to 2.0% butene/0.25% oxygen, and the reactor cooled after only one half hour at these conditions (the minimum needed to perform the GC analyses to verify the gas composition), the O/Pt ratio had decreased but only to 2.1. After reheating the reactor and letting the surface equilibrate in the 2% butene/0.25% oxygen mixture, the O/Pt ratio dropped still further to about 1.6. Therefore, **different** O/Pt ratios were obtained for the **same** gas phase composition. The same O/Pt ratio of 1.6 was also reached, in a separate experiment, when the re-oxidized catalyst was switched to these butene/oxygen partial pressures directly.

Exposing the surface to 40% butene/0.25% oxygen caused the surface to be almost completely covered with carbon, making the surface analysis unreliable. Switching back to 2% butene/0.25% oxygen did not cause the surface carbon to desorb sufficiently for reliable analyses. The electrons from the Pt 3d peak at 76 eV have an escape depth of only about 3 Å, whereas the electrons from the O 1s peak at 533 eV have an escape depth of about 8 Å. The platinum signal would therefore be much more susceptible to interference from the presence of a carbon overlayer than would oxygen.

Therefore, concentrating on the data taken before the reactor was exposed to 40% butene/0.25% oxygen, the reactor apparently was oxidized by

pretreatment in air, exposing the reactor to 0.15% butene/0.25% oxygen caused the catalyst surface to reduce only slightly. Switching the gas to 2.0% butene/0.25% oxygen and cooling the reactor immediately caused the oxide to start to decompose. The surface oxygen concentration was significantly higher than when the reactor was re-heated in the same 2% butene/0.25% oxygen and the surface permitted to equilibrate over a further 16 hour period.

When the reactor was exposed to a step increase in the butene partial pressure (section 4.1.5), the rate of butadiene production increased slowly over a 24 hour period, with the rate of deep oxidation to CO and CO_2 decreasing correspondingly. When performing surface analyses and the reactor was exposed to similar a step change in butene partial pressure, the selectivity changed identically to the previous study and the surface oxygen concentration decreased somewhat within one half hour of the switch and still further after another 16 hours, i.e two <u>different surface</u> atomic compositions were observed for the <u>same gas</u> phase composition.

It is therefore likely that the hysteresis observed when cycling the butene and/or oxygen partial pressures arose from the surface oxidation/reduction reaction, probably the formation and reduction of a platinum oxide.

4.2.2.5 Depth Profiling

The 1000 Å thick film of Ta_2O_5 on Ta was sputtered off the surface in about 8.8 minutes. As mentioned above, the sputter yields are not known for platinum oxide on platinum and the values quoted were only rough estimates. Nonetheless, the data do appear to indicate that pretreatment in air probably led to multilayer oxide formation since the O signal prior to sputtering, was the same value for air pretreatment (figure 4.41(a)) and

for pretreatment in 0.0025 atm butene, 0.0025 atm oxygen (figure 4.41(b)), whereas the film thickness was approximately double, about 40 Å versus 20 Å.

The profiles for the sample pretreated in 0.02 atm butene, 0.0025 atm oxygen for 1/2 hour (figure 4.41(c)) was almost the same as (b) indicating that one half hour in the higher concentration of butene did not reduce the O concentration (see section 4.2.2.4) nor the profile. This agrees with the surface O/Pt ratio.

The carbon profiles were similar to that observed for adventitial carbon (figure 4.40(a) and (b)) but were slightly deeper. The carbon films were probably less than 20 Å thick except when the samples were pretreated in 0.40 atm butene, 0.0025 atm oxygen, when they were about 120 Å thick and when pretreated in 0.01 atm butene when they were 80 Å thick. This agrees with the data for surface carbon oxidation (section 4.2.1.2) where the equivalent of 2 - 12 monolayers of carbon had existed on the surface. Although the surface was covered by carbon to this extent, the catalyst was still active, which tends to further confirm the model of Davis, Zaera and Somorjai (1982) that the surface has a steady state coverage of carbon up to several molecules high.

4.2.2.6 Comparison with Literature

The oxide formed in the presence of air and decomposed in the presence of butene/oxygen over about a twelve hour period. This is somewhat longer than was observed in section 3.3.3 for the decomposition of a similar oxide film in the absence of oxygen. The model proposed in that section for the decomposition of the oxide was:

$$O_{oxide} + \text{site} \longrightarrow 2\ O(a) \qquad (5)$$

In other words, the decomposition requires an empty site for the reaction. in the presence of butene, the majority of these sites will be occupied by

butene, this would inhibit the oxide decomposition reaction. Furthermore, in the oxide formation/decomposition study, the catalyst was pretreated in CO (or C_2H_4) for about 30 minutes, then exposed to air for periods from 1 to 100 minutes. The rate of oxide decomposition also decreased significantly with increasing oxidation times because of site blockage by the oxide itself. In the experiments discussed here, the reactor was pretreated in air up to 727°C, cooled in air to 513°C and oxidized for about 16 hours. This would cause a far greater layer of platinum oxide to form on the surface, possibly several monolayers thick. The decomposition of this multilayer oxide may also proceed by a different and slower reaction. Therefore the two rates of oxide decomposition observed in the presence and absence of butene are entirely consistent.

The formation and decomposition of an oxide film on platinum powder was investigated by Turner and Maple (1985), and their rate constant was consistent with that observed in the absence of butene (as discussed in section 3.3.4, above). Vayenas and Michaels (1982) implicated the formation and decomposition of an oxide film in the oscillation reactions observed over a similar platinum film. Their data indicated that platinum oxide should be stable up to about 600°C at 1 atm total pressure. In the presence of excess ethylene, the oxide would decompose, releasing the excess oxygen in the form of CO_2. No oscillations were observed in the study presented here, instead, the formation and destruction of the oxide film was used to account for the slow hysteresis observed. Yeates et al. (1985) analysed the rate of formation and destruction of platinum oxide on Pt(111) single crystals and hypothesised that these reactions were catalysed by the presence of silicon impurities, and that the rate therefore was dependent on the concentrations of impurities in the

catalyst. The study of Vayenas, Lee and Michaels (1981) used a fluxed platinum ink which may have had a higher concentration of glass impurities, which would catalyse the oxide formation/decomposition reaction, resulting in oscillations between the two states, rather than a slow hysteresis as was observed in this study.

Michaels (1983) in a separate study of the electrochemical oxidation of ethylbenzene over platinum in a similar zirconia-yttria reactor, observed that the cell voltage took several hours to come to equilibrium after a change had been made in either the gas phase composition or the current passing through the zirconia-yttria electrolyte. His data could be due to a slow oxide formation/decomposition step, as was observed here.

McCabe and Schmidt (1976) studied the thermal desorption spectra of CO adsorbed on clean and oxidized Pt. They recorded the spectra by sequentially exposing the oxidized surface to CO and temperature programming the crystal up to 700 K (427°C). They observed no decrease in the surface coverage by oxide with exposure of the oxide to these temperatures in the presence of desorbing CO. This would agree with our data, in that the oxide would be expected to decompose extremely slowly at the temperatures they used, and also with the data of Amirnazmi and Boudart (1975) where the rate of NO decomposition over Pt foil was reversibly poisoned by the formation of PtO_2 over about 1 1/2 hours, at 1000°C.

4.2.3 Butene Oxidation in a Fuel Cell

4.2.3.1 Cell Voltage at Open Circuit

In the absence of butene the Nernst equation was obeyed and gave a measure of oxygen concentration (see section 3.1):

$$V_{cell} = \frac{RT}{4F} \ln \frac{p_{O2}(inside)}{0.21} \qquad (1.31)$$

where 0.21 is the partial pressure of oxygen in the reference gas exposed to the external electrode, air, and 4 is the number of electrons that are transferred, via O^{2-} anions, per O_2 molecule.

In the presence of butene/oxygen mixtures, and at open circuit, the cell voltages both exhibited V-shaped curves with minima co-inciding with the switches between state 1 and state 2 regimes (figures 4.21, 4.22). Under state 1 conditions, the cell voltage could be described by:

$$V_{cell} = \frac{RT}{2F} \ln \frac{p_{O2}}{p_{butene}} + \text{constant} \qquad (6)$$

However, when the butene partial pressure was decreased to the point where all the butene was converted, the cell voltage changed from increasing with decreasing p_{butene} and dropped precipitously to about 0.08 V. This voltage, according to the Nernst equation, represented the oxygen partial pressure in the presence of diluent He and CO_2.

These observations are similar to data reported by Colvin, Butler and Anderson (1982), when they exposed a similar zirconia-yttria electrochemical reactor to butane/oxygen mixtures. They found that the cell voltage increased with both butane and oxygen partial pressures when no additional catalyst was present, but when an additional catalyst was added to completely oxidize the butane, the cell voltage reflected the oxygen partial pressure in the gas with CO_2 simply behaving as a diluent.

In a parallel paper (Anderson and Graves, 1981), they modelled the cell voltage in terms of the relative rates of surface adsorption, desorption and reaction on the surface. They did not however consider a mixed potential, such as has been proposed for CO oxidation by Williams, McGeehin and Tofield (1982), and also by Okamoto, Kawamura and Kudo (1981, 1983a,b, 1984a,b) where adsorbed CO reacts directly with the electrolyte oxygen anions:

$$CO(a) + O^{2-}(\text{electrolyte}) \rightleftharpoons CO_2(g) + 2e^-(Pt) \quad (7)$$

$$O^{2-}(\text{electrolyte}) \rightleftharpoons 1/2\ O_2(g) + 2e^-(Pt) \quad (8)$$

When oxidizing CO over Pt in a zirconia-yttria reactor at 250-400°C, Okamoto, Kawamura and Kudo (1983a) did not observe minimina, but when p_{CO} was large ("region 3" in their data), they did observe the same dependencies of cell voltage on p_{O2} and p_{CO} as was found for p_{O2} and p_{butene} (equation 7).

When Sigal and Vayenas (1963) oxidized ammonia in a similar, high temperature fuel cell, the data could be modelled by assuming reaction between adsorbed ammonia and the oxygen anions:

$$2NH_3 + 5O^{2-}(\text{electrolyte}) \longrightarrow 2NO + 3H_2O + 10e^- \quad (9)$$

Further, when the potential of a zirconia-yttria electrochemical cell, used to investigate the characterisitics of H_2/H_2O mixtures, was decreased below -500mV (Schouler and Isaacs, 1981) the dominant electrode reaction changed from oxygen evolution:

$$O^{2-}(\text{electrolyte}) \rightleftharpoons 1/2\ O_2 + V_O'' + 2e^- \quad (10)$$

where V_O'' is an oxide vacancy, to hydrogen oxidation:

$$H_2 + O^{2-}(\text{electrolyte}) \rightleftharpoons H_2O + V_O'' + 2e^- \quad (11)$$

i.e. direct reaction between oxygen anions in the electrolyte and hydrogen.

Following these examples, it seems reasonable to propose that the cell voltages observed are mixed potentials:

$$C_4H_6(a) + O^{2-}(\text{electrolyte}) + [P1] \longrightarrow CO + CO_2 + H_2O + V_O'' + 2e^- \quad (12)$$

$$O^{2-}(\text{electrolyte}) \rightleftharpoons O(a) + V_O'' + 2e^- \quad (13)$$

If this is the case then the high cell potentials do not correspond to extremely low surface oxygen activities, as would be demanded were only the Nernst equation obeyed (where a voltage of 0.60 V corresponds to an oxygen activity of $3x10^{-16}$ atm.).

At 513°C, the Gibbs energy for the reaction in equation 12 is -621.72 kcal/mol (from data in Stull, Westrum and Sinke, 1969). This corresponds to an equilibrium voltage of 1.123 volts ($\Delta G=-nFE^o$; n=24). The voltage from equation 13 will obey the Nernst equation (1.31), and be about 0.070 volts (at 513°C and p_{O2}=0.0025). The observed cell voltages lie between these two values, the actual values will depend on the relative rates of each reaction (their exchange current densities), which cannot be determined from this data.

4.2.3.2 Effect of Current

When a positive current was applied to the reactor (O^{2-} anions flowing from the air side of the zirconia-yttria electrolyte to the reactant side) the rate of butadiene increased very slightly and then became zero, or negative order, in current, depending on the p_{O2} in the gas phase (figures 4.4 to 4.6). In contrast, the rate of deep oxidation was first order in current, with <u>all</u> the oxygen that was pumped through the electrolyte being incorporated into the deep oxidation products (CO and CO_2). This can be seen in table 4.1 where the flux of oxygen in the deep oxidation products CO, CO_2 and H_2O was equal to the flux of electrical oxygen (ratio = 0.984 - 1.091). At the same time, there was no change in r_{O2} (the flux of gas

phase oxygen).

When a negative current was applied (O^{2-} anions being pumped from the reactant-side to the air-side), the rates of all the butene reactions were unaffected. The gas phase oxygen was simply pumped through the zirconia-yttria electrolyte (in table 4.1, the ratio of the flux of gas phase oxygen to electrical oxygen = 0.99 - 1.12). At a current of 60 mA, the flux of electrochemical oxygen (1.556×10^{-7} mol/s) is approximately the same as the rate of reaction of oxygen with butene ($1.444\text{-}1.526 \times 10^{-7}$ mol/s at zero or positive currents). Since pumping oxygen away from the catalytic surface at a rate equal to the reaction rate had no effect on the rates, then, either the reactions are zero order in oxygen, or, oxygen must be in equilibrium between the gas phase and the surface. If this were not the case, and adsorption of oxygen were the rate limiting step, then I would have expected the butadiene and deep oxidation rates to have decreased when pumping oxygen away from the surface through the electrolyte. Since, as reported above, and discussed below, the butadiene and deep oxidation rates were dependent on p_{O2}, it therefore appears that equilibrium exists between oxygen in the gas phase and oxygen adsorbed on the **catalytic** surface.

If oxygen was also in equilibrium between the **electrochemical** surface and the gas phase, and a mixed potential did not exist (equation 12), then I would have expected the gas phase oxygen concentration to have increased when applying a positive current (the exact opposite of the effect of a negative current). This was not observed, and the oxygen was instead incorporated into CO, CO_2 and H_2O. This supports the hypothesis of a mixed potential.

In the presence of gas phase oxygen, and at low p_{O2}/p_{butene} ratios, the rate of butadiene production was positive order in oxygen pressure and only became negative order at high p_{O2}. This behavior is mimicked by the

electrochemical data. At low currents, the rate of butadiene production does increase slightly, but then becomes negative order at higher currents. Oxygen does not diffuse readily on platinum surfaces (Engel and Ertl, 1979) and therefore at high currents it is likely that the platinum surface in the region of the three phase boundary (between the gas, the electrode and the electrolyte) may have become rich in oxygen. This would cause this localized region to behave according to state 2 characterisics, and for all the butene that reacts there to be oxidized to CO and CO_2.

4.2.4 Effect of Spiking the Feed

There were no effects whatsoever on spiking the feed with **CO_2** (figure 4.26) and it therefore seems reasonable to assume that CO_2 does not adsorb on the platinum catalyst to any significant extent at the reactor temperatures. This is in keeping with all literature reports.

Carbon monoxide reacts to form CO_2 when added to the 2% butene/0.08% oxygen feed (figure 4.25). At the concentrations added (up to 0.7%, which was ~10 times larger than the maximum concentration formed during the experiments), it does not have any effect on the rate of butene consumption or butadiene production. Apparently, by increasing the partial pressure of CO above the catalyst, CO is unable to desorb, as would normally occur, and therefore is further oxidized to CO_2. It should be noted that the net rate of deep oxidation (the sum of CO and CO_2) remains unchanged, and therefore the effects of product CO may be ignored.

Hydrogen has the effect of initialy decreasing the rate of CO_2 production, under state 1 conditions, and then having no further effect (figure 4.28). The rate of production of water increases linearly with hydrogen addition. As discussed in the experimental section, it was not

possible to measure the concentration of hydrogen in the exit gas. The x-axis of figure 4.28 is the concentration of hydrogen **fed** to the reactor and was calculated from the concentration and flowrate of the feed. This contrasts with all other concentration data presented in this thesis which reflect the concentrations in the **exit.** It is quite likely that no free hydrogen was present in the exit stream and that under reaction conditions, all the hydrogen was combusted to water on the catalytic surface.

When hydrogen was added to the reactor under state 2 conditions (high p_{O2}, large rate of deep oxidation), it had a negligible effect on the rate of CO_2 production .

Michaels (1983) reported that the addition of hydrogen to a similar reactor, being used for the dehydrogenation of ethylbenzene, had the effect of decreasing CO_2 formation, and that this effect was linear with p_{H2}. He proposed that ethylbenzene was dehydrogenated to styrene over the platinum surface and that the added hydrogen occupied sites that would otherwise be used for cracking the benzene ring in the ethylbenzene.

The effect of hydrogen may be explained if we assume that the surface consists of both oxidized and un-oxidized platinum, simultaneously, and that hydrogen inhibits the formation of CO_2 on the un-oxidized Pt surface, but does not effect the formation of CO_2 on the PtO_2 surface. The initial drop in the rate of CO_2 formation in figure 4.28 would then be due to H_2 completely poisoning the rate over the un-oxidized Pt. Beyond this initial drop the rate is independent of p_{H2} because H_2 has no effect on the rate over the PtO_2 surface. The lack of any effect of hydrogen under state 2 conditions, when the surface would be predominantly PtO_2, would confirm the hypothesis that hydrogen does not poison the reaction over the oxide

Irrespective of the mechanism, the important result is that hydrogen

had no effect on the rate of butene consumption or butadiene formation and may therefore be ignored in the model to be developed.

The effect of **butadiene** is more pronounced than for any other component (figure 4.29). Addition of up to 6% butadiene has almost no effect on the rates of production of CO and CO_2, however it does inhibit the formation of butadiene from butene. Butadiene probably adsorbs on the same surface as butene and therefore blocks catalytic sites, inhibiting the reaction. It should be noted, however, that the maximum concentration of butadiene in any experiment was 0.29% (for the data of figure 4.19) and 0.36% (figure 4.20), the oxygen and butene cycles at 544°C. At these butadiene concentrations, the rates had not decreased significantly (figure 4.29). To a first approximation, for modelling purposes, the poisoning effect of butadiene may therefore be ignored.

4.2.5 Kinetics of Butene Conversion

The data, for the effects of butene and oxygen on the rates of butadiene and deep oxidation production, appear to fit a trend whereby one set of orders of reaction are found for the "state 1" conditions, at low oxygen/high butene partial pressures and completely different trends under "state 2" conditions, at high oxygen/low butene partial pressures.

The states 1 and 2 may be related to the surface composition by considering the following:

1. In the study of oxygen desorption from the surface of the platinum catalyst (section 3.3.3), the data could be explained by a model that assumed that an oxide formed on the surface of the catalyst, and that the rate determining step for desorption of oxygen was the decomposition of the oxide.

2. When measuring the exchange current density of the reactor relative to the temperature and oxygen partial pressures (section 3.2.2), it was found that a model explaining the exchange current density arising from the dissociative adsorption of oxygen on the platinum surface broke down at temperatures below about 577°C and high oxygen partial pressures. The observed effects could be explained by a surface platinum oxide having formed which reduced the srea available for oxygen adsorption.
3. Auger spectroscopy data of the platinum surface pretreated at 513°C in air indicated that the surface coverage of oxygen was far higher than was found for adventitial oxygen (the same platinum film pretreated in hydrogen, to remove oxide, then cooled and exposed to ambient air during transport to the spectrometer). It was hypothesised that this oxygen, being far more prevalent, and stable, on the surface arose from an oxide rather than chemisorbed oxygen.

On the basis of all the above data and in reference to literature measurements (see section 1.2.2.3) of oxide formation on Pt single crystals (Yeates et al. 1985, etc.) on platinum sponges deposited on zirconia-yttria solid electrolytes (Vayenas et al. (1982)) and on platinum wires (Berry, 1978), it is proposed that under **state 1** conditions (low oxygen/high butene partial pressures) the surface is predominantly **un-oxidized platinum** and that the rate determining steps are the surface reactions over **platinum.** Under **state 2** conditions (high oxygen/low butene partial pressures) the surface is predominantly **platinum oxide** and the rate determining steps for production of CO and CO_2 are the surface reactions over the **oxide** surface.

It is further proposed that butene and oxygen react over the platinum surface to form both butadiene, and CO and CO_2 in a parallel mechanism,

whereas oxygen and butene react to form **only** CO_2, no butadiene, over the platinum oxide surface. Also, that under high p_{O2}, the oxide may form on the clean platinum surface.

The reaction orders may then be explained in terms of these two surfaces, platinum and platinum oxide, assuming that the entire surface is either oxidized Pt or unoxidized Pt (i.e. reduced) Pt and that the fractions of each are θ_{ox} and θ_r respectively.

4.2.5.1 Qualitative Description of Results Relative to Model

The observed rates of reaction are the summation of the rates over the platinum and oxide surfaces. At low oxygen partial pressures, it would be expected that platinum would be more stable than the oxide and under these conditions, the rates of deep oxidation and butadiene formation are both one half order in oxygen and first order in butene. This would imply that butadiene is formed by a Langmuir-Hinshelwood mechanism of adsorbed butene and dissociatively adsorbed oxygen reacting to form an intermediate that forms butadiene. With reference to the "spiking" data (section 4.2.4), the product butadiene probably also adsorbs on the surface, however under the reaction conditions it is formed to such a small extent that it is unlikely to interfere with the rate.

At high butene partial pressures pressures, the rates of both deep oxidation and butadiene formation decrease with butene partial pressure. This is in keeping with the Langmuir-Hinshelwood mechanism because the surface is now almost saturated with butene, leaving no sites for oxygen adsorption, and increasing p_{butene} decreases the number of sites for oxygen adsorption still further, inhibiting the reactions.

The plot of selectivity versus conversion does not appear to pass through 100% selectivity at zero conversion (figure 4.42) as would be

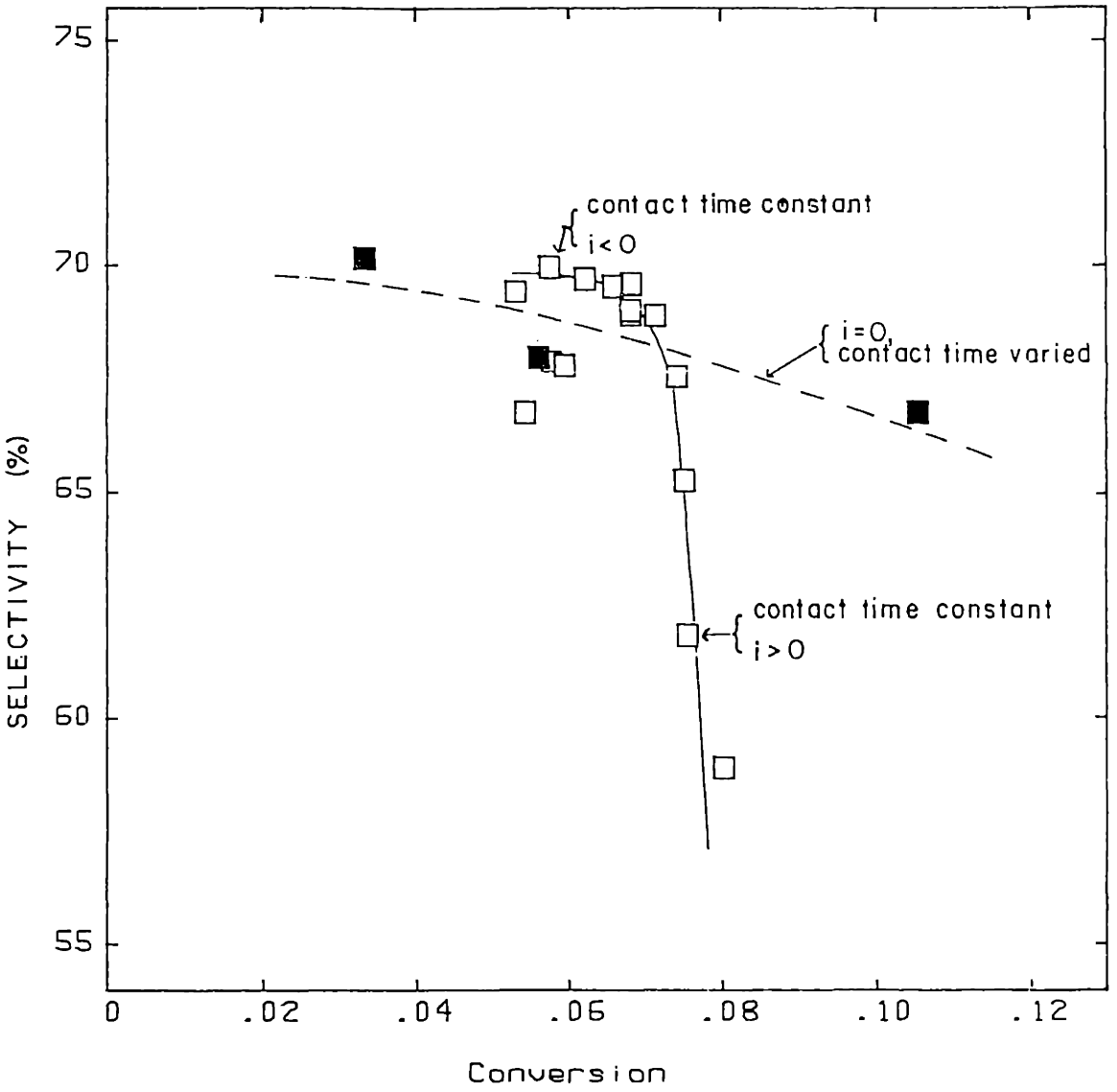

Figure 4.42: Selectivity vs conversion for different contact times, P_{butene}=0.02 atm, p_{O2}=0.0075 atm, T=513°C, and for the application of positive and negative currents

expected for a consecutive mechanism (Kiperman, 1981). It is therefore likely that CO and CO_2 form, on the un-oxidized platinum surface, in parrallel to butadiene production, with the rate controlling step being the formation of the initial transition state.

At high oxygen partial pressures, platinum oxide is the predominant surface species, however due to the slow kinetics of the surface reaction, some platinum surface still remains exposed and it appears as if there may be some inhibition of the formation of butadiene over the clean Pt surface by saturation with oxygen at high p_{O2}. This is probably not an artifact from the decrease in the platinum area, since the negative order kinetics were observed when decreasing the oxygen partial pressure after the surface had been pre-oxidized.

Under state 2 conditions (high p_{O2}/p_{butene}), deep oxidation was first order in oxygen and negative order in butene. This would also conform to a Langmuir-Hinshelwood mechanism whereby butene adsorbed on the oxide (with different adsorption equilibrium characteristics than the platinum surface) would react with co-adsorbed molecular oxygen. The rate would then be controlled by the fractions of butene and oxygen on the surface, which are themselves dependent on the partial pressures.

4.2.5.2 Rationalization of the Model

On a series of oxides, Matsuura (1977) found that high heats of adsorption of an olefin on the surface resulted in a highly active but non-selective catalyst for butene or propylene oxidation, whereas, catalysts with lower heats of adsorption gave better selectivity to partial oxidation products.

Mc Cabe and Schmidt (1976) examined the adsorption of CO on clean and oxidized Pt(110) planes. Using flash desorption techniques they found

significantly higher binding energies of the CO on the oxide than on the clean platinum plane (desorption occurred at 580 K on the oxide and 430 K on clean Pt). This they hypothesised was due to a decrease in the number of Pt d-electrons available for chemisorption, hence increasing the strength of chemisorption.

On clean platinum, butadiene forms by reaction with adsorbed oxygen. If, like CO, the butene is also more strongly adsorbed on the oxide, than clean Pt, then it will have a higher heat of adsorption and, with respect to Matsuura's results, be less selective for partial oxidation. In accordance with McCabe and Schmidt's reasoning, there will be a decrease in the electron density in the carbon-carbon bonds in the butene adsorbed on the oxide, thus weakening them. When reaction occurs with oxygen, butene would then break apart more readily than when adsorbed on the clean surface, and so undergo deep oxidation rather than partial oxidation.

This does apparently occur, since Somorjai (1981) reported that the hydrogenation activity of platinum catalysts was uneffected by the presence of surface oxides, but that the hydrogenolysis activity was greatly enhanced. Also, Herz and Marin (1980) obvserved a decrease in the rate of CO oxidation over Pt catalysts, at 473 K, when they were oxidized. They presumed this was because oxide that formed on the surface could adsorb CO but not dissociate oxygen, and therefore was inactive at this low temperature.

4.2.5.3 Model Assumptions

The model has been further developed to explain, quantitatively, these experimental data. It requires the following assumptions for the adsorptions and reactions:

platinum:

(i) Butene, butadiene and oxygen adsorb on vacant, or unoccupied, sites on the platinum surface which are iso-energetic. The fraction of vacant sites is $\theta_{v,r}$.

(ii) Butene adsorbs molecularily, and is in rapid equilibrium between the gas phase and the surface, and occupies fraction $\theta_{Bu,r}$.

(iii) Oxygen adsorbs dissociatively, and is in rapid equilibrium between the gas phase and the surface, and occupies fraction $\theta_{0,r}$.

(iv) Adsorbed butene and oxygen atoms react simultaneously to form butadiene, which is in rapid equilibrium between the gas phase and the surface.

(v) Adsorbed butene and oxygen also react in a parallel reaction to form deep oxidation products, CO and CO_2 which desorb rapidly and irreversibly.

platinum oxide:

(i) Butene and oxygen adsorb on vacant sites on the platinum oxide surface. The fraction of vacant sites is $\theta_{v,ox}$.

(ii) Butene adsorbs on the oxide surface, is in rapid equilibrium between the gas phase and the surface and occupies fraction $\theta_{Bu,ox}$.

(iii) Oxygen adsorbs molecularily on the oxide surface and is in rapid equilibrium between the gas phase and the surface and occupies a fraction $\theta_{02,ox}$

(iv) Adsorbed oxygen and butene react to form an intermediate product which reacts further with oxygen to form CO and CO_2 which desorb rapidly and irreversibly.

4.2.5.4 Model Formulation

When the above assumptions are expressed mathetically:

Adsorption on Pt:

$O_2(g) + 2\ \text{sites} \rightleftharpoons 2\ O(a)$ therefore:

$$K_O P_{O2}^{1/2} = \frac{\theta_{O,r}}{\theta_{v,r}} \quad (14)$$

$Bu(g) + 1\ \text{site} \rightleftharpoons Bu(a)$ therefore:

$$K_{Bu} P_{Bu} = \frac{\theta_{Bu,r}}{\theta_{v,r}} \quad (15)$$

$Bd(g) + 1\ \text{site} \rightleftharpoons Bd(a)$ therefore:

$$K_{Bd} P_{Bd} = \frac{\theta_{Bd,r}}{\theta_{v,r}} \quad (16)$$

Adsorption on platinum oxide:

$Bu(g) + 1\ \text{site} \rightleftharpoons Bu(a)$ therefore:

$$K'_{Bu} P_{O2} = \frac{\theta_{Bu,ox}}{\theta_{v,ox}} \quad (17)$$

$O_2(g) + 1\ \text{site} \rightleftharpoons O_2(a)$ therefore:

$$K'_{O2} P_{O2} = \frac{\theta_{O2,ox}}{\theta_{v,ox}} \quad (18)$$

Reactions on platinum:

$Bu(a) + O(a) \xrightarrow{k_{Bd}} Bd(a) + H_2O(g)$ therefore:

$$\frac{d[Bd]}{dt} = k_{Bd}\, \theta_{O,r}\, \theta_{Bu} \quad (19)$$

$$Bu(a) + O(a) \xrightarrow{k_{DO}} [P_1] \xrightarrow{+(7+n)O(a)} nCO_2 + (4-n)CO + 4H_2O$$

where $0 \leq n \leq 4$, and $\frac{d[DO]}{dt} = k_{DO}\, \theta_{O,r}\, \theta_{Bu,r}$ (20)

$$Bd(a) + O(a) \xrightarrow{k_{DO2}} [P_2] \xrightarrow{+(5+k)O(a)} kCO_2 + (4-k)CO + 3H_2O$$

where $0 \leq k \leq 4$, and $\frac{d[DO]}{dt} = k_{DO2}\, \theta_{O,r}\, \theta_{Bd,r}$ (21)

Reactions on platinum oxide:

$$Bu(a) + O_2(a) \xrightarrow{k'_{DO}} [P_3] \xrightarrow{+(6+m/2)O_2(a)} mCO_2 + (4-m)CO$$

$$\text{where } 0 \leq m \leq 4, \text{ and } \frac{d[DO]}{dt} = k'_{DO} K'_{O2} P_{O2} \theta_{Bu,ox} \quad (22)$$

Expressing the rates in terms of measurable parameters:

Manipulating equations (14),(15) and (16):

$$\theta_{v,r} = \frac{\theta_r}{(1 + K_O P_{O2}^{1/2} + K_{Bu} P_{bu} + K_{Bd} P_{Bd})} \quad (23)$$

and similarily for the platinum oxide surface by manipulating equations (17) and (18):

$$\theta_{v,ox} = \frac{\theta_{ox}}{(1 + K'_{O2} P_{O2} + K'_{Bu} P_{Bu})} \quad (24)$$

Also:

$$\theta_{ox} + \theta_r = 1, \text{ or } \quad \theta_r = 1 - \theta_{ox} \quad (25)$$

Butadiene formation:

Applying equations (14), (15), (23) and (25) to equation (19):

$$r_{butadiene} = \frac{d[Bd]}{dt} = \frac{k_{Bd} K_{Bu} K_O P_{O2}^{1/2} P_{Bu}}{(1 + K_O P_{O2}^{1/2} + K_{Bu} P_{Bu} + K_{Bd} P_{Bd})^2} (1-\theta_{ox})^2 \quad (26)$$

this equation can be simplified somewhat by considering the experiments. In all the experiments, the conversion to butadiene was low and the maximum concentration of butadiene obtained in any experiment was 0.6%, most of the time it was an order of magnitude lower. With reference to figure 4.29 ("spiking" the feed with butadiene), 0.6% butadiene would reduce the rate of butadiene formation by about 8%, and it therefore seems reasonable to ignore butadiene for modelling purposes, thus Equation (26) becomes:

$$r_{butadiene} = \frac{k_{Bd}\, K_{bu}K_O\, P_{O2}^{1/2}\, P_{Bu}}{\{1 + K_O P_{O2}^{1/2} + K_{Bu}P_{Bu})\}^2} \quad (1 - \theta_{ox})^2 \qquad (27)$$

This equation is able to account qualitatively for the experimental observations. Under state 1 conditions, the surface is predominantly platinum and the rate is positive one half order in oxygen partial pressure but decreasing with increasing oxygen partial pressure. The rate is negative order in butene because the butene term in the denominator predominates, i.e., if:

$$K_{Bu}P_{Bu} >> 1 + K_O P_{O2}^{1/2}$$

then:

$$r_{butadiene} \approx (k_{Bd}\, K_O P_{O2}^{1/2}) \;/\; K_{Bu}P_{Bu}$$

and the rate of production of butadiene is negative order in butene partial pressure.

Under state 2 conditions, a significant fraction of the surface is covered by platinum oxide and butadiene is not produced over this surface. The butadiene that is produced therefore comes from the small amount of platinum surface still remaining exposed to the reactants.

Deep oxidation:

Applying equations (14), (15), (23) and (25) to equation (20) and equations (17), (18), (24) and (25) to equation (22):

$$r_{deep\ oxidation} = \frac{d[DO]}{dt} = \{ r_{DO\ on\ platinum} \} + \{ r_{DO\ on\ platinum\ oxide} \} =$$

$$= \frac{k_{DO}\, K_{Bu}K_O\, P_{O2}^{1/2}\, P_{Bu}}{(1 + K_O P_{O2}^{1/2} + K_{Bu}P_{Bu} + K_{Bd}P_{Bd})^2} \quad (1 - \theta_{ox})^2$$

$$+ \frac{k'_{DO}\, K'_{Bu}P_{Bu}\, K'_{O2}P_{O2}}{(1 + K'_{O2}P_{O2} + K'_{Bu}P_{Bu})^2} \quad \theta_{ox}^2 \qquad (28)$$

The deep oxidation data may be divided into the two regimes corresponding to the two "states" of the catalyst. In state 1, CO and CO_2 are formed over the platinum surface, and therefore the rate of deep oxidation should be controlled by the first term in equation (28). The rate of formation of deep oxidation products, CO and CO_2 are apparently half order in oxygen partial pressure (figure 4.9) as would be expected from the first term in equation (28). The rate is nearly zero order with respect to butene partial pressure (figure 4.10) because the data lie in the interim region between the fist order and negative order regimes for the first term in equation (28).

Equation (28) could also have been obtained by a different set of assumptions. For example, an alternative mechanism would be between adsorbed oxygen and adsorbed ("active", in the jargon of Yeates et al., 1985) coke precursors, which are themselves in equilibrium with the surface covered by butene ($\theta_{Bu,r}$). Carbon has also been seen as a reactant and poison in HCN synthesis from CH_4 and NH_3 over Pt (Hasenberg and Schmidt, 1986).

At high p_{O2} and/or low p_{Bu}, deep oxidation products are formed predominantly by the reactions over the platinum oxide surface and therefore the second term in equation (28) will predominate. The rate of deep oxidation is first order in oxygen partial pressure and negative order in butene partial pressure, indicating that in the second term:

$$K'_{Bu}p_{Bu} \gg 1 + K'_{O2}p_{O2}$$

therefore:

$$r_{\text{deep oxidation, state 2}} \approx \frac{k''_{DO}\, p_{O2}}{p_{Bu}} \qquad (29)$$

$$\text{where:} \quad k''_{DO} = k'_{DO}\, K'_{O2} \,/\, K'_{Bu}$$

which agrees with the experimental observations that under state 2

conditions, the rate of deep oxidation is first order in oxygen and negative order in butene.

4.2.5.5 Application of the Model to the Matrix Data

This model is able to explain most of the data obtained in the "matrix" study of the reaction. In particular it explains the observation whereby the rate of butadiene production is positive first order in butene partial pressure while the rate of deep oxidation is, simultaneously, negative order in butene partial pressure: the butene is poisoning the oxide surface, inhibiting deep oxidation, whereas on the platinum surface the coverage is not as great (the adsorption coefficient is lower) and the rate increases with increasing butene pressure because the coverage increases.

The data under state 1 conditions may be quantitatively compared to the model by inverting and re-arranging equation (28) to:

$$\left\{ \frac{P_{Bu}\, P_{O2}^{1/2}}{r_{butadiene}} \right\}^{1/2} = \frac{1}{(k_{Bd}K_{O}K_{Bu})^{1/2}(1-\theta_{ox})} \{1 + K_{O}P_{O2}^{1/2} + K_{Bu}P_{Bu}\} \qquad (30)$$

The first set of data, taken over a limited range of oxygen and butene partial pressures as a matrix, were plotted according to this linearization are shown in figures 4.43 and 4.44. The state 1 data fit the model well in both plots, yielding four values, two slopes and two intercepts. These were used to obtain estimates of the rate parameters to be used in the non-linear least squares fit (see below).

4.2.5.6 Platinum Oxide Formation

The description of the model to this point is independent of the

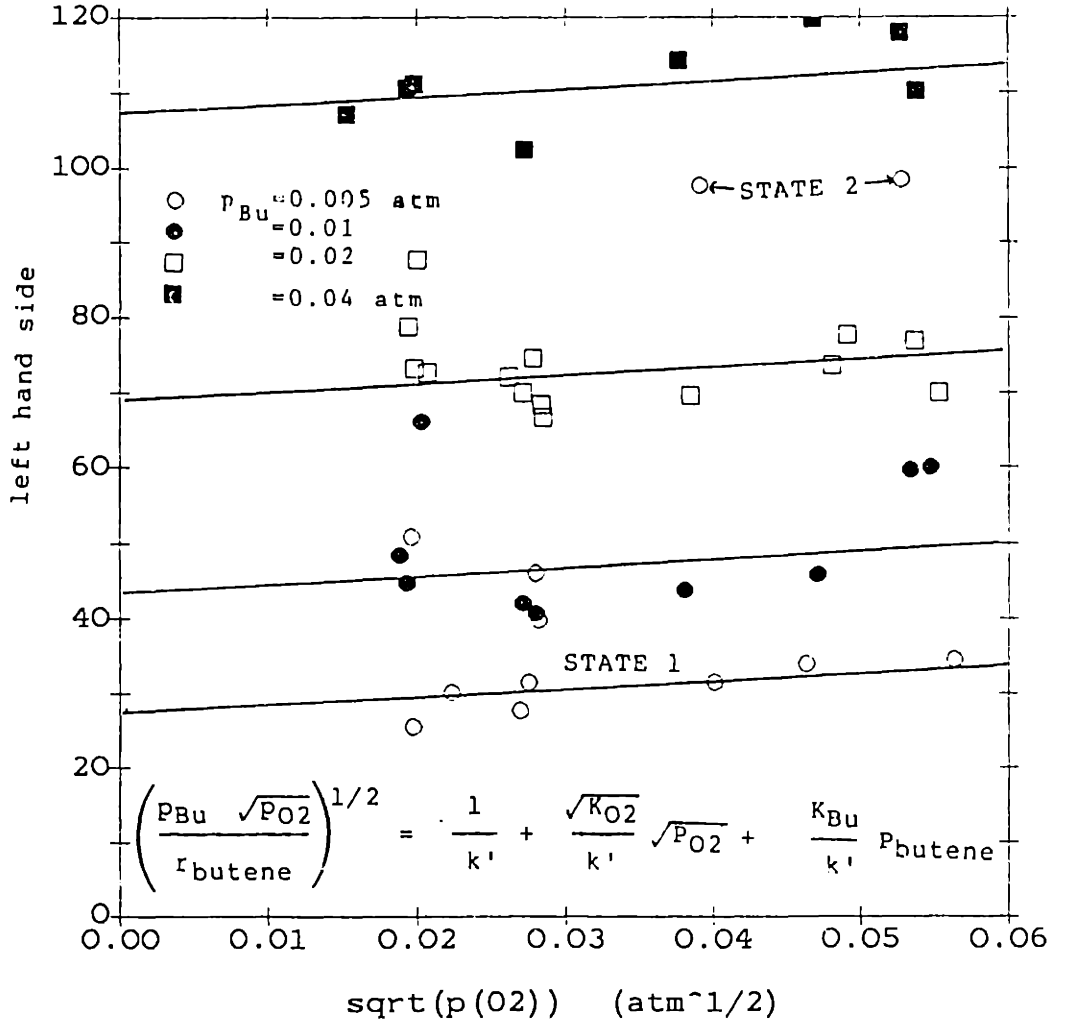

Figure 4.43: Application of model to butadiene conversion ("matrix" data) for constant p_{butene}

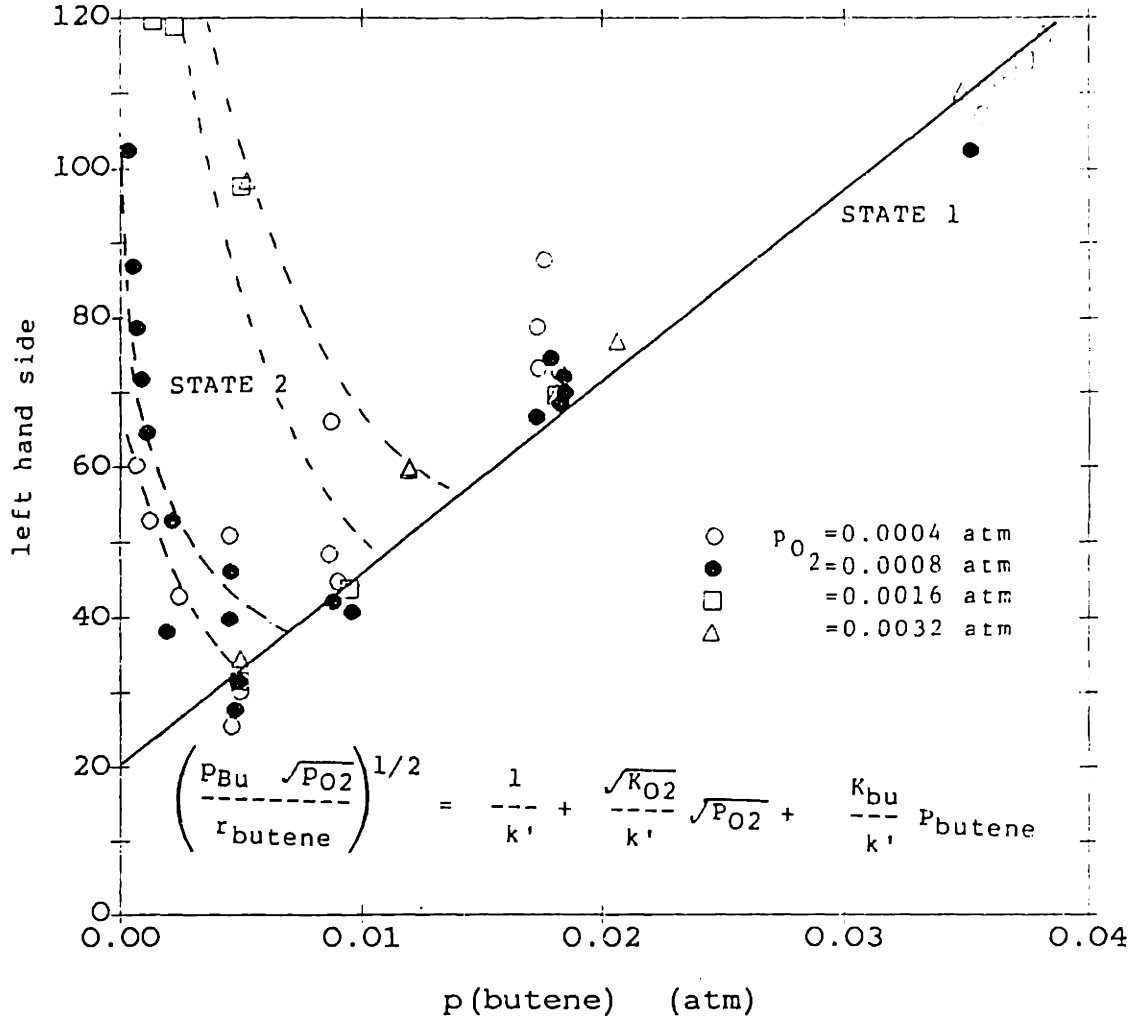

Figure4.44: Application of model to butadiene conversion ("matrix" data) for constant p_{O2}

mechanism of oxide formation, mearly that it does exist, that it forms in excess oxygen and that butene reacts over the oxide to form CO_2 only. It is possible to evaluate the parameters in the model by the linearization techniques, however, a more precise method is to determine the parameters by non-linear least squares fitting of the data and model (Absil, Butt and Dranoff, 1984). In order to do this it is necessary to describe θ_{oxide} and, therefore, the oxide formation/decomposition reaction in terms of measureable parameters.

The model that is proposed for oxide formation/decomposition is identical to the model considered to explain the oxygen desorption kinetics in section 3.3.3), i.e.:

$$2\ O(a) \underset{k_r}{\overset{k_x}{\rightleftharpoons}} \theta_{ox} + site \tag{31}$$

for which:

$$\frac{d\theta_{ox}}{dt} = k_x\ \theta_{0,r}^2 - k_r\ \theta_{ox}\ \theta_{v,r} \tag{32}$$

When applying equations (14),(15),(23) and (25) to equation (32):

$$\frac{d\theta_{ox}}{dt} = \frac{k_x\ K_0^2\ P_{02}\ (1-\theta_{ox})^2}{\{1 + K_0 P_{02}^{1/2} + K_{Bu} P_{Bu}\}^2} - \frac{k_r\ \theta_{ox}\ (1 - \theta_{ox})}{\{1 + K_0 P_{02}^{1/2} + K_{Bu} P_{Bu}\}} \tag{33}$$

This equation can be integrated as follows:

let $$a = \frac{k_x\ K_0^2\ P_{02}}{\{1 + K_0 P_{02}^{1/2} + K_{Bu} P_{Bu}\}^2}$$ and $$b = \frac{k_r\ \theta_{ox}\ (1-\theta_{ox})}{\{1 + K_0 P_{02}^{1/2} + k_{Bu} P_{Bu}\}}$$

then equation (21) becomes:

$$\frac{d\theta_{ox}}{dt} = a(1 - \theta_{ox})^2 - b\ \theta_{ox}\ (1 - \theta_{ox}) \tag{34}$$

this is separable and can be integrated by partial fractions:

$$1/b\ \ln(1 - \theta_{ox}) + 1/b\ \ln\{a(1 - \theta_{ox}) - b\theta_{ox}\} = t + c$$

or

$$\ln(1 - \theta_{ox}) - \ln \{a - \theta_{ox}(a + b)\} = bt + bc \qquad (35)$$

boundary condition: at t=0, $\theta_{ox} = \theta_{ox,i} = \theta_{ox}$ at initial conditions

therefore:

$$c = \frac{1}{b} \ln \left\{ \frac{1 - \theta_{ox,i}}{a - \theta_{ox,i}(a + b)} \right\}$$

$$= 1/b\ c_2$$

and then:

$$\ln \left\{ \frac{1 - \theta_{ox}}{[a - \theta_{ox}(a + b)]\ c_2} \right\} = bt \qquad (36)$$

rearranging:

$$\theta_{ox} = \frac{1 - ac_2e^{bt}}{1 - (a+b)c_2e^{bt}} \qquad (37)$$

i.e. θ_{ox} is a function of the oxygen and butene partial pressures and the time that the surface has been exposed to these pressures.

If the system is left at the same conditions to reach steady state, then:

$$\theta_{ox} = a\ /\ (a+b)$$

or:

$$\theta_{ox} = \frac{K_A K_0^2 p_{O2}^{1/2}}{(1 + K_A K_0^2 p_{O2}^{1/2} + K_0 p_{O2}^{1/2} + K_{Bu} p_{Bu})} \qquad (38)$$

where $K_A = k_x/k_r$

and the fraction of surface covered by oxide is in terms of measureable parameters, p_{O2} and p_{butene}.

4.2.5.7 Quantitative Description of Model

The model therefore can be described by equations (27), (28) and (37). In these equations there are a total of nine (9) adjustable parameters: the adsorption equilibria, K_0 and K_{Bu} on un-oxidized platinum, K'_{Bu} on the

oxidized platinum; the rate constants k_{Bd}, for butadiene formation and k_{DO} for deep oxidation on un-oxidized Pt and k'_{DO} for deep oxidation over oxidized Pt; and k_r and k_x the oxide formation/decomposition rate constants. The variables that account for the data are the butene and oxygen partial pressures, and the time that the catalyst has been at the particular reaction conditions, and the surface oxide coverage at the previous p_{O2} and p_{butene} conditions.

The number of adjustable parameters may be reduced somewhat by examination of the experimental data as follows:

1. In accordance with experimental observations, the parameters for adsorption and reaction over the oxide surface may be combined, as was done in equation (29), eliminating two parameters:

   $$k''_{DO} = k'_{DO} K'_{O2} / K'_{Bu}$$

2. There is some question as to the validity of the model for oxide formation/decomposition. The model chosen was the one found applicable to the surface titration experiments. There is no independent data for when butene is present, indicating that the particular mechanism chosen is any more applicable than any other. The surface coverage by oxide from the previous p_{O2} and p_{butene} settings is also highly dependent on the mechanism. To avoid this restriction, it is possible to assume that the surface is in equilibrium. This is most definitely not the case experimentally, since if the surface existed in equilibrium between the oxide and clean surface, then the data would not be dependent on the previous history of the catalyst, and no envelope of data would be seen. However, if equilibrium is assumed (equation 38), k_r and k_x the decomposition and formation rate constants are replaced by K_A the equilibrium constant for the oxide formation/decomposition. The

number of parameters are therefore reduced to 6.

3. The data were fitted using the value for the equilibrium constant for the formation of the platinum oxide as found in the surface titration experiments, and assuming the enthalpy of formation from the literature of 42 kcal/mole (Berry, 1982). The equilibrium constant at 477°C is the ratio of the rate constants for the formation and decomposition of the oxide: 0.135 min^{-1}/0.72 min^{-1} = 0.188. The values used were 0.488, 0.0723 and 0.0186 for 466, 513 and 544°C, respectively. This reduces the number of adjustable parameters to 5.
4. The equilibrium constant for oxygen adsorption on the un-oxidized platium surface was taken from the measurements in section 3.2.2.1, figure 3.8. This figure is the Van't Hoff plot for the oxygen adsoption equilibrium as determined by measurement of the exchange current density at different p_{O2}'s and temperatures, and modelling of the data according to Langmuir-Hinshelwood adsorption of oxygen on the un-oxidized Pt. The model broke down at temperatures below 577°C probably because of the formation of oxide, which occupies sites for oxygen adsorption. The equilibrium constants were therefore evaluated by extrapolation from the linear region above 577°C, where oxide was unstable, and would not have formed on the Pt surface. The values of K_{O2} determined from figure 3.8 were 22360, 2800 and 720, which correspond to 149.5, 52.9 and 26.8 for K_O ($K_O=K_{O2}^{1/2}$), for 466, 513 and 544°C respectively. This thereby reduces the number of independent parameters to only four.

4.2.5.7.1 Parameter Estimation

The data and model were fit using a multi-parameter multi-variable non-linear least squares program. This was based on a generalized minimization criterion for the regression of multiresponse data that was derived by Box and Draper (1965). This had been converted into a computationally efficient program by Jutan (1976), a copy of which was obtained from Truskey (1985) which contains more information on the method, than presented here, and a listing of the program (or one may be obtained from the author).

The inputs required by the program are initial guesses for the parameters and a mathematical description of the model. The program uses the initial guesses of the parameters to calculate estimates of the determinant of the matrix of differences between the each observation and response expected from the calcuation of model's prediction. This matrix is then minimized and the sum of squares of deviations between the data and the model is calculated. This is used, in turn, to obtain an estimate of the parameters. This continues iteratively until the parameters change by less than some desired tolerance. The program uses Marquardt's method for the iterative process.

Also calculated by the program is the correlation matrix of the parameters. Correlation coefficients are always between +1 and -1. A correlation coefficient with an absolute value greater than 0.95 suggests that the parameters are highly correlated, indicating that the model contains redundancies.

To re-iterate, the program fits the data of both butadiene production and deep oxidation **simultaneously**, and the fits cover 2 to 3 orders of magnitude of oxygen **and** butene partial pressures.

4.2.5.7.2 Parameter Estimates

The data and model were fitted accordingly and estimates of the parameters obtained. The parameters obtained are shown in table 1.

Table 1: Parameters from Fits of Model and Data (with standard deviations)

Parameter	Temperature (°C)			Activ. Energy or Ads. Enthalpy (kcal/mole)
	466	513	544	
K_O	149.5	51.0	26.8	53.1
K_{Bu}	1072±185	69.1±7.7	17.4±2.2	63.8
k_{Bd}	$2.59\pm.26\times10^{-7}$	$9.57\pm.73\times10^{-7}$	$1.83\pm.23\times10^{-6}$	30.2
k_{DO}	$5.56\pm.74\times10^{-7}$	$1.23\pm.10\times10^{-6}$	$3.42\pm.35\times10^{-6}$	27.1
k''_{DO}	$3.84\pm.68\times10^{-6}$	$2.33\pm.23\times10^{-4}$	$8.90\pm.91\times10^{-3}$	117.3
K_{Pt}	0.286	0.0516	0.0186	42.0

These parameters were then used to obtain theoretical estimates of the rates and plotted with their experimental data in figures 4.45 to 4.50. As can be seen in these figures, the model fits the data reasonably well and is bracketed by the data as would be expected. The correlation coefficients between the parameters in the model were all less than 0.6 and most of them were less than 0.2. This indicates that the parameters used were independent of each other and that it is unlikely that any more parameters may be eliminated and a good fit of the model and data still be obtained.

The fit of the model to the data where oxygen was varied at 466°C is only satisfactory (figure 4.45). When the restriction on the equilibrium of adsorption of oxygen on the surface was lifted, and the data fitted with five adjustable parameters, a far better fit of the data was obtained

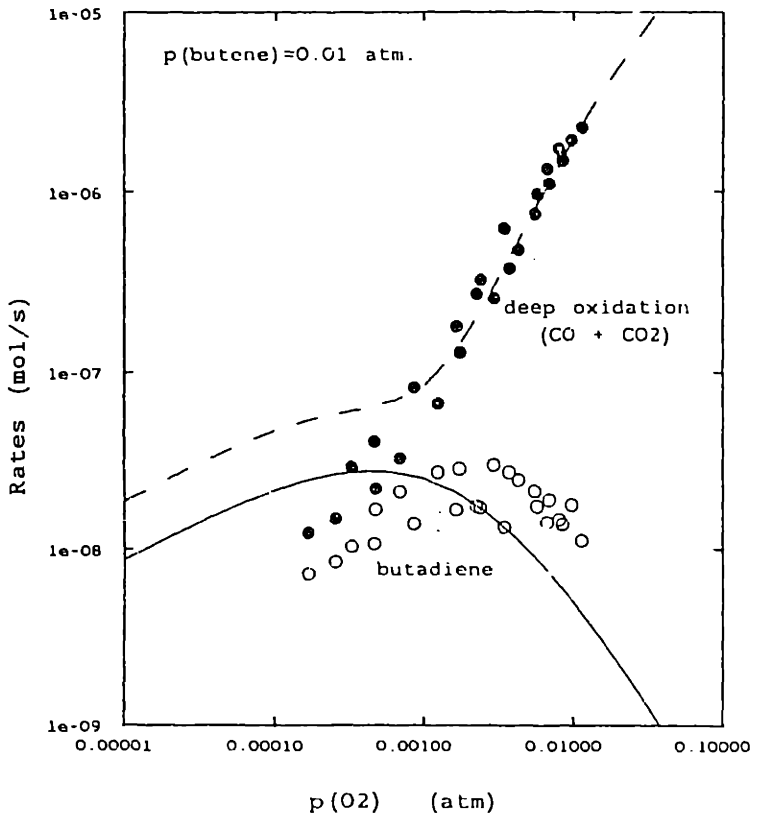

Figure 4.45: Rate of butene oxidation vs p_{O2} at p_{butene}=0.01 atm, T=466°C.
Fit of model with K_O and K_{Pt} from electrochemical measurements

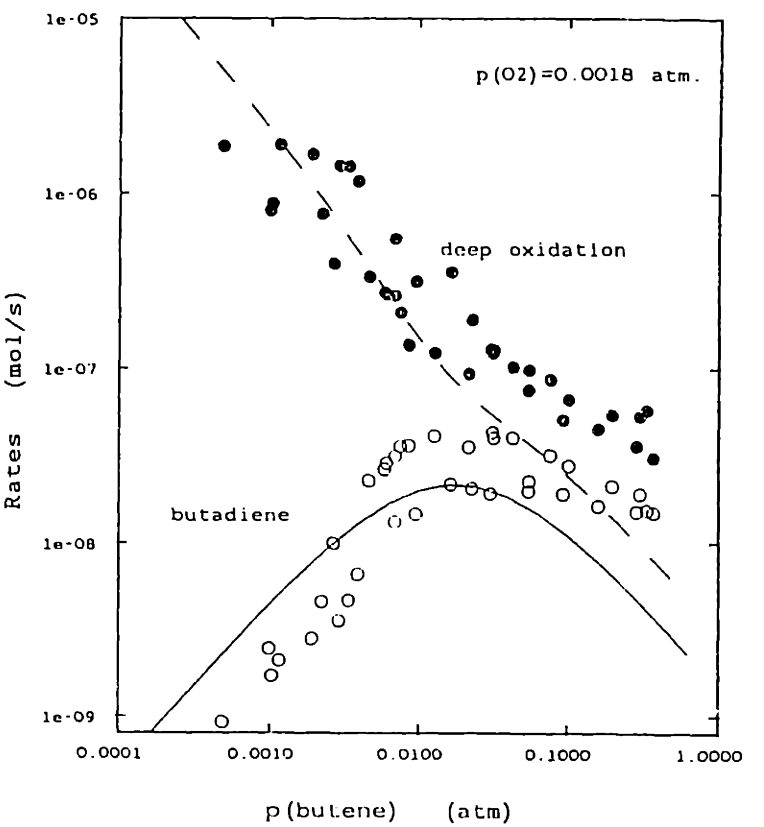

Figure 4.46: Rate of butene oxidation vs p_{butene} at p_{O2}=0.0018 atm, T=466°C.
Fit of model with K_O and K_{Pt} from ele ctrochemical measurements

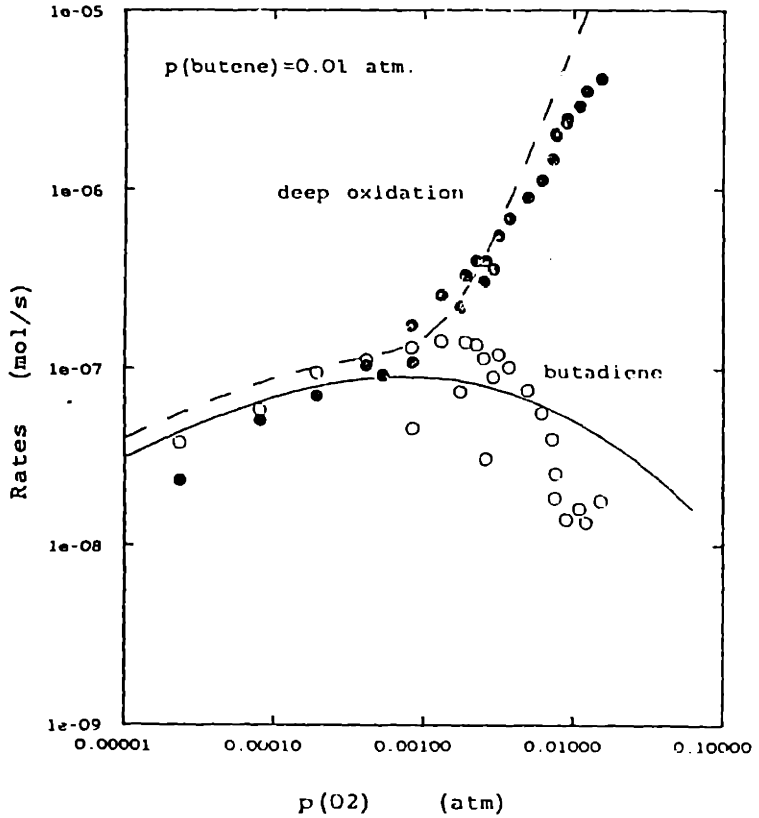

Figure 4.47: Rate of butene oxidation vs p_{O2} at p_{butene}=0.01 atm, T=513°C.
Fit of model with K_O and K_{Pt} from electrochemical measurements

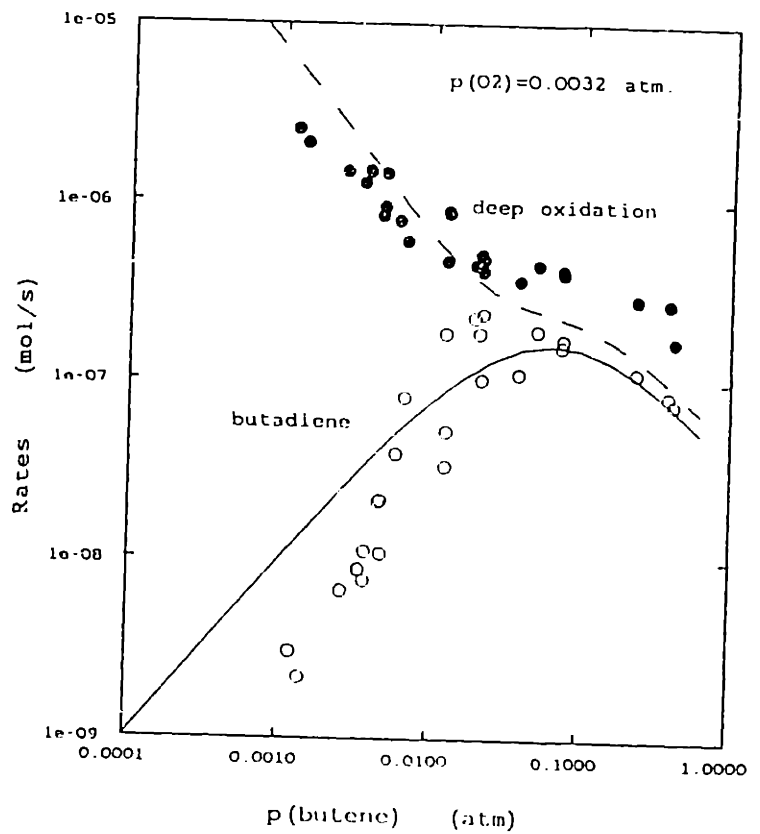

Figure 4.48: Rate of butene oxidation vs p_{butene} at p_{O2}=0.0032 atm, T=513°C.
Fit of model with K_O and K_{Pt} from electrochemical measurements

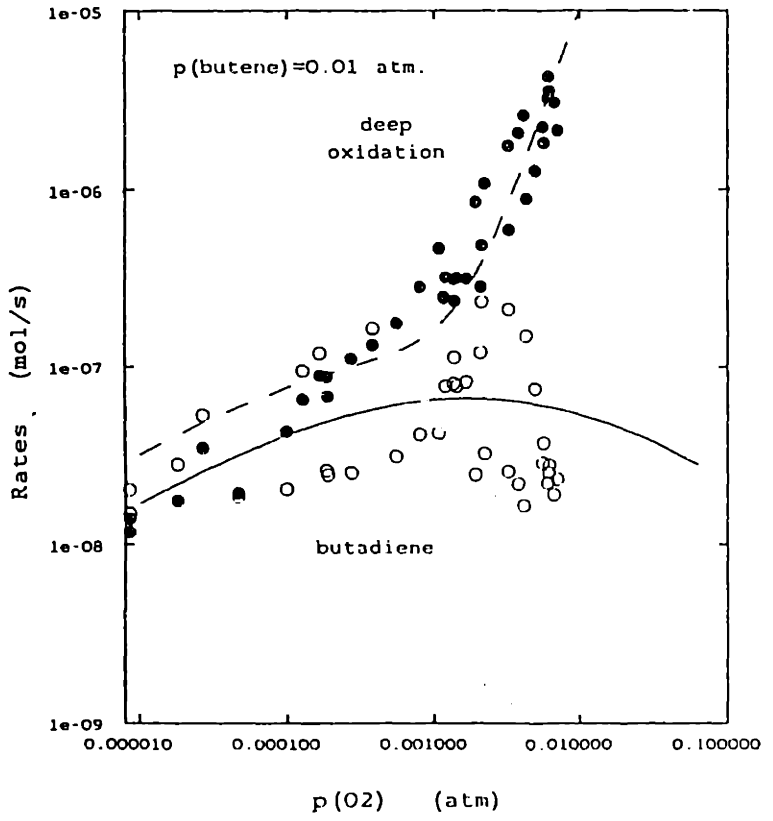

Figure 4.49: Rate of butene oxidation vs P_{O2} at P_{butene}=0.01 atm, T=544°C.
Fit of model with K_O and K_{Pt} from electrochemical measurements

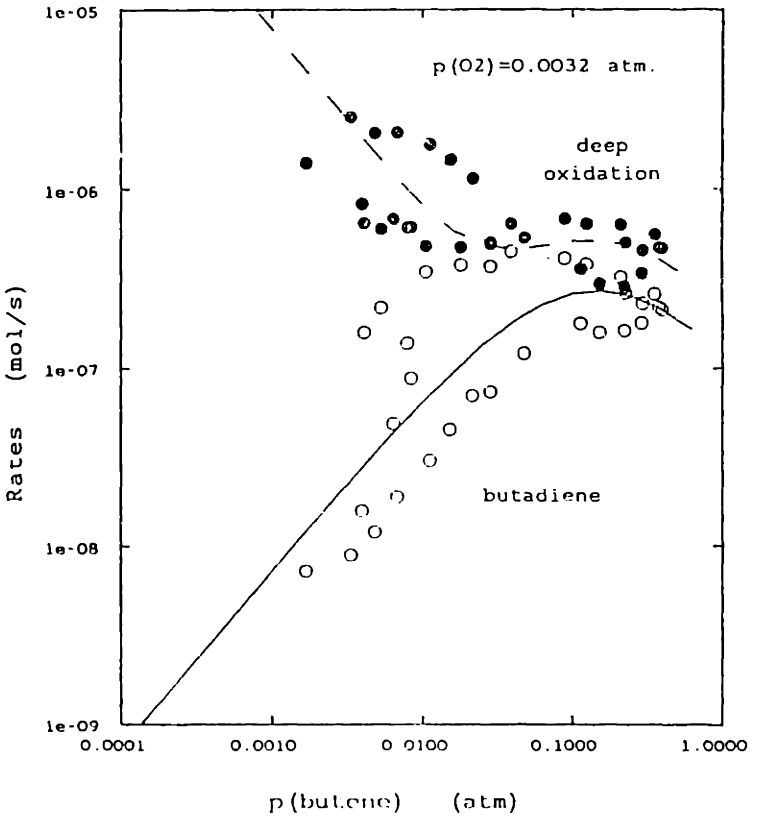

Figure 4.50: Rate of butene oxidation vs P_{butene} at P_{O2}=0.0032 atm, T=544°C.
Fit of model with K_O and K_{Pt} from electrochemical measurements

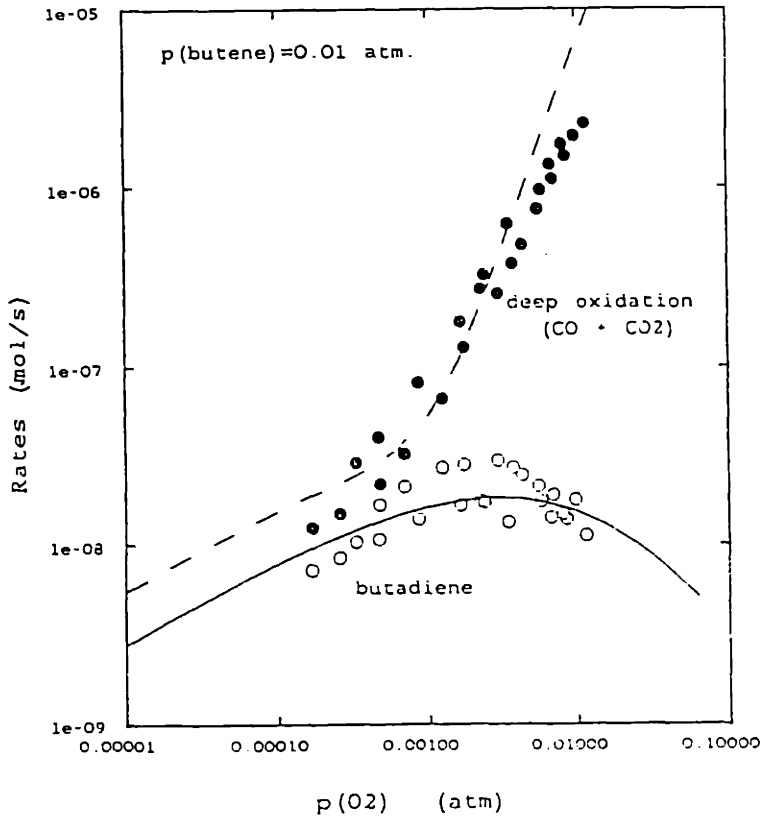

Figure 4.51: Rate of butene oxidation vs P_{O2} at P_{butene}=0.01 atm, T=466°C. Fit of model with K_{pt}, but not K_O, from electrochemical measurements

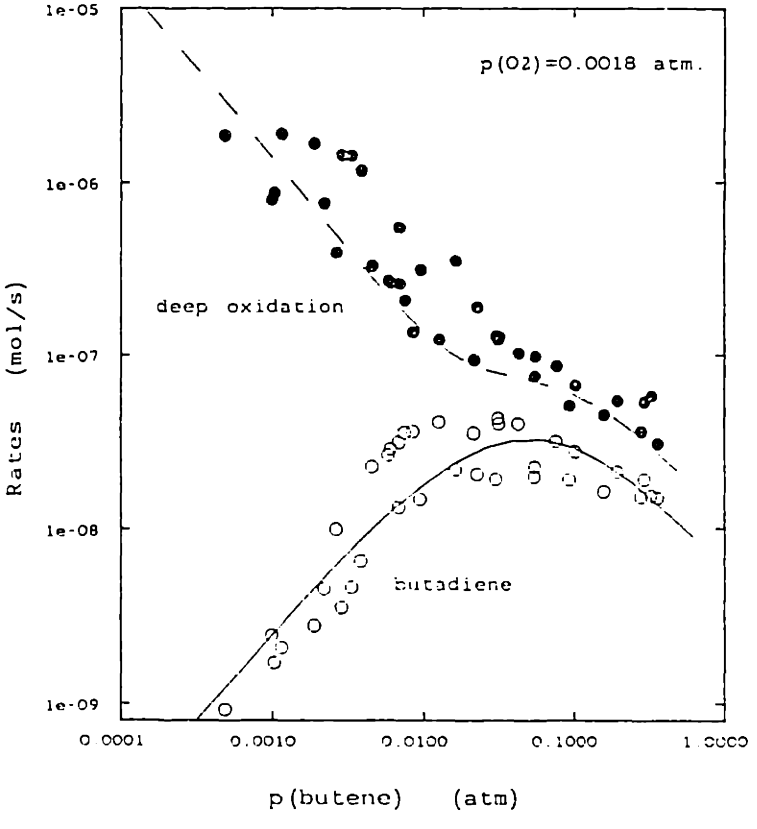

Figure 4.52: Rate of butene oxidation vs P_{butene} at P_{O2}=0.0018 atm, T=466°C. Fit of model with K_{pt}, but not K_O from electrochemical measurements

(figures 4.51 and 4.52), i.e. at 466°C, the model gives only a semi-quantitative fit to the data.

Comparing figures 4.11 and 4.51, for decreasing p_{O2} the experimental data in figure 4.11 lie below the model estimates for butadiene and above the model estimates for deep oxidation in figure 4.51. When decreasing p_{O2} from a higher value, if the surface does not come to equilibrium immediately, a larger fraction of the surface will be oxidized than at equilibrium. Therefore the model will overpredict the rate of butadiene production and underpredict the rate of deep oxidation, as observed experimentally. Similarily, for increasing p_{O2}, if the surface is not at equilibrium, there will be less oxide on the surface than expected by the model and the rates of butadiene formation and deep oxidation will be under- and over-predicted, respectively. Similar logic applies to the data where p_{butene} was cycled (figures 4.12 and 4.52). The data at the other temperatures also consistently followed these trends.

The rate constants obtained are plotted as Van't Hoff and Arrhenius plots in figures 4.53 and 4.54. The activation energies for butadiene formation and deep oxidation were 30.2 kcal/mole and 27.1 kcal/mole, respectively. The apparent activation energies for the other two parameters, the enthalpy of adsorption and the combined parameters over the oxide surface were 70 and 120 kcal/mole respectively.

4.2.5.7.3 Contour Plots/Oxide Phase Diagram

The values of K_{Pt}, K_O and K_{Bu} at 513°C were used with equation (38) to produce contour plots of equilibrium surface platinum oxide coverage (θ_{ox}; figure 4.56). Superimposed on this figure are the realms over which the data were taken. For example, when oxygen was cycled from 0.002% to 1.5%

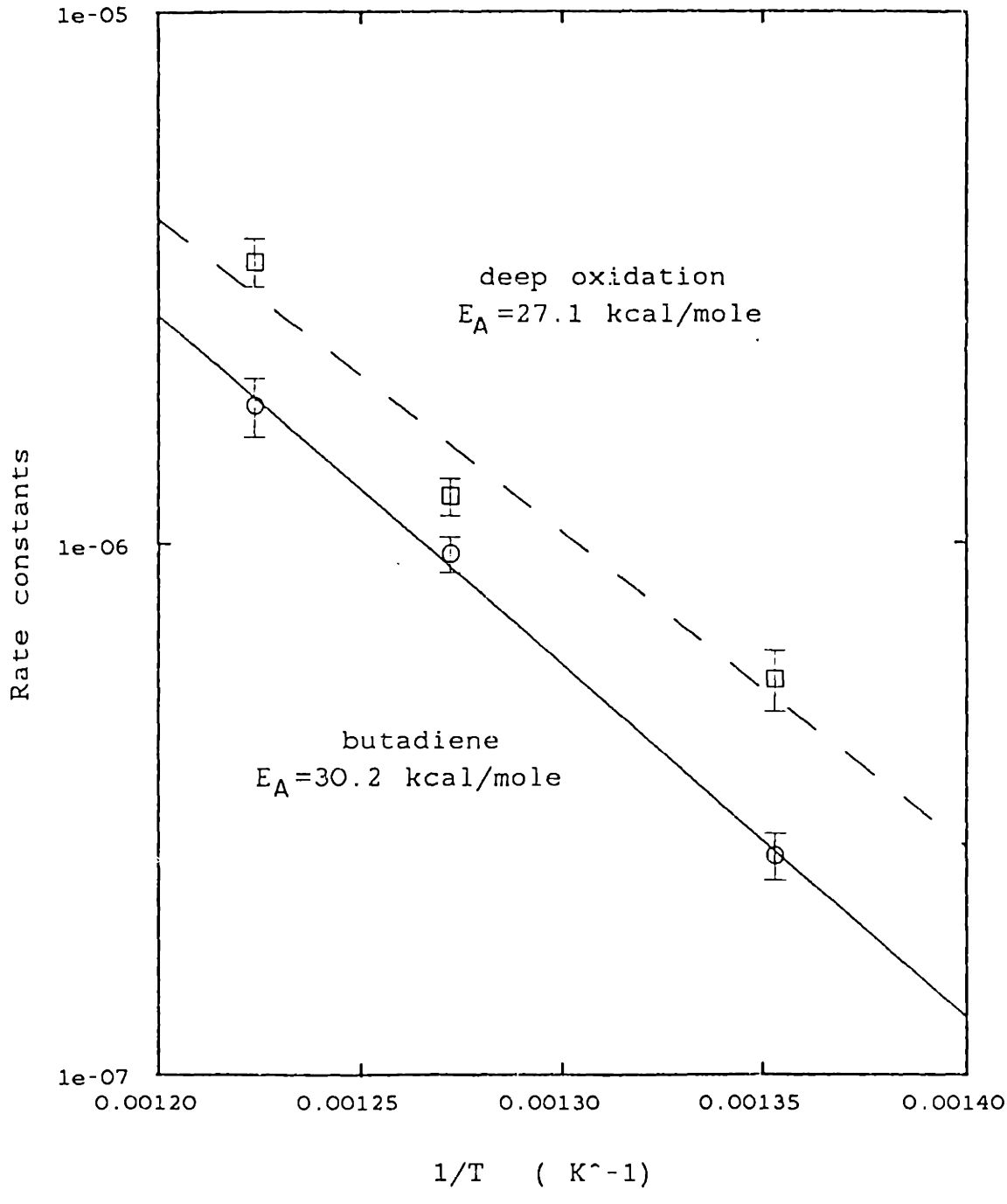

Figure 4.53: Arrhenius plots for butadiene and deep oxidation rate constants over un-oxidized platinum surface

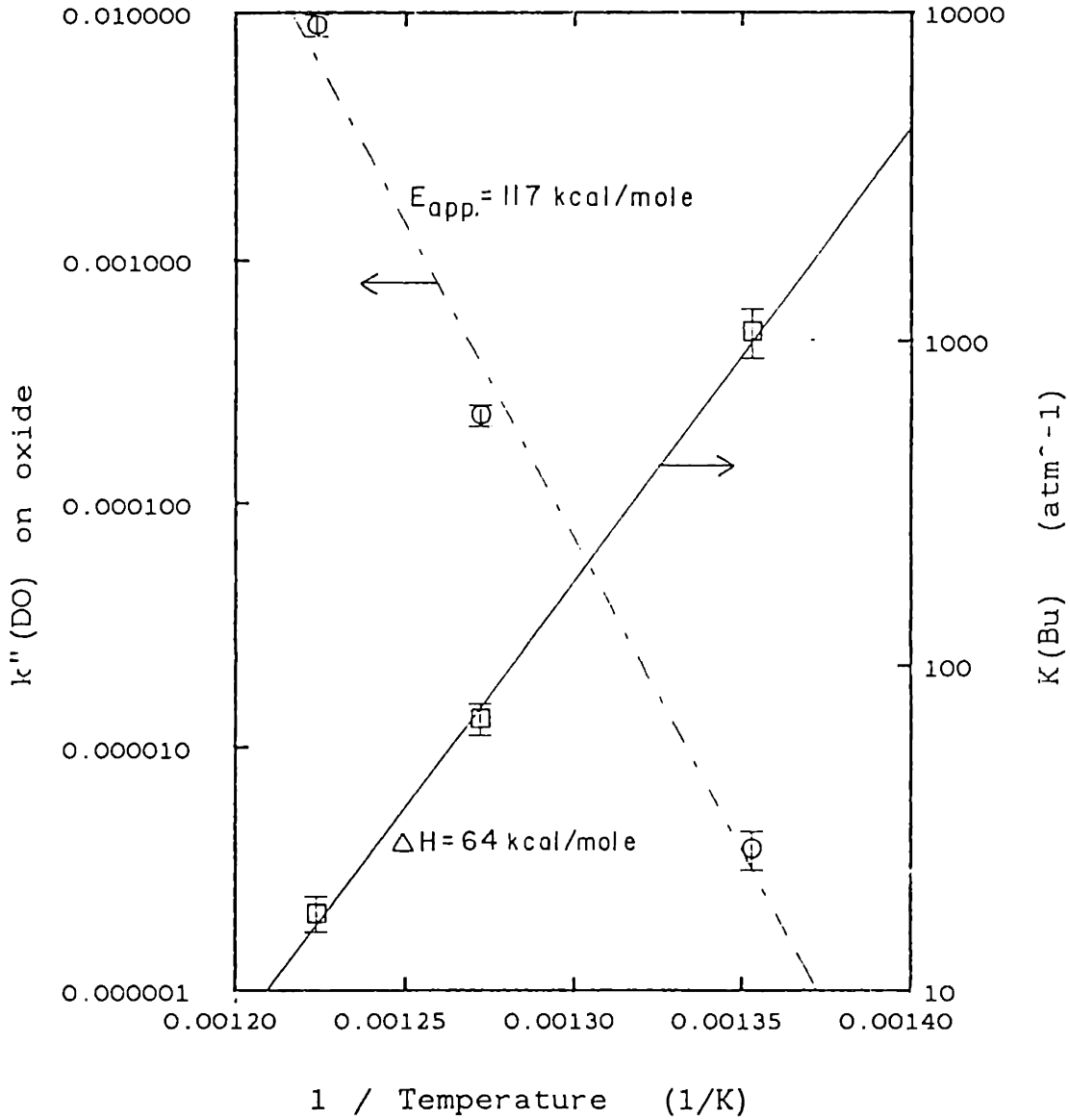

Figure 4.54: Arrhenius plot for combined rate constant ($k'_{DO}K'_{O2}/K'_{Bu}$ for deep oxidation of butene over PtO_2 and van't Hoff plot for adsorption of butene on un-oxidized Pt

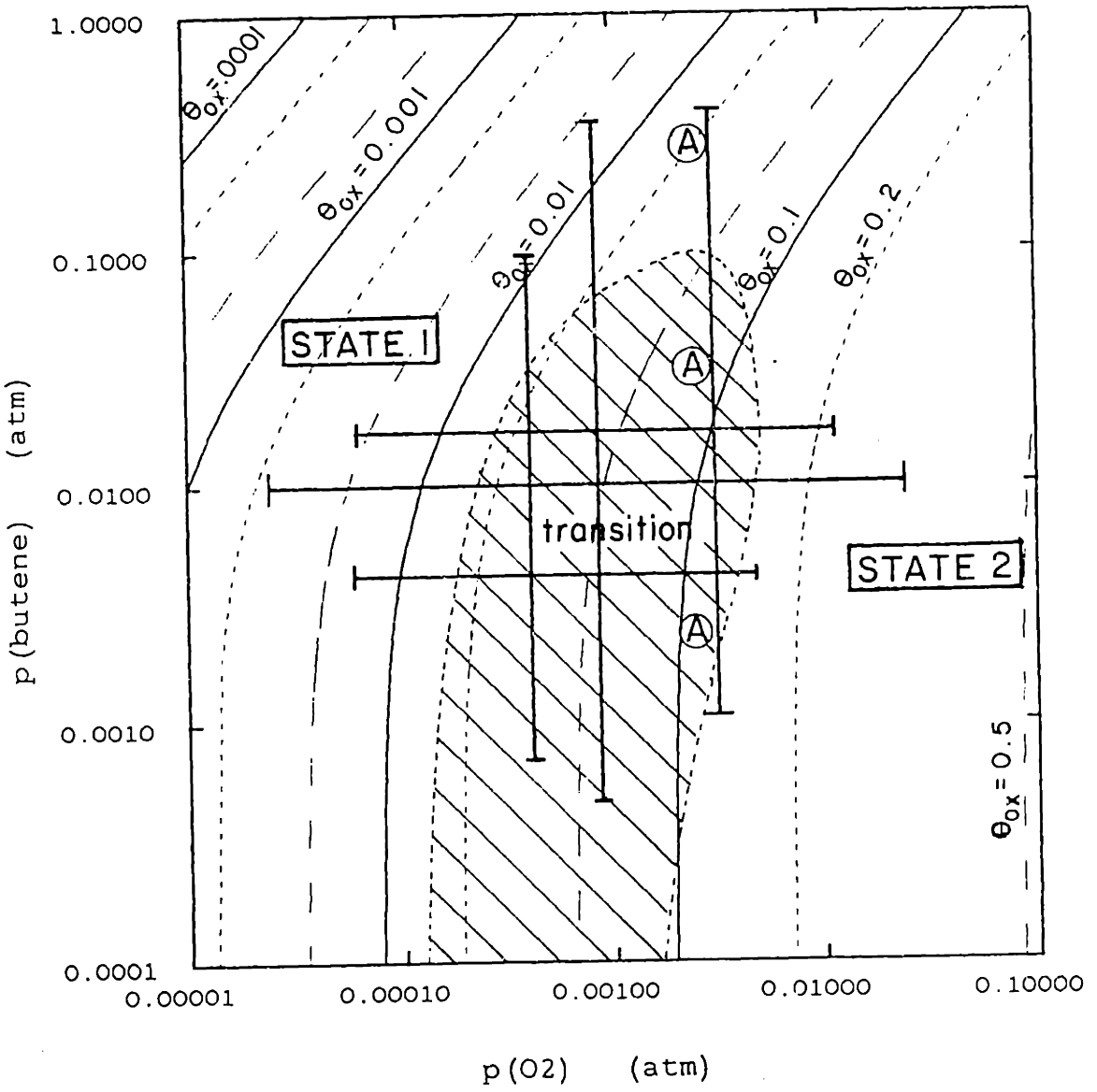

Figure 4.5 : Approximate equilibrium contours for platinum oxide on platinum catalyst, T=513°C. The solid lines in the figure are the conditions over which experimental data were taken.

while p_{butene} was constant at 1.0% (figures 4.14 and 4.47), the oxide coverage increased from 0.001 to 0.25. "State 1" behavior corresponded to coverage of 0.001 and "state 2" to coverage of 0.25. When 25% of the surface was covered with oxide, the rate for butadiene production decreased accordingly, as presumably did the rate of deep oxidation over the Pt surface. The total rate of deep oxidation was, however, up to three orders of magnitude greater than the rate of butadiene, and therefore it was dominated by the reaction over the oxide, i.e. the oxide is considerably more active for deep oxidation than the Pt surface.

The conditions at which the Auger data were taken are indicated by "A"'s in figure 4.56. The change in surface O/Pt from 3.5 to 1.9 corresponds to θ_{ox} changing from about 15% to about 6%, according to figure 4.56. The Auger values indicate a more significant transition than this and therefore the values in the figure may be somewhat low. The shaded region in the figure indicates the transition region between the two states which occurred because the oxide formation/decomposition was not in equilibrium as assumed in the model.

4.2.5.7.4 Comparison of Values Obtained

The enthalpy of adsorption of oxygen on the clean platinum surface was determined by the exchange current density measurements in section 3.3.3 and was about 54 kcal/mole. This is the value that was entered as a constant in the model, it compared to literature values of 38 to 55 kcal/mole, and is discussed in section 3.3.3.

The oxidation of CO over platinum catalysts has been more widely studied than the oxidation of butene. Many models have been proposed for the reaction, with different activation energies. Sales, Turner and Maple

(1984) analysed the literature and found activation energies from 10 to 20 kcal/mole for a Langmuir-Hinshelwood mechanism between adsorbed oxygen and CO. Kiss and Gonzalez (1985) studied the reaction over Rh supported on SiO_2 and found an activation energy of 22.9 to 25.4 kcal/mole, depending on the relative concentrations of CO and oxygen used.

For the oxidation of butene, Schwartz, Holbrook and Wise (1971) reported an activation energy for the complete (deep) oxidation of butene to CO_2 in excess air of 17.4±2.4 kcal/mol and Cant and Hall (1970) reported an activation energy of 18.5±0.5 kcal/mole. Yao (1984) studied the oxidation of CO and olefins over Pt wires and on Al_2O_3 supports and reported activation energies of 16 to 28 kcal/mole (section 1.2.2). The experimental value for the activation energy for the oxidation of butene to CO and CO_2 of 18.9 kcal/mole agrees well with these literature values.

In contrast, the activation energy for the partial oxidation of butene to butadiene is higher than that for deep oxidation, 26.1 kcal/mole versus 18.9 kcal/mole. This was initially thought to be an error, however, on further examination, it does not appear to be an abberation or a product of the fitting and modelling. If the activation energy for partial oxidation were higher than for deep oxidation, then at higher temperatures, the selectivity to butadiene should increase. This is observed experimentally (see figure 4.56). This is also borne out by the limited data presented in a patent by Thomas (1967). The patent proposes producing butadiene by reacting mixtures of butene and oxygen over a platinum gauze at temperatures "preferably" 800 to 900°C, with contact times of "less than 0.1 second, and may be as low as 0.0001 second". Unfortunately, no selectivity data were presented, but they commented that when the ratio of butene to oxygen dropped below 2:1, increased amounts of CO and H_2O were produced. This appears to indicate that the selectivity of the high temper-ature

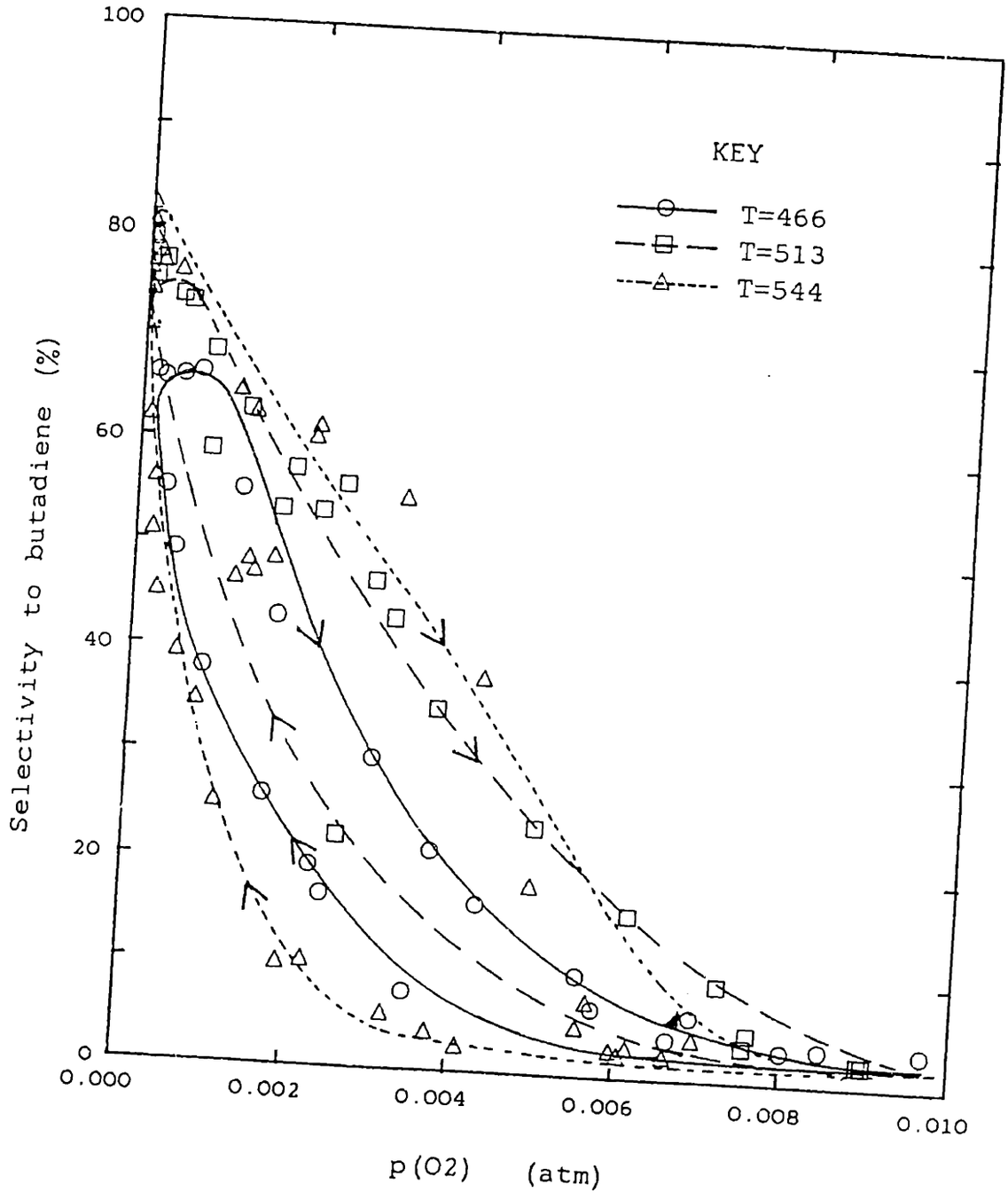

Figure 4.56: Butadiene selectivity at p_{butene}=0.01 atm, effect of temperature

oxidation was reasonable, and that little CO_2 was produced. If this were the case, then his approach would tend to confirm the results of greater selectivity at higher temperatures found here.

The size of the activation energy for butadiene production, and the kinetics being dependent on $p_{O2}^{1/2}$ and p_{butene}, leads us to speculate that the mechanism for the reaction probably goes through a transition state that involves both the oxygen and butene and that the dehydrogenation occurs by a concerted reaction, rather than in two steps of dehydrogenation and then oxidation of the hydrogenation.

There is little data with which to compare the enthalpy of adsorption of butene on the platinum surface. The activation energy for desorption of butene from Pt (111) was 10.5 ± 1.7 kcal/mol according to Salmeron and Somorjai (1983). The activation energy for desorption of CO from Pt (111) varied between 29.6 (McCabe and Schmidt (1977)) and after reviewing a number of papers, Sales, Turner and Maple (1984) reported estimates of 20-35 kcal/mole. The latter paper involved an attempt to model oscillations of CO oxidation on platinum catalysts, they assumed zero activation energy for adsorption, which would give an enthalpy of 20-35 kcal/mole.

The apparent enthalpy of adsorption of butene on the un-oxidized platinum surface obtained by the fits of the model to the data, of about 70 kcal/mole, therefore appears to be too large and may be an aberation of the fitting procedure. The same may be said for the apparent activation of the deep oxidation over the oxide surface. The fitted parameter, $k''_{DO} = k'_{DO}/K'_{Bu}$ and therefore the apparent activation energy should be the sum of the activation energy for k'_{DO} and the enthalpy of adsorption for butene on the oxide surface. Even considering this, the apparent activation energy of about 120 kcal/mole is excessively high.

This model does, however, give consistent values for the parameters, unlike several other models that were applied to the data. The model is simplified description of the reality, rather than the reality per se. A number of assumptions were made in its development that are contradictions of the experimental data: it was assumed that the surface oxidation/oxide decomposition reaction was in equilibrium and the presence of carbon on the surface was ignored.

At 544°C, the slow hysteresis reaction took almost 24 hours to come to a final steady state. It is possible that at 466°C the time allowed for the experiments, about 24 hours, may have been too short and the surface may never have come to equilibrium. At 466°C, the difference in the rates between increasing and decreasing p_{O2}/p_{butene} ratios was less than at 544°C. The model does is too simple to predict difference in increasing and decreasing ratios, but one would anticipate the rate of oxide formation/decomposition to be higher at higher temperatures, which would result in smaller differences, the opposite of the experimental observations. This may indicate that the slower surface reaction was "frozen" at the lower temperatures.

At the end of each period of taking data, the carbon that had been on the surface was oxidized in air and the CO_2 evolved measured. The amounts indicated that the carbon coverage was the equivalent of more than a monolayer of the surface. Also, when the surface that had been pretreated in 40% butene/0.25% oxygen was analysed by Auger spectroscopy, no surface components other than carbon could be detected, yet this catalyst had not lost any catalytic activity. In the model it was assumed that the carbon had no effect on the reactions. This is a simplification.

In conclusion, the model is able to give a semi-quantitative description of the data, with the activation energies for the surface reactions agreeing reasonably well with the literature.

4.3 CONCLUSIONS

4.3.1 Effect of Time on Stream

When a pre-oxidized reactor was exposed to butene/oxygen mixtures, the selectivity to butadiene increased over the first ten hours and then remained constant irrespective of the length of time (up to 600 hours). The activity of the catalyst was approximately constant during the first ten hours (butene was oxidized to CO and CO_2, instead of butadiene), and remained so until more than 100 hours on stream. Beyond one hundred hours, the activity declined steadily. When the surface carbon was titrated with air, it was found to be present at levels of about a monolayer up to 100 hours on stream, and to increase to levels equivalent to almost 12 monolayers. It therefore appeared as if carbon deposition on the surface was responsible for the non-selective decay observed beyond 100 hours.

When the catalyst was exposed to step increases in the p_{butene}/p_{O2} ratio, the selectivity to butadiene increased. When samples of the surface were analysed by surface spectroscopic techniques after similar step changes, the surface concentration of oxygen was found to decrease in parallel to the butadiene rate increase. This decrease in the surface oxygen content may have arisen from the decomposition of platinum oxides which had formed on the surface in the presence of excess oxygen, or from impurities, which had surface segregated and oxidized in the presence of excess oxygen, redissolving in the bulk Pt. Iron and Ag impurities were

seen in the sample that had been exposed to air, which were not seen in samples that had been reduced in either hydrogen of butene. Some silicon impurities were observed in the sample pretreated in hydrogen. The impurities are present as a consequence of using commercial inks for the electrode/catalyst preparations.

4.3.2 Conversion of Butene in a Fuel Cell

When butene was used as the fuel for a zirconia-yttria high temperature fuel cell, the only products obtained were those of the deep oxidation of butene, CO and CO_2, butadiene was not selectively produced. When butene/oxygen mixtures were fed to the electrochemical reactor and the current was "reversed", so that oxygen was pumped from the reactor, the rates of butadiene formation and deep oxidation of butene over the platinum surface were unaffected, even when the current was as large as the rate of oxygen reacted to butadiene and CO and CO_2. The rates were not zero order in oxygen, therefore oxygen was probably in equilibrium between the gas phase and surface.

At open circuit, the cell voltage varied according to:

$$V_{cell} = \frac{RT}{2F} \ln \left(\frac{P_{O2}}{P_{butene}} \right)$$

The simultaneous dependence of the cell voltage on the butene and oxygen partial pressures, together with the size of the voltage (0.4-0.7 volts) indicated that the voltage may be due to a mixed potential. The voltage and reaction rates were also unaffected by the flowrate from the external recycle pump, indicating that mass transfer was not a problem and not the scource of the voltage.

4.3.3 Butene Conversion

When butene and oxygen were fed to the reactor in the gas phase, butene was converted to butadiene, CO and CO_2, no oxygen containing products were observed. At low p_{02}/p_{butene}, the selectivity to butadiene was about 80% at low p_{02} and remained approximately constant for small increases in p_{02}. The rate of butadiene production and deep oxidation were both one half order in oxygen and negative order in butene. At high $p_{02}^{1/2}/p_{butene}$ ratios the selectivity to butadiene decreased to about 4%. Under these conditions, the rate of butadiene production was first order in butene and negative order in oxygen, the rate of deep oxidation was negative one order in butene and first order in oxygen.

The data could be semi-quantitatively modelled in terms of butadiene, and CO and CO_2 being produced in parallel reactions over the platinum surface under low p_{02}/p_{butene} conditions. At high $p_{02}^{1/2}/p_{butene}$ ratios, the surface coverage was modelled as becoming net oxidizing, permitting platinum oxide to form at the expense of the un-oxidized platinum surface. Butene is oxidized only to CO and CO_2 over the oxide surface.

Values for the adsorption equilibrium constant of oxygen on the un-oxidized surface and the equilibrium constant for oxide formation had been measured independently (chapter 3). These, with simplifications to the model, reduced the number of adjustable parameters to four. The model was fit **simultaneously** to butadiene production and deep oxidation data for butene and oxygen partial pressures varied over 2 to 3 orders of magnitude each. Reasonable fits were obtained with the activation energies for butadiene formation and deep oxidation being 30.2 and 27.3 kcal/mole respec-tively, which agree reasonably well with the literature. This simple model was therefore able to describe the trends of the experimental data semi-quantitatively.

5. CONCLUSIONS

5.1 Oxygen over Platinum

1. The **transfer coefficients** for the electrochemical reaction at the electrode/electrolyte interface reaction were found to be 1.0, indicating that the rate controlling step is probably the transfer of O^- anions across the interface

2. The **exchange current density** of the interface varied with $p_{O2}^{1/4}$ at low p_{O2} and high temperatures, and as $p_{O2}^{-1/4}$ at low temperatures and high p_{O2}. The data were fitted to a Langmuir-Hinshelwood model of adsorption of oxygen on the platinum surface and yielded an enthalpy of adsorption of 53± 5 kcal/mole.

At low temperatures, the exchange current density data deviated from the simple Langmuir-Hinshelwood model, probably because of the formation of platinum oxide on the surface which would reduce the area available for oxygen adsorption.

2. The desorption of oxygen from the platinum surface was successfully modelled by the **decomposition of an oxide** layer that was stable and had formed during pre-oxidation, but is unstable when flushing the reactor with helium. The rate controlling step for desorption is the reaction between an oxide moeity and a vacant site.

The decomposition was found to be approximately independent of temperature (activation energy=0±1 kcal/mole), whereas, the initial coverage of oxygen prior to flushing with helium (found by extrapolation back to zero time) increased with an apparent activation energy of about 6 kcal/mole. It is possible that oxygen exists as a sub-surface species, the concentration of which may increase with temperature.

5.2 Oxygen and Butene over Platinum

1. When **butene** was used as the fuel for a zirconia-yttria high temperature **fuel cell,** the only products obtained were those of the deep oxidation of butene (CO, CO_2 and H_2O), butadiene was not selectively produced. When butene/oxygen mixtures were fed to the electrochemical reactor and the current was "reversed", so that oxygen was pumped from the reactor, the rates of butadiene formation and deep oxidation of butene over the platinum surface were unaffected, even when the current was as large as the rate of oxygen reacted to butadiene and CO and CO_2. The rates were not zero order in oxygen, therefore oxygen was probably in equilibrium between the gas phase and surface.

2. When **butene and oxygen** were fed to the reactor **in the gas phase,** butene was converted to butadiene with a selectivity of about 75% under "state 1", low p_{O2}/p_{butene}, conditions. Under these conditions, the surface is predominanatly Pt. CO and CO_2 are produced in a reaction in parallel to the butadiene reaction over Pt, at approximately the same rate as butadiene.

At higher p_{O2}/p_{butene} ratios platinum oxide is formed at the expense of un-oxidized platinum. This creates "state 2" conditions where the rate of deep oxidation is now controlled by the rate over the oxidized surface. The selectivity drops because butene is oxidized only to CO and CO_2 over the oxide surface, and the rate of deep oxidation over the oxide is up to three orders of magnitude faster than the rate of butadiene formation over the Pt surface.

3. Under state 1 (low p_{O2}/p_{butene} ratio) conditions, **"spiking" the feed** with CO_2 or water had no effect on the rates of butadiene formation or deep

oxidation, whatsoever. "Spiking" the feed with CO enhanced the rate of CO_2 formation but had no effect on butadiene. "Spiking" with butadiene inhibited the rate of butadiene, because of poisoning, but only at concentrations higher than obtained experimentally.

Under state 1 conditions, "spiking" with hydrogen had no effect on the rate of butadiene formation, but inhibited the rate of deep oxidation, therefore increasing the selectivity from about 75% to over 85%. In contrast, under state 2 (high P_{O2}/P_{butene} ratio) conditions, spiking the feed with hydrogen had no effect at all, i.e. H_2 inhibits the deep oxidation on the Pt, but not the PtO_2, surface.

4. Scanning electron micrographs and **surface analysis** indicated that the surface was predominantly Pt, but after pre-treatment in air, small inclusions composed of Fe, Ni, Cr and Si were observed, probably the product of processing by the manufacturer. The concentrations were sufficiently small to be ignored, but were also seen in XPS and Auger spectra.

Auger spectra of the surface after pre-treatments in different oxygen and butene partial pressures tended to confirm the surface platinum oxide theory, and different O/Pt surface concentrations were observed for the same gas composition, depending on the length of time the surface had been exposed to this environment.

APPENDIX A. The Butler-Volmer equation

The Butler-Vulmer equation is used extensively in chapter 2 of this thesis to evaluate the mechanism of the electrochemical reaction at the zirconia-yttria-platinum-gas interface. The derivation given below is adapted from Bockris and Reddy (1970).

Assume that a simple reaction occurs at the electrode interface whereby an ionic species A^+ picks up an electron to become a new species D:

$$A^+ + e^- \text{---} D \qquad (1)$$

The frequency, k, with which the ion can overcome the energy barrier between the electrode and the electrolyte is given by the Boltzman distribution:

$$k = k'T/h \exp\{-\Delta G^{o\ddagger}/RT\} \qquad (2)$$

where k' is the Boltzmann constant, h Planck's constant and $\Delta G^{o\ddagger}$ is the standard free energy for activation over the energy barrier.

The rate for transfer is given by the product of frequency with concentration:

$$r = k'T/h\ c_{a+} \exp\{-\Delta G^{o\ddagger}/RT\} \qquad (3)$$

where c_{a+} is the concentration of the ionic species A^+ to be transfered over the energy barrier.

For the transfer of the ion between the electrolyte and a charged electrode, there will be a potential difference, $\Delta\Phi$, which will hinder or assist the transfer and so increase or decrease the height of the activation barrier. For the transfer of a single ion from the "outer Helmhlotz plane" (the point in the electrolyte at which the interface starts to influence the electrolyte) to the electrode, only that fraction, β, called the "symmetry factor", of the potential prior to the barrier will reduce the potential difference. Therefore the potential difference in the

forward direction would be $\beta\Delta\phi$ and $(1-\beta)\Delta\phi$ in the reverse direction. Considering the relationship between free energy and voltage this potential difference would result in a free energy contribution of $\beta F\Delta\phi$.

Therefore in the presence of an electric field, the energy barrier would change to:

$$\Delta G^{o\ddagger} = \Delta G_c^{o\ddagger} + \beta F \Delta\phi \qquad (4)$$

where $\Delta G_c^{o\ddagger}$ is the chemical free energy change and $\beta F\Delta\phi$ is the electrical free energy change, and the rate of transfer would be:

$$r = k'T/h \; c_{a+} \exp\{-\Delta G_c^{o\ddagger}/RT\} \; \exp\{-\beta F\Delta\phi\}$$

$$= k_f \, c_{a+} \exp\{-\beta F\Delta\phi\} \qquad (5)$$

where k_f is the non-electrical rate constant in the forward (electrolyte to electrode) direction.

The current is obtained by the product of the rate with the charge per mole of ionic species:

$$i = Fr$$

therefore:

$$i_f = k_f \, c_{a+} \, F \exp\{-\beta F\Delta\phi/RT\} \qquad (6)$$

and similarily for the reverse process of transfer of ions from the electrode to the electrolyte:

$$i_b = k_b \, c_d \, F \exp\{(1-\beta)F\Delta\phi/RT\} \qquad (7)$$

When no external potenetial is applied to the electrode/electrolyte interface, it will be at equilibrium and the forward and backward rates will be equal:

$$i_o = i_f = k_f \, c_a \, F \exp\{-\beta F\Delta\phi/RT\} \qquad (8)$$

$$= i_b = k_b \, c_d \, F \exp\{(1-\beta)F\Delta\phi/RT\} \qquad (9)$$

and equal to i_o, the so-called exchange current density. The exchange current density therefore measures the rate of transfer of ions and

electrons across the interface when there is NO NET flow of current, under equilibrium conditions. It is therefore analagous to the pre-exponential factor A in the Arrhenius expression for rates versus temperature:

$$r = A \exp\{-E_a/RT\}$$

When an external current is applied, the potential difference between the electrode and electrolyte, ϕ_i will increase from the equilibrium value by:

$$\phi_i = \phi + \eta \qquad (10)$$

i.e. , the activation overvoltage, is the difference between the potential under an applied voltage and at equilibrium. The corresponding current density is then given by:

$$i = i_b - i_f$$

$$= k_b\, c_d\, F \exp\{(1-\beta)F\Delta\phi_i/RT\} - k_f\, c_a\, F \exp\{-\beta\, F\Delta\phi_i/RT\}$$

applying equation (10):

$$i = [k_b\, c_d\, F \exp\{(1-\beta)F\Delta\phi_i/RT\}\exp\{(1-\beta)F\,\eta/RT\}] -$$

$$[k_f\, c_a\, F \exp\{-\beta\, F\Delta\phi_i/RT\}\exp\{-\beta F\,\eta/RT\}$$

using equations (8) and (9):

$$i = i_o\,[\exp\{(1-\beta)F\eta/RT\} - \exp\{-\beta\, F\eta/RT\}] \qquad (11)$$

Equation (11) is known as the Butler-Volmer equation, as applied to a single electron transfer process.

6.1.1 Butler-Volmer Equation for Multi-electron Transfers

Equation (11) applies only for a single electron/ion transfer and will now be extended to a multistep reaction (e.g. $A^{n+} + ne^- \text{ --- } Z$) involving the transfer of n electrons and assuming that the rate determining step (rds) is irreversible:

step 1 $\quad A + e^- \rightleftharpoons B$

step 2 $\quad B + e^- \rightleftharpoons C$

. . .

step γ_f $\quad P + e^- \rightleftharpoons R$

rds $\quad (R + re^- \longrightarrow S)$

step $\gamma_b = n - \gamma_f - r\nu$ $\quad S + e^- \rightleftharpoons T$

. . .

step n $\quad Y + e^- \rightleftharpoons Z$

Since steps 1 to γ_f are in equilibrium and since each step involves the transfer of a single electron:

$$c_B = K_1 \, c_A \exp\{-F\Delta\phi/RT\}$$

$$c_C = K_2 \, c_B \exp\{-F\Delta\phi/RT\} = K_1K_2 \, c_A \exp\{-2F\Delta\phi/RT\}$$

. .

$$c_R = \prod_i K_i \, c_A \exp\{-\gamma_f \, F\Delta\phi/RT\}$$

The rate of production of Z is controlled by the rate determining step (rds) which must occur ν times. Therefore the forward current for the n electron process, i_f', is:

$$i_f' = i_Z = i_R^{1/\nu}$$

Now, the rds uses r electrons:

$$i_R = F \, k_f \, c_R \exp\{-r\beta \, F\Delta\phi/RT\}$$

therefore:

$$i_f' = F \, k_f \left[\prod_i K_i c_a \right]^{1/\nu} \exp\{-\gamma_f/\nu F\Delta\phi/RT\} \exp\{-r\beta \, F\Delta\phi/RT\}$$

$$= F \, k_f \left[\prod K_i c_a \right]^{1/\nu} \exp\{(-\gamma_f/\nu + r\beta) \, F\Delta\phi/RT\}$$

using equation (8) and (10) above:

$$i_f' = i_o' \exp\{-(\gamma/\nu + r\beta)\, n/RT\}$$

where i_o' is defined as the exchange current density for n electrons.

Simplifying:

$$i_f = i_o \exp\{- \alpha_f F /RT\} \qquad \text{where: } \alpha_f = (\gamma/\nu + r\beta) \qquad (12)$$

Similarily, for the back reaction of $(S \longrightarrow R + ne^-)$:

$$c_s = \prod_{n-\gamma_f-r}^{n} K_i C_z \exp\{ \gamma_b F \Delta\phi/RT\}$$

also $\quad i_{backwards} = i_A = i_S^{1/\nu}$

and $\quad i_s = F\, k_s\, c_s \exp\{-r(1-\beta)F\Delta\phi/RT\}$

therefore

$$i_b' = i_o' \exp\{(\gamma_b/\nu - r + r\beta) F\eta /RT\}$$

and

$$i_b = i_o \exp\{\alpha_b F\eta/RT\} \qquad \text{where: } \alpha_b = \gamma_b/\nu - r + r\beta \qquad (13)$$

Thus for a multi-step reaction, the Butler-Volmer equation can now be written, by combining equations (12) and (13), as:

$$i = i_o(\exp\{ \alpha_b F\eta/RT\} - \exp\{- \alpha_f F\eta/RT\}) \qquad (14)$$

where $_b$ and $_f$ are known as the transfer coefficients and also

$$\alpha_b + \alpha_f = n/\nu \qquad (15)$$

6.1.2 Limiting cases of the Butler-Volmer equation

6.1.2.1 High overpotential

When is large and the reaction is far from equilibrium, the rate of the forward reaction >> rate of the backward reaction, therefore:

$$i_f = i_o \exp (- \alpha_c F\eta/RT) \qquad (16)$$

or

$$\ln i_f = \ln i_o - \alpha_c F\eta/RT \qquad (17)$$

and similarily at large negative overpotentials:

$$\ln i_b = \ln i_o + \alpha_a F\eta/RT \qquad (18)$$

Therefcre it is possible to determine the forward and backward transfer

coefficients from a plot of log current versus overvoltage (the Tafel plot).

6.1.2.2 Low overpotential

When the net overpotential is low, the exponent in the Butler-Volmer equation can be expanded in a Taylor expansion. Neglecting all the higher order terms:

$$i = i_o [1 + \alpha_a F \eta/RT - (1 - \alpha_c F \eta/RT)]$$
$$= i_o F (\alpha_a + \alpha_c)/RT \qquad (19)$$

Therefore if $(\alpha_a + \alpha_c)$ is known from the high overvoltage approximation, it is possible to determine the exchange current density from the slope of the current versus plot. It is also possible to determine i_o from the intercept of the Tafel plot, but the low overvoltage plot requires less data and is more reliable.

APPENDIX B. Equipment Model Numbers

Equipment Type		Specification	Manufacturer
Gases	butene	1.0%, 10.0%, 100%	Matheson Gas Products,
	butadiene	1.0%, 10.0%	Gloucester, MA. Certified
	oxygen	0.5, 2.0, 10.0, 100%	Standards, prepared from CP grade
	ethylene	2.17%	components by dilution
	hydrogen	10.4%	with helium.
	CO	2.06%	(diluted in nitrogen)
	CO_2	2.58%	" " "
	air	-	Matheson dry gas
	helium	-	Airco purified
Gas regulators*		Type 3104	Matheson
Needle valves		Series 4171 and 4172	Matheson
Rotameter housing		Model 7440	Matheson
Rotameter tubes		#600, 601 602 as required	Matheson "tube cube"
Gas filters		#450 with disposable zeolite 13X cartridges (type 451)	Matheson
Recycle pump		Type MB-21	Metal Bellows Corp, Sharon, MA
Gas Chromatograph		Model 3760	Varian Instrument Group Florham Park, NJ
GC Integrator		Model 3390A	Hewlett Packard
GC Columns		Poropak Q	Supelco Inc, Bellefonte, PA
		4% picric acid on Carbopack	" " " "
		Carbosieve S	" " " "
GC Valves		1/8" 4-port (reactor feed) 1/16" 8-port (column switching) 1/16" 10-port (sampling)	Valco Instruments Co. Houston, TX

* all regulators and valves made from stainless steel

Equipment Type	Specification	Manufacturer
Selector Valve	4-port; Series 43Y	Whitey Co., Highland Heights, OH
Shut-off Valves	various, 316 SS	Whitey Co., Highland Heights, OH
Tubing fittings	various, 316 SS	Swagelock, Crawford Fitting Co
Tubing	1/8" and 1/4"	316 Stainless Steel
CO_2 Analyser	Model 864 (infrared)	Beckman Instruments, Fullerton,CA
Zirconia-yttria reactor	Composition 1372	Corning/Zircoa Products, Solon, OH
Platinum catalyst/ electrodes	Ink #A-3788 and #A-4338	Engelhard Industries/Hanovia Thick Film, East Newark, NJ
Temperature Controller	Model 1523 (P.I.D)	Love Controls Corp, Wheeling, IL
Temperature Readout	Model 199 (type K)	Omega Engineering Inc, Stamford, CT
Temperature Programmer	Model JGB	West Instrument/Gulton Measurement East Greenwich, RI
Digital multi-meter	Model 8050A	John Fluke Mfg. Co. Inc. Mountlake Terrace, WA
"	Model 3466A	Hewlett Packard
Galvanostat/ Potentiostat	Model 549	Eco Instruments, Newton, MA
Electrometer	Model 602	Kiethley Instruments Inc, Cleveland, OH
Chart recorder	SuperScribe Series 4900	Houston Instruments, Austin, TX
Function generator	Model 3312A	Hewlett Packard
Lock-in Analyser	Model 3204	EG&G/Princeton Applied Research
X-Y Recorder	Model 7044B	Hewlett Packard
2-Channel Oscilloscope	Model 2335	Tektronix, Beaverton, OR

APPENDIX 3. THERMAL CRACKING OF BUTENE

C.1 Experimental

The effect of temperature on the reaction rates were investigated to permit the differentiation between thermal cracking occuring in the gas phase and reactions occurring on the platinum surface.

The kinetics of thermal cracking were investigated in three sets of experiments. The first was performed in a 1" O.D. quartz tubular reactor. This was similar to the annular reactor without the ZrO_2-Y_2O_3 central tube. Butene in He (0.5-4.0%) was fed at various flowrates yielding contact times of 4-14 seconds. The products were determined by GC (see section 2.2). The second set of experiments investigated the effect of the platinum catalyst for dehydrogenation of butene in the absence of oxygen, and to observe the point at which the change from dehydrogenation to thermal cracking occurred. In this case a very low flowrate of 1% butene in He (22ml/min, the standard flowrate was 120 ml/min) was used.

In the third set, the effect of the ZrO_2-Y_2O_3 surface was investigated by using the annular reactor, but with no Pt electrodes on the ZrO_2-Y_2O_3 tube, and also the effect of adding oxygen in the butene on the thermal cracking knetics. A mixture of about 2% butene and 0.24% oxygen was fed to the annular reactor with the recycle pump in place.

The active volume of the reactor was determined using the "effective volume" of Hougen and Watson (see Fromment and Bischoff, p401, 1979). The equivalent reactor volume is the volume, V_r, at a reference temperature, T_1 and pressure, p_1, which would give the same conversion as the actual reactor with its temperature and pressure profiles, i.e.:

$$r_{T1,p1}\, dV_r = r_{T,p}\, dV$$

and the equivalent reactor volume for a reaction of order, n, is given by:

$$V_r = \int_0^V \left(\frac{pT_1}{p_1 T} \right)^n \exp \left[\frac{E}{R} \left(\frac{1}{T_1} - \frac{1}{T} \right) \right] dV \qquad (1)$$

The temperature profile of the tubular furnace (figure A.1) was determined by recording the temperature along the central axis of the inner zirconia-yttria tube with a thermocouple. The effective volume was therefore calculated by graphical integration of equation (1) assuming an activation energy of 60 kcal/mole, and a reaction order of 1. After calculation of the activation energy experimentally, this was used to re-calculate the equivalent reactor volume, with only a small change resulting.

C.2 Results

In the first set of experiments, the thermal cracking of butene was studied in a SiO_2 tube. The rate at 550°C was below the GC's detectability. The kinetics for thermal cracking at 600°C were first order in butene (figure A.2) for $0.005 < p(\text{butene}) < .04$ atm, and varying the contact time (from 2 to 6 seconds) had no effect on the rates. The rate of butene conversion was measured at 550, 600, 650 and 700°C and the rate constants calculated assuming the reactor behaved as an integral reactor (figure A.3). The effective volume of the reactor was 40.0 cm^3.

The second set of data were performed in the annular reactor with its platinum electrode. The rate of thermal cracking of butene was calculated from the rates of propylene and ethylene production assuming selectivities for these products of 23.5 and 17.0%, respectively. The rate constant for butene conversion was calculated from this value (assuming a first order reaction and an equivalent reactor volume of 5.22 cm^3). The rate constant for butene dehydrogenation to butadiene was calculated by the difference between the experimental rate constant and that for the thermal cracking

...

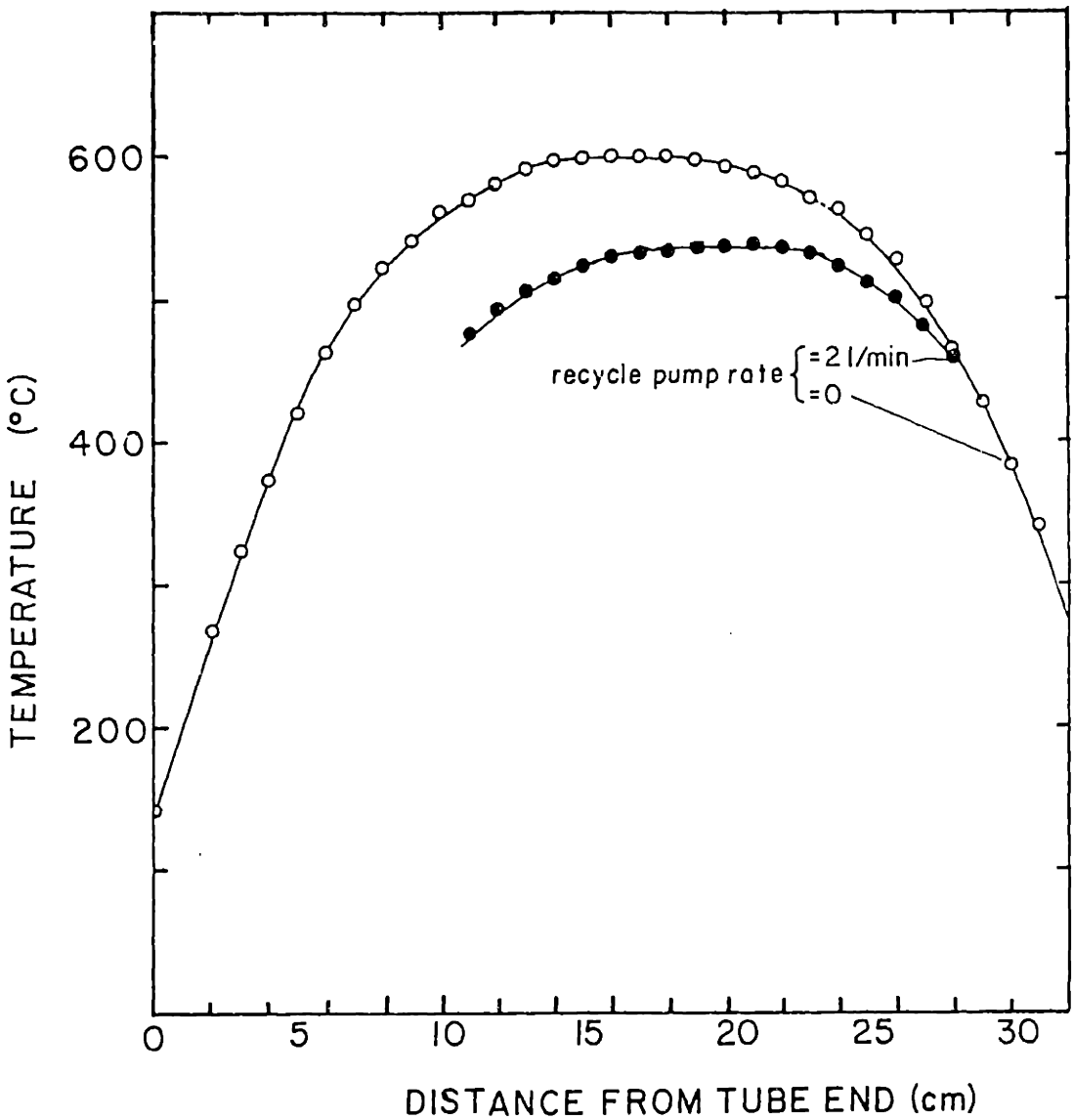

Figure A.1: Temperature profile for annular reactor with and without recycle pump in operation

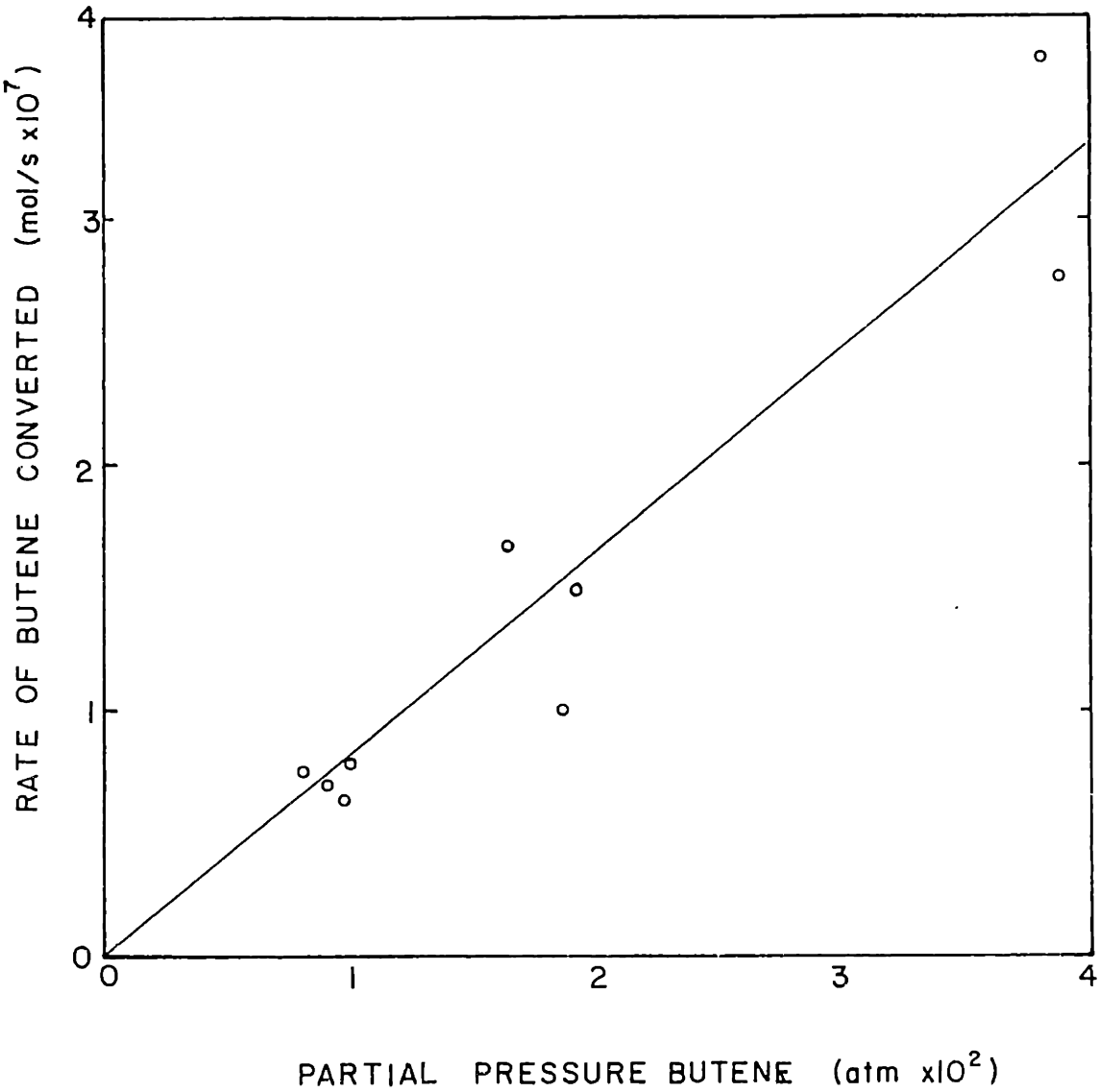

Figure A.2: Thermal cracking of 1-butene at 600°C in 1" diameter SiO_2 tubular reactor

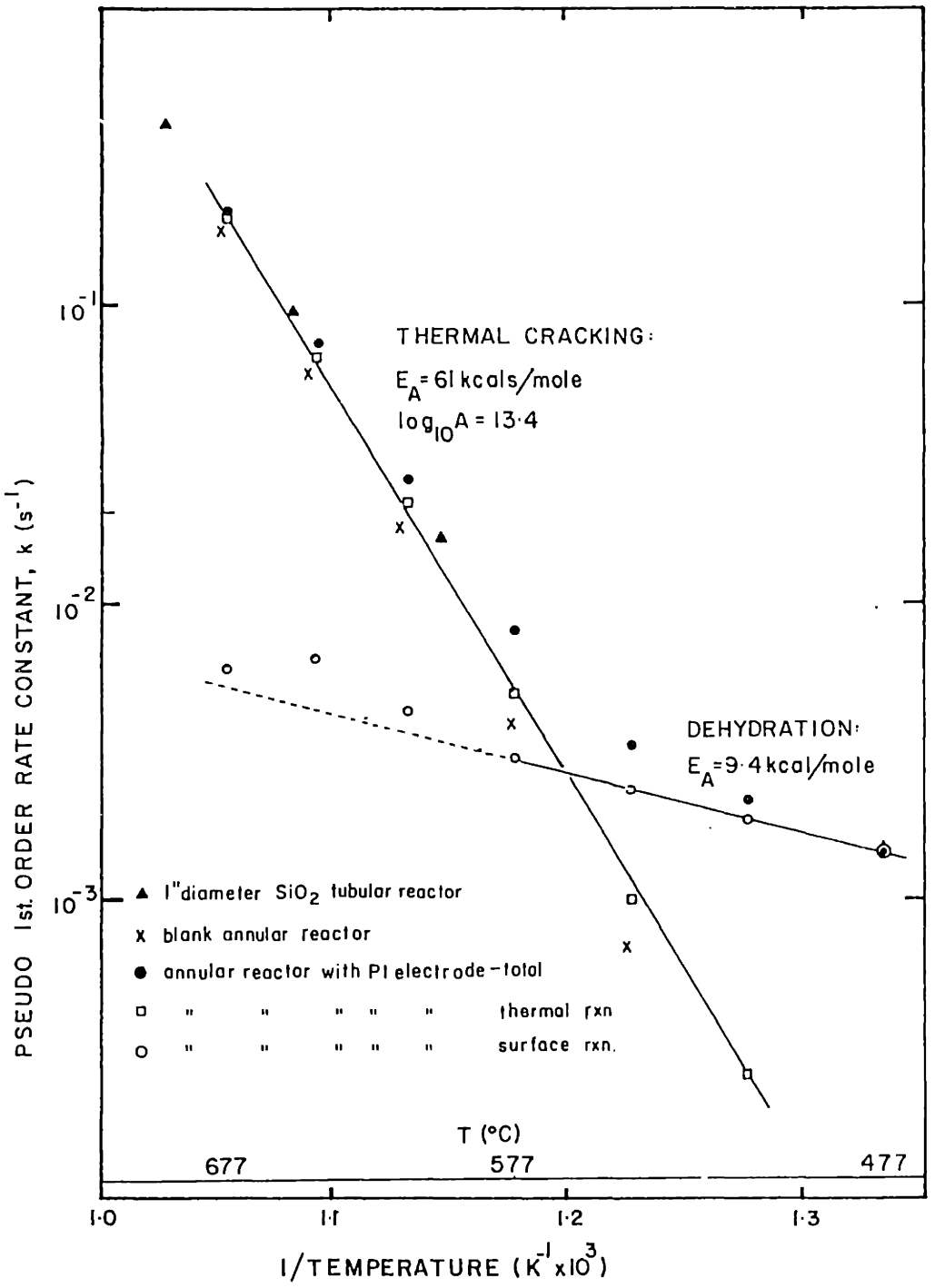

Figure A.3: Arrhenius plot for thermal cracking of 1-butene

(figure A.3).

The effect of adding oxygen to the gas stream was investigated by passing a stream of 2% butene and 0.08% oxygen through the reactor, with no Pt electrodes, between 477 and 700°C. Below 578°C, it was almost impossible to determine the conversion because it was so low. The conversion of butene increased up to 23.6% at 677°C (950 K) and the rate constant was calculated by ignoring the oxygen and assuming a first order reaction with an equivalent reactor volume of 9.7 cm^3 (figure A.3).

The data from all three experimental runs agree with each other and have an activation energy of about 61 kcal/mol and a pre-exponential factor of about $10^{13.36}$ s^{-1}.

The product distributions measured for the thermal cracking are shown in table A.2.

Table A.2: Product distribution for thermal cracking of 1-butene.

Reactor	1" SiO_2 Tubular Reactor	Annular Reactor	Blank Annular Reactor	Powers & Corcoran (1976)	Leftin (1979)
Temp (°C)	700	677	677	575	871
Butene (atm)	.0195	.0120	.015	.001	.40
Diluent	He	.00023 atm O_2 in He	.0024 atm O_2 in He	Ar	H_2O
Contact time (s)	≈2	17.9	2.61	4	.047
Recycle ratio	0	>100	20	-	-
Component		Selectivity (mol %)			
CO	0	.73	2.69	-	-
CH_4	11.6	10.5	7.62	26.9	11.69
CO_2	0	.22	.86	-	-
C_2H_4	21.1	17.7	13.56	12.0	16.09
C_2H_6	0	.98	.90	-	.77
C_3H_6	24.3	21.2	20.5	23.5	23.29
cis-2-butene	.50	.97	1.13	4.8	1.22
trans-2-butene	.93	1.27	1.34	5.5	1.70
butadiene	17.9	20.4	25.1	19.1	21.88
1-pentene	1.77	.55	1.47	2.8	-

C.3 Discussion

At 677°C, the predominant reaction is the thermal cracking of butene, but it becomes insignificant at temperatures below about 600°C. From the data in figure A.3, the rate constant for thermal cracking of butene is about 0.001 s^{-1} at 544°C. This corresponds to a rate of butene cracking of 1.45×10^{-7} [Butene] mol/s for a reactor volume of 9.7 cm^3, or a rate of

thermal cracking of 5.8×10^{-8} mol/s at 40% butene. The rate of butadiene formation given under these conditions (figure 4.50) is about 3×10^{-7} mol/s, and the rate of butene conversion was 4.99×10^{-7} mol/s, i.e. the expected rate of thermal cracking was always about an order of magnitude less than the rate of the surface reaction.

The selectivities for thermal cracking agree between the three sets of data and with the literature data (Table A.2). The values from Leftin (1979) differ slightly the other data because of the higher temperatures used and larger conversions, permitting secondary reactions to occur. During surface reaction experiments, the presence of ethylene and propylene were therefore used as markers to indicate the occurence of thermal cracking; their rates were never significant.

The activation energy for thermal cracking of 61 kcal/mole and pre-exponential factor of $10^{13.4}$ s^{-1} agree with the literature values of 57.2 kcal/mole and $10^{13.3}$ s^{-1} (Leftin, 1979), 76kcal/mole (Powers and Corcoran, 1976) and 59.0 kcal/mole and $10^{13.1}$ s^{-1} (Shibatani and Kinoshita, 1973). The pre-exponential factor of $10^{13.4}$ is also as expected for a thermal reaction (10^{13}).

C.4 Conclusion

1. Thermal cracking of butene is given by:

$$\text{rate} = 10^{13.4}\ s_{-1}\ \exp(61100/RT)$$

2. The rate of thermal cracking of butene is unaffected by the presence of oxygen. Oxygen simply serves to change the ultimate product distribution observed.

3. The rate of thermal cracking at all the temperatures used in this thesis is sufficiently low to be ignored.

APPENDIX 4: "CSTR-NESS" OF RECYCLE REACTOR

The degree of mixing and the quality of the recycle reactor as a CSTR was investigated by measuring the residence time distribution of the reactor using the so-called "E-curve" method of Dankwertz (1953, see also Fromment and Bischoff, 1979 and Levenspiel, 1972).

This method involves injecting a delta function of a tracer into the reactor and observing the output from the reactor. If the reactor were to behave as a perfect plug flow reactor, the output would be a similar delta function, which would have been broadened by any dispersion that may have occurred. If the reactor behaves as a perfect CSTR (Continuous Stirred Tank Reactor), the ouput from the reactor is a decaying exponential which is given by:

$$E(\theta) = 1/T \quad \exp-(\theta/T)$$

where θ is the time and T the contact time in the reactor.

Experimentally, the GC was by-passed and the output from the reactor, heated to 530_oC, connected directly to the continuous infra-red CO_2 detector. The reactor and detector were equilibrated using helium and the the input to the reactor was switched briefly to 100% CO_2 and then back to helium, in an attempt to experimentally create a delta function. The CO_2 output was recorded for delta functions injected into the reactor at different recycle pumping rates (different recycle ratios). The CO_2 output was digitized and normalized:

$$E(\theta) = \frac{C(\theta)}{\int_0^\infty C(\theta)d\theta}$$

where $C(\theta)$ is the concentration of CO_2 at time, θ. The time was similarily normalized using:

$$\theta' = \theta / T$$

where:

$$= \frac{\int_0^{\infty} \theta\, C(\theta)\, d\theta}{\int_0^{\infty} C(\theta)\, d\theta}$$

The data were plotted according to the normalized concentration and time in figure A.4. When the recycle ratio was less 8, spikes from where the input CO_2 had not mixed with the bulk of the gas appeared in the output. At recycle ratios greater than 8, the output approximated an exponential decay, as would be expected from a CSTR.

The variance of the output was calculated using (Fromment and Bischoff, p604, 1979):

$$\sigma^2 = \int_0^{\infty} (\theta')_2\, E(\theta')\, d\theta'$$

The variance of the data increased from 0.13 for no recycle to 0.6 for recycle ratios>8. The variance is a measure of the degree of "CSTR-ness" of the reactor and is inversely related to the equivalent number of CSTR's in series; i.e. this variance implies that the output from the reactor is equivalent to the output from 1.67 CSTR's in series which had been fed with a perfect dirac delta function. The input to the reactor was not a perfect delta function and the CO_2 was itself a small CSTR of about 5 cm_3 volume (determined by by-passing the reactor). These combine

to explain the variance not being 1.0.

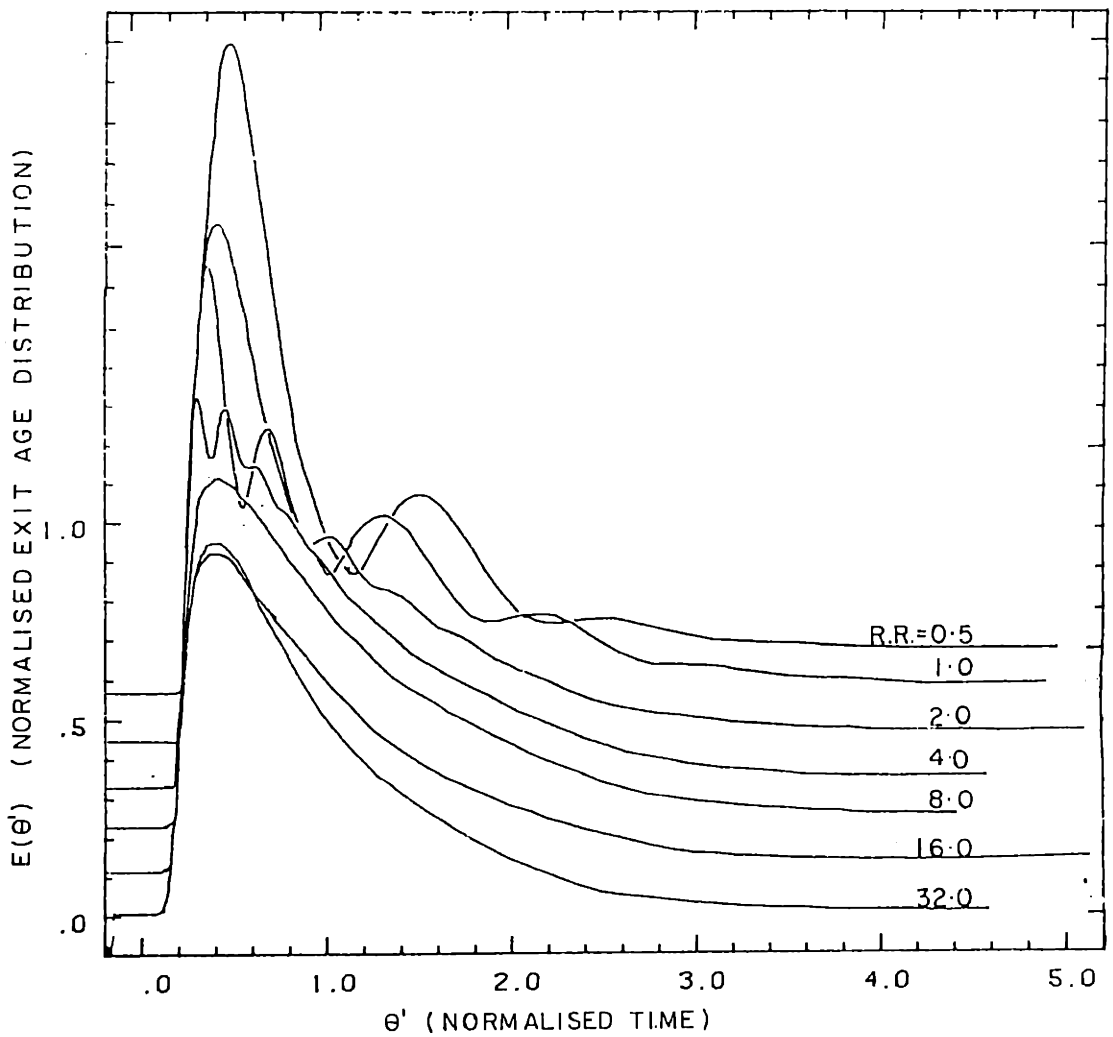

Figure A.4: Normalized exit concentration of CO_2 tracer vs normalized time for different recycle ratios, annular reactor.

REFERENCES

R.P.L. Absil, J.B. Butt and J.S. Dranoff: On the estimation of catalytic rate equation parameters. J. Catal. 87, 530-535 (1984).

C.B. Alcock and G.W. Hooper: Thermodynamics of the gaseous oxides of the platinum group metals. Proc. Royal Soc. A 254, 551 (1960).

A. Amirnazmi and M. Boudart: Decomposition of nitric oxide on Pt. J. Catal. 39, 383 (1975).

J.E. Anderson and Y.B. Graves: Steady-state characteristics of oxygen concentration cell sensors subjected to non-equilibrium gas mixtures. J. Electrochem. Soc. 128, 294 (1981).

D.H. Archer, L. Elikan and R.L. Zahradnik: The performance of solid-electrolyte cells and batteries on CO-H_2 mixtures. A 100-watt solid-electrolyte power supply. In B.S Baker (Ed.): Hydrocarbon fuel cell technology, Academic Press, NY (1965).

J. Barbier, G. Corro, Y. Zhang, J.P. Bournonville and J.P. Franck: Coke formation on Pt-Al_2O_3 catalyst of wide varying dispersion. Appl. Catal. 13, 245 (1985).

R.W. Bartlett: Platinum oxidation kinetics with convective diffusion and surface reaction. J. Electrochem. Soc. 114, 547 (1967).

R.J. Behm, P.A. Thiel, P.R. Norton and P.E. Binder: The oxidation of CO on Pt/(100): mechanism and structure. Surface Sci. 147, 143 (1984).

F.J. Berry: Tin-antimony oxide catalysts. Adv. in Catal. 30, 97 (1981).

R.J. Berry: Study of multilayer surface oxidation of platinum by electrical resistance technique. Surface Sci. 76, 415 (1978).

A. Bielanski and J. Haber: Oxygen in catalysis on transition metal oxides. Catal. Rev.-Sci. Eng. 19 (1), 1 (1979).

J. O'M. Bockris and A.K.N. Reddy: Modern electrochemistry. Plenum Press, New York (1970).

H.P. Bonzel, A.M. Franken and G. Perug: The segregation and oxidation of silicon on Pt/(111) or The question of "platinum oxide." Surface Sci. 104, 625-642 (1981).

H.P. Bonzel and R.Ku.: Mechanisms of the catalytic CO oxidation on Pt/(110). Surface Sci. 33, 91 (1972).

G.E.P. Box and N.R. Draper: The Bayesian approach of common parameters from several responses. Biometrika 52, 355 (1965).

D. Brennan, D.O. Hayward and B.M.W. Trapnell: The calorimetric determination of the heats of adsorption of oxygen on evaporated metal films. Proc. R. Soc. London Ser. A 256, 81 (1960).

D. Briggs and M.P. Sheah: Practical surface analysis by auger and X-ray photoelectron spectroscopies. John Wiley and Sons (1983).

N.W. Cant and D.E. Angove: The origin of apparent deactivation during oxidation of CO over SiO_2-supported Pt at moderate temperatures. J. Catal. 97, 36 (1986).

N.W. Cant and W.K. Hall: Catalytic oxidation. II. Silica supported noble metals for the oxidation of ethylene and propylene. J. Catal. 16, 220 (1970).

J.J. Carberry: Chemical and catalytic reaction engineering. McGraw-Hill, New York (1976).

S. Carra and L. Formi: Catalytic dehydrogenation of C_4 hydrocarbons over Cr_2O_3/Al_2O_3. Catal. Rev.-Sci. Eng. 5 (1), 159 (1971).

S. Chandra: Superionic solids: Principles and applications. North Holland Publ. Co., Amsterdam (1981).

M. Chen and L.D. Schmidt: Morphology and sintering of Pt crystallites on Amorphous SiO_2. J. Catal. 55, 348 (1978).

C.B. Choudary, H.S. Maiti and E.C. Subbarao: Defect structure and transport properties. In E.C. Subbarao (Ed.), Solid Electrolytes and their Applications, Plenum Press, NY (1980).

J.R. Christie, D. Taylor and C. McCain: Isotropic exchange studies and selective oxidation of propene on mixed tin-antimony oxides. J. Chem. Soc. Far. Trans. I 72, 334 (1976).

A.D. Colvin, J.W. Butler and J.E. Anderson: Catalytic effects on ZrO_2 oxygen sensors exposed to non-equilibrium gas mixtures. J. Electroanal. Chem. 136, 179-183 (1982).

Y.M. Cross and D.R. Pyke: An x-ray photoelectron spectroscopy study of the surface composition of tin and antimony mixed metal oxide catalysts. J. Catal. 58, 61 (1979).

P.V. Danckwerts: Continuous flow systems. Distribution of residence times. Chem. Eng. Sci. 2, 1 (1953).

S.M. Davis, F. Zaera, B.E. Gordon and G.A. Somorjai: Radiotracer and thermal desorption studies of dehydrogenation and atmospheric hydrogenation of organic fragments obtained from [C-14] ethylene chemisorbed on Pt(111) surfaces. J. Catal. 92, 240-246 (1985).

S.M. Davis, F. Zaera and G.A. Somorjai: The reactivity and composition of strongly adsorbed carbonaceous deposits on platinum. Model of the working hydrocarbon conversion catalyst. J. Catal. 77, 439 (1982).

W.A. Dietz: Response factors for gas chromatographic analyses. J. of Gas Chromatography 68 (1967).

L.H. Dreger and J.L. Margrave: Vapor pressures of platinum metals. I. Platinum and palladium. J. Phys. Chem. 64, 1323 (1960).

J.J. Ehrhardt, E. Hafele, H.-G. Lintz and A.F. Martins: Surface preparation for solid electrolyte aided studies in heterogeneous catalysis. Ber. Bensenges Phys. Chem. 89, 984 (1985).

T. Engel and G. Ertl: Elementary steps in the catalytic oxidation of carbon monoxide on platinum metals. Adv. Cat. 28, 1-78 (1979).

T.H. Etsell and S.N. Flengas: The electrical properties of solid oxide electrolytes. Chem. Rev. 70 (3), 339 (1970).

P. Fabry and M. Kleitz: Influence of the metal and the electrolyte composition on the characteristics of the oxygen electrode on reaction on solid oxide electrolyte. Electroanal. Chem. and Inter. Electrochem. 57, 165-177 (1974).

R.D. Farr and C.G. Vayenas: Ammonia high temperature solid electrolyte fuel cell. J. Electrochem. Soc. 127 (7), 1478 (1980).

G.F. Fromment and K.B. Bischoff: Chemical reactor analysis and design. John Wiley and Sons, New York (1979).

J.H. Gland: Molecular and atomic adsorption of oxygen on the Pt/(111) and Pt/(s)-12/(111)/x/(111) surfaces. Surface Sci. 93, 487 (1980).

J.H. Gland and V.N. Korchak: The adsorption of oxygen on a stepped Pt single crystal. Surface Sci. 75, 733 (1978).

J.H. Gland, B.A. Sexton and G.B. Fisher: Oxygen interactions with the Pt/(111) surface. Surface Sci. 95, 587 (1980).

I.M. Gur, I.D. Raistrick and R.A. Huggins: Steady state D.C. polarization characteristics of the O_2, Pt/stabilized zirconia interface. J. Electrochem. Soc. 127 (12), 2620 (1980).

T.M. Gur, I.D. Raistrick, R.A. Huggins: AC admittance measurements on stabilized zirconia with porous platinum electrodes. Solid State Ionics 1, 251 (1980).

D.M. Haarland and F.L. Williams: Simultaneous measurement of CO oxidation rate and surface coverage on Pt/Al_2O_3 using I.R. spectroscopy: rate hysteresis and CO island formation. J. Catal. 76, 450 (1982).

J.H. Harding. Thermodynamic and transport properties of superionic conductors and electrode materials. In J.W. Perran (Ed.), Nato Advanced Study Institute on the physics of superionic conductors and electrode materials. Plenum Press, New York (1980).

D. Hasenberg and L.D. Schmidt: HCN synthesis from CH_4 and NH_3 on Pt. J. Catal. 97, 156 (1986).

L.L. Hegedus and R.W. McCabe: Catalyst Poisoning. Marcel Dekker, Inc., New York (1984).

H.J. Herniman, D.R. Pyke, R. Reid: An investigation of the relationship between the bulk and surface composition of tin and antimony mixed oxide catalysts and the oxidative dehydrogenation of 1-butene to butadiene. J. Catal. 58, 68 (1979).

J-M.J. Herrmann, J-L. Portefaix, M. Forissier, F. Figueras and P. Pichat: Electrical behavior of powdered tin-antimony mixed oxide catalysts. J. Chem. Soc. Far. Trans. I 75, 1346 (1979).

R.K. Herz and S.P. Marin: Surface chemistry models of CO oxidation on supported Pt catalysts. J. Catal. 65, 281 (1980).

L. Hilaire, G.D. Guerrero, P. Legare, G. Maire and G. Krill: A photoemission study of the oxidation of platinum in Pt-based alloys: Pt-Pd; Pt-Ru; Pt-Ir. Surface Sci. 146, 569 (1984).

A.B. Hope: Ion transport and membranes. Butterworths, London (1971).

E.A. Irvine and D. Taylor: Dehydrogenation and isomerization of n-butenes on mixed tin-antimony oxide catalysts. J. Chem. Soc. Far. Trans. I 74, 1590 (1978).

E.A. Irving and D. Taylor: Acidic properties of mixed tin and antimony oxides. J. Chem. Soc. Far. Trans. I 74, 206 (1978).

H.S. Isaacs, L.J. Olmer, E.J.L. Schouler and C.Y. Yang: Electrode reactions at solid oxide electrolytes. Solid State Ionics 3, 503-7 (1981).

A. Jutan: A parameter estimation program for multiresponse data using a Bayesian approach. McMasters University Technical Publication No. SOC-117.

D.J. Kaul and E.E. Wolf: FTIR studies of surface reaction dynamics: temperature and concentration programming during CO oxidation on Pt/SiO_2. J. Catal. 89, 348 (1984).

J.A. Kilner and R.J. Brook: A study of oxygen ion conductivity in doped non-stoichiometric oxides. Solid State Ionics 6, 237 (1982).

S.L. Kiperman: Kinetic problems in selectivity. Kinetika i Kataliz 22 (1), 30 (1981).

M.U. Kislyuk and T.N. Bakuleva: Adsorption of oxygen on the surface of polycrystalline platinum. Arguments in favor of islet character of adsorption. Kinetika i Kataliz 24 (6), 1455-1462 (1982).

J.T. Kiss and R.D. Gonzalez: Deactivation of selected noble metal catalysts during CO oxidation: An in situ IR and kinetic study. Ind. Eng. Chem. Prod. Res. Dev. 24, 216 (1985).

M. Kleitz and J. Dupuy (Eds.): Electrode Processes in Solid State Ionics. D. Reidel Publishing Co., Holland (1976).

O. Kubaschewski and C.B. Alcock: Metallurgical Thermochemistry, 5th Edition. Pergamon Press, Oxford (1979).

S.H. Langer and I.A. Colucci-Rios: Chemicals with power. Chemtech 15 (4), 226 (1985).

S.H. Langer and K.T. Pate: Selective electrogenerative reduction of nitric oxide. Ind. Eng. Chem. Proc. Des. Dev. 22, 264 (1983).

S.H. Langer, G.P. Sakeliaropoulos: Electrogenerative and voltameriotic processes. Ind. Eng. Chem. Proc. Des. Dev. 18 (4), 587 (1979).

H.P. Leftin: Steam pyrolysis of normal butenes. Adv. in Chem. Ser. 183, 21 (1979).

P. Legare, L. Hilaire and G. Maire: Interaction of polycrystalline Pt and Pt-Si alloys with oxygen; XPS study. Surface Sci. 141, 604-616 (1984).

R. Lewis and R. Gomer: Adsorption of oxygen on platinum. Surface Sci. 12, 157 (1968).

H.A. Liebhafsky and E.J. Cairns: Fuel cells and fuel batteries. John Wiley and Sons, New York (1968).

D.T. Lynch, G. Emig and S.E. Wanke: Oscillations during CO oxidation over supported metal catalysts. J. Catal. 97, 456 (1986).

J.C. McAteer: Study of the oxidative reactions of butenes over mixed tin-antimony oxides. J. Chem. Soc. Far. Trans. I 75, 2768 (1979).

R.W. McCabe, T. Pignet and L.D. Schmidt: Catalytic etching of Pt in NH_3 oxidation. J. Catal. 32, 114 (1974).

R.W. McCabe and L.D. Schmidt: Adsorption of H_2 and CO on clean and oxidized (110) Pt. Surface Sci. 60, 85-98 (1976).

R.W. McCabe and L.D. Schmidt: Binding states of CO and H_2 on clean and oxidized (111) Pt. Surface Sci. 65, 189-209 (1977).

M.R. McClellan, R. McFeely and J. Gland: Molecular and atomic oxygen adsorption on the kinked Pt/(321) surface. Surface Sci. 124, 184 (1983).

T. Mahoney, Engelhard Corporation, Personal Communication (1986).

I. Matsuura: The nature of the sites on olefin oxidation catalysts. Proc. 6th Int. Cong. Catalysis, London (1976) (The Chemical Soc., 1977), 819.

T. Matsushima, D.B. Almy and J.M. White: The reactivity and Auger chemical shift of oxygen adsorbed on platinum. Surface Sci. 67, 89 (1977).

J.N. Michaels: Electro-oxidative dehydrogenation of ethylbenzene. Ph.D. Thesis, M.I.T. (1983).

D. Mukesh, C.N. Kenney and W. Morton: Concentration oscillations of carbon monoxide, oxygen and 1-butene over a platinum supported catalyst. Chem. Eng. Sci. 38 (1), 69 (1983).

J.S. Newman: Electrochemical Systems. Prentice-Hall, Englewood Cliffs, New Jersey (1973).

H. Niehus and G. Comsa: Surface and subsurface oxygen adsorbed on Pt/(111). Surface Sci. 43, L147-L150 (1980).

J.H. Norman, H.G. Staley and W.E. Bell: Mass spectrometric-Knudsen cell study of gaseous oxides of platinum. J. Phys. Chem. 71, 3686 (1967).

P.R. Norton, J.A. Davies and T.E. Jackman: Absolute coverages of CO and O on Pt/(111); comparison of saturation CO coverages on Pt(100), (110) and (111) surfaces. Surface Sci. 122, L593 (1982).

E.J. Nowak: Prediction of platinum loss during ammonia oxidation. Chem. Eng. Sci. 24, 421 (1969).

H. Okamoto, H. Obayashi and T. Kudo: Non ideal emf behavior of zirconia oxygen sensors. Solid State Ionics 3/4, 453 (1981).

H. Okamoto, G. Kuwamura and T. Kudo: Interpretation of the electromotive forces of solid electrolyte concentration cells during carbon monoxide oxidation on Pt. J. Catal. 82, 322 (1983).

H. Okamoto, G. Kawamura and T. Kudo: Electromotive forces studies of carbon monoxide oxidation of platinum. J. Catal. 82, 332 (1983).

H. Okamoto, G. Kawamura and T. Kudo: Study of oxygen adsorption on platinum through observation of exchange current in a solid electrolyte concentration cell. Electrochimica Acta 28 (3), 379 (1983).

H. Okamoto, G. Kawamura and T. Kudo: Relation between surface adsorption states and emf in a solid electrolyte concentration cell during CO oxidation on Pt studied by local current measurement. J. Catal 86, 437-440 (1984).

H. Okamoto, G. Kawamura and T. Kudo: Carbon monoxide oxidation on platinum studied by local current and emf in a solid electrolyte concentration cell. J. Catal. 87, 1 (1984).

L.J. Olmer and H.S. Isaacs: The effect of electrode surface impurities on the oxygen electrode reaction at zirconia electrolytes. J. Electrochem. Soc. 129 (2), 345 (1982).

J.J. Ostermaier, J.J. Katzer and W.H. Manogue: Platinum catalyst deactivation in low-temperature ammonia oxidation reactions. 1. Oxidation of ammonia by molecular oxygen. J. Catal. 41, 277-292 (1976).

J.M. Parera, N.S. Figoli and E.M. Traffano: Catalytic action of Pt on coke burning. J. Catal. 79, 481 (1983).

M. Peuckert and H.P. Bonzel: Characterization of oxidized platinum surfaces by XPS. Surface Sci. 145, 239 (1984).

S. Pizzini: General aspects of kinetics of ion-transfer across interfaces. In W. Van Gool (Ed.), Fast Ion Transport in Solids. North-Holland Publishing Co., Amsterdam (1973).

D.R. Powers and H. Corcoran: Pyrolysis of 1-butene and cis-2-butene. ACS Symp. Series 32, 117 (1976).

D.R. Pyke, R. Reid and R.J.D. Tilley: Structures of tin oxide-antimony oxide catalysts. Chem. Soc. Faraday I, 76, 1174-1182 (1980).

V. Ragaini: The isomerization of n-butenes over platinum black in the absence of molecular hydrogen. J. Catal. 34, 1 (1974).

L.F. Razon and R.A. Schmitz: Intrinsically unstable behavior during the oxidation of carbon monoxide on platinum. Catal. Rev.-Sci. Eng. 28 (1), 89-164 (1986).

B.C. Sales, J.E. Turner and M.B. Maple: Oscillatory oxidation of CO over Pt, Pd and Ir catalysts: theory. Surface Sci. 114, 381-354 (1982).

M. Salmeron and G.A. Somorjai: Desorption, Decomposition and D_2 exchange reactions of unsaturated hydrocarbons (C_2H_4, C_2H_2, C_3H_6, C_4H_8) on Pt/(111) crystal face. J. Phys. Chem. 86, 341-350 (1982).

J. Sasaki, J. Mizusaki, S. Yamauchi and K. Fueki: Studies on electrode processes of stabilized zirconia cells by complex impedance method. Solid State Ionics 3/4, 531 (1981).

C.N. Satterfield: Heterogeneous Catalysis in Practice. McGraw-Hill (1980).

H. Schafer and A. Tebben: Gleichgewichtsmessungen im system platin-sauerstoff; gasformiges platindioxyd. Z. Anorg. Allgem. Chem. 304, 317 (1960).

E.J.L. Schouler and H.S. Isaacs: The reaction kinetics of electrodes on zirconia in H_2/H_2O gases. Solid State Ionics 5, 555 (1981).

A. Schwarz, L.L. Holbrook and H. Wise: Catalytic oxidation studies with Pt and Pd. J. Catal. 21, 199 (1971).

V. Sharchenko: Oxidative dehydrogenation of hydrocarbons. Int. Chem. Eng. 9, 1, (1969).

M. Sheintuck: Nonlinear kinetics in catalytic oxidation reactions, periodic and aperiodic behavior and structure sensitivity. J. Catal. 96, 326 (1985).

H. Shibatani and H. Kinoshita: Thermal decomposition of alkenes. III. Kinetic study of thermal decomposition of 1-butene. Nippon Kagaku Kaishi, 1005 (1973).

C.T. Sigal and C.G. Vayenas: Ammonia oxidation to nitric oxide in a solid electrolyte fuel cell. Solid State Ionics 5, 567-570 (1981).

G.A. Somorjai: Chemistry in Two-dimensions - Surfaces. Cornell University Press, Ithaca, New York (1981).

H.S. Spacil and C.S. Tedmon: Electrochemical dissociation of water vapor in solid oxide electrolyte cells. I. Thermodynamic and cell characteristics. J. Electrochem. Soc. 116, 1627 (1969).

R.M. Spotnitz, C.E. Loeffler and S.H. Langer: Electrogenerative oxidation of SO_2. J. Appl. Electrochem. 11, 403 (1981).

B.C.H. Steele: High temperature fuel cells and electrolysers in M. Kleitz and J. Dupuy (Eds.), Electrode Processes in Solid State Ionics. D. Reidel Publishing Co., Holland (1976).

H. Steininger, S. Lehwald and H. Ibach: Adsorption of oxygen on Pt/(111). Surface Sci. 123, 1-17 (1982).

J.S. Sterrett and M.G. McIlvreid: Kinetics of the oxidative dehydrogenation of butene to butadiene over a ferrite catalysts. Ind Eng. Chem. Process Des. Dev. 13, 54 (1974).

D.R. Stull, E.F. Westrum and G.C. Sinke: The Chemical Thermodynamics of Organic Compounds. John Wiley and Sons, New York (1969).

E.C. Subbarao (Ed.), Solid Electrolytes and Their Applications. Plenum Press, New York (1980).

E.F. Sverdrup, C.J. Warde and A.D. Glasser: A Fuel Cell Power System for Central-Station Power Generation Using Coal as a Fuel in "From Electrocatalysis to Fuel Cells," G. Sanstede (Ed.), p. 253, U. Washington Press, Seattle (1972).

K.C. Taylor: Automobile catalytic converters. Catal. Sci. and Tech. 5, 120 (1984).

C.E. Teague: The high temperature ammonia fuel cell: production of nitric oxide with concentration of electricity. M.Sc. Thesis, M.I.T. (1981).

D.Y. Wang and A.S. Nowick: Catholic and anodic polarization phenomena at platinum electrodes with doped CeO_2 as electrolyte: 1. steady state overpotential. J. Electrochem. Soc. 126 (7), 1155 (1979).

C.D. Wagner, U.M. Riggs, L.E. Davis, J.F. Moulder and G.E. Muilenberg: Handbook of X-Ray Photoelectron Spectroscopy. Perkin-Elmer Corporation, Physical Electronics Division (1979).

M.J. Verkerk, M.W.J. Hammink and A.J. Burggraaf: Oxygen transfer on substituted ZrO_2, Bi_2O_3 and CeO_2 electrodes with Pt electrodes. I: Electrode resistance by DC polarization. J. Electrochem. Soc. 130 (1), 70 (1983).

C.G. Vayenas and J.N. Michaels: On the stability limit of surface platinum oxide and its role in the oscillatory behavior of platinum catalyzed oxidations. Surface Sci. 120, L405-L408 (1982).

C.G. Vayenas, G. Georgakis, J. Michaels and J. Tormo: The role of PtO_2 in the isothermal rate oscillations of ethylene oxide on platinum. J. Catal. 67, 348 (1981).

C.G. Vayenas, B. Lee and J.N. Michaels: Kinetics, limit cycles and mech. of ethylene oxidation on Pt. J. Catal. 66, 36-48 (1980).

J.E. Turner and M.B. Maple: Oxide formation and reduction over Pt, Pd and Ir; a driving mechanism for oscillations in the CO oxidation reaction. Surface Sci. 147, 647 (1984).

C.L. Thomas: Catalytic Processes and Proven Catalysts. Academic Press, New York (1970).

C.L. Thomas: Butadiene preparation from butene by catalytic oxidation. U.S. Patent # 3 444 260 (5/16/69).

W.H. Weinberg and R.P. Merrill: Crystal field surface orbital-bond energy bond order (CFSO-BEBO) calculations of adsorption. II: CO, O and CO_2 on Pt(111) and O on Ni (111). Surface Sci. 39, 206 (1973).

J.M. White and A. Golchet: Rates and coverages in low pressure Pt-catalysed oxidation of CO. J. Catal. 53, 266 (1979).

M. Wilf and P.T. Dawson: The adsorption and desorption of oxygen on the Pt/(110) surface; a thermal desorption and LEED/AES study. Surface Sci. 65, 399 (1977).

D.E. Williams, P. McGeehin and B.C. Tofield: Solid electrolyte mixed potential phenomena. Ext. Abs., Spring Meet. Electr. Soc., May 1982, 82-1, 1176 (1982).

K.R. Williams (Ed.): An Introduction to Fuel Cells. Elsevier Publishing Co., Amsterdam (1966).

W.L. Worrell: Oxide solid electrolytes. In solid electrolytes, Ed. S. Geller. Springer-Verlag, Berlin (1977).

R.C. Yeates, J.E. Turner, A.J. Gellman and G.A. Somorjai: The oscillatory behavior of the CO oxidation reaction at atmospheric pressure over Pt single crytals: surface analysis and pressure dependent mechanism. Surface Sci. 149, 175-190 (1985).

Y-F.Y. Yao: The oxidation of CO and hydrocarbons over noble metal catalysts. J. Catal. 87, 152-162 (1984).

M.G. Zabetakis: Flammability Characteristics of Combustible Gases and Vapors. U.S. Bureau of Mines, Bulletin # 627 (1965).